Multi-functional Self-healing Materials for Structural Application

Elisa Calabrese

UNIVERSITY OF SALERNO

DEPARTMENT OF INDUSTRIAL ENGINEERING

Ph.D. Course in Industrial Engineering
Curriculum in Chemical Engineering - XXXI Cycle

MULTI-FUNCTIONAL SELF-HEALING MATERIALS FOR STRUCTURAL APPLICATION

Supervisor
Prof. Liberata Guadagno

Ph.D. student
Elisa Calabrese

Scientific Referees
Prof. Pasquale Longo
Dr. Carlo Naddeo
PhD. Marialuigia Raimondo
Eng. Salvatore Russo

Ph.D. Course Coordinator
Prof. Ernesto Reverchon

Acknowledgements

These three years have come to an end and first of all I would like to express my profound gratitude to my supervisor, Professor Liberata Guadagno, who, with her enormous professional experience, has been able to give me the necessary tools to successfully carry out this PhD research activity.

She taught me to move forward with humility and strong critical spirit, transferring me the passion to face all the challenges.

I would like to express my gratitude to my scientific referees, Prof. Pasquale Longo, Dott. Carlo Naddeo, PhD Marialuigia Raimondo and Ing. Salvatore Russo, for their support and for their valuable advice.

A special thanks goes to Carlo and Regina, which have strongly supported me during these three years. I shared with Regina important life and work experiences, which have contributed to my human and professional growth.

I would like to thank IASS project (European Union's Seventh Framework Programme for research, technological development and demonstration under Grant Agreement No. 313978) and MASTRO project (European Union Horizon 2020 Programme under Grant Agreement No. 760940), whose funds have allowed to reach the results of this research.

I would like to extend my particular thanks to all my colleagues from the Chemical Foundations of Technologies laboratory I4 (DIIN) and of the Chemistry laboratory 2 (DCB), with particular reference to the expert engineer Luigi Vertuccio, and the PhD Giuseppina Barra and the PhD Annaluisa Mariconda, who were dear friends and excellent researchers.

Last but not least, a very special thanks goes to all my family, in particular, to my husband Francesco and my children, Chiara and Alfonso Maria, who are a firm reference point in my life and who in these years have supported me with patience and love. Thanks to my parents, who supported me morally, helping to realize this dream.

Thank you
Elisa Calabrese
University of Salerno
January 2019

Publication list related to the Ph.D. research activity

International research papers

1) P. Longo, A. Mariconda, **E. Calabrese**, M. Raimondo, C. Naddeo, L. Vertuccio, S. Russo, G. Iannuzzo, L. Guadagno, (2017). Development of a new stable ruthenium initiator suitably designed for self-repairing applications in high reactive environments, *Journal of Industrial and Engineering Chemistry*, **54**, pp. 234-251. **DOI: 10.1016/j.jiec.2017.05.038.**

2) L.Guadagno, L. Vertuccio, C. Naddeo, **E. Calabrese**, G. Barra, M. Raimondo, A. Sorrentino, W. H. Binder, P. Michael, S. Rana, (2019). Self-Healing Epoxy Nanocomposites via Reversible Hydrogen Bonding, *Composites Part B*, **157**, pp. 1-13. **DOI: 10.1016/j.compositesb.2018.08.082 (Open Access)**.

3) **E. Calabrese***, P. Longo, C. Naddeo, A. Mariconda, L. Vertuccio, M. Raimondo, L. Guadagno, (2018). Design of Self-Healing Catalysts for Aircraft Application, *International Journal of Structural Integrity*, **9** (6), 723-736. **DOI: 10.1108/IJSI-12-2017-0077. ***Corresponding author.

4) **Book chapter** of Springer Book on Aircraft Materials: Self-Healing Mechanisms in Multifunctional Structural Materials. L. Guadagno, C. Naddeo, L. Vertuccio, **E. Calabrese**, G. Barra, M. Raimondo. (**Accepted**)

5) Liberata Guadagno, Luigi Vertuccio, Carlo Naddeo, **Elisa Calabrese**, Giuseppina Barra, Marialuigia Raimondo, Andrea Sorrentino, Wolfgang H. Binder, Philipp Michael, and Sravendra Rana, (2018). Development of aeronautical epoxy nanocomposites having an integrated self-healing ability, *MATEC Web of Conferences***,** **233**, 00021 **DOI: 10.1051/matecconf/201823300021**.

Publication list related to the Ph.D. research activity

International conferences

1) **GRICU GET INNOVATION, Anacapri (NA), Italy, September 12-14, 2016**.
   E. Calabrese, L. Guadagno, P. Longo, C. Naddeo, M. Raimondo, A. Mariconda, L. Vertuccio (2016). New Ruthenium Catalyst for Self-Healing Applications in Highly Reactive Environments. **Poster contribution**.

2) **NanoInnovation edition 2016, Rome – Italy, 20-23 September 2016.**
   Guadagno Liberata, Longo Pasquale, Mariconda Annaluisa, **Calabrese Elisa**, Raimondo Marialuigia, Naddeo Carlo, Vertuccio Luigi, Russo Salvatore, Iannuzzo Generoso (2016). Synthesis of a new ruthenium catalyst for self-healing applications in aeronautics. **Poster contribution**.

3) **NanoInnovation edition 2016. p. 1, Rome – Italy, 20-23 September 2016**.
   Guadagno Liberata, Longo Pasquale, Mariconda Annaluisa, **Calabrese Elisa**, Raimondo Marialuigia, Naddeo Carlo, Vertuccio Luigi, Russo Salvatore, Iannuzzo Generoso (2016).
   A new synthesized ROMP catalyst stable in strongly interactive environments designed for self-repairing structural applications.

4) **7th EASN International Conference on Innovation in European Aeronautics Research, 26-29 September 2017, Warsaw, Poland.**
   E. Calabrese, P. Longo, A. Mariconda, M. Raimondo, C. Naddeo, L. Luigi, L. Guadagno. Development of self-healing mechanisms in aeronautical vehicles, (2017). **Oral contribution.**

5) **5th ICEAF International Conference of Engineering Against Failure – 20-22 June 2018, Chios Island, Greece.**
   E. Calabrese, P. Longo, C. Naddeo, A. Mariconda, L. Vertuccio, M. Raimondo, L. Guadagno (2018). Microencapsulated Self-Healing Composites. **Oral contribution.**

6) **8th EASN-CEAS International Workshop Manufacturing for Growth & Innovation, 4-7 September 2018, Glasgow, UK.**
E. Calabrese, L. Guadagno, L. Vertuccio, C. Naddeo, G. Barra, M. Raimondo, W. H. Binder, P. Michael, S. Rana, (2018). Development of Aeronautical Epoxy Nanocomposites Having Integrated Self-Healing Ability. **Oral contribution**.

7) **IWDRC Second International Workshop on Dynamic Response of Composite Materials, 27-28 September 2018, Ischia (Naples), Italy.**
L. Guadagno, L. Vertuccio, C. Naddeo, G. Barra, M. Raimondo, W. H. Binder, P. Michael, S. Rana, **E. Calabrese**, (2018). Development of Aeronautical Epoxy Nanocomposites Having Integrated Self-Healing Ability. **Oral contribution**.

International Patent

1) L. Guadagno, P. Longo, A. Mariconda, **E. Calabrese**, M. Raimondo, C. Naddeo, L. Vertuccio, S. Russo, G. Iannuzzo (2015). Grubbs-Hoveyda Type Catalyst for Metathesis Reactions in Highly Reactive Environments.
European patent application, **EP3141303 (A1)**, Leonardo S.p.A 00195 Roma / IT. Date of Publication: 2017-03-15.

Ph.D. Schools Participation

1) **GRICU PhD NATIONAL SCHOOL 2016**: "Chemical engineering for sustainable production of energy and fine chemicals", Anacapri September 14th-16th 2016.

2) **GRICU PhD NATIONAL SCHOOL 2018:** "Advanced chemical reactor Circular economy concepts in process engineering", Pisa May, 16th-19th 2018.

Index

Figures Index

Tables Index

Abstract

Main objective of this PhD thesis is the development of a new generation of self-healing multifunctional composites able to overcome some of the current limitations of aeronautical materials, such as: absence of auto-repair mechanisms integrated in the composite structure, reduced electrical conductivity and poor impact damage resistance.

Structural aeronautical systems experience a broad spectrum of environmental and operational loads and atmospheric hazards (hail, lightning, storms etc.). Severe and/or prolonged load exposures may trigger the damage accumulation process even in recently deployed structures. Modern airframe design is exploiting new exciting developments in materials and structures to construct ever more efficient air vehicle able to enable 'smart' maintenance including self-repair capabilities. Relevant challenges for many of the already developed self-repairing systems are to enhance the structural stability, and the resistance to the atmospheric hazards through specific functions integrated in the material. The traditional approach to the development of aeronautic materials is to address the load-carrying and other functional requirements separately, resulting in a suboptimal load-bearing material with the penalty of added weight. The research activity of this PhD thesis is aimed to develop self-healing, load-bearing materials with all functionalities integrated in a single material able to meet many important requirements of this kind of materials. The main concept underpinning this PhD project is the use of the nanotechnology strategy for the production of new, high mechanical performance multifunctional materials. Based on recent developments in the field of nanotechnologies and successful strategies identified in recently papers and patents, the main objectives of this thesis have been achieved. The performed research activities allowed the implementation of a new generation of self-healing composites, which also considers relevant aspects related to the need of developing environmentally-friendly materials for transports.

In this project, many different approaches have been considered for each functionality in order to reduce the risk of failure. Alternative concepts with respect to designs already proposed in literature have been explored. Multifunctional resins prepared using chemicals not commercially available yet have been developed and characterized.

Abstract

Chapter I
Introduction

I.1 Preface

Global competition and the necessity to maintain global leadership in the field of structural materials (air transport field, aircrafts, ships, wind turbine blades, satellite control boards, electronic devices, etc.) dictate the need for cost efficient, environmental friendly aviation products and services, while at the same time preserving top quality. Maintaining and extending industrial leadership and protecting the environment are very ambitious long-term goals also addressed by Europe's vision for aviation Flightpath 2050. As any evolutionary technologies are mature near to their maximum potential, new disruptive breakthrough technologies are needed to reach these ambitious goals. The development of technologies and methodologies which have the potential to save costs throughout the life cycle of an aircraft for example must be driven towards solutions to fulfil the following requirements:

- strict requirements to pollution control during manufacturing process and their use in service;
- low consumption of fuel and resources;
- reduction the manufacturing and operating costs (life cycle costs) etc.

The demonstrated benefits of composite materials, compared to metallic one, have led to the recent trend of increased use of the former with respect to metal alloys most of all in the field of primary aeronautical structures. At the same time, several drawbacks of these materials prohibit their use to the extent where their full potential could be exploited. In this regard, strong limitations are due to the impossibility of current aeronautical materials to satisfy special needs which meet the high standards and fulfil the requirements in the field. Environmental and operational loads and atmospheric hazards (hail, lightning, storms etc) may significantly affect the integrity of the composite structures. The images in Figure I.1 show the most common phenomena responsible for damages in the primary structures

of aeronautical vehicles (lightining strike, impact of hail on the fuselage crown during a storm, the strong impact of the stones on the keel or of the birds during landing**,** the accidental falls of heavy objects on the structures during the assembling phases and the development of flames).

Figure I.1 *Most common phenomena damaging aeronautical vehicles*

If exposed to such high environmental and operational loads, also recently deployed structures can undergo a process of accumulation and propagation of damage. An important contribution to increased exploitation of composite materials can be given by an implementation of a strategy of damage auto-repairing, monitoring and other specific functions integrated in the material structure. The main objective of this PhD research project was just that to propose strategies that can give this contribution in the field of structural materials.

I.2 Aims of the Thesis

The aim of this Ph.D. thesis is to evaluate the current shortcoming in the field of self-healing materials for their applications in aeronautics. In particular, the critical points which still prevent the application and the widespread use of these materials have been analyzed, in order to develop a new generation of multifunctional self-healing composites able to overcome the current limitations such as:

- poor impact damage resistance;
- absence of auto-repair mechanisms in the composite structures;
- reduced electrical conductivity.

A very innovative aspect of this research is that the activities related to the different functionalities are designed to merge all functionalities in a single multifunctional load-bearing material. In opposition to the classic approach, which addresses the functional requirements separately, this research activity is aimed to develop self-healing, load-bearing structures, having all the functionalities integrated in a single material able to meet many important requirements of structural materials such as aeronautical materials for primary structures (see Figure I.2).

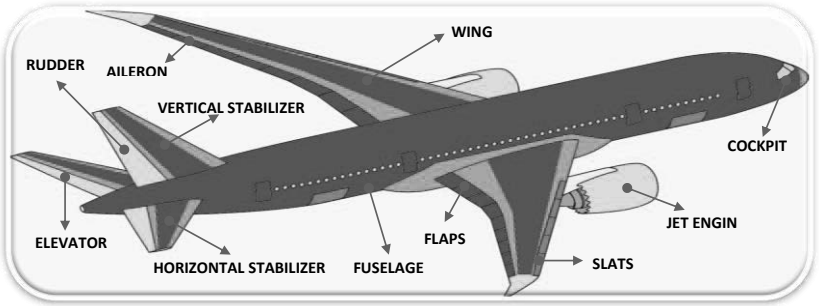

Figure I.2 *Structural parts of the aircraft*

Structural parts of the primary structure sustain aerodynamic loads. If parts of the primary structure are damaged, the stability of the vehicle is completely compromised. Contrary to the primary structure, secondary structures permit to keep control of the aircraft even after possible damages.

In particular, based on recent developments in the field of nanotechnologies, and successful strategies recently identified in literature, promising multifunctional resins able to impart regenerative ability and simultaneously to increase flame resistance and electrical conductivity, can be employed as structural materials in many fields of structural materials (Guadagno *et al*. 2011a, 2014a, 2015a, 2015b, 2017a, 2017b; Longo *et al*. 2017a; Shaygannia *et al*. 2015). During this PhD research work, the possibility of industrialization of the most promising results already reported in literature, was seriously taken into account.

The basic contents of the patents and the already performed work described in different papers (Guadagno *et al.* 2017b; Vertuccio *et al*. 2017) have represented a robust starting point for the development of this PhD project.

I.3 Research strategies

In order to achieve the objectives of this thesis project and to develop polymeric composites, able to overcome the above-mentioned current limitations of structural materials, different approaches have been considered for each functionality.

The research strategies proposed and realized for each functionality are summarized in the Table I.1.

Table I.1 *Research strategies related to the different functionality*

RESEARCH STRATEGIES	
Poor impact damage resistance	**Reduced electrical conductivity**
Current limit: absence of auto-repair mechanisms in the composite structures	
First approach Development of self-healing systems based on the microencapsulation concept	**First approach** Use of covalently functionalized electrically conductive carbon nanofillers embedded in the polymeric matrix
Second approach Development of supramolecular self-healing systems	**Second approach** Use of unfunctionalized electrically conductive carbon nanofillers embedded in a polymeric matrix suitable modified to host auto-repair mechanisms

Concerning the strategy to impart self-healing function to multifunctional resins, the first approach, based on microencapsulated systems and discussed in the Chapter II, has led to the design and development of a new ruthenium catalyst, which has allowed overcoming some drawbacks related to the possibility to extend self-healing materials to advanced applications. (Guadagno *et al.* 2017a*;* Longo *et al.* 2017a).

These drawbacks mainly regarded:

- the thermal stability of the Ring Opening Metathesis Polymerization (ROMP) catalyst inside the epoxy resin during the curing cycle;
- the impossibility to use, as hardeners, aromatic primary amines (e.g. 4,4-diaminodiphenyl sulfone, DDS) in combination with catalysts active in the ROMP; the limit related to this drawback is the poor mechanical performance of the material;
- the impossibility to use curing cycles at high temperatures, as those scheduled for aeronautic materials designed for primary structures; the limit related to this drawback is the poor mechanical performance of the material;
- the impossibility to use the catalyst dispersed in the form of molecular complex in chemically very reactive environments, such as fluid epoxy mixtures containing reactive epoxy rings; the limits related to this drawback is due to the high cost of the materials and the reduced efficiency of the self-healing function.

The new catalyst has been used in the form of molecular complex inside epoxy mixtures allowing a strong reduction of the manufacturing costs and a relevant enhancement in the mechanical properties. Its chemical stability allows to use aromatic primary amines, used as hardeners in aeronautical resins, without undergoing deactivation.

Concerning the second approach for self-healing functionality, discussed in the Chapters III and IV in combination with the possibility to impart electrical conductivity to the materials, relevant achievements in the field of supramolecular chemistry and in the field of hybrid materials and functionalized nanofillers are now available to be used for developing emerging composites with unique properties and functionalities.

Hybrid materials or nanomaterials can be functionalized with hydrogen bonding moieties to activate self-healing mechanisms, which are very advantageous not only to restore the structural integrity (self-healing function) in multiple cycles, even at the same position of the sample (Herbst *et al.* 2013), but also to restore other functionalities. Thus, a large variety of SH-systems have been prepared, with auto-repairing at different time and length-scales (Herbst *et al*. 2012), and crosslinked (Döhler *et al.* 2015) or even blend-systems, which allow the mixed-composition of different polymeric systems (Chen *et al.* 2015a, 2015b).

In this research work, attractive reversible hydrogen bonding forces between molecules, acting as self-healing fillers, and chemical groups of epoxy precursors have been explored with the aim to use these forces to impart auto-repair ability to the epoxy resins.

In particular, hydrogen bonding moieties able to act as donor and acceptor of hydrogen bonding have been covalently bonded on multi-wall carbon nanotubes. The carbon nanotubes have been embedded in the epoxy formulation to explore the possibility to simultaneously impart electrical conductivity and auto-repair functions**.**

In the following sections, it will be discussed the state of the art related to the progress achieved in the field of self-healing materials and of all the problems that still need to be solved for a real application of these materials in load-bearing structures.

I.4 State of art

I.4.1 Classification of self-healing mechanisms

The concept of self-healing materials finds a great source of inspiration by the nature, such as biological systems in which the damage triggers an autonomic healing response. The big challenge in the design of synthetic materials lies in the fundamental difference between biological systems and synthetic materials, which have no the metabolic capability of the formers. The study of how to impart auto-repair function to polymeric materials is an

emerging and fascinating area of research that could significantly extend the working life and safety of the polymeric components for a broad range of applications. Thermoplastic and thermosetting polymers represent the intelligent invention and technological driving force of the twentieth century. The possibility to add self-repair function to these materials is under investigation from researchers around the globe (White *et al.* 2001; Kessler *et al*. 2003; Rule *et al*. 2005a; Toohey *et al*. 2007, 2009a, 2009b; Wu *et al.* 2008; Cho et al. 2009; Guadagno *et al.* 2010a, 2011a, 2014a, 2014b, 2016a; Liu *et al*. 2011; Binder 2013; Jin *et al.* 2013; Raimondo and Guadagno 2013; Raimondo *et al.* 2015, 2016; Amendola *et al*. 2015; Chowdhury *et al* 2015; Chung *et al.* 2015; Everitt *et al*. 2015).

Several self-healing concepts for polymeric materials have been published over the last 20 years. Depending on the chemical nature of the polymeric materials, different approaches have been proposed to prepare and characterize self-healing systems.

Self-healing mechanisms can be generally categorized into two main groups: *extrinsic* and *intrinsic self-healing mechanisms*. These two mechanisms are differentiated by the self-healing chemistries that the polymer composite undergo in response to the damage.

For *extrinsic self-healing mechanisms*, sequestered healing agents from the embedded containers in the matrix recover the damage. Extrinsic self-healing is also considered as autonomous self-healing, where the damage within a material structure is recovered by the prefilled healing agent as an isolated phase within different types of container and then embedded in the matrix. In conjunction with the type of containers, the repair mechanisms can be classified into (i) *microcapsule self-healing mechanism*, and (ii) *vascular network self-healing mechanism*. The self-healing concept of these two mechanisms is the same, when a crack is formed and eventually breaks the containers, the healing agent within the containers is released and heals the crack planes.

In contrast, an *intrinsic self-healing mechanism* is driven by the chemical bonding of the matrix itself, which has the ability to restructure after a drastic damage in the presence of external stimuli such as UV light, heat, or chemicals. Intrinsic self-healing function in thermoplastic materials is designed with inherent repeatable reform abilities after damages. In this last case, the presence of healing agent and catalyst is not required. The intrinsic healing of thermoplastic structure is achieved at the molecular level due to the low glass transition temperatures (Tg) of thermoplastic polymers, where the heating and cooling process will lead to molecular inter-diffusion, randomisation, recombination of chain ends, etc. Unlike extrinsic self-healing, this simpler concept of self-healing mechanism can be more competitive in terms of product manufacturing and applications. Although no monomer or catalyst is required, different external stimuli to trigger the

self-healing are essential, depending on the types of self-healing mechanism (Hia *et al*. 2016).

I.4.2 Self-healing polymer composites

Polymers and polymer composites have been widely used in engineering fields because of their advantages including lightweight, good processability, chemical stability in any atmospheric conditions, etc. However, long-term durability and reliability of polymeric materials are still problematic when they serve for developing structural materials. Exposure to harsh environment would easily lead to degradations of polymeric components. Comparatively, micro cracking is one of the fatal deteriorations generated in service, which would bring about catastrophic failure of the materials and hence significantly shorten lifetimes of the structures. Since the damages deep inside materials are difficult to be perceived and to repair in particular, it would be better to integrate in them the self-healing ability (Yuan *et al*. 2008a).

Currently, most industrial polymeric materials can be used to develop self-healing materials.

A great number of self-healing materials has been demonstrated based on extrinsic or intrinsic materials. In the case of extrinsic autonomy thermosetting materials, the advancement in the knowledge and the developments of new mechanisms were much slower with respect to the self-healing systems based on soft materials and or on the activation of the self-healing function by means of external stimuli.

However, the hardest challenge in the field of composite material is to develop “autonomic self-healing materials” for structural application. A truly self-healing material is capable of repairing itself in its intrinsic environment, and it does this without any external intervention as soon as the damage occurs.

In the case of soft materials characterized by relatively low values in the glass transition temperature, the movement of the macromolecular chains (or segment of chains) makes possible the application of different self-healing mechanisms. In the structural material, the stiffness or limited movement of the chains, o part of chains among the crosslinking points in the network (for thermosetting materials) severely limits the choice of the self-healing mechanisms and the chances of successful results. In fact, the development of smart composites capable of self-repairing in load-bearing structures is still at the planning stage owing to complex issues to overcome.

It is worth noting that in this PhD research activity the attention has been focused on autonomy self-healing materials, where the self-healing function is inherent in the material nature and composition. Therefore, in this section on state of the art, all the self-healing intrinsic materials based on autorepair mechanisms activated by external stimuli (for ex. Diels-Alder reactions,

photochemical self-healing system, etc.) which can be of limited interest for the aim of this PhD thesis, are excluded. In particular, this thesis is focused on the development of multifunctional self-healing systems, where the self-healing function is based on ROMP reactions (microencapsulated systems) or on other strategies from the supramolecular chemistry.

I.4.3 Microencapsulated self-healing system

One of the first promising extrinsic self-healing system for structural materials (based on epoxy resins-Epon 828) was the microencapsulated system, proposed by White et al. (White *et al.* 2001) (see Fig. I.3), which is suitable for thermosetting materials.

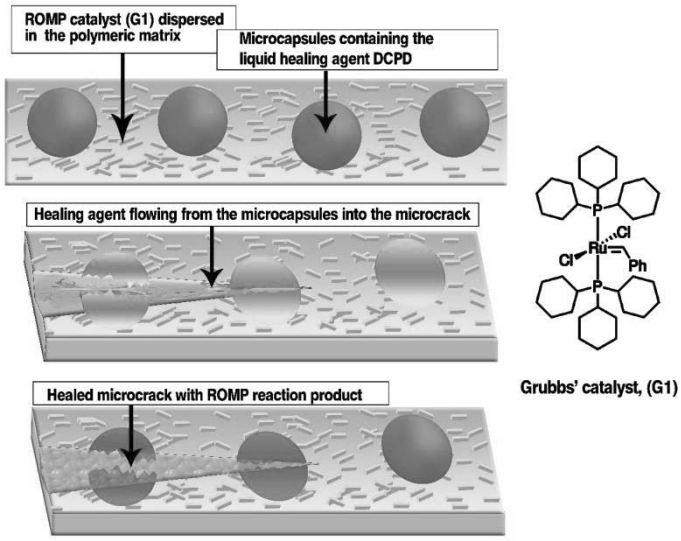

Figure I.3 *Scheme of the first self-healing system relied on capsule-based concept*

This system consists of incorporating a micro-encapsulated healing agent and a catalytic chemical trigger within an epoxy matrix. An approaching crack ruptures embedded microcapsules releasing a polymerizer agent into the crack plane through capillary action. Polymerization of the healing agent via Ring Opening Metathesis Polymerization (ROMP) is triggered by contact with the embedded catalyst particles, bonding the crack faces.

After the milestone work reported by White and co-workers, self-healing chemistry for thermosetting polymers rapidly expanded in the past decade. The employment of the healing agent has been proposed again in the subsequent literature, even if it has been stored in other type of vessels

(hollow fibres, storage vessels or more complex microvascular network etc.) embedded into the materials in advance (Kessler and White 2001; Kessler *et al.* 2003; Brown *et al.* 2004, 2005a, 2005b; Rule *et al*. 2005a, 2005b; Jones *et al.* 2006, 2007; Wilson *et al*. 2008a). Thermosetting auto-repair polymers, which have been proposed so far, include different catalysts, for example, Grubbs' first-generation catalyst (G1) (Motuku *et al*. 1999; Brown *et al.* 2003; Dry 2007; Toohey *et al.* 2007; Van der Zwaag 2007), second-generation Grubbs' catalyst (G2), Hoveyda–Grubbs' first- or second-generation catalyst (HG1 or HG2) etc. (see Fig. I.4 for chemical formulas of the ruthenium catalysts) (Guadagno *et. al*. 2011a).

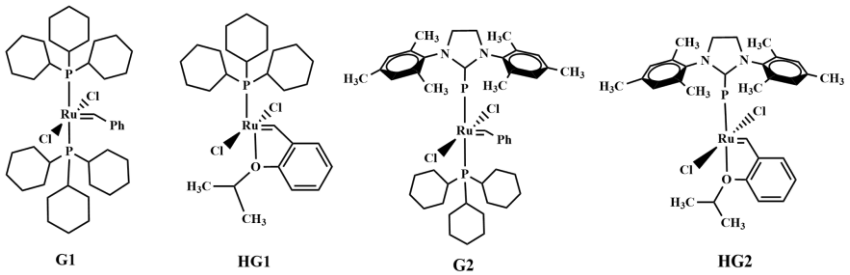

Figure I.4 *Chemical formulas of the Ruthenium based catalysts*

Figure I.5 shows design of the self-healing system relied on capsule-based concepts containing HG1 catalyst.

Wilson and coworkers evaluated the activity of G1, G2 and HG2 catalysts with various monomeric healing agents (Wilson *et. al.* 2008b).

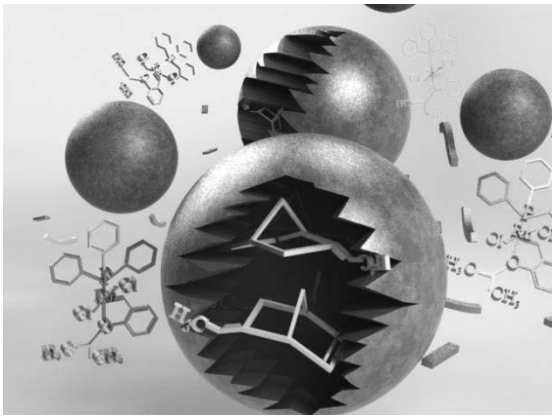

Figure I.5 *Scheme of the first self-healing system containing HG1 catalyst particles*

Guadagno et al. developed several microencapsulated self-healing systems using the following self-healing components embedded in epoxy mixtures:

- Microcapsules filled with 5-ethylidene-2-norbornene (ENB), and Hoveyda–Grubbs' first-generation catalyst particles (HG1) (Guadagno *et al.* 2014a), (see Fig. I.6),
- ENB(95%)/dicyclopentadiene (DCPD)(5%)-filled microcapsules, with the outer shell composed of poly(urea-formaldehyde) and the inner shell of ethylene maleic anhydride (EMA) copolymer (Brown *et al*. 2003; Raimondo and Guadagno 2013) (see Fig. I.7), and Hoveyda–Grubbs' second-generation catalyst (HG2) (Guadagno *et al.* 2011a) or HG1 (Guadagno *et al*. 2014a, 2014b, 2016a; Raimondo and Guadagno 2013; Raimondo *et al*. 2015, 2016).

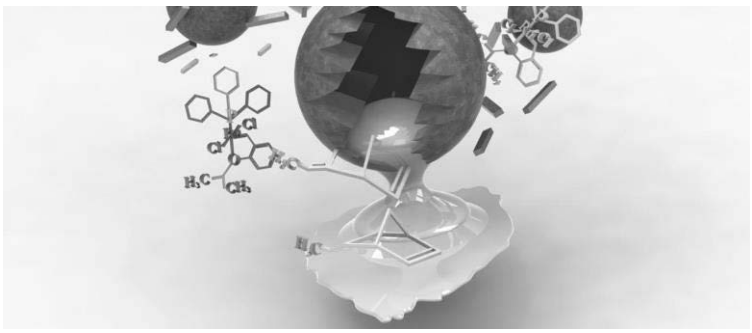

Figure I.6 *Scheme of self-healing system based on ENB-filled microcapsules and HG1 catalyst particles dispersed in the matrix*

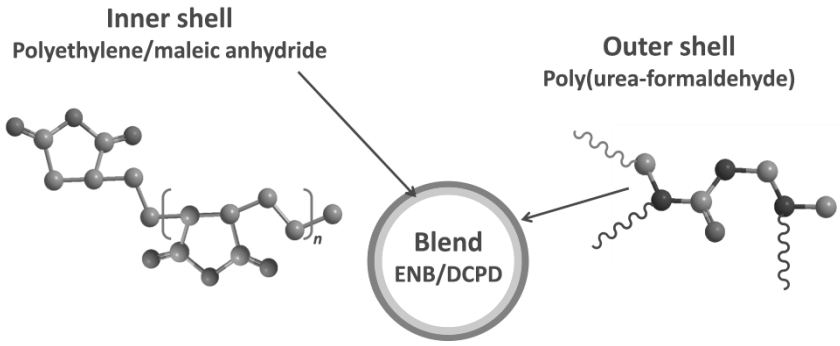

Figure I.7 *Scheme of the microcapsules containing ENB/DCPD blend as healing agent*

The above-described systems represent an efficient solution for epoxy structural composites where no soft matter or thermoplastic matrix is involved. However, in order to fully apply these systems, some drawbacks

were re-evaluated for advanced applications where high mechanical performance are required (aerospace, aeronautics etc.). One of these concerns the thermal stability of the different ruthenium catalysts inside the epoxy resin during the curing cycle. The usually significantly high temperatures of the curing cycles scheduled for epoxy formulations designed for high mechanical performance, the thermolytic decomposition etc. can limit the usefulness of the ruthenium catalysts in self-healing composites based on epoxy resins. This is a crucial aspect for self-healing systems for structural applications. Generally, for the mechanical targets fixed for the materials used for structural aims, a glass transition temperature after wet aging of 170°C/180°C minimum is required, thus putting a curing temperature equal to or less than 100°C as too low to this purpose. To achieve this goal, it is necessary to choose a proper chemical formulation and to make a post cure with a temperature that could be as high as 180°C. Concerning the stability of the catalysts at different temperatures, as mentioned before, Wilson and co-workers have evaluated the reactivates of G1, G2 and HG2 catalysts with various monomeric healing agents also with a view toward improving the self-healing performances in a variety of epoxy matrices (Wilson *et. al.* 2008b). In their work, they have evaluated the thermal stability of these three catalysts embedded into the epoxy matrices with the aim of studying their stability to processing conditions during the manufacturing conditions. To evaluate the thermal stability of the catalysts under simulated high-temperature processing conditions, the authors prepared fracture specimens with a Tapered Double-Cantilever Beam (TDCB) geometry. Different types of fracture tests were performed, among which self-activated tests. For these last experiments, the catalyst was embedded in the epoxy matrix and the healing agent alone was injected into the crack plane. The samples were left to heal for 24 h. Self-activated M1 samples (epoxy matrix EPON 828 cured with the hardener diethylenetriamine, DETA) containing 1.5 wt % of an as-received catalyst were prepared and subjected to customary curing cycles followed by an additional post-curing at 125°C for 4 h before fracture testing. Samples were then fractured and DCPD (10 μL) was injected into the crack plane. The samples were then left to heal at either (room temperature) RT or 125°C for 24 h. Samples healed at RT showed a retention of healing performance of 77%, 84%, and 18% for G1, G2, and HG2 catalysts, respectively. Samples healed at 125°C showed significant improvements over those healed at RT, in fact for G1, G2 and HG2 catalysts, the retention of healing performance was 109%, 216% and 57% respectively. The authors of Ref. (Guadagno *et al.* 2011a) have dealt with the same issue from different angles trying to understand the reason for the low retention of healing performance obtained using HG2 catalyst. In a recent paper, they have shown critical issues in the use of epoxy precursors in conjunction with Hoveyda–Grubbs' II metathesis catalyst (Guadagno *et al.* 2011a). In recent papers, they have shown the

results related to the healing efficiency and dynamic mechanical properties of self-healing epoxy formulations cured up to 170, 180°C using as catalyst Hoveyda–Grubbs' I (HG1) metathesis catalyst (Guadagno *et al.* 2014a).

It was found that the healing chemistry based on the ROMP of healing agents can be very different depending on the chemical nature of the catalyst and the healing agent. The performed experiments highlighted that the chemical nature of the epoxy matrix plays an important role in determining the mechanical properties of the resulting material.

The effect of matrix nature and curing cycle on the healing efficiency and dynamic mechanical properties of self-healing epoxy resins were also investigated for epoxy formulations solidified by choosing processing conditions that contemplate permanence at high temperatures up to 170°C, 180°C (Guadagno *et al.* 2014a).

As self-healing components, ENB and HG1 catalyst particles were chosen. Microcapsules resembling snarls of tubular nanovessels (see Fig. I.8) and catalyst particles were dispersed inside an epoxy mixture tailored to meet specific needs of structural materials (as higher storage modulus, higher glass transition temperature with respect to already published epoxy formulations).

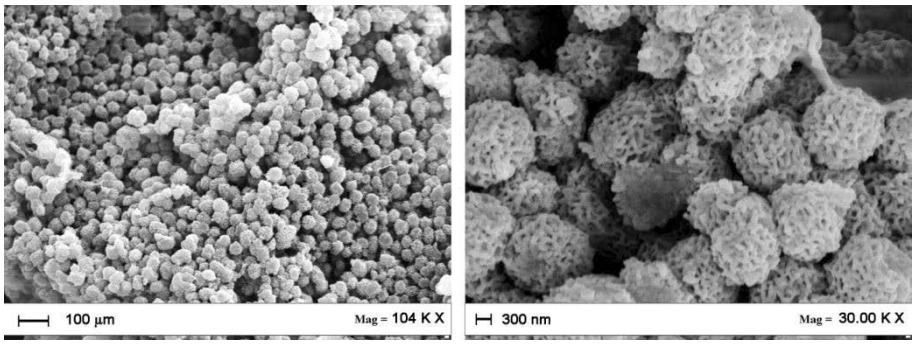

Figure I.8 *SEM images at different magnifications of the synthesized microcapsules in the form of spherical snarls*

Self-healing efficiency η assessed by fracture test, as described in section *II.2.2.3 Healing activity and self-healing efficiency evaluation*, was calculated for different self-healing formulations. In all the analysed systems, the healing efficiency measured by means of in situ tests using tapered double–cantilever beam (TDCB) specimens was found very high (also higher than 100%). In particular, it was found to be affected by microcapsule and catalyst concentrations and their morphological parameters. Three epoxy matrices were investigated:

a) EHA epoxy matrix was prepared by mixing the epoxy precursor EPON 828 (E) with an epoxy flexiblizer (H) - trade name HELOXY 71- which was used in a percentage of 37 % by weight to improve

the toughness of the material and consequently growth stability; this formulation for the epoxy matrix was used for the self-healing system already described in literature (Guadagno *et al.* 2010a, 2013a, 2014b; Guadagno and Raimondo 2012; Raimondo and Guadagno 2012, 2013).

b) EBA1 matrix was prepared by mixing the epoxy precursor EPON 828 with an epoxy reactive monomer 1,4 Butandioldiglycidylether (B) at a concentration of 90%: 10% (by wt) epoxide to flexibilizer.

c) EBA2 matrix was prepared by mixing the epoxy precursor E with an epoxy reactive monomer 1,4 Butandioldiglycidylether (B) at a concentration of 80%: 20% (by wt) epoxide to flexibilizer.

For these formulations, the curing agent (A) employed was an anionic initiator, 2,4,6-tris[(dimethylaminomethyl) phenol] (Trade name Ancamine K54) already used in literature (White *et al.* 2001). The catalyst used in all the epoxy matrices was Hoveyda-Grubbs'1st (HG1). It was purchased from Aldrich. The catalyst particles were reduced in the form of thin powders before dispersion into the epoxy matrix. ENB-filled microcapsules with the outer shell composed of poly(urea-formaldehyde) and the inner shell of ethylene maleic anhydride copolymer (EMA), were prepared by *in situ* polymerization in an oil-in-water emulsion in accordance with procedure previously described in literature (Brown *et. al.* 2003).

The healing efficiency was found to be 97.8% for a percentage of 10% of microcapsules, 111% for a percentage of 17% of microcapsules, and 123% for a percentage of 20% of microcapsules. Considering a constant amount of catalyst (fixed at 5 wt%), an increase in the microcapsule concentration was found to improve the healing efficiency of the formulated materials. A more complete picture is shown in Figure I.9.

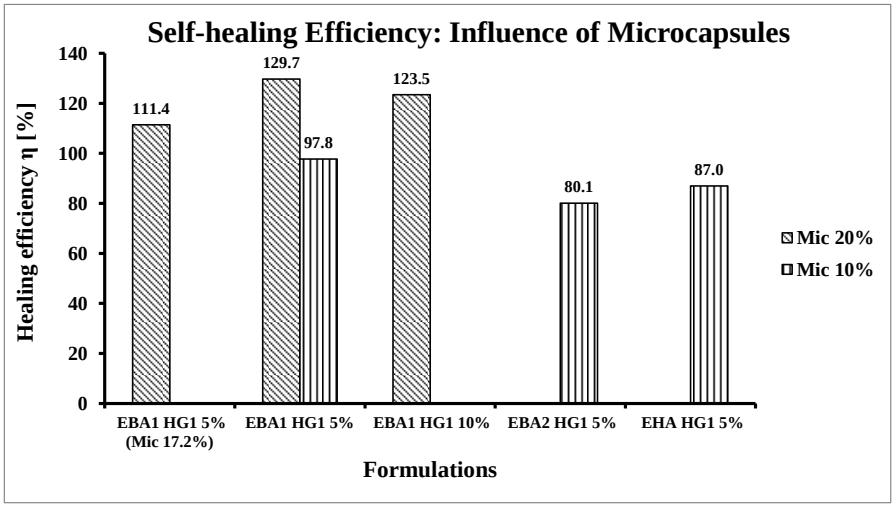

Figure I.9 *Self-healing efficiency of samples with different amounts of microcapsules (Curing: T_{max}=170°C)*

Increasing the catalyst concentration was found to improve healing efficiencies when the capsule concentration was held fixed (Brown *et al*. 2005b).

A very similar result was found by Brown et al. (Brown *et al.* 2002) who performed experiments of healing efficiency on pure epoxy (Epon 828) cured with DETA for 24 h at room temperature, followed by 24 h at 30°C. They used DCPD as healing agent and Grubbs' first-generation catalyst.

Figure I.10 shows the influence of the curing cycle on the healing efficiency values for some of the analyzed formulations and for the two different curing cycles. Samples EBA1 cured up 170°C showed the highest values of efficiency. For samples EBA1 (10 wt% of reactive diluent) cured up 170 °C with a microcapsule concentration higher than 10 wt%, the self-repair effect allows the healed material to have a critical load ($P_{Chealed}$) higher than the critical load ($P_{Cvirgin}$) of the virgin material and efficiency higher than 100%.

The lower efficiency of the samples cured up to 180°C, with respect to samples cured up to 170°C, is most probably due to an initial thermolytic decomposition of the HG1 catalyst.

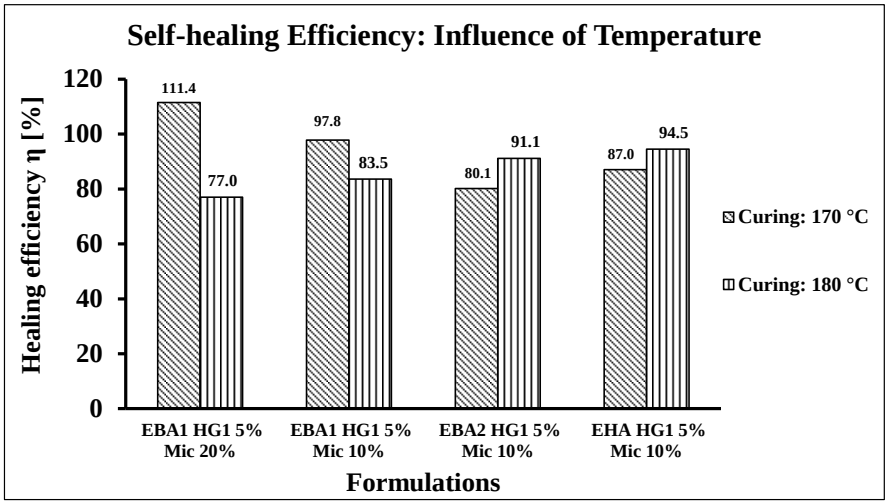

Figure I.10 *Self-healing efficiency with different formulations and curing cycles*

The healing efficiency was also found to be affected by the nature of the epoxy matrix.

Figure I.11 shows the comparison of healing efficiency for self-healing systems with different epoxy matrices (EHA, EBA1, EBA2), at the different curing temperature. The crack healing efficiency, η, was found to be 97.75% for a percentage of 10% of microcapsules for EBA1 blend, while slightly lower efficiency was recorded for the same formulation cured up 180°C. At curing temperature up to 180°C, high values of efficiency (94.50%) were recorded for EHA samples.

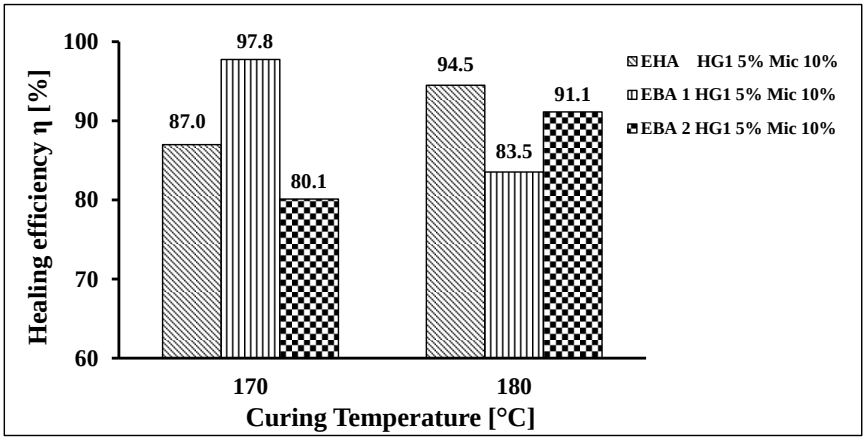

Figure I.11 *Comparison of healing efficiency for self-healing systems with different epoxy matrices (EHA, EBA1, EBA2), at the different curing temperature*

The authors developed the self-healing technology for use in structural materials that are not easily accessible for maintenance. These self-healing materials were designed to repair damage that begins at the micron scale, effectively stopping the propagation of the damage and extending the lifetime of the material. The microcapsules were designed to be robust enough to survive the manufacturing process and the development of the material in its intended application. A range of self-healing chemistries can be microencapsulated to maximize compatibility with matrix materials. On top of this, the size of the microcapsules and the thickness of their shell walls can be customized for various applications and chemical environments. Additional functionalities can be added to the self-healing material to provide different solutions.

As found with the mechanical tests, a good adhesion between the capsules and the polymer matrix was achieved for all the formulated systems. It not only allows an effective crosslink formation along the sample, but also prevents the dewetting of the microcapsules ensuring an efficient utilization during the crack propagation. The very high level of crack healing efficiency attained demonstrates the ability of these systems to regenerate the pristine properties.

Even if very good healing efficiencies were found, the developed systems required high costs for the ROMP catalyst and most of all they have shown do not meet some of the mechanical requirements necessary for specific scopes (structural parts of aircrafts, ships, wind turbine blades, satellite control boards etc.). In particular, the maximum value reached in the Tg was found to be between 100°C and 125°C; the value of the storage modulus was

found to range between 2500 Mpa and 2000 Mpa (in the temperature range from -50°C to + 80°C).

These relatively poor mechanical properties (for the above listed specific applications) were found due to the impossibility to use aromatic primary amines in the developed self-healing epoxy formulations because they deactivate ROMP catalysts (Longo *et al.* 2017a). Several issues, related to transferring these self-healing systems from the laboratory-scale to possible real applications in the aeronautic field, such as the possibility to choose systems with increased glass transition temperature, high storage modulus and high values in the healing functionality under real working conditions, have been analyzed and alternative solutions for the formulations of multifunctional self-healing resins were proposed.

I.4.3.1 Carbon filler-based microencapsulated self-healing systems

In order to increase the mechanical performance and to integrate other relevant functions in the material (flame resistance, electrical conductivity to enhance the lightning strike resistance), carbon nanotubes and graphene-based materials were embedded in the epoxy matrix trying to preserve the catalytic sites of the self-healing function (Mariconda *et al.* 2015; Guadagno *et al*. 2017c).

In particular, electrically conductive nanoparticles, functionalized to act as support for the catalyst and simultaneously impart self-healing and electrical conductivity properties to the polymeric matrix, have been successfully prepared. Highly dispersed copper nanoparticles, immobilized onto carbon nanomaterials were prepared and used as a recyclable and reusable catalyst to achieve Cu (I)-catalyzed [3 + 2] cycloaddition “click” chemistry (Shaygannia *et al.* 2015). In particular, carbon nanoparticles supported catalysts exhibit excellent properties due to their high surface area, thermal stability, and porous surfaces. These characteristics make them particularly suitable to act as scaffold to prevent the agglomeration of the immobilized metallic particles (Scheuermann *et al.* 2009; Gu *et al.* 2014; Sarkar *et al*. 2014; Shaygannia *et al.* 2015).

Among the carbon-based nanoparticles, graphene immobilized catalyst has been recently proposed for application in several technological fields (Yang *et al.* 2003; Eigler *et al.* 2013; Eigler and Hirsch 2014; Nia *et al.* 2015; Shaygannia *et al.* 2015). The functionalization also favors the nanomaterial dispersibility, which is improved via covalent and non-covalent functionalization (Sahoo *et al.* 2010; Georgakilas *et al.* 2012; Osim *et al.* 2013).

Concerning the covalent functionalization, the possibility to covalently bond ROMP catalysts to multiwall carbon nanotubes (MWCNTs) (see Fig. I.12) or graphene-based particles has been investigated.

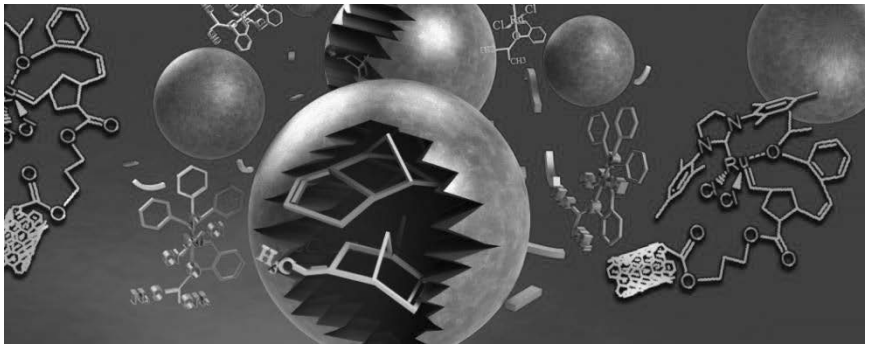

Figure I.12 *Scheme of self-healing system based on ROMP reactions activated by Ruthenium catalysts covalently bonded to MWCNTs*

Concerning this aspect, it was already observed that graphene-based nanomaterials can be designed as a self-assembly structure in the epoxy matrices using edge-carboxylated layers approach (Guadagno *et al.* 2015c). The functionalization on graphene sheets facilitates the interfacial interaction between polymer and carbon layer. It also enhances the electrical percolation paths and mechanical performance of structural epoxy matrices. It has been deduced that the surface chemistry of graphene surface can be tuned at nanoscale level, to pave the way towards an effective strategy to also transfer graphene properties to polymeric matrices.

In particular, in the above described context, Graphene Oxide (GO) was used to support ruthenium catalysts with the aim to activate self-healing reactions in multifunctional materials able to integrate simultaneously the healing reactions with the very interesting properties of graphene-based materials (Mariconda *et al*. 2015) (see Fig. I.13).

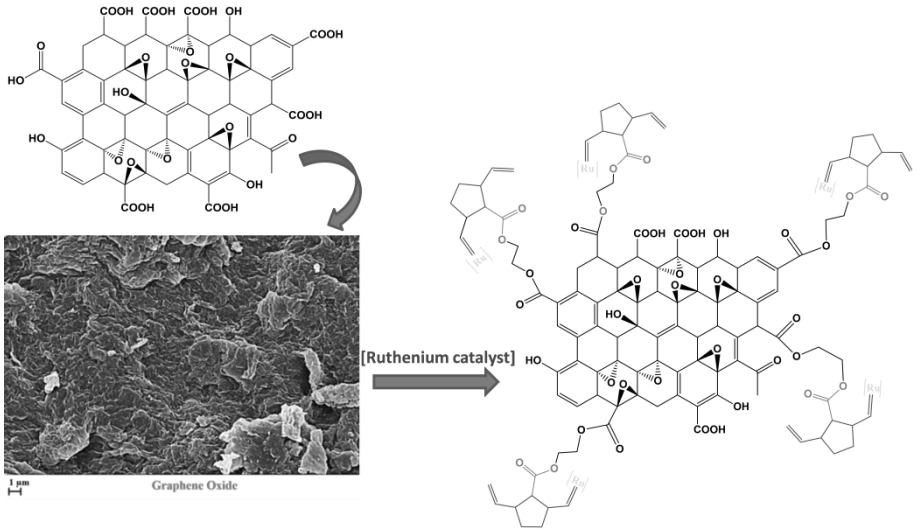

Figure I.13 *Functionalization of graphene oxide with Ruthenium catalyst*

Grubbs catalysts 1st (G1) and 2nd generation modified (G2*o*-tol), Hoveyda-Grubbs catalysts 1st (HG1) and 2nd generation (HG2) were covalently bonded to GO preserving the same catalytic activity of the catalysts not bonded to the graphene sheets. GO-G2o-tol and GO-G1 were found to deactivate during the process of preparation of the self-healing epoxy mixtures at 90°C. Evidence of the self-healing activity of the various catalytic complexes was studied for both uncured and cured samples. Results showed that GO-HG1 and GO-HG2 were not deactivated and hence they were found to be able to trigger self-healing reactions based on the ROMP of ENB. This behavior was found due to the formation of 16 electron Ru-complexes that are more stable than the 14 electron complexes of GO-G1 and GO-G2 catalysts (Mariconda *et al.* 2015). A strong increase in the storage modulus was found (as expected), but no in the glass transition temperature. Also, in this case, it was found that no aromatic amines could be used to solidify the epoxy matrix in such a way to obtain very high mechanical performance. A strategy to overcome this drawback was experimented. The catalytic sites (containing Ru on the graphene sheets) were protected polymerizing few units of polymeric monomers around the ruthenium atoms forming a globular shell around the catalyst sites (Guadagno *et al*. 2017c) (see Fig. I.14).

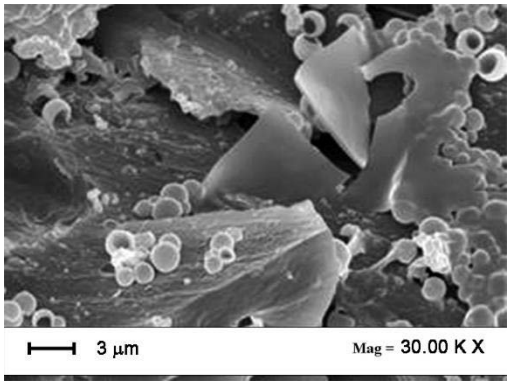

Figure I.14 *Globular shell around the catalyst sites attached on graphene sheets*

This system allowed high curing temperatures, but the open part of the shell is low and this strongly influences the kinetics of the ROMP reactions inside cracks of the selected epoxy matrix.

Unfortunately, as highlighted above, many structural applications require that the function of self-healing must be active also under extreme environmental conditions and the self-healing mechanisms must be quickly activated to avoid the crack propagation (when the entity of the propagation is relevant, there is no healing of the material). Furthermore, the materials for many very interesting structural applications must be characterized by very high mechanical performance, electrical conductivity, low moisture content, long durability etc.

Also, other problems concern the cost of the catalyst, its poisoning with aromatic primary amines, and the thermal stability which is compromised at the cure temperatures necessary to impart good mechanical performance to the epoxy matrix (cured with aromatic primary amines). Performed experiments evidenced that, in the case of the catalyst particles solubilized at molecular level (to reduce the cost of the self-healing materials) the catalyst particles, which are locally in contact with the oxirane rings (during the curing reactions) deactivate, hence reducing the actual amount of active catalyst. Additional experiments were performed on this issue to better understanding the reason of the deactivation for the most promising ROMP catalysts (catalysts active in the ring opening metathesis polymerization). An equimolecular reaction between epoxide ring and alkylidene of ruthenium compound was found to be responsible for the deactivation (Raimondo *et al.* 2015).

I.4.3.2 Microencapsulated self-healing Carbon Fibers Reinforced Composites (CFRC)

In order to activate self-healing reactions in epoxy matrices cured at high temperature (between 130°C and 170°C), Leonardo S.p.A. adopted a new strategy to manufacture Carbon Fibers Reinforced Composites (CFRCs) for the realization of structural aeronautic components in order to address their vulnerability to impact damage in the real service conditions (Raimondo *et al.* 2016). In this strategy, the employed solid catalyst particles retain an intact heart of catalyst, which is not deactivated in contact with the oxirane rings of the epoxy matrix. The developed self-healing panels were based on ring-opening metathesis polymerizations reaction of microencapsulated 5-ethylidene-2-norbornene/dicyclopentadiene cyclic olefins using Hoveyda-Grubbs' first-generation catalyst as catalyst.

The self-healing resin was infused into a carbon fiber dry preform using an unconventional bulk film infusion technique, which allowed minimizing the filtration effects via a better compaction, and reduced resin flow paths. Infrared spectroscopy proved to be an useful technique to identify metathesis products and therefore catalyst activity in the self-healing panel after damage. The damage resistance of the manufactured CFRPs was evaluated through hail and drop tests (see Fig. I.15). Although aerospace and aviation technology allow aircraft to avoid a great many storms and other dangers, wildlife impacts and hail still cause millions of dollars in plane crashes and aircraft property damage—not to mention the danger to human life. Efficient self-healing mechanisms can help to avoid this type of risk. The developed panels have been tested for different values of impact energy (Tool Drop Test), after which it has been possible to compare the characteristics of damage resistance and to measure the maximum residual deformation. The estimate of the latter (also said indentation) has been obtained with a digital comparator. For the impact of 20 J (using a tip diameter of 1 inch) it has been possible to measure an indentation of 0.14 mm without drilling. Figure I.15 shows the Tool Drop Test set up and the depth measuring after impact.

Figure I.15 *Tool Drop Test set up (on the left) and depth measuring after impact (on the right)*

Hail Impact Tests have been performed considering the requirements of hail impact for the design of a fuselage in composite material (Ground hail). They are the following: a) Hail diameter 2.4 inches (Cum Prob .98) and b) Energy 50 J. The panels have been subjected to impact tests "Gas Gun" at different levels of energy and then inspected by means of Non-Destructive Inspection (NDI).

To simulate the damage caused by the impact of hail on aeronautical structures, a plant for the launch of pneumatic darts has been used. Table I.2 shows the experimental values concerning the performed experiments. Figure I.16 shows the photo of one of the tested panels and Figure I.17 shows the Hail Impact Test set up and Test fixture.

Table I.2 *Experimental values concerning the performed experiments*

PANEL	IMPACT	PRESSURE VALVE	HAIL WEIGH	SPEED	ENERGY
[N°]	[LOCATION]	[bar]	[g]	[m/s]	[j]
1	A	1.00	163	41.6	141
2	A	0.78	108	36	70
2	B	0.90	163	38	118

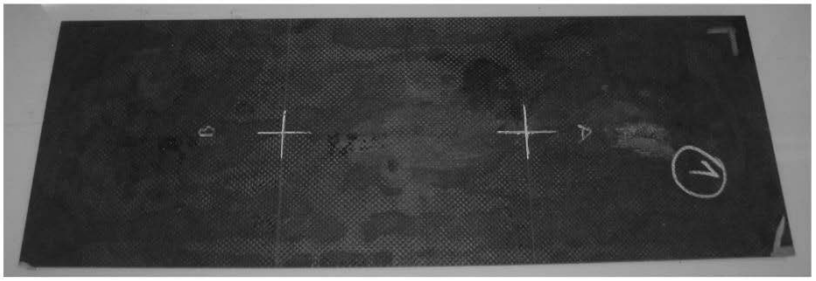

Figure I.16 *Photo of the one of the tested panels*

Figure I.17 *Hail Impact Test set up (on the left) and Test fixture (on the right)*

The result shows that, with the energies reported in Table I.2, the panel was not damaged because it returns in a perfectly elastic way in its un-deformed condition after the impact. It is worth noting that the mechanisms proposed for the auto-repair action are very fast. From the first NDI no cracks are observed in the panels also for maximum energy value tested.

The self-healing manufactured panels showed, after damage, catalytic activity with the metathesis product formation poly(ENB/DCPD), (see Fig. I.18), as also evidenced by an infrared peak at 966 cm^{-1}.

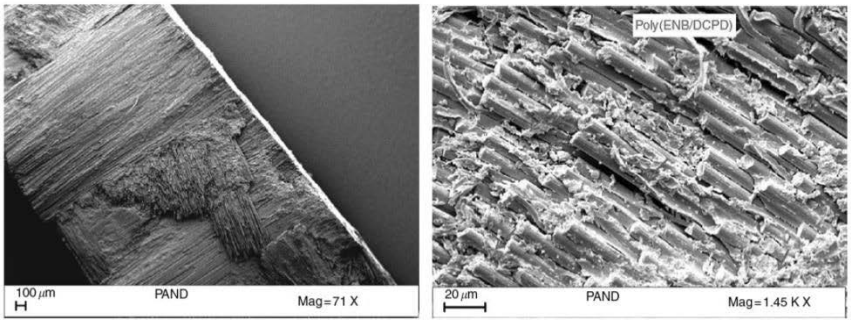

Figure I.18 *FESEM of fracture surface of the delaminated Panels*

The damage response of CFRPs, detected in accord to the requirements of hail impact for the design of a fuselage in composite material, was found very good, also at low working temperatures (values as low as −50°C). These results encouraged further research to reduce the cost of the CFRCs and further enhance the stability of the catalyst during the curing cycles of the panels.

A part the excess of catalysts to be used, another problem addressed by Leonardo Finmeccanica was the development of a new catalyst able to resist in presence of the common industrial hardeners (primary aromatic amines such as 4,4-diaminodiphenyl sulfone, DDS) at high values of temperature (during the curing cycle) (Guadagno *et al.* 2017a).

A reduction of material costs and the possibility to apply the ROMP initiators in epoxy resins aimed at manufacturing load-bearing structures was obtained using a new catalyst, synthetized for this purpose during this PhD research activity (see Chapter II) (Guadagno *et al.* 2017a; Longo *et al.* 2017a).

It is worth noting that, in the field of structural composites, solutions able to overcome shortcomings related to the microencapsulated systems will also allow to fulfill other requirements of structural materials without additional costs. For instance, the inclusion of microcapsules in CFRCs (self-healing aeronautic laminates) aimed at imparting self-healing ability, is of relevant benefit also for the very appreciable damping performance of these kind of self-healing composites compared to standard CFRC composites (Viscardi *et al.* 2017).

This peculiar property of the microencapsulated systems further allows to reduce the cost related to the noise/vibration control of aircraft structures. The numerical analysis performed by means of ACTRAN® solver confirmed an enhanced performance of the innovative material design, in terms of structural vibration as well as of sound pressure level inside the cabin, motivating the development of advanced technologies up to industrial scale in future industrial activities.

I.4.4 Supramolecular self-healing systems

Recently, alternative strategies to the microencapsulated systems have been proposed. In this new approach, chain dynamics and principles of polymeric physics are an important aspect for the design of self-healing structural polymer. In order to design materials with dynamic properties, a reversible bonding system is required to enable a self-healing material, including aspects of supramolecular polymer chemistry. Thus, non-covalent bonds such as hydrogen bonds and π-π-stacking are crucial elements on which the possibility of multiple healing cycles can be considered (in contrast to covalently linked networks) (Herbst *et al.* 2013; Guadagno *et al.* 2017b).

The field of supramolecular chemistry utilizes multiple, reversible, and in certain cases, cooperative intermolecular interactions to create new materials with unique properties and functionalities (Faghihnejad *et al*. 2014). The non-covalent intermolecular interactions typically utilized in the design of supramolecular materials and polymers include hydrophobic (Annable *et al*. 1996; Tam *et al.* 1998), hydrogen bonding (Sijbesma et al. 1997; Sivakova *et al.* 2005; Cordier *et al.* 2008), metal-ligand (Beck and Rowan 2003; Weng *et al.* 2006) and ionic interactions (Eisenberg *et al.* 1990). Over the last two decades many synthesis strategies have been developed to design new supramolecular polymers with unique characteristics such as enhanced bulk properties (i.e., plateau modulus, tensile modulus), self-healing capability, stimulus-responsiveness and the ability to assemble into well-defined nanostructures. In this field, self-healing polymer materials or composites have attracted considerable attention over the past decade due to their controllable and reversible molecular interactions, interesting mechanical properties and potential applications. Many conventional healing approaches used in thermoplastic polymers and thermoset composites such as microencapsulation and thermally reversible crosslinks (covalent bonds) require treatments at high temperature (i.e., high energy input) which are not required using this approach.

Recently, the authors of Ref. (Gauadagno *et al.* 2017b) applied a such strategy to develop self-healing aeronautical resins by introducing nanometric flexible cages of hybrid materials into the host structure matrix. These nanometric flexible cage have been found to be able to enhance other properties such as flame resistance, mechanical properties and thermal stability (Gauadagno *et al.* 2017b).

Concerning this last strategy, the work performed for this PhD thesis has highlighted that hydrogen bonding moieties can be covalently attached to specific nanofillers (see Fig. I.19) to activate self-healing mechanisms integrated in multifunctional materials (Guadagno *et al.* 2019).

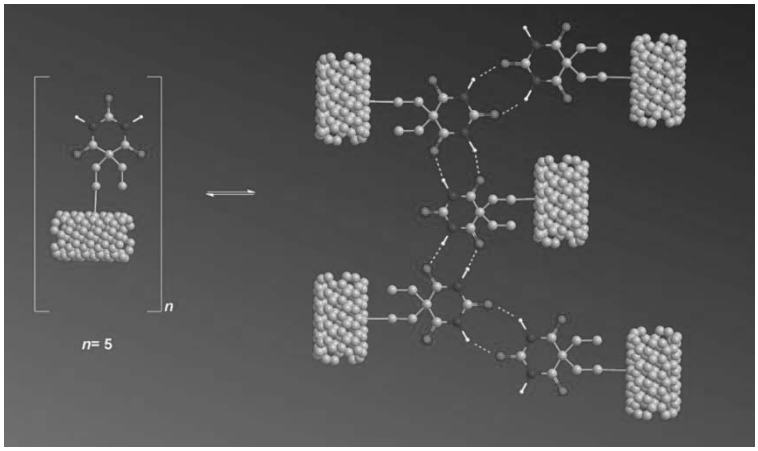

Figure I.19 *Example of H-bonding moieties covalently bonded to MWCNTs for reversible hydrogen bonds*

It is worth noting that the main challenge to overcome in applying this type of mechanisms is the limited dynamic properties of thermosetting matrix segments. The performed studies have highlighted that this mechanism can be integrated in epoxy mixture (able to reduce moisture content) solidified with primary aromatic amines and therefore characterized by high values in the glass transition temperature and storage modulus. The presence of graphene/polyhedral oligomeric silsesquioxane (GPOSS) in the nanofilled epoxy matrix strongly increases flame resistance and allows a decrease in the resin viscosity. This is a desirable effect as it count-balances the increase in the viscosity due to the addition of nanofillers in the epoxy formulation. The increase in viscosity is an effect, which must be carefully considered because it causes several processing problems such as difficulties in the dispersion stage of the nanofiller and/or filtration during the infusion process for the manufacturing of carbon fiber reinforced composites. Dynamic mechanical results have shown that sample containing carbon nanoparticles tend to create a phase with increased mobility of the chains. This particular phase arrangement is most likely responsible for better promoting reversible hydrogen bonds determined by interaction between epoxy resin and nanocages of POSS compounds. The presence of a more mobile phase in the multifunctional formulation can be advantageously exploited to enhance the self-healing efficiency up to 400% and then to strongly reduce the fatigue crack growth rate of CFRs laminates impregnated with multifunctional formulations (Kadlec *et al.* 2016).

As mentioned above, mechanisms based on hydrogen bonding have also been explored during this PhD research activity (Guadagno *et al.* 2019). Structural multifunctional self-healing resins, based on dynamic hydrogen bonds and capable to overcome many current industrial limitations, have been developed, with the aim to formulate auto-repair nanocomposites.

Chapter II
Microencapsulated self-healing system

II.1 Introduction

II.1.1 Development of microencapsulated self-healing systems based on ROMP reaction

The aim of this chapter is that to expose the main aspects concerning the development of microencapsulated self-healing systems, the main problems encountered in the application of these systems in the structural field and the winning solutions proposed during this PhD activity.

Inspired by living systems, self-healing materials are characterized by intrinsic ability to autonomically repair damage, thus providing a means to significantly extend the service life and reliability (Wu et al. 2008; Binder 2013; Jin *et al*. 2013). As already explained in the previous section *I.4 State of art*, several conceptual approaches have been explored to integrate self-healing ability in different materials, depending on their nature. Self-healing mechanisms integrated in thermosetting resins have been extensively studied (White *et al.* 2001; Kessler *et al.* 2003; Rule *et al.* 2005a; Amendola *et al*. 2015; Chowdhury *et. al.* 2015; Guadagno *et al.* 2010a, 2011a, 2014a, 2014b, 2016a; Raimondo *et al.* 2015, 2016; Everitt *et al*. 2015). Recently, a range of epoxy blends were investigated to evaluate mechanical properties and suitability for use as healing agents for the repair healing resins; FRP specimens were designed to encourage the controlled formation of damage which can be repaired by infusion of the resin blends. It has been found that the toughened epoxies were capable of providing complete recovery of stiffness (Everitt *et al*. 2015). Using the ROMP reaction, White et al. were able to self-heal the cracks in thermoset material based on microencapsulated system (White *et al.* 2001). Chung et al. (Chung *et al.* 2015) and Cho et al. (Cho *et al.* 2009) recently tested other self-healing

materials using microencapsulated systems. In Reference of Billiet *et al.* 2013, the authors used the monomer dimethylphenol (DMP) and styrene-butadiene-styrene triblock copolymer (SBS) rubber as healing agent. These components were used as core material to manufacture microcapsules incorporated into manufacturing self-healing asphalt. The healing mechanism was hypothesized due to a polymerization of DMP into poly (phenylene oxide) PPO by metals already existing in asphalt and the catalytic action of oxygen molecules in the air (Chung *et al*. 2015). Cho *et al.* developed microencapsulated systems, where the healing agent was a mixture of polydimethylsiloxane and polydiethoxysiloxane with hydroxyl end group and the catalyst was di-*n*-butyltin dilaurate able to heal microcracks on metal surface by condensation polymerization (Cho *et al.* 2009). Supramolecular chemistry which utilizes multiple, reversible, and in certain cases, cooperative intermolecular interactions can be advantageously exploited to create new materials with unique properties and functionalities (Gonzàlez-Rodrìguez and Schenning 2011; Busseron *et al.* 2013; Stupp and Palmer 2014). Reversible coordination abilities of polyphenols to metal ions can be useful employed to impart self-healing behaviour to novel conjugate hydrogels (Halake and Lee 2017).

Ring-opening metathesis polymerization (ROMP) has provided a powerful means for enabling self-healing mechanisms in epoxy systems for structural application (Schrock 1990; Navak *et al.* 1992; Kanaoka and Grubbs 1995; Schwab *et al*. 1996; Weck *et al.* 1996; Ivin and Mol 1997; Bazan *et al.* 1999; Grubbs and Khosravi 1999; Buchmeiser 2000; White *et al.* 2001; Frenzel and Nuyken 2002; Zhang and Rong, 2011; Binder 2013). However, ROMP initiators suffer from a lack of functional-group tolerance (Navak *et al.* 1992; Ivin and Mol 1997; Grubbs and Khosravi 1999; Buchmeiser 2000; Frenzel and Nuyken 2002), which can limit their applicability to activate self-healing mechanisms in structural materials. In fact, although in the last years, the implementation of ruthenium catalyzed olefin metathesis has benefitted from a broad functional group tolerance, as for the development of *N*-heterocyclic carbene ruthenium initiators (Weskamp *et al.* 1998a, 1998b, 1999a, 1999b; Huang *et al.* 1999), nitrogen bases, as the DDS hardener which is employed for the curing of high-performance structural materials, have remained challenging often-requiring initiator protection (Guadagno et al. 2017b). One of the most promising extrinsic ROMP-based self-healing systems for structural materials was firstly proposed in the year 2001 by White et al. (White *et al.* 2001) and, as already underlined, it constituted a significant break-through and milestone in self-healing chemistry, which allowed self-repair mechanisms for thermosetting polymers to grow rapidly over the past decade. These systems incorporate vessels containing healing agent (microencapsulated dicyclopentadiene (DCPD) or microvascular network etc.) and a catalytic chemical trigger within an epoxy matrix (usually EPON 828). The

microcapsules usually have been prepared via a urea-formaldeyde (UF) polycondensation (Brown *et al.* 2003). A rupture would cause cracks on the embedded microcapsules, thus allowing them to release a polymerizer agent into the crack plane. Polymerization of the healing agent is realized through Ring-Opening Metathesis polymerization (ROMP) which is triggered by contact with the embedded initiator and bonds the crack faces. Although some progress has been made in implementing the first proposed epoxy systems, most of the repair mechanisms are still based on ROMP reactions. Studies have been carried out using Grubb's first-generation initiator (G1) and other ruthenium initiators (Motuku *et al.* 1999; Jones *et al.* 2006; Toohey et al. 2007; Van der Zwaag 2007; Guadagno *et al.* 2010a, 2011a; Dry 2015). These systems allow to impart auto-repair function to epoxy resins. However, several drawbacks still need to be considered for more advanced applications where high mechanical performance is required (aircrafts, ships, wind turbine blades, satellite control boards etc). In particular, the epoxy formulations designed for high-performance mechanical polymers require a minimum value in the glass transition temperature (Tg) (after wet aging) of 170°C-180°C. This value in Tg of the resin can be obtained only using as "hardener agents" aromatic primary and secondary amines. Furthermore, the processing conditions able to impart high mechanical performance to the material usually require curing cycles also up to 180°C during the curing of the resin. High temperatures and very reactive environments (such as epoxy resins) cause deactivation or thermolytic decomposition of the ROMP initiators, which in turn limit the efficiency of self-healing function. As mentioned before, another critical point is related to the curing agent employed to solidify the epoxy system. Primary and secondary amines and most of all aromatic primary amines impose severe limits in the applicability of the self-healing chemistry based on ROMP reactions because they deactivate the ROMP initiators even at low temperatures (in the phase of preparation of the self-healing mixture). In order to overcome this drawback, the hardener ancamine or other tertiary amines have been used to solidify the matrix hosting ROMP initiators. Although tertiary amines allow formulating self-healing systems, there is a limit in max value of Tg due to the curing mechanism of tertiary amines because the final result is a polyether.

In fact, in the case of tertiary amines, no nitrogen bases can poison the ROMP initiator because the polymerization mechanisms consume the unshared electron pair of nitrogen atoms already in the first stage of polymerization at low temperature, but also in this case, many problems remain. The reaction with tertiary amines results from the unshared electron pair on the nitrogen atom. Since there are no secondary hydroxyl groups generated, the resin may be said to homopolymerize; in fact, tertiary amines lead to polyetherification by nucleophilic ring opening of oxirane ring (see Fig. II.1), which results in networks with significant lower mechanical

performance with respect to resins solidified using primary or secondary amines.

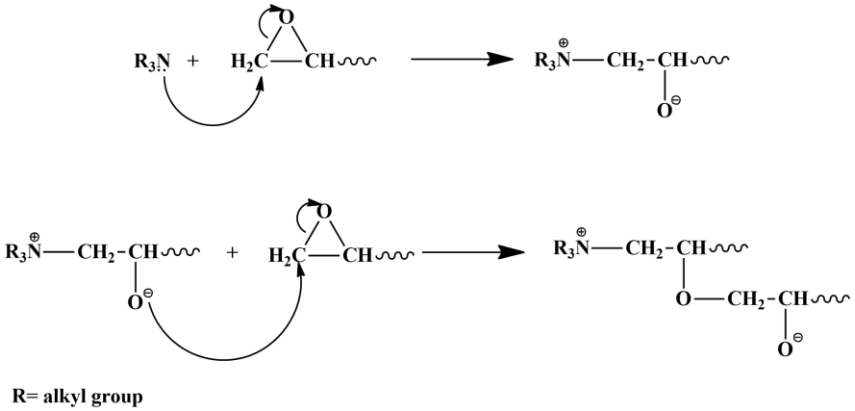

Figure II.1 *Reaction scheme for the homopolymerization of epoxide*

For example, the epoxy matrix composed of EPON 828 (the more common bifunctional epoxy precursor) hardened with diethylenetriamine (DETA), which has primary amino groups, is unable to host initiators for ROMP reaction because the hardener deactivates the initiator (Brown *et al*. 2002; Kessler *et al*. 2003; Rule *et al*. 2005a).

In recent publications, critical issues have been highlighted in the use of epoxy precursors in conjunction with Hoveyda-Grubbs' II (HG2) metathesis initiator (Guadagno *et al*. 2011a), as well as in the healing efficiency of self-healing epoxy formulations hardened at 170°C-180°C, when Hoveyda–Grubbs' I (HG1) metathesis initiator is employed (Guadagno *et al*. 2014b). Ethylene norbonene (ENB) and Hoveyda Grubbs I (HG1) initiator particles were used as self-healing components, and *in-situ* measurements of the healing efficiency, on tapered double cantilever beam (TDCB) specimens, provided very high values (even higher than 100%). More specifically, the healing efficiency has been found to be affected by the concentrations and morphological parameters of both the microcapsule and the initiator. Self-healing technologies for structural materials, able to repair the damage at macro-scale (Raimondo *et al.* 2016), thus effectively preventing the propagation of the impairment and ultimately extending the lifetime of the material, have been already proposed in literature.

Despite the positive results on the healing efficiencies, for specific industrial applications, the performance related to several mechanical properties has been found lacking due to the impracticality of introducing aromatic primary amines in the developed self-healing epoxy formulations, as these deactivate the ROMP initiators also using different strategies to preserve the initiator (Guadagno *et al*. 2011a). No self-healing thermosetting materials based on ROMP mechanisms (microencapsulated systems or

systems with microvascular networks) hardened with primary aromatic amines have been proposed until now in literature. Experiments have been performed highlighting that, when initiator particles are solubilized at molecular level (to reduce the cost of the self-healing materials), the particles which are in contact with the oxirane rings (during the curing reactions) are deactivated, hence reducing the actual amount of the active initiator. The deactivation also occurs in presence of tertiary amines (then in absence of primary and secondary amines) when ROMP initiators are solubilized at molecular level in epoxy precursors hardened at high temperature (up to 180°C). Experiments performed on this issue showed that an equimolecular reaction between the epoxide ring and the alkylidene of the ruthenium compound causes the deactivation of the ROMP initiator (Raimondo *et al.* 2015).

It was therefore concluded that it is only possible to enable self-healing reactions in epoxy matrices when cured at high temperature (130°C-170°C) using solid initiator particles; these retain an intact "heart" of initiator which is not deactivated when in contact with the oxirane rings of the epoxy matrix. Appropriate curing cycles able to open the oxirane rings before the equimolecular reaction between epoxy ring and initiator have been described in a recent patent, but also in this last case, no aromatic primary amines have been used to solidify the epoxy mixture (Guadagno and Raimondo 2013b).

II.1.2 Drawbacks of the ruthenium ROMP initiators and research strategies

Metathesis initiators developed until now to manufacture self-healing epoxy resins of composite structures have proven to be affected by two relevant drawbacks:

- poor mechanical performance of the developed materials;
- production cost not suitable for industrial production.

Concerning the first point, the developed systems (containing the ROMP initiators) did not meet the mechanical requirements suggested by many industrial manufacturers for specific applications (aircrafts, ships, wind turbine blades, satellite control boards, etc.). The poor mechanical performance of the microencapsulated systems has been found due to the impossibility to use hardeners as aromatic primary amines (e.g. DDS), in combination with initiators active in the Ring Opening Metathesis Polymerization (ROMP), and to the impossibility to use curing cycles at high temperatures as those scheduled for materials designed for load-bearing structures. Concerning the second point, the cost of self-healing systems based on ROMP reactions activated by a suitable amount of ruthenium initiators (~5% wt/wt in form of solid particles) is very expensive. To

succeed in overcoming the above-mentioned shortcoming, a winning approach might be the reduction of the amount of ROMP initiator embedded in the matrix, for example by dispersing it at molecular level in the initial fluid epoxy mixture.

In the attempt of significantly reducing the criticalities above mentioned, a new ruthenium-based initiator for the ring opening metathesis polymerization has been synthesized. It should be emphasized that since the discovery of well-defined Ru-alkylidene initiators (for example, first generation Grubbs initiator) active in the Ring Opening Metathesis Polymerization, many studies have been directed to design and develop new Ru-based initiator with improved applicability (Nguyen *et al.* 1992; Nguyen and Grubbs 1993; Schwab *et al.* 1996). Important progress has been achieved by:

- replacing a phosphine in the first-generation initiators with a ligand N-heterocyclic carbene (NHC), which constituted the second-generation Grubbs initiators class (Weskamp et al. 1998a, 1998b, 1999a, 1999b; Huang et al. 1999; Scholl *et al.* 1999);
- synthesizing initiators containing an alkylidene bonded to an aryl with a chelating ether group, which formed the class of the Hoveyda–Grubbs second generation initiator (Garber *et al.* 2000; Gessler *et al.* 2000).

The introduction of *N*-heterocyclic carbene ligands (NHC) in the ruthenium-based complexes marked a turning point in the development of ever more efficient metathesis initiators (Deshmukh and Blechert 2007; Schrodi and Pederson 2007; Samojłowicz et al. 2009; Vougioukalakis and Grubbs 2010) significantly improving the activity and selectivity (Savoie et al. 2009; Vieille-Petit et al. 2009, 2010; Keitz and Grubbs 2010; Tiede et al. 2010a, 2010b), while the introduction of the ether-chelating group has significantly improved the stability. In light of the results achieved in literature, new studies have been carried out with the aim to synthetize a new initiator stable at very high temperatures in a very reactive environment such as an epoxy mixture hardened at high temperature and/or with hardeners consisting of aromatic primary amines. During this research activity, a very promising result has been achieved in this direction consisting in the synthesis of an initiator of the Hoveyda–Grubbs second generation type, having phenyl groups as substituents of the backbone and mesytilene as substituents of the nitrogen of the imidazolium ligand, believing that these groups could significantly increase the stability of the
initiator.

The presence of the phenyl groups on the backbone stabilizes the bond of NHC with the metal for inductive effect, and the mesitylene groups on nitrogen atoms are those, which make the ligand less susceptible to give decomposition reactions (Jazzar *et al.* 2002; Hong *et al*. 2007; Chung and Grubbs 2008). The new initiator proposed in research work is able to

promote high catalytic activity in the ROMP reactions. It is named with the acronym $HG2_{MesPhSyn}$ and it is shown in Figure II.2.

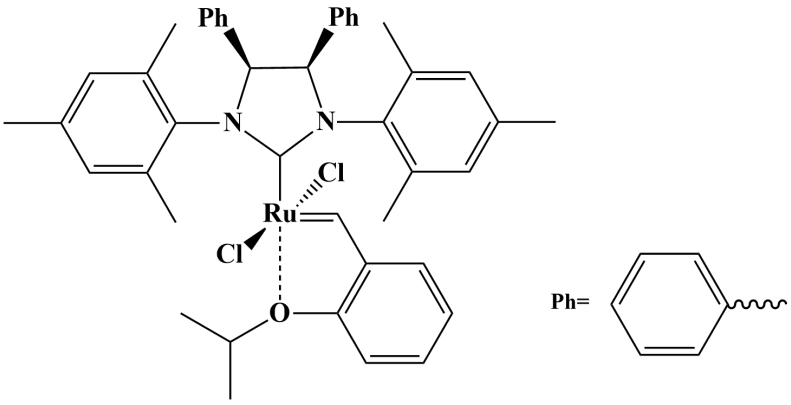

$HG2_{MesPhSyn}$

Figure II.2 *Chemical formula of $HG2_{MesPhSyn}$ initiator*

The synthesis and characterization of this new ruthenium initiator, will be discussed in the following sections.

Furthermore, aspects related to the influence of the stereochemistry of the ROMP-catalysts have been investigated. In particular the $HG2_{MesPhAnti}$ (see Fig. II.14 for the chemical formula) complex with the *anti*-orientation of the phenyl groups has also been synthesized, with the aim to highlight the relevant role of the stereochemistry of two ruthenium catalysts on the self-healing efficiency of aeronautical resins (Calabrese *et al.* 2019).

II.2 Experimental section

II.2.1 Materials

All reactions involving metal complexes have been performed under nitrogen atmosphere using standard Schlenk or glove-box techniques. All reagents have been purchased from Sigma-Aldrich Company and were of reagent grade quality. These products have been used without any further purification. Solvents have been dried and distilled before use. Deuterated solvents have been degassed under a N_2 flow and stored over activated 4 Å molecular sieves. Flash column chromatography of organic compounds has been performed using silica gel 60 (230-400 mesh), and flash column chromatography of ruthenium compounds has been performed using silica gel 60 (230-400 mesh) from TSI Scientific (Cambridge, MA). Analytical

thin-layer chromatography (TLC) has been performed using silica gel 60 F254 precoated plates (0.25 mm thickness) with a fluorescent indicator. Visualization of TLC plates has been performed by UV light and $KMnO_4$ or I_2 stains.

II.2.1.1 Epoxy matrices

Two different epoxy matrices whose acronyms hereafter are EB2A and TBD, have been used to analyze the activation of the metathesis reactions in the epoxy formulations during damages events. The first is based on a very common bifunctional epoxy precursor already used in the literature for developing self-repairing structural materials (Motuku *et al.* 1999; White *et al.* 2001; Brown *et al.* 2002, 2003; Kessler *et al.* 2003; Rule *et al.* 2005a; Jones *et al.* 2006; Dry 2007; Toohey *et al.* 2007; Van Der Zwaag 2007; Guadagno *et al.* 2010a, 2011a; 2014a, 2014b, 2016a; Raimondo *et al.* 2015, 2016). This resin has been hardened at high temperature (up to 180°C) with a tertiary aliphatic amine already used by other author (at lower temperature) and with solid ROMP initiators (Guadagno *et al.* 2010a, 2011a, 2014a, 2014b). The second is based on a tetrafunctional precursor that requires high temperatures for the curing cycle. In this second case, the use of hardener composed of aromatic primary amines allows to obtain high mechanical performance (high glass transition temperature (Tg), high values in the storage modulus in a wide range of temperature, high thermal stability etc.).

II.2.1.1.1 Epoxy matrix EB2A

The epoxy matrix EB2A has been prepared by mixing an epoxy precursor (bisphenol A diglycidyl ether, trade name EPON 828 - acronym E) with a reactive diluent (1,4- butanediol-diglycidylether - Acronym B) at a concentration of 80%: 20% (by wt) epoxide to flexibilizer giving the EB2 sample. This reactive diluent has proven to be effective to reduce the viscosity of epoxy precursors (Guadagno *et al.* 2014c, 2015d; Nobile *et al.* 2015) allowing to improve handling and ease of processing and to optimize consequently performance properties. The compounds E and B, both containing epoxy-moieties, have been obtained by Sigma-Aldrich. The curing agent investigated for this study was an anionic initiator phenol, 2,4,6-tris[(dimethylamino) methyl] (Trade name ancamine K54 - acronym A). The curing agent Ancamine K54 has been added at a concentration of 10% (by wt) with respect to the mixture EB2 giving the sample EB2A. Figure II.3 shows the chemical structures of compounds used for the mixture EB2A.

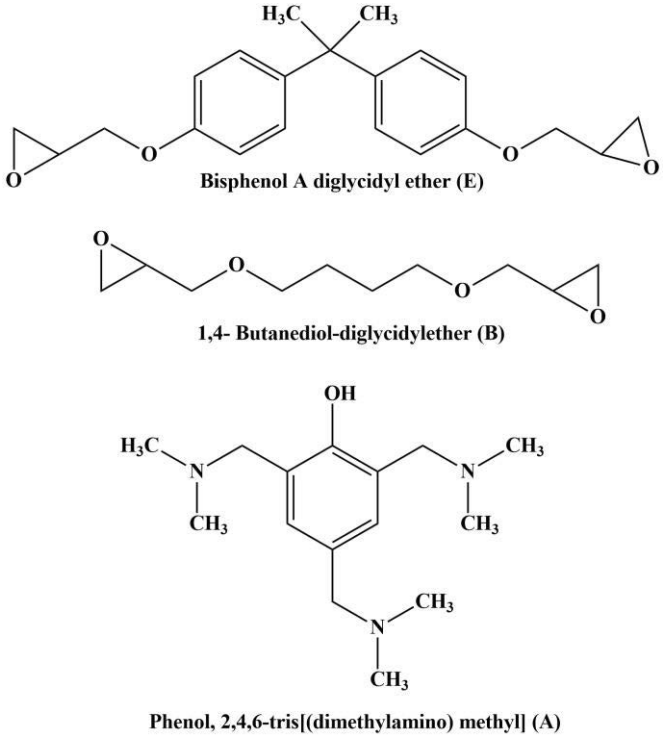

Figure II.3 *Chemical formulas of the compounds used for the mixture EB2A*

II.2.1.1.2 Epoxy matrix TBD

The epoxy matrix composite has been prepared by mixing the tetrafunctional epoxy precursor, tetraglycidyl methylene dianiline (TGMDA - acronym T) (epoxy equivalent weight 117-133 g/eq), with an epoxy reactive monomer 1-4 butanedioldiglycidyl ether (BDE - acronym B) at a concentration of 80%: 20% (by wt) epoxide to flexibilizer giving the TB sample. The compounds T and B, both containing epoxy-moieties, have been obtained by Sigma-Aldrich. The curing agent investigated for this study is an aromatic primary amine 4,4-diaminodiphenyl sulfone (DDS - acronym D). The curing agent has been added at stoichiometric amount with respect to the epoxy rings (TGMDA and BDE) giving the sample TBD. Figure II.4 shows the chemical structures of compounds used for the mixture TBD.

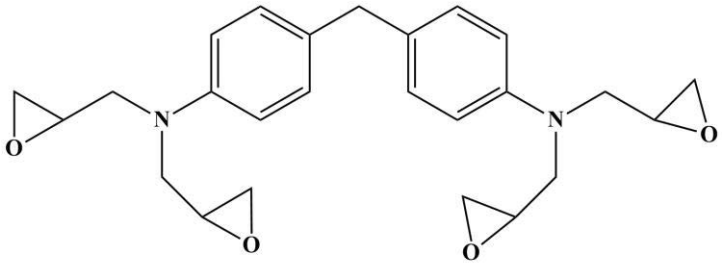

Tetraglycidyl methylene dianiline (T)

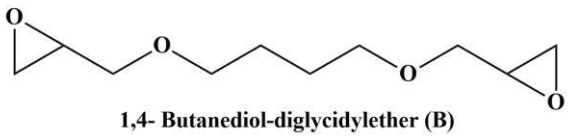

1,4- Butanediol-diglycidylether (B)

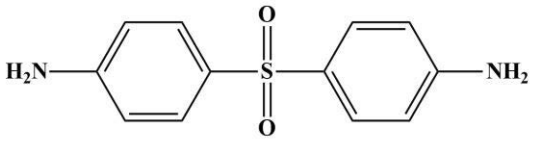

4,4-Diaminodiphenyl sulfone (D)

Figure II.4 *Chemical formulas of the compounds used for the mixture TBD*

II.2.1.2 Microcapsule manufacture

Microcapsules containing as "healing agent" a blend of two olefins 5-ethylidene-2-norbornene (ENB) and dicyclopentadiene (DCPD), with the outer shell composed of poly (urea formaldehyde) and the inner shell of ethylene maleic anhydride (EMA) copolymer (see Fig. I.7 of Chapter I), have been prepared by *in situ* polymerization in an oil in water emulsion which can be obtained encapsulating water immiscible liquids by the reaction of urea with formaldehyde at acidic pH. The pH was measured by pHMeter BASIC 20 which was purchased from Crison Instruments. The parameters used in the procedure (stirring rate, pH control, choice of appropriate workhead) have made it possible to obtain microcapsules characterized by a particular morphological feature, in the form of spherical nanovessels (see Fig. II.5).

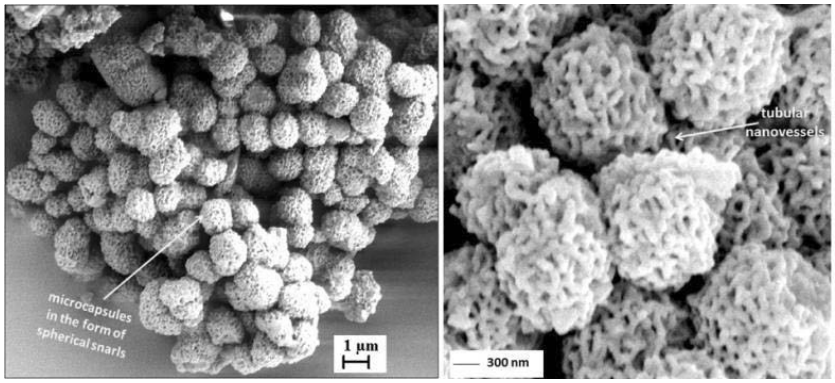

Figure II.5 *FESEM image of the microcapsules (capED5) in the form of spherical snarls*

At room temperature 400 ml distilled water and 100 ml of a 2.5 wt% aqueous solution of EMA copolymer were mixed in a 800 ml glass beaker. EMA copolymer was completely dissolved in distilled water at 100°C until obtaining a perfectly clear solution. The beaker containing the emulsion was suspended in a temperature-controlled water bath on a programmable digital stirring hotplate with external temperature immersion probe (Dataplate Digital Hotplate, Cole Palmer). The hotplate stirrer with external temperature probe was purchased from General Control S.p.a. The oil-in-water emulsion was kept under stirring at a speed of 1800 rpm with a high shear digital mixer/emulsifier (Silverson Machines Ltd mod. L4RT) driving a three bladed, 63.5 mm diameter low shear mixing propeller (Cole Parmer) placed just above the bottom of the beaker. The digital mixer with electronic speed control (nominal maximum speed 8000 rpm) equipped with interchangeable heads (mixing or disintegrating), was purchased from Crami Amalfiter Group S.R.L. The Silverson rotor/stator workhead rapidly disintegrates and disperses agglomerates to give an uniform and homogeneous mix. In our experimental work, a general-purpose disintegrating head was used with the aim of obtaining a vigorous mixing action. The use of this head, the stirring rate control and a careful control of the pH strongly affect the morphology of the oil/water mixture and then the morphology of the vessel walls. Under agitation, the wall forming materials 10 g urea, 1 g ammonium chloride and 1 g resorcinol were dissolved in the solution. Then, the pH was raised from 2.60 to 3.50–3.60 by dropwise addition of 10% NaOH solution. Surface bubbles were eliminated by the addition of four drops 1octanol. Then, a slow stream of 120 ml of ENB was added to form a suspension of fine droplets and allowed to stabilize for 10 min. After stabilization, 25.34 g of 37 wt% aqueous solution of formaldehyde was added, keeping pH at a constant value of 3.50–3.60. Since no phase separation was observed, the stirring rate was initially lowered to 1000 rpm and then at 500 rpm. This low stirring speed of 500 rpm was kept

constant until the end of the microencapsulation process. The mixture was covered with aluminium foil and the temperature was raised to 55°C at a rate of 1 °C min^{-1}. After 4 h of continuous agitation the obtained suspension of microcapsules was removed and allowed to slowly cool to room temperature and the mixer and hot plate were switched off. Once cooled to room temperature, the suspension of microcapsules was filtered with discs of filter paper which were placed inside the Büchner funnel. The microcapsules were rinsed with deionized water and air dried for 48 h.

DCPD was added to ENB with the aim of increasing the cross-linked fraction of the metathesis products. The composition of the healing agent inside the microcapsules is ENB(95%)/DCPD(5%) (Guadagno *et al.* 2014a, 2016a, Raimondo *et al.* 2015, 2016).

II.2.1.3 Synthesis of $HG2_{MesPhSyn}$ initiator

II.2.1.3.1 First step

Under nitrogen atmosphere, tris (dibenzylideneacetone)-dipalladium (0) ($Pd_2(dba)_3$) (0.11 g, 0.12 mmol), 2,20-bis(diphenylphosphino)-1,10-binaphthyl (BINAP) (0.18 g, 0.29 mmol), sodium tert-butoxide (NaO*t*Bu) (0.71 g, 7.39 mmol) and toluene (8 ml) have been introduced in a flask equipped with a reflux condenser and stirred for 20 min. After this time, meso-1,2-diphenylethylenediamine (0.52 g, 2.46 mmol) and 2-bromomesitylene (0.74 ml, 4.93 mmol) have been added and the solution has been heated to 105°C for 16 h. The reaction mixture has been then cooled at room temperature, diluted with hexane and filtered through a plug of silica gel. The product has been eluted from silica gel with methylene chloride. The solvent has been removed under vacuum to give the product as a pale yellow solid S1(see Fig. II.9) (0.88 g, 1.96 mmol, 79%).

NMR characterization: ^{1}H NMR (400 MHz, CD_2Cl_2): δ 7.19 (m, 6H), 6.84 (m, 4H), 6.78 (s, 4H), 4.96 (d, 2H), 4.35 (d, 2H), 2.13 (s, 6H), 2.09 (s, 12H). ^{13}C NMR (100 MHz, CD_2Cl_2): δ 142.2, 140.4, 130.4, 129.8, 128.4, 127.7, 126.8, 66.1, 20.6, 20.0 (see Figs. II.10 and II.11).

II.2.1.3.2 Second step

Triethylorthoformate (0.89 ml, 5.36 mmol), diamine (0.31 g, 0.68 mmol) and ammonium tetrafluoroborate (0.09 g, 0.87 mmol) have been introduced in a 10 ml round-bottom flask equipped with a magnetic stirrer. The reaction mixture has been heated at 120°C for 5 h. After cooling to room temperature, the product has been precipitated and washed with Et_2O (3x10 ml) and hexane. The solid obtained has been dissolved in the minimum amount of CH_2Cl_2 and then filtered. The solvent has been removed under vacuum. The product has been dissolved in the minimum amount of ethanol and recovered

by precipitation as a light brown solid S2 (see Fig. II.9) (0.22 g, 0.41 mmol, 60%).

NMR characterization: ^{1}H NMR (300 MHz, $CDCl_3$): δ 8.52 (s,1H), 7.29 (m, 6H), 7.16 (m, 4H), 6.89 (s, 4H), 6.63 (s, 2H), 2.52 (s, 12H), 2.21 (s, 6H). ^{13}C NMR (100 MHz, CD_2Cl_2): δ 160.5, 141.1, 131.5, 130.0, 129.4, 129.1, 72.0, 21.2, 19.8 (see Figs. II.12 and II.13).

II.2.1.3.3 Third step

In a glove box, a solution of S2 (0.160 g, 0.29 mmol), potassium bis(trimethylsilyl)amide (KHMDS) (0.064 g, 0.32 mmol) in 15 ml of toluene has been stirred at room temperature for five minutes. $(PCy_3)Ru(=CH\text{-}o\text{-}OiPrC_6H_4)Cl_2$ (0.092 g, 0.15 mmol) has then been added, the reaction flask has been removed from the glove box and heated at 70°C for 1.5 h. The mixture has been allowed to cool at room temperature and the crude product has been purified by flash column chromatography on silica gel TSI (see Fig. II.6a) (*n*-hexane/Et_2O = 5:1-3:1). The solvent has been removed under vacuum to give initiator $HG2_{MesPhSyn}$ as a green powder (see Fig. II.6b) (0.081 mmol, 63.1 mg, 54%) (see Fig. II.9). The NMR spectra of $HG2_{MesPhSyn}$ are shown in Figsures II.17 and II.18.

NMR characterization: ^{1}H NMR (400 MHz, $CDCl_3$): δ 16.33 (s, 1H), 7.53–6.99 (m, 18H), 5.89 (d, 1H), 5.72 (d, 1H), 4.89 (q, 1H), 2.59–2.21 (18H), 1.30 (d, 3H), 1.21 (d, 3H). ^{13}C NMR (100 MHz, CD_2Cl_2): δ 298.5, 219.3, 152.0, 145.1, 139.0, 129.9, 128.2, 127.6, 122.4, 122.3, 113.0, 75.2, 74.2, 73.2, 29.7, 22.8, 22.0, 20.6, 20.5, 20.2, 19.7.

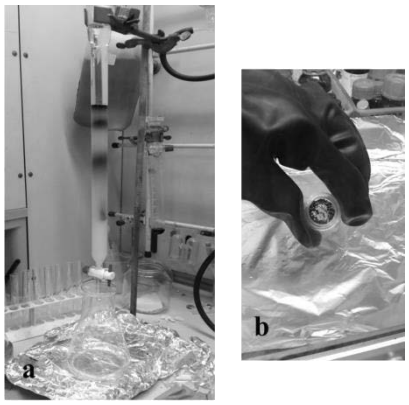

Figure II.6 *a) Flash column chromatography used for the purification of the $HG2_{MesPhSyn}$ catalyst (green band); b) green powder of $HG2_{MesPhSyn}$ catalyst after purification*

II.2.2 Methods

II.2.2.1 Nuclear magnetic resonance (NMR) spectroscopy

NMR spectra have been recorded on a Bruker AVANCE 400 spectrometer (400 MHz for ^{1}H; 100 MHz for ^{13}C). The ^{1}H and ^{13}C NMR chemical shifts are referenced to Me_4Si (d = 0 ppm) using the residual portion impurities of the deuterated solvents as internal standard. Spectra are reported as follows: chemical shift (ppm), multiplicity, integration and coupling constant (Hz). Multiplicities are abbreviated as follows: singlet (s), doublet (d), triplet (t), quartet (q), multiplet (m), and broad (br).

II.2.2.2 Fourier Transform Infrared (FTIR)Spectroscopy

FTIR spectra have been collected at a resolution of 2.0 cm^{-1} with a FTIR (BRUKER Vertex70) spectrometer equipped with deuterated triglycine sulfate (DTGS) detector and a KBr beam splitter, using KBr pellets. The frequency scale was internally calibrated to 0.01 cm^{-1} using a He–Ne laser. 32 scans were collected and averaged to reduce the noise.

II.2.2.3 Healing activity and self-healing efficiency evaluation

The test of healing activity has been carried out by means of FTIR investigation. Self-healing efficiency assessed by fracture test has also been performed. The healing efficiency η of the sample EBA + 0.5% $HG2_{MesPhSyn}$ cured up to 180°C has been evaluated by fracture tests. For quasi-static fracture conditions crack healing efficiency η, see eq. (II.1), is defined as the ability of a healed sample to recover fracture toughness:

$$\eta = \frac{K_{IChealed}}{K_{ICvirgin}} \qquad \text{(II.1)}$$

where $K_{ICvirgin}$ is the fracture toughness of the virgin specimen and $K_{IChealed}$ is the fracture toughness of the healed specimen. Using a protocol already established in literature (Wool and O'Conner 1981; White *et al.* 2001), healing efficiency is measured by carefully controlled fracture experiments for both the virgin and the healed sample. These tests utilize a Tapered Double-Cantilever Beam **(**TDCB) geometry (see Fig. II.7) which ensures controlled crack growth along the centreline of the specimen and provides a crack length independent measure of the fracture toughness.

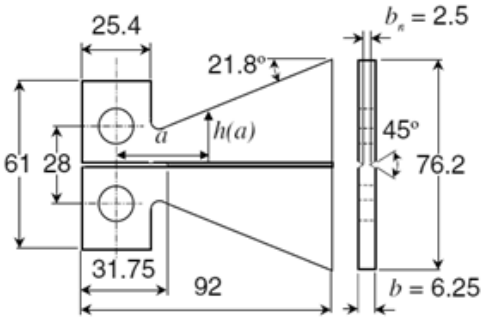

Figure II.7 *TDCB geometry and dimensions (mm)*

Healing evaluation begins with a virgin fracture test of an undamaged TDCB sample. A pre-crack is introduced to sharpen the crack-tip. The sample is then mounted on a load frame and loaded under displacement control causing the pre-crack to propagate along the centreline of the sample until failure. The crack is then closed and allowed to heal at room temperature with no external intervention. After healing, the sample is loaded again until failure. With this geometry, the efficiency measurement simply requires knowledge of the critical fracture load, P_C, of virgin and healed specimen, see eq. (II.2):

$$\eta = \frac{P_{Chealed}}{P_{Cvirgin}} \qquad \text{(II.2)}$$

Equation (II.2) can be derived from equation (II.1) by considering that $K_{IC} = \alpha P_C$; where $\alpha = 11.2 \times 10^3 m^{-3/2}$, for the TDCB used geometry. This procedure has been recognized to be very effective to measure the healing efficiency. In the current work, fracture specimens have been tested by INSTRON mod. 5967 Dynamometer under displacement control using a load cell of 30KN and a 250 mm/min displacement rate and measuring load and displacement values (see Fig. II.8). Samples have been loaded at first failure and then unloaded allowing the crack face to come back into contact. After a sufficient time (24 h) for healing efficiency to reach a steady state the healed samples have been tested again. Values of healing efficiency (η) have been calculated using equation (2).

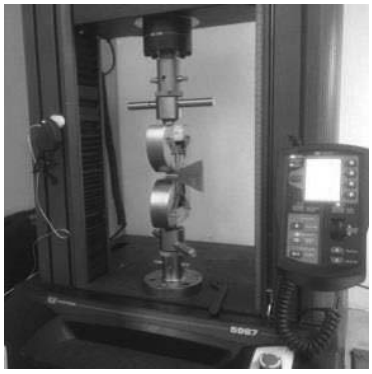

Figure II.8 *Equipment to evaluate the healing efficiency*

II.2.2.4 Evaluation of the cross-linked fraction of poly-ENB

The cross-linked fraction of metathesis polymer has been determined, according to the ASTM method D2765-84, as the percent of the original weight of the sample extracting for 33 h in boiling decahydronaphthalene (decaline, a mixture of *cis* and *trans* isomers). The extraction has been followed by drying at 150°C in a vacuum oven.

II.2.2.5 Electrospray Ionization Mass Spectrometry (ESI-MS)

ESI-MS has been performed on a Waters Quattro Micro triple quadrupole mass spectrometer.

II.2.2.6 Field Emission Scanning Electron Microscopy (FESEM)

Micrographs of the epoxy matrices were obtained using FESEM (mod. LEO 1525, Carl Zeiss SMT AG, Oberkochen, Germany). All samples were placed on a carbon tab previously stuck to an aluminium stub and were covered with a 250 Å- thick gold film using a sputter coater (Agar mod. 108 A – Agar Scientific, Stansted, UK), before being subjected to morphological analysis.

II.3 Results and discussion

II.3.1 Synthesis and characterization of $HG2_{MesPhSyn}$ initiator

In the attempt to enhance initiator efficiency, phosphine-free NHC Ru pre-initiator with encumbered *syn* backbone substituents with phenyl groups have been prepared. The synthesis of the NHC ligand precursor with *syn* phenyl groups on the backbone has been easily accomplished in two steps starting from the commercially available meso-1,2-diphenylethylenediamine,

allowing significant time saving. The synthesis of the initiator has been carried out through three basic reactions (see Fig. II.9).

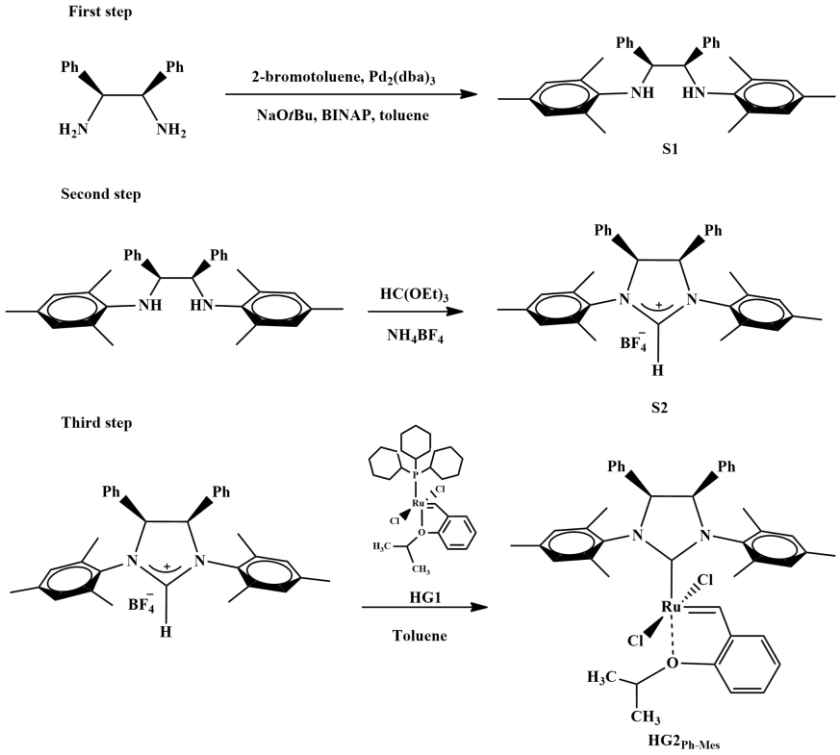

Figure II.9 *Steps of synthesis of the initiator HG2$_{MesPhSyn}$*

The NMR spectra of S1 solid are shown in Figures II.10 and II.11, and are consistent with the proposed structure, e.g. the doublets at 4.96 and 4.35 ppm into ^{1}H NMR spectrum can be attributed to C*H* and NC*H*Ph, respectively, and the signals at 20.6 and 20.0 ppm into ^{13}C NMR spectrum can be assigned to methyls in position 4, and to methyls in the positions 2,5 of the mesitylenes, respectively; while the signal at 140.4 ppm can be assigned to quaternary carbons of the mesitylenes.

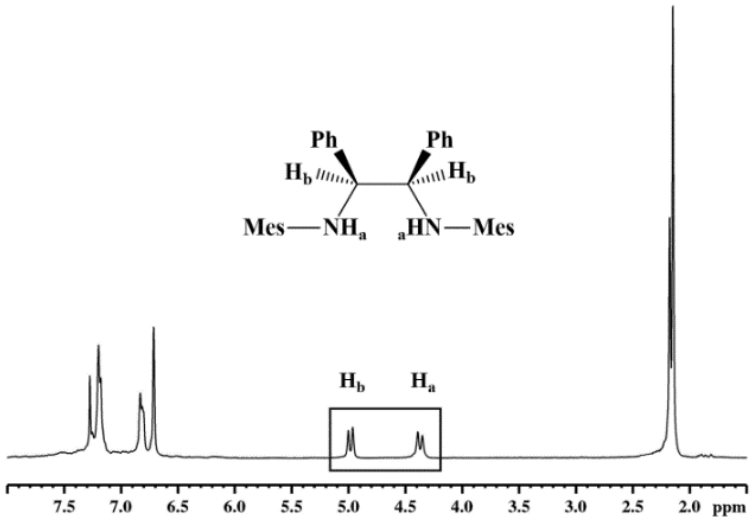

Figure II.10 *[1]H NMR (400 MHz, CDCl3): N,N'-dimesityl-meso-1,2-diphenyl-ethylen-diamine (S1)*

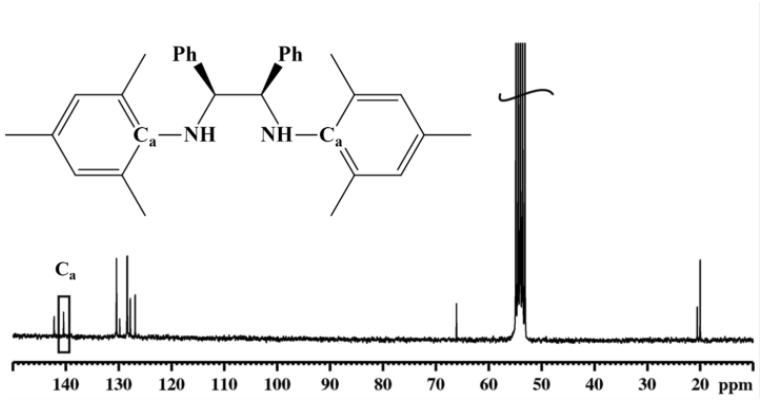

Figure II.11 *[13]C NMR (100 MHz, CD_2Cl_2) of N,N'-dimesityl-meso-1,2-diphenyl-ethylen-diamine (S1)*

The NMR spectra of S2 solid are shown in Figures II.12 and II.13. The signal at 8.52 ppm in the ^{1}H NMR and the signal at 160.5 ppm in the ^{13}C NMR, are indicative of the occurred cyclization of diamine, in fact they are attributable to *CH* group between the nitrogen atoms.

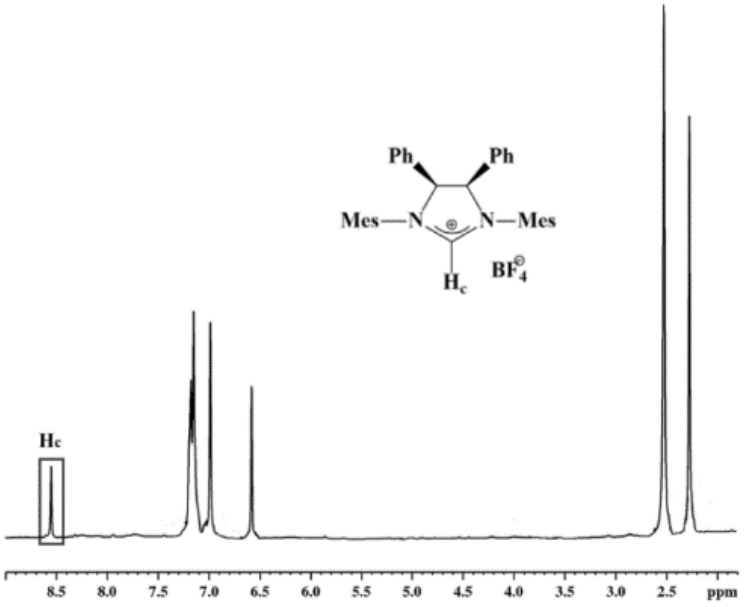

Figure II.12 *^{1}H NMR (300 MHz, $CDCl_3$): N,N'-dimesityl-meso-1,2-diphenyl-ethyl-imidazolium-tetrafluoroborate (S2)*

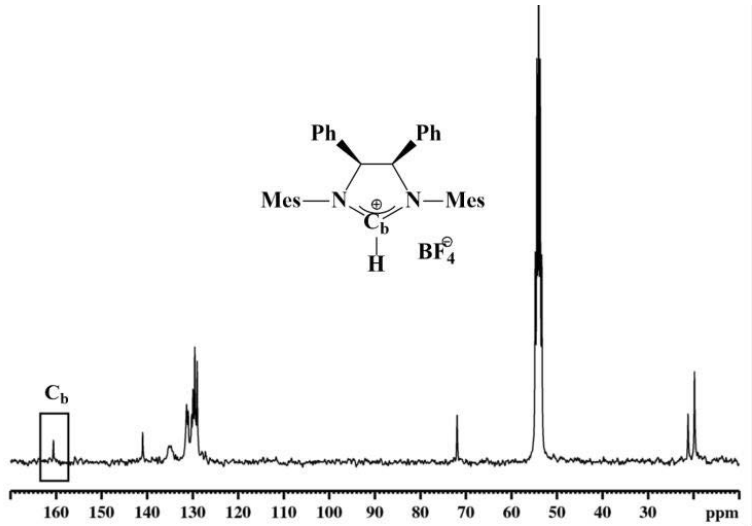

Figure II.13 *^{13}C NMR (100 MHz, CD_2Cl_2): N,N'-dimesityl-meso-1,2-diphenyl-ethyl-imidazolium-tetrafluoroborate (S2)*

It is worth noting that the stereochemistry of the starting material is preserved during the second step of the synthesis procedure, as it is confirmed by the synthesis of the other stereoisomer $HG2_{MesPhAnti}$. The

chemical formula is shown in Figure II.14, where also the formula of $HG2_{MesPhSyn}$ initiator is shown for comparison.

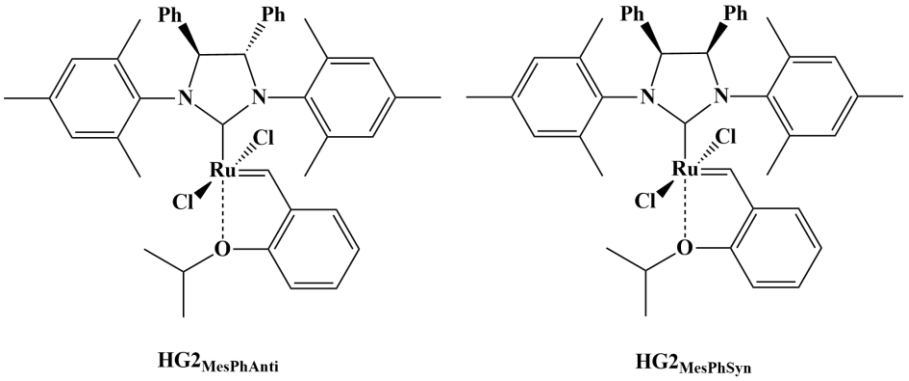

Figure II.14 *Chemical formulas of $HG2_{MesPhAnti}$ and $HG2_{PhMesSyn}$ initiators*

By comparing the spectra of each reaction intermediate for the synthesis of both complexes, we can observe that the protons on the backbone of the NHC ligand have always different chemical shifts. The ^{1}H-NMR spectra (400 MHz, $CDCl_3$) show a signal at 4.79 ppm (s, $2H_a$) for the product A, and a signal at 4.96 ppm (s, $2H_a$) for the product S1 (see Fig. II.15).

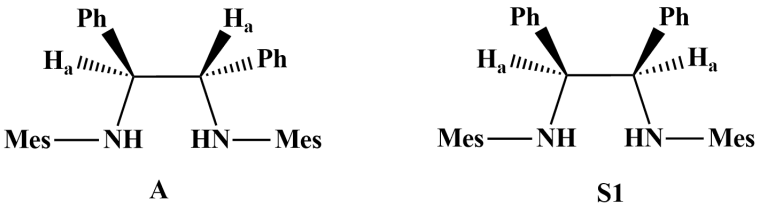

Figure II.15 *Chemical formulas of A and S1 products*

The ^{1}H-NMR spectra (400 MHz, CD_2Cl_2) show a signal at 6.07 ppm (s, $2H_b$) for the product B, and a signal at 6.52 ppm (s, $2H_b$) for the product S2 (see Fig. II.16).

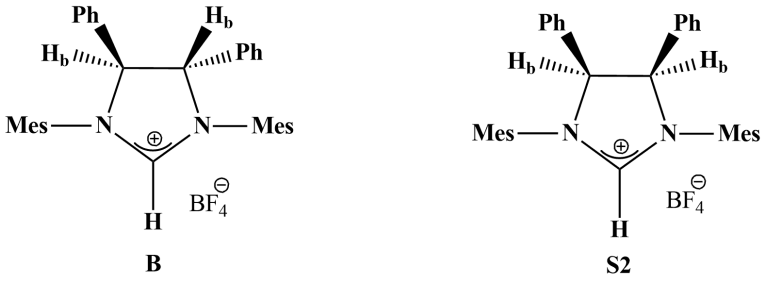

Figure II.16 *Chemical formulas of B and S2 products*

Furthermore, in agreement with another published paper (Grisi *et al*. 2009), the protons on the backbone have always chemical shifts lower in products with the phenyl groups in *anti* than the protons in the compounds with the phenyl groups in *syn*.

This explanation shows that the stereochemistry of the starting material is preserved during the second step of the synthesis procedure.

The NMR spectra of $HG2_{PhMesSyn}$ are shown in Figs. II.17 and II.18. The signal at 16.33 ppm, in the ^{1}H NMR spectrum, is due to the benzylidenic proton (H_d); whereas the signals at 298.5 and 219.3 ppm, in the ^{13}C NMR spectrum, are due to the benzylidenic carbon (C_c) and the carbene of the imidazole group, respectively.

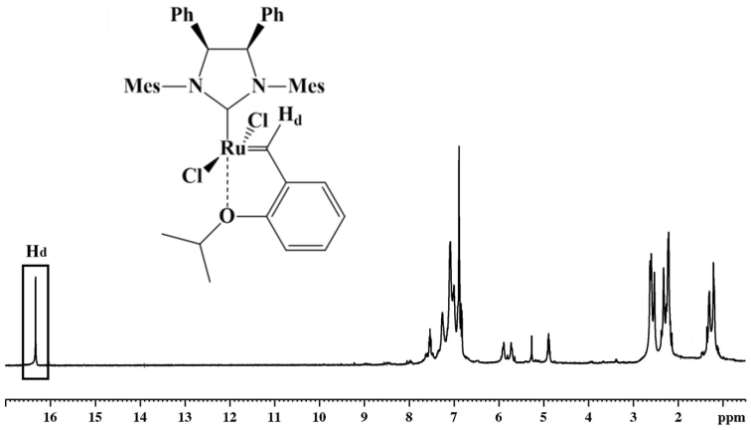

Figure II.17 *^{1}H NMR (400 MHz, $CDCl_3$ of ($HG2_{MesPhSyn}$): (meso)-(1,3-bis-mesityl)l-(4,5-diphenyl-imidazolin-2-ylidene)-dichloro-(2-isopropoxybenzylidene)-ruthenium(II)*

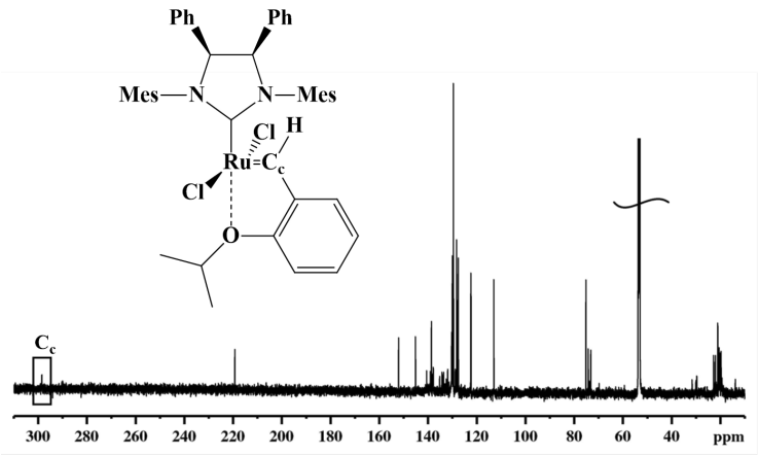

Figure II.18 *^{13}C NMR (100 MHz, CD_2Cl_2) of ($HG2_{MesPhSyn}$): (meso)-(1,3-bis-mesityl)l-(4,5-diphenyl-imidazolin-2-ylidene)-dichloro-(2-isopropoxybenzylidene)-ruthenium(II)*

The results of the Electrospray Ionization Mass Spectrometry (ESI-MS) confirm the obtaining of $HG2_{PhMesSyn}$ initiator (see Fig. II.19). In fact, two expected peaks corresponding to the values of ESI+MS: m/z = 743.0 [M^+(-Cl^-)] and 709.1[M^+(-2Cl^-_)] are observed. Furthermore, ESI-MS spectrum shows multiple peaks of fragment ions according to isotopic percentages abundances of the ruthenium atom.

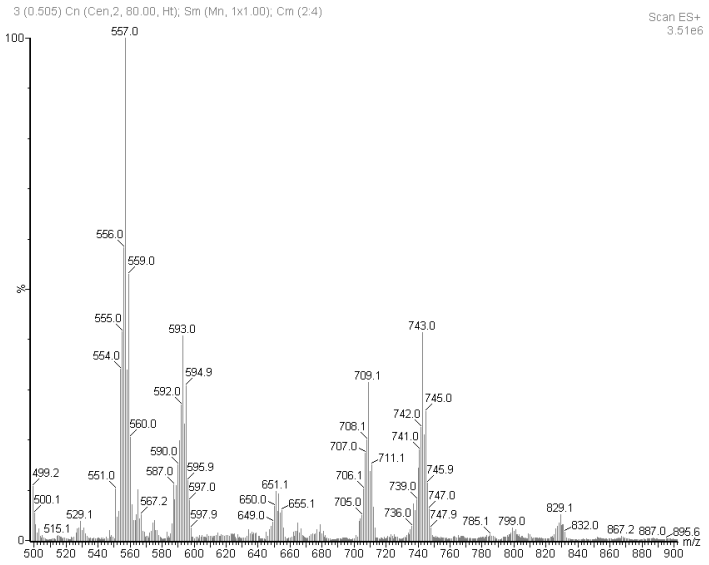

Figure II.19 *ESI-MS spectrum of $HG2_{MesPhSyn}$*

II.3.2 Evaluation of the $HG2_{MesPhSyn}$ initiator activity

The activity of the new synthesized complex $HG2_{MesPhSyn}$ has been evaluated through the Ring Opening Metathesis Polymerization (ROMP) of two monomers: 2-norbornene (NBE) and 5-ethylidene-2-norbornene (ENB) (see Tables II.1 and II.2). Furthermore, $HG2_{MesPhSyn}$ metathesis efficiency has been compared to that of the two commercial pre-initiators, [1,3-bis-(2,4,6-trimethyl phenyl)- 2-imidazolin-2-ylidene]-dichloro-(o-isopropoxybenzylidene)-ruthenium (II)(HG2) and [1,3-bis(2-methyl phenyl)-2-imidazolin- 2-ylidene]-dichloro-(2-isopropoxybenzylidene)-ruthenium(II) $HG2_{oTol}$ (the formulas are shown in Fig. II.20).

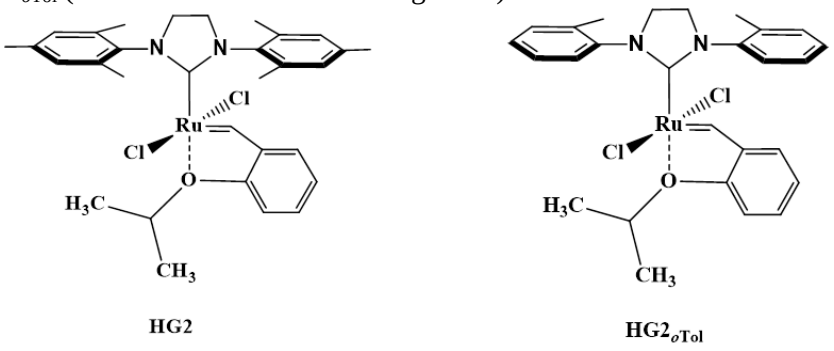

Figure II.20 *Chemical formulas of HG2 and $HG2_{oTol}$ initiators*

All polymerizations have been carried out in solution of tetrahydrofuran (THF) at 25°C. A molar ratio monomer/initiator of 3000/1 has been used for the polymerization tests. In the performed experiments, the initiator has been mixed with the monomer and stirred in 99 mL of THF, in a round bottom flask. The metathesis reactions have been stopped by adding few drops of ethyl-vinyl ether and the obtained polymers have been coagulated in methanol, filtered and washed with CH_2Cl_2. Figure II.21 shows the scheme of polymerizations of 2-norbornene (NBE) and 5-ethylidene-2- norbornene (ENB) by ROMP reaction.

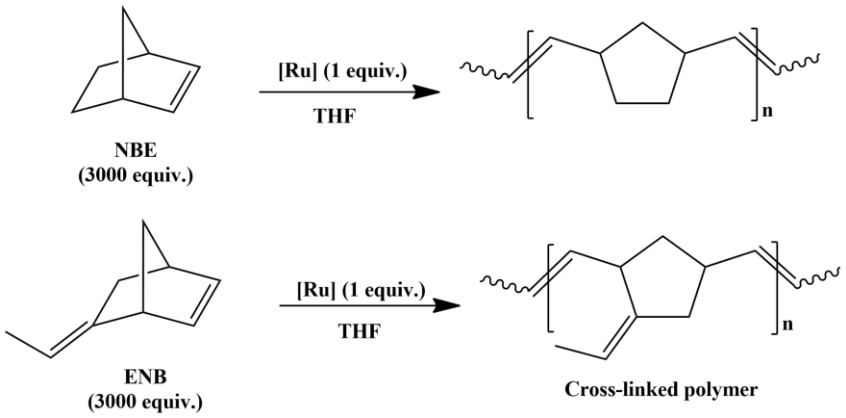

Figure II.21 *Polymerizations of NBE and ENB by ROMP reaction*

In the polymerization of 2-norbornene all the analysed pre-initiators show high conversion (see Table II.1).

Table II.1 *Results on the polymerization of 2-norbornene (NBE) with different initiators*

Run[a]	Initiator	Monomer moles $\times 10^{-2}$	Polymer g	Yield %	***E/Z***[b]
I	$HG2_{oTol}$	1.15	1.09	100	0.71
II	HG2	1.12	1.01	95.8	0.60
III	$HG2_{MesPhSyn}$	1.10	0.867	83.7	0.61

[a]Reaction conditions: monomer/initiator = 3000/1; solvent THF; reaction time = 60 s.
[b]Ratio based on data from ^{1}H NMR and ^{13}C NMR of isolated products.

$HG2_{oTol}$ and HG2 initiators show higher activities than $HG2_{MesPhSyn}$. This different behaviour can be due to steric factors. The effect of steric factors of ruthenium-based initiators on the activity of ROMP reactions have been also evidenced by Chung et al. (Chung and Grubbs 2008). E/Z in Table I.1 is the ratio between the *cis* and *trans* isomers; it has been obtained from ^{1}H NMR and ^{13}C NMR of the isolated products. The value of E/Z ratio for the new synthetized pre-initiator is comparable with HG2 and $HG2_{oTol}$. The ^{1}H-NMR spectrum of poly-NBE, obtained using the new synthetized pre-initiator, is shown in Figure II.22.

NMR characterization: ^{1}H NMR (300 MHz, TDCE at 90°C): δ (ppm) 5.18 (s, $2H_{cis}$), 5.01 (s, $2H_{trans}$), 2.58 (br s, 2H), 2.25 (br s, 2H), 1.66 (br m, 3H), 1.12 (br m, 2H), 0.82 (br m, 1H).

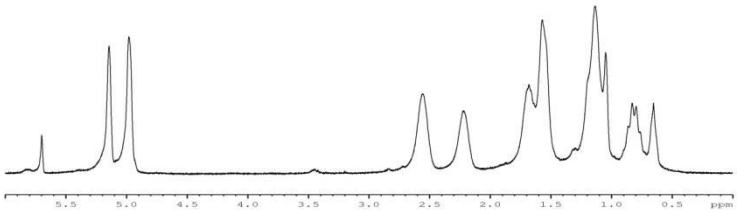

Figure II.22 *^{1}H NMR spectrum of Poly-NBE obtained using as initiator $HG2_{MesPhSyn}$*

In the ROMP of 5-ethylidene-2-norbornene, the initiator $HG2_{MesPhSyn}$ also shows good conversions for short times (see Table II.2).

Table II.2 *Results on the polymerization of 5-ethylidene-2-norbornene (ENB) with different initiators*

Run[a]	Initiator	Monomer moles $\times 10^{-2}$	Polymer g	Yield %	Insoluble fraction (%)
I	$HG2_{oTol}$	1.13	1.10	80.9	78
II	HG2	1.12	1.22	90.4	82
III	$HG2_{MesPhSyn}$	1.11	1.08	81.2	81

[a]Reaction conditions: monomer/initiator = 3000/1; solvent THF; reaction time = 60 s.

A very important aspect concerning the ROMP of ENB monomer, in particular for self-healing applications, is related to the degree of cross-linking of the metathesis product. The degree of the cross-linked fraction has been evaluated through the extraction of the insoluble fraction in *cis-trans* decahydronaphthalene (decaline) as described in section *II.2.2.4 Evaluation of the cross-linked fraction of poly-ENB*. The ^{1}H NMR spectrum of poly-ENB was not reported because the polymer is not soluble in any deuterated solvent.

II.3.3 Control of the $HG2_{MesPhSyn}$ initiator thermal stability

The thermolytic stability of the new initiator $HG2_{MesPhSyn}$ has been evaluated in nitrogen atmosphere and compared to that of HG2 and $HG2_{oTol}$ initiators. The thermal stability has been verified by introducing dust of the

ruthenium compounds in a vial. This last has been placed in an oil bath at 180°C for 2 h. Then the solid has been dissolved into 0.5 mL of $CDCl_3$ and analysed by ^1H NMR. ^1H NMR analysis has been carried out for monitoring and estimating the initiators stability. In the spectra of the initiators, the presence of the characteristic resonance signal of the benzylidenic proton can be considered for directly assaying the degradation state of the initiator. It is interesting to note that, after a thermal treatment at 180°C for 2 h in nitrogen atmosphere, the ^1H NMR spectra of all initiators reveal the signal of Ru=CH, but for HG2 and $HG2_{oTol}$ this signal is lower than that of $HG2_{MesPhSyn}$. This confirm that $HG2_{MesPhSyn}$ initiator shows greater stability, showing all ^1H NMR signals unchanged. The same treated samples have been used for a test polymerization in solution of THF to evaluate the activity. After heat treatment the $HG2_{MesPhSyn}$ initiator activity is only slightly diminished from 81 to 76%, while the other two initiators give lower yields as shown in Table II.3.

Table II.3 *Polymerization of 5-ethylidene-2-norbornene (ENB) with different thermally treated initiators*

Run[a]	Initiator[b]	Monomer moles $\times 10^{-2}$	Polymer g	Yield %
I	$HG2_{oTol}$ 2h 180°C	1.10	0.89	67.8
II	HG2 2h 180°C	1.09	0.73	55.4
III	$HG2_{MesPhSyn}$ 2h 180°C	1.11	1.02	76.1

[a]Reaction conditions: monomer/initiator = 3000/1; solvent THF; reaction time = 60 s.
[b]The initiator has been thermally treated at 180°C for 2 h.

These results confirm the exceptional thermal stability of the new initiator, closely related to its structural characteristics. Each polymerization has been performed 4 times in order to verify the reproducibility of the results. The error on the yield percentage has been found to be less than 5% for all experiments shown in Tables II.1-3.

II.3.4 Control of the $HG2_{MesPhSyn}$ initiator chemical stability in presence of oxirane rings and primary amine

In order to evaluate initiator stability with epoxy groups, present in elevated concentration in the resin, at a solution of $HG2_{MesPhSyn}$ in 1,1,2,2-tetrachloroethane-d_2 has been added cyclohexene oxide. The reactivity of

this compound with the initiator has been analyzed at different ruthenium-complex/cyclohexeneoxide ratio (1/1 and 1/150) and at different temperature (80, 100, 110, 120, 130 and 140°C) by means of ^{1}H NMR. The results are shown in Figure II.23.

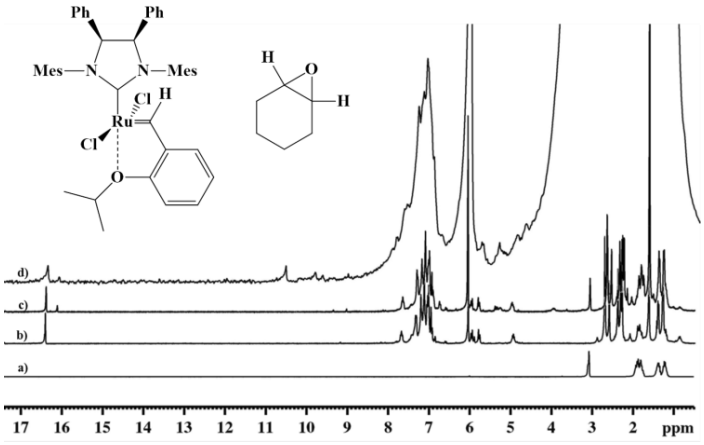

Figure II.23 *^{1}H NMR spectra of samples dissolved in 1,1,2,2-tetrachloro-ethane-d_2 (TCDE): a) cyclohexene oxide; b) $HG2_{MesPhSyn}$; c) $HG2_{MesPhSyn}$ and cyclohexene oxide in a molar ratio 1/1 treated at 140°C for 35 min; d) $HG2_{MesPhSyn}$ and cyclohexene oxide in a molar ratio 1/150 treated at 140°C for 35 min*

It is worth to note that 140°C is the maximum operating temperature for our NMR spectrometer. Spectra show all the signals characteristics of $HG2_{MesPhSyn}$ and cyclohexene oxide, highlighting that no reaction takes place between these two compounds (see spectrum of the Fig. II.23c) indicating that no thermal decomposition occurs, on the contrary of what happens with HG1 and cyclohexene oxide (Raimondo *et al*. 2015). In particular, the signal at 16.44 ppm (in TCDE) due to proton on alkylidene carbon of $HG2_{MesPhSyn}$, and the signal at 3.10 ppm attributable to protons of methine carbons of cyclohexene oxide, are clearly visible. A very small partial decomposition of the pre-catalyst occurs under the conditions of the spectrum in the Fig. II.23d (signal at 10 ppm). However, despite the very drastic chosen conditions, the signal at 16.44 ppm still remains highlighting that the initiator is active. It is worth noting that, in our previous experience, we have already observed that the epoxy mixture is less reactive than cyclohexene oxide. Furthermore, ROMP catalysts embedded in the epoxy matrix show a better thermal stability with respect to the catalysts directly treated at 140°C with cyclohexene oxide (Raimondo *et al*. 2015). On the other hand, the performed tests highlight the potential use of the synthetized catalyst in self-healing systems manufactured by a processing curing up to 180°C.

Similar experiments have been carried out by adding to the solution of ruthenium initiator the 4,40-diaminodi-phenyl sulfone (DDS). Spectra shown in Figure II.24 highlight that the synthetized initiator is not deactivated also after treatments at high temperature. In fact, spectra show all signals characteristics of $HG2_{MesPhSyn}$ and DDS and in particular the signal at 16.44 ppm (in TCDE) due to proton on benzylidenic carbon of $HG2_{MesPhSyn}$, and the signal at 4.16 ppm due to the amine protons of DDS.

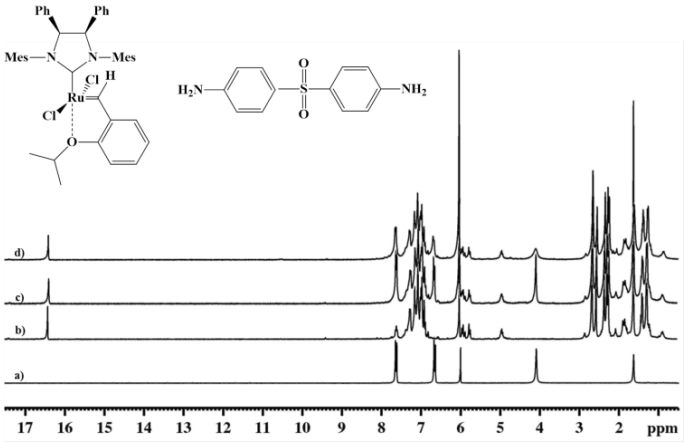

Figure II.24 *^{1}H NMR spectra of samples dissolved in 1,1,2,2-tetrachloro-ethane-d_2 (TCDE): a) DDS; b) $HG2_{MesPhSyn}$; c) $HG2_{MesPhSyn}$ and DDS in a molar ratio 1/1 at RT; d) $HG2_{MesPhSyn}$ and DDS in a molar ratio 1/1 treated at 120°C for 30 min*

Concerning the moisture sensitivity, $HG2_{MesPhSyn}$ initiator shows a behaviour similar to the HG2 complex which is tolerant to air and moisture (Scholl *et al.* 1999).

II.3.5 Control of the chemical stability of $HG2_{MesPhSyn}$ initiator in the epoxy-based mixtures

II.3.5.1 Chemical stability of the $HG2_{MesPhSyn}$ initiator in epoxy mixture assessed by metathesis test

II.3.5.1.1 Formulation EB2A

The catalytic activity of the synthetized initiator has been checked in presence of oxirane rings by FTIR investigation. Infrared spectroscopy provides a useful way to identify metathesis products and therefore initiator activity. Indeed, to verify complete dispersion and dissolution of the initiator

and its catalytic activity, infrared spectroscopic investigation has been carried out. As described in the section *II.2.2.2 Fourier Transform Infrared (FTIR) Spectroscopy*, a very similar investigation has been performed using the initiator solubilized in the form of molecular complex inside two different epoxy mixtures based on common epoxy precursors for structural applications:

a) formulation EB2A based the bi-functional epoxy precursor EPON 828
b) formulation TBD based on the tetra-functional epoxy precursor (TGMDA).

The thermal stability has been evaluated in this hostile environment up to 180°C by means of FTIR investigation. It is worth noting that, for these tests, $HG2_{MesPhSyn}$ initiator has been solubilized in the epoxy matrix EB2A at the molecular level. In particular, the epoxy specimen EB2A+0.5%$HG2_{MesPhSyn}$ has been prepared by solubilizing the $HG2_{MesPhSyn}$ initiator at concentration of 0.5% (by wt) with respect to the mixture EB2. The optical image in Figure II.25 of the cured specimen in the shape of circular disk shows the transparent mixture containing the completely dissolved initiator.

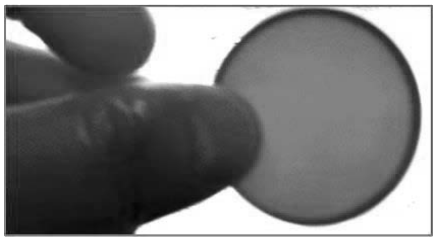

Figure II.25 *Photo of the cured specimen in the shape of circular disk*

A further evidence that the initiator is molecularly dissolved in the resin has been obtained by means of SEM investigation. The results are shown in Figure II.26, where the SEM image of the resin containing the initiator molecularly dissolved is compared to the SEM image of the resin containing the initiator in the form of solid particles.

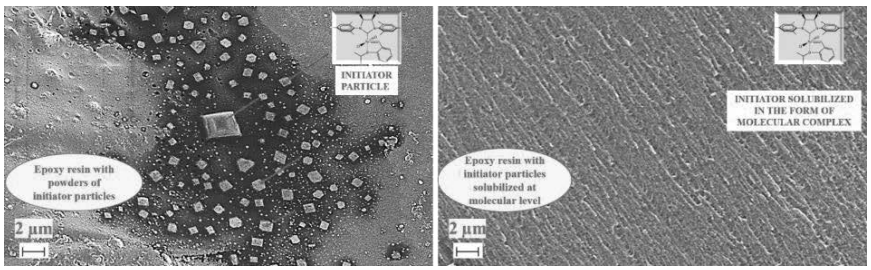

Figure II.26 *SEM images of the resin containing the initiator molecularly dissolved (on the right) and the resin containing embedded the initiator in the form of solid particles (on the left)*

As previously described, the initiator $HG2_{MesPhSyn}$ has been completely solubilized by mechanical agitation in the liquid epoxy mixture (EB2) composed of epoxy precursor (E) and reactive diluent (B). It is worth noting that the mixture has been loaded with a very low percentage of $HG2_{MesPhSyn}$ (0.5% by weight) with respect to the epoxy resin EB2. The initiator has been embedded into the EB2 formulation at the temperature of 90°C and kept at this temperature for 1 h using an oil bath until complete solubilisation. As previously described, to verify the catalytic activity, spectroscopic investigation has been carried out. For this purpose, the mixture containing initiator $HG2_{MesPhSyn}$ has been stratified on a slide for light microscopy. Subsequently, two drops (2x50 mL) of 5-ethylidene-2-norbornene (ENB) have been added to the stratified mixtures. The control of the catalytic activity has been performed by evaluating the formation of the metathesis product. For the presence of initiator $HG2_{MesPhSyn}$, a thin solid film of metathesis product has been immediately obtained. FTIR spectrum obtained for EB2+0.5%$HG2_{MesPhSyn}$ (in the form of liquid mixture) shows a peak at 966 cm^{-1} (see Fig. II.27), which is a clear indication of the formation of the metathesis product and hence of the fact that the activity of the initiator has not been compromised by the chemical nature of the oligomers, by the temperature and by the treatments of mechanical mixing.

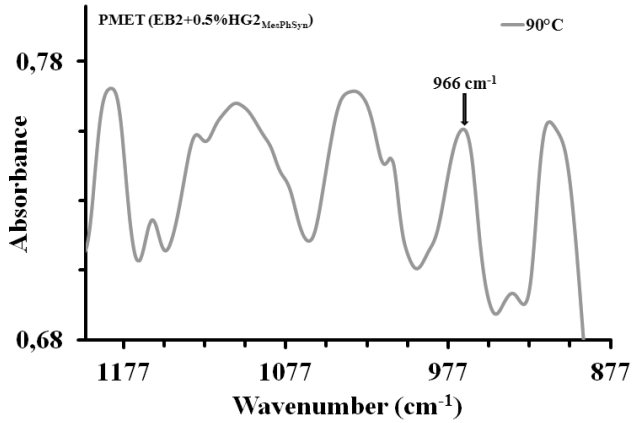

Figure II.27 *FTIR spectrum of the solid film (metathesis product) obtained by polymerization of ENB with $HG2_{MesPhSyn}$ (0.5 wt%) solubilized in the EB2 mixture at 90°C*

The highlighted peak at 966 cm^{-1} is attributable to ring-opened poly (ENB). This peak is assigned to the trans substituted alkenes, characteristic of the ring opened cross-linked product [poly(ENB)] providing evidence that the initiator is active in the ROMP reaction. Similar results have also been obtained for all the samples EB2A+0.5% $HG2_{MesPhSyn}$ cured up to 110°C, 130°C, 160°C and 180°C confirming the high thermal stability and chemical inertness of the initiator (solubilized at molecular level) towards the epoxy groups. Figure II.28 shows the FTIR spectra of the metathesis products of the cured material respectively after the intermediate stages, and the second stage carried out with the three variants stated above, to which ENB has been added in the same way as was done after the preliminary step of dissolution of the initiator.

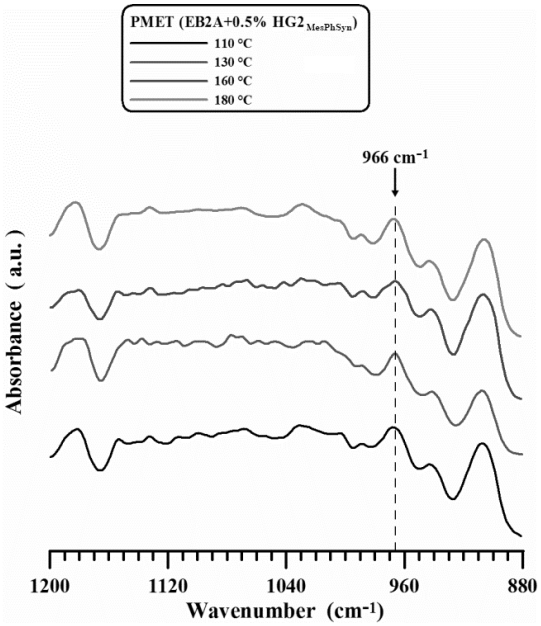

Figure II.28 *FTIR spectra of the solid film (metathesis product) obtained by polymerization of ENB with HG2$_{MesPhSyn}$ (0.5 wt%) solubilized in the EB2A mixture cured up to 180°C*

In particular, the samples EB2A+0.5%HG2$_{MesPhSyn}$ cured up to 110°C, 130°C, 160°C and 180°C have been cut by a serrated blade and the powder ENB healing agent have been added before dispersing the sample powder into the KBr disks for FTIR investigation. The presence in all cases of the peak at 966 cm^{-1}, indicating formation of the metathesis product, proves that the catalytic activity of the HG2$_{MesPhSyn}$ initiator within the epoxy matrix remain unchanged after the treatments described. It can be seen that, after the treatment at 110°C, the mixture can be cured up to 180°C for 1 h without compromising the catalytic activity of the initiator. From the FTIR spectra, we can also observe that, even for a very low percentage of initiator (0.5% by wt), HG2$_{MesPhSyn}$ shows thermal stability and chemical inertness towards the epoxy groups. The result of Figure II.28 (red spectrum) also proves that the initiator, even if in the form of molecular complex at very low amount, is active in the epoxy formulations also after curing cycles up to 180°C, which is the temperature of industrial manufacturing processes. This high chemical stability is because no equimolecular reaction between epoxy rings and initiator complex occurs during the curing cycle. In opposite to the result shown in Figure II.28, where an intense peak of the metathesis product is observed, no signal of metathesis product is observed for the sample containing HG2 initiator (see Fig. II.29), although this last sample contains an amount of initiator 10 times greater than the sample of Figure II.28 and it has been cured up to 110°C.

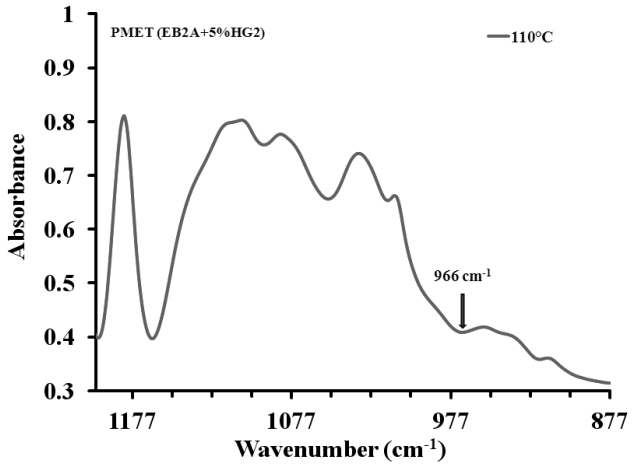

Figure II.29 *FTIR spectrum of the solid powders obtained by treatment of ENB with HG2 (5 wt%) solubilized in the EB2A mixture cured up to 110°C*

This last result highlights that the ROMP initiator (HG2) is completely deactivated even at the lower temperature of 110°C.

II.3.5.1.2 Formulation TBD

$HG2_{MesPhSyn}$ initiator-based epoxy mixture has been prepared by solubilizing $HG2_{MesPhSyn}$ initiator in the epoxy matrix TBD at the molecular level (as for the previous formulation EBA) using a very low amount of initiator, 0.5% (by wt) with respect to the mixture TB. In particular, the initiator in the epoxy specimen TBD+0.5%$HG2_{MesPhSyn}$ has been solubilized by mechanical agitation in the liquid epoxy mixture TB at the temperature of 120°C and kept at this temperature for 1 h using an oil bath. Then, the 4,4-diaminodiphenyl sulfone (DDS) curing agent (an aromatic primary amine) has been added to the transparent mixture containing the completely dissolved initiator. Subsequently, the epoxy hardener DDS has been mechanically stirred in this mixture (containing the initiator) for another hour at 120°C (which is the time for the complete solubilization of the hardener). In this case, a higher temperature has been employed with respect to the previous formulation EBA (120°C with respect to 90°C) because the DDS, in the form of fine solid powder, requires a higher temperature to completely solubilize (contrary to the ancamine, which is a liquid component). It is worth noting that until now this type of hardener has never been used before in combination with epoxy mixture containing ROMP initiators. This hardener is used to solidify materials for many industrial applications where high mechanical performance is required. To verify the

catalytic activity of this initiator, spectroscopic investigation has been carried out as mentioned before. For this purpose, the mixture containing initiator $HG2_{MesPhSyn}$ has been stratified on a slide for light microscopy. Subsequently, two drops of 5-ethylidene-2-norbornene (ENB) have been added to the stratified mixtures. In this case the control of the catalytic activity was performed by evaluating the formation of the metathesis product. A thin solid film of metathesis product has been immediately obtained. FTIR spectrum obtained for TB+0.5% $HG2_{MesPhSyn}$ shows a peak at 966 cm^{-1} (see Fig. II.30), which is an indication that the activity of the initiator has not been compromised by the chemical nature of the hardener (DDS), oligomers (TGMDA), temperature and treatment of mechanical mixing.

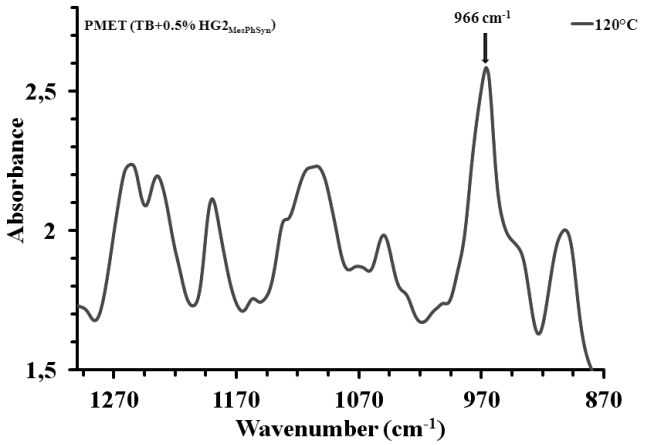

Figure II.30 *FTIR spectrum of the solid film (metathesis product) obtained by polymerization of ENB with $HG2_{MesPhSyn}$ (0.5 wt%) solubilized in the TB mixture at 120°C*

The characteristic peak at 966 cm^{-1}, attributable to ring-opened poly(ENB), highlights that the initiator is active also after 1 h at 120°C in presence of DDS. The mixture has then been cured in a two-stage process as for the formulation EB2A. Fig. II.31 shows FTIR spectrum of the metathesis product of the cured material to which ENB has then been added in the same way as was done after the preliminary step of dissolution of the initiator. The sample TBD+0.5%$HG2_{MesPhSyn}$ cured up to 180°C for 1 h has been cut by a serrated blade. The powder, which has been produced from the sample, has been collected in a mortar and 2 drops of ENB healing agent have been added before dispersing the sample powder into the KBr disks for FTIR investigation. In addition, in this case, the presence of the metathesis peak at 966 cm^{-1} proves that the catalytic activity of the $HG2_{MesPhSyn}$ initiator within the epoxy matrix remained unchanged after the treatment at 180°C.

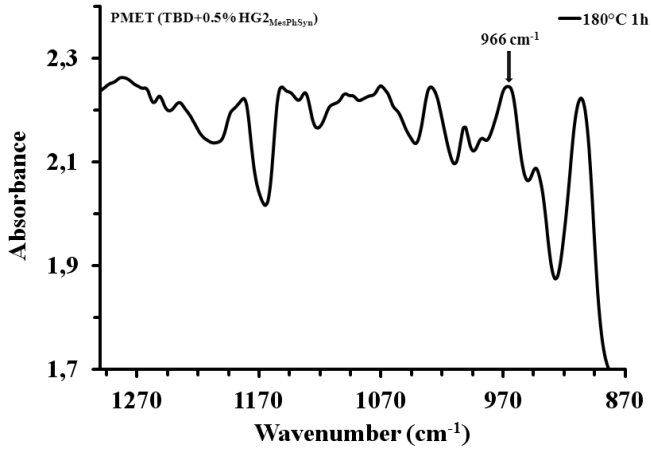

Figure II.31 *FTIR spectrum of the solid film (metathesis product) obtained by polymerization of ENB with HG2$_{MesPhSyn}$ (0.5 wt%) solubilized in the TBD mixture cured up to 180°C for 1 h*

Figure II.32 shows the comparison between the FTIR spectrum of the metathesis product of the sample TBD+0.5%HG2$_{MesPhSyn}$ cured up to 180°C for 1 h and the FTIR spectrum of the epoxy mixture TBD cured under the same conditions (without initiator). Sample TBD shows, as expected, the absence of the metathesis peak at 966 cm^{-1}, characteristic of the ring opened cross-linked product poly-ENB.

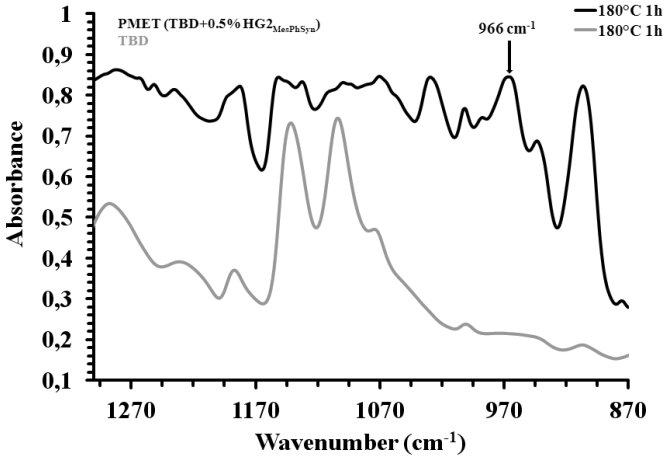

Figure II.32 *FTIR spectra of the solid film (metathesis product) obtained by polymerization of ENB with HG2$_{MesPhSyn}$ (0.5 wt%) solubilized in the TBD mixture cured up to 180°C for 1 h and of the epoxy mixture TBD cured up to 180°C for 1 h*

This comparison highlights that no peaks around 966 cm^{-1} are present in the FTIR spectrum of the cured sample (in absence of metathesis reaction), hence this peak is only due to the metathesis product. In conclusion, the initiator is active in the solid sample solidified using DDS (aromatic primary amine) which requires high temperature (up to 180°C) for the curing process. For comparison, the FTIR spectrum of the cured epoxy sample ED + HG2(10%), containing EPON 828 resin, DDS hardener and HG2 initiator (10% wt%), after the treatment with ENB is shown in Fig. II.33. Contrary to the result shown in Fig. II.31, no signal of metathesis product is observed for this sample cured up to 180°C, clearly proving that the primary aromatic diamine DDS poison the HG2 initiator responsible for the healing mechanisms.

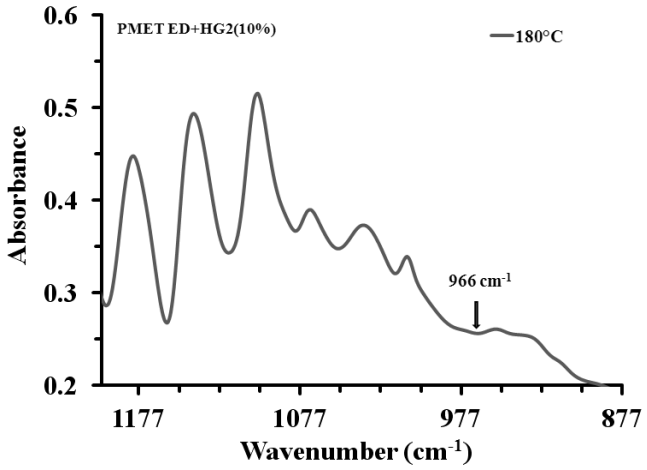

Figure II.33 *FTIR spectrum of the solid powders obtained by treatment of ENB with HG2 (10 wt%) solubilized in the ED epoxy mixture (containing DDS as hardener) cured up to 180°C for 1 h*

A similar result is obtained using HG1 initiator, as shown in the Fig. II.34. In the FTIR spectrum of the cured sample EB2+DDS+HG1(7%), after the treatment with ENB, no signal of metathesis product was found for this sample cured up to 150°C, clearly proving the evidence that the primary aromatic diamine (DDS) poisons the initiator HG1 and hence no healing mechanisms can be active after the curing cycle of the resins containing embedded the initiator.

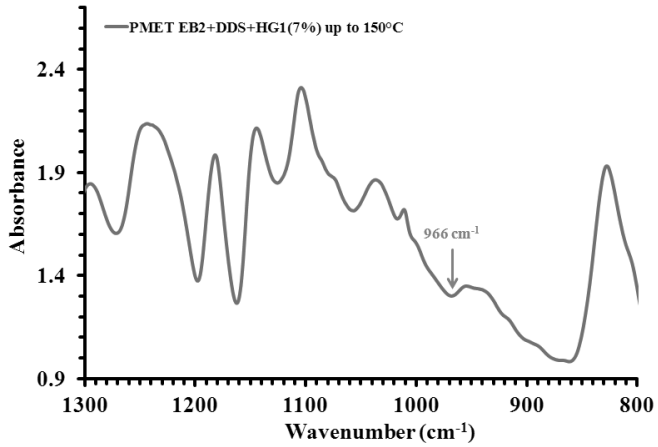

Figure II.34 *FTIR spectrum of the sample EB2+DDS+HG1(7%) cured up to 150°C after the treatment with ENB*

Similar results are obtained using G1 and G2 in combination with tetrafunctional epoxy precursors.

The fact that $HG2_{MesPhSyn}$ is active in presence of aromatic amines after curing cycles at high temperatures is an unexpected result. In fact, in spite of the fact that the implementation of ruthenium catalyzed olefin metathesis has benefitted from a broad functional group tolerance, nitrogen bases as the DDS hardener have remained challenging often-requiring initiator protection to achieve good yields with reasonable initiator loadings. In the case of the new synthetized initiator, also a very low amount of initiator is able to activate the ROMP reaction (also after the curing cycle of the resin containing embedded the $HG2_{MesPhSyn}$ initiator dispersed in the resin in the form of solubilized complex).

II.3.5.2 Chemical stability of the $HG2_{MesPhSyn}$ initiator in self-healing epoxy mixture

Complete self-healing formulations have been manufactured using the formulations EB2A and TBD with microcapsules embedded in the resins.

II.3.5.2.1 Self-healing efficiency assessed by fracture test for EB2A formulation

Values of healing efficiency η have been calculated using Eq. (II.2) (see section *II.2.2.3 Healing activity and self-healing efficiency evaluation*). Figure II.35 shows the Load–Displacement curves for the self-healing sample EB2A+0.5%$HG2_{MesPhSyn}$+18%capED cured up to 180°C. It is worth

noting that the percentage of the initiator is very low, only 0.5 wt%. It is solubilized in the epoxy matrix in the form of molecular complex as previously described. Two different cycles have been carried out, after the first closure of the crack, the sample has been kept at rest for 24 h and a first cycle has been performed after the healing of the sample. The healing has been stressed again and kept at rest for 3 h (second cycle). It has shown a healing efficiency of 94%.

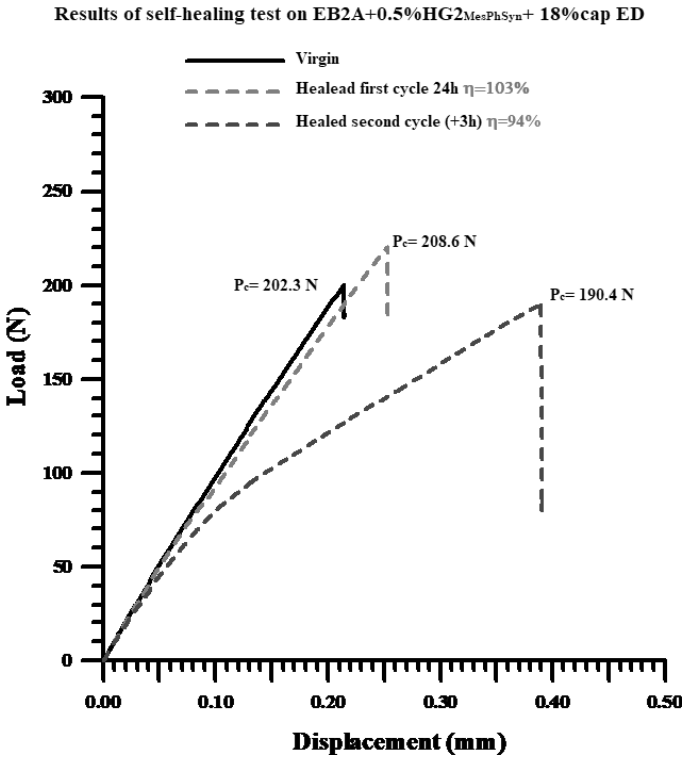

Figure II.35 *Load–Displacement curves of the virgin sample (black curve), the healed sample after the first cycle (grey curve), the healed sample after the second cycle (blue curve)*

These data highlight that many critical points relate to high performance self-healing structural materials can be avoided:

1) the thermal stability and chemical inertness towards the epoxy groups allow to use the new synthetized initiator dissolved in the resin in the form of molecular complex and then in a very low amount;

2) high temperatures during the curing cycles do not deactivate the initiator; the solubilization of the initiator, in the form of molecular complex, can enable a considerable saving on the amount of initiator to be used in the production of self-healing composite materials.

II.3.5.2.2 Self-healing efficiency assessed by metathesis test for TBD formulation

The self-healing epoxy mixture has been obtained by dispersing ENB(95%)/DCPD(5%)-filled microcapsules (cap ED) at a concentration of 16% (by wt) with respect to the mixture TB into the epoxy formulation TBD +0.5%$HG2_{MesPhSyn}$ and finally adding the hardener agent DDS thus obtaining self-healing epoxy sample TBD+0.5% $HG2_{MesPhSyn}$+16% cap ED. The self-healing epoxy mixture has been cured in a two-stage process. The first stage has been carried out at a temperature of 80°C for 3 h, while the second stage has been carried out at the higher temperatures of 180°C for 3 h. The evaluation of catalytic activity has been performed by FTIR analysis. To verify complete dispersion and dissolution of the initiator, and its catalytic activity, experimental tests have been carried out as previously described. Fig. II.36 shows the FTIR spectrum of the metathesis product of the self-healing epoxy sample TBD+0.5%$HG2_{MesPhSyn}$+16%capED cured up to 180°C for 3 h. The metathesis peak at 966 cm^{-1} can be observed also for the self-healing epoxy sample TBD+0.5%$HG2_{MesPhSyn}$+16%capED cured up to 180°C for 3 h.

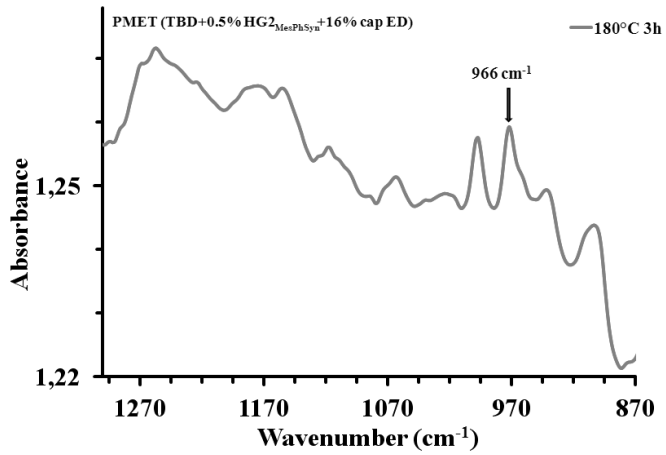

Figure II.36 *FTIR spectrum of the metathesis product of the self-healing epoxy sample cured up to 180°C for 3 h*

This important result indicates that the catalytic activity of $HG2_{MesPhSyn}$ is preserved in the resin also in the presence of microcapsules after very critical curing cycles. The example related to this last formulation highlights that the initiator is active in the sample solidified using DDS (aromatic primary amine) and containing vessels filled with the healing agent. In this case, the vessels are in the form of microcapsules containing a blend of ENB/DCPD, which is active also at very low temperature. The cure degree, calculated by thermal analysis, of the sample TBD+0.5%$HG2_{MesPhSyn}$+16%capED cured up to 180°C for 3 h has been found to be 94% as that of structural resins characterized by high mechanical performance targeted for aeronautical application (Guadagno *et al.* 2014c).

The FTIR spectrum of this sample, in the spectral range of 2500–3800 cm^{-1} (see Fig. II.37) shows the absence of the two weak absorption bands (N-H stretching vibrations, one at 3471 cm^{-1} and the other near 3373 cm^{-1}). These bands represent, respectively, the "free" asymmetrical and symmetrical N-H stretching modes".

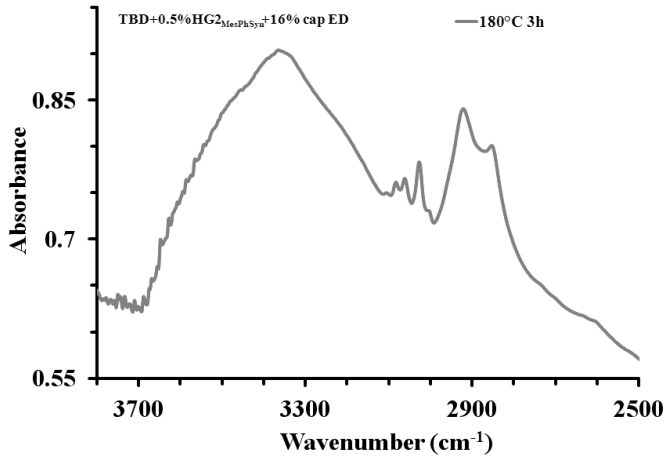

Figure II.37 *FTIR spectrum of the metathesis product of the self-healing epoxy sample cured up to 180°C for 3 h in the wavenumber range of 3800–2500 cm^{-1}*

The absence of these signals proves that the sample is almost completely cured as also evidenced by thermal analysis. This is a very relevant result because a high curing degree is usually required for structural application. The new synthetized initiator has proven to be active also inside an epoxy formulation hardened up to 200°C.

The evaluation of healing efficiency by TDCB fracture test was not performed for the formulation based on the TGMDA epoxy precursor, due to the high rigidity of the matrix, which did not allow the control of fracture

propagation along the centerline of the sample, and therefore the correct execution of the test.

The need to tackle this problem was one of the reasons that led to the development of new formulations, based on a tetra-functional epoxy precursor, toughened by the addition of an elastomeric phase, as discussed in the Chapter III.

II.3.6 Role of the stereochemistry on the self-healing efficiency

II.3.6.1 Introduction

In this section the study of $HG2_{MesPhAnti}$ catalyst activity has been performed. The results have been compared with those related to HG2MesPhSyn. The metathesis tests have been performed by FTIR investigation.
The purpose of this investigation is to study the role of the stereochemistry of two new ruthenium catalysts on the self-healing efficiency of aeronautical resins.

A detailed evaluation on the stereochemistry evidences the crucial role of the spatial orientation of phenyl groups in the N-heterocyclic carbene ligands in determining the temperature range within the curing cycles is feasible without deactivating the self-healing mechanisms (ROMP reactions) inside the thermosetting resin. In fact, while the $HG2_{MesPhSyn}$ complex, with the *syn*-orientation of the phenyl groups, is able to activate metathesis reactions within the highly reactive environment of the epoxy thermosetting resins, cured up to 180°C, the other stereoisomer, with the *anti*-orientation of the phenyl groups, does not preserve its catalytic activity in these conditions.

In this section, a comparison between the self-healing functionality of two catalytic systems, performed using metathesis tests and FT-IR spectroscopy, will be discussed.

The synthesis of the $HG2_{MesPhAnti}$ catalyst has been realized through the same reaction steps already described for the synthesis of the $HG2_{MesPhSyn}$ (see sections *II.2.1.3 Synthesis of $HG2_{MesPhSyn}$ initiator* and ***II.3.1** Synthesis and characterization of $HG2_{MesPhSyn}$ initiator*). The synthesis differs only for the use of a different amine as a reagent in the first step, that is (1*R*,2*R*)-1,2-diphenylethylenediamine (shown in the Fig. II.15 and indicated with the symbol A) in place of meso-1,2-diphenylethylenediamine. Furthermore, all reaction intermediates were characterized by NMR spectroscopy, as previously mentioned (see section *II.3.1 Synthesis and characterization of $HG2_{MesPhSyn}$ initiator*).

Here, for clarity, it is shown only the spectra of the final product, $HG2_{MesPhAnti}$ catalyst (see Fig. II.38 and Fig.39)

NMR characterization: ^{1}H NMR (300 MHz, CD_2Cl_2): δ 1.18 (d, 6H), 1.93 (s, 6H), 2.31 (s, 3H), 2.39 (s, 3H), 2.68 (s, 3H), 2.88 (s, 3H), 4.87 (m, 1H), 5.86 (s, 2H), 6.84 – 7.57 (ArH, 18H), 16.35 (s, 1H).

^{13}C NMR (100 MHz, CD_2Cl_2): δ 14.38, 19.51, 21.57, 28.14, 30.40, 35.94, 73.37, 74.52, 75.68, 113.50, 122.84, 129.03, 129.73, 129.83, 130.14, 130.27, 145.80, 152.57, 214.55, 298.32.

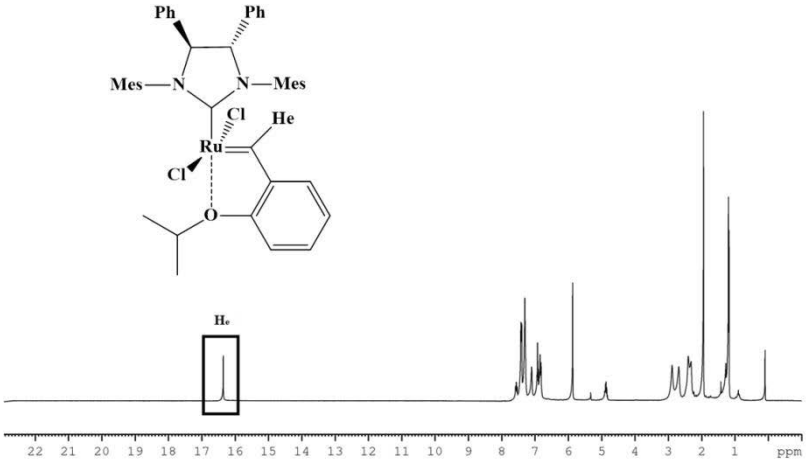

Figure II.38 *^{1}H NMR (300 MHz, CD_2Cl_2) of $HG2_{MesPhAnti}$*

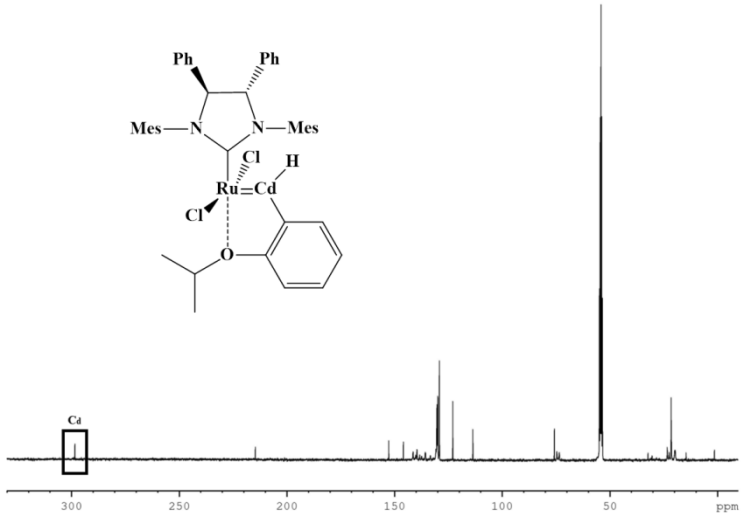

Figure II.39 *^{13}C NMR (100 MHz, CD_2Cl_2) of $HG2_{MesPhAnti}$*

The signal at 16.35 ppm, in the ^{1}H NMR spectrum, is due to the benzylidenic proton (H_e), whereas the signals at 298.32 and 214.55 ppm, in

the ^{13}C NMR spectrum, are due to the benzylidenic carbon (C_d), and the carbene of the imidazole group, respectively.

II.3.6.2 Metathesis tests and FTIR investigation

The Ring Opening Metathesis Polymerization (ROMP) activity of $HG2_{MesPhAnti}$ within the epoxy mixture, according to the reaction previously shown in Figure II.21, was evaluated by metathesis tests and spectroscopic investigation.

The two synthetized complexes only differ for the spatial orientation of the phenyl groups in the N-heterocyclic carbene ligand (see Fig. II.40). It is clearly observable that $HG2_{MesPhSyn}$ catalyst has the phenyl groups on the backbone oriented on the same side of the plane on which the carbene ligand lies (see Fig. II.40a); while the $HG2_{MesPhAnti}$ catalyst has the phenyl groups oriented, respectively, one on this plane and the other on the opposite side ((see Fig. II.40b) (Costabile and Cavallo 2004; Perfetto *et al*., 2013, 2014).

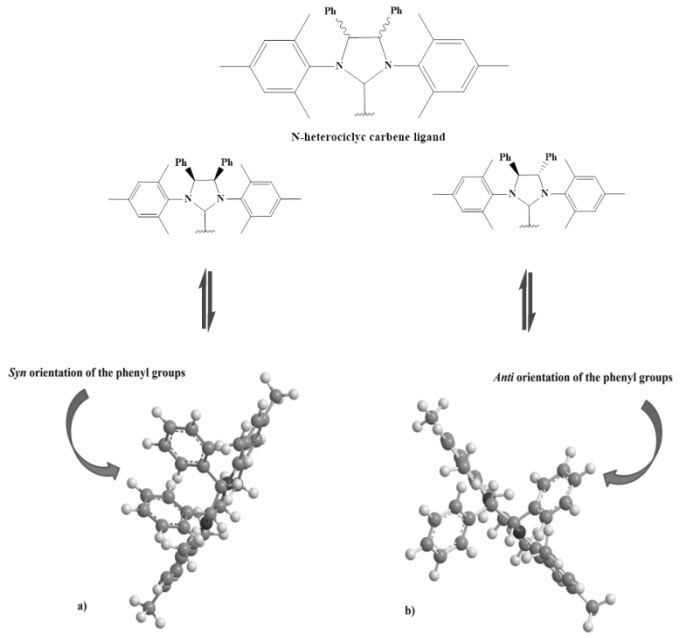

Figure II.40 *Rappresentation of the spatial orientation of the phenyl groups in the N-heterocyclyc carbene ligand for $HG2_{MesPhSyn}$ (a) and $HG2_{MesPhAnti}$ (b) catalysts*

The ROMP activity was evaluated by solubilizing the catalyst at molecular level within the EB2A epoxy mixture, according to the already

described experimental procedure (see section II.3.5.1.1 *Formulation EB2A*), at concentration of 0.5% (by wt) with respect to the EB2 blend, obtaining the sample EB2A+0.5%$HG2_{MesPhAnti}$.

The first metathesis test was performed by adding few drops of self-healing liquid monomer, 5-ethylidene-2-norbornene/dicyclopentadiene (ENB), on a small amount of the EB2+0.5%$HG2_{MesPhAnti}$ mixture, heated at 90°C and layered on a slide for optical microscopy. The blend containing the catalyst, produced the polymeric film of poly-ENB, shown in Fig. II.41 and characterized by FTIR spectroscopy.

Figure II.41 *Polymeric film of the metathesis product poly-ENB*

All the proposed spectra show the comparison between the spectrum of the sample containing the catalyst $HG2_{MesPhAnti}$ and that of the sample containing the catalyst $HG2_{MesPhSyn}$, performed in the same conditions, in order to fully understand the different behaviour of the two initiators.

The FTIR spectra (see Fig. II.42) indicate the presence of the characteristic metathesis peak at 996 cm^{-1} confirming the formation of the polymeric product poly-ENB and highlighting that both catalysts preserve their activity within the EB2 epoxy blend after heating up to 90°C.

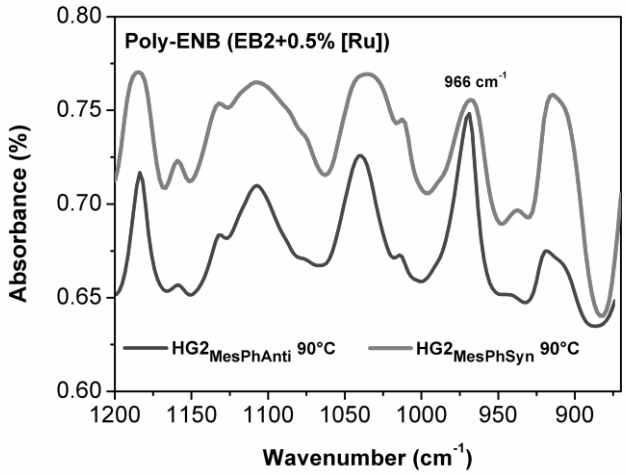

Figure II.42 *FTIR spectra of the polymeric films obtained by treatment of ENB with Ruthenium catalyst (0.5% wt%) solubilized in the EB2 mixture heated at 90°C*

The symbol [Ru] is the generic way used to indicate the two-ruthenium complex $HG2_{MesPhSyn}$ and $HG2_{MesPhAnti}$.

The subsequent metathesis test was carried out by adding few drops of the liquid monomer on the collected powders of the solid epoxy mixture EB2A+0.5%$HG2_{MesPhAnti}$, cured up to 110°C. FTIR spectra, shown in Figure II.43, confirm that both catalysts preserve their activity also after a curing cycle up to 110°C.

In fact, in the FT-IR spectra of the epoxy mixture containing $HG2_{MesPhAnti}$ and $HG2_{MesPhSyn}$, respectively, it is possible to observe the peak of the metathesis product-around 970 cm^{-1} characteristics of double *trans* bonds in the polymer chain.

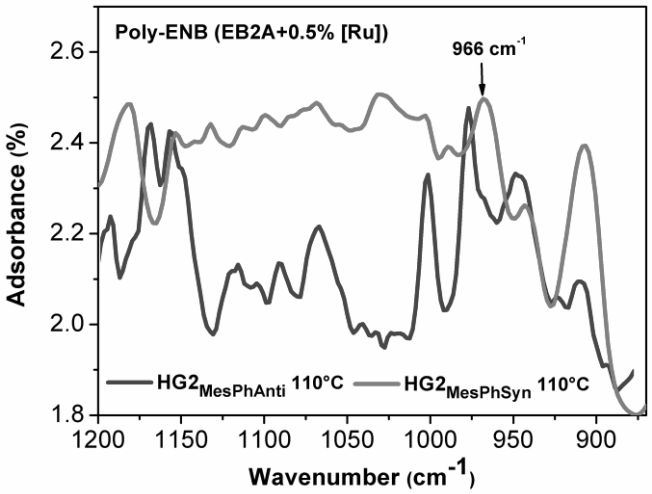

Figure II.43 *FTIR spectra of the solid powders obtained by treatment of ENB with Ruthenium catalyst (0.5% wt%) solubilized in the E2BA mixture cured up to 110°C*

The same procedure was followed for the metathesis test performed on the epoxy mixture EB2A+0.5%$HG2_{MesPhAnti}$, cured up 130°C, and this test highlighted the loss of activity by the $HG2_{MesPhAnti}$ ruthenium catalyst. In fact, FTIR spectrum shown in Figure II. 44 (blue curve) highlights the absence of the characteristic metathesis peak at 966 cm^{-1}. In comparison, the spectrum related to the blend containing the $HG2_{MesPhSyn}$ shows the metathesis peak, confirming the preservation of its activity.

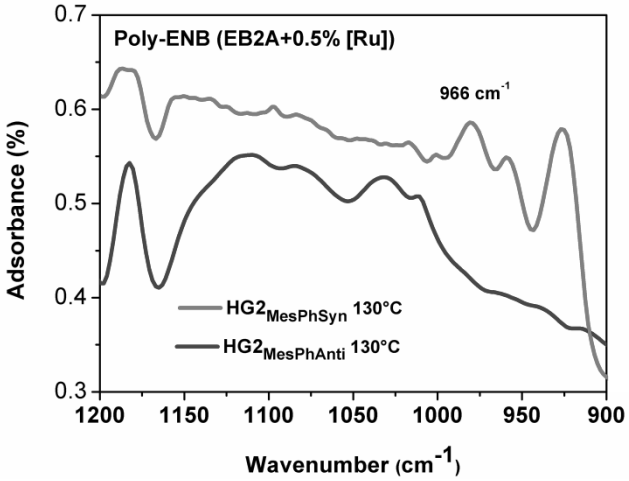

Figure II.44 *FTIR spectra of the solid powders obtained by treatment of ENB with Ruthenium catalyst (0.5% wt%) solubilized in the EB2A mixture cured up to 130°C*

These results are certainly due the higher thermal and chemical stability of the $HG2_{MesPhSyn}$ complex, which does not decompose within the highly reactive environment of the epoxy resins suitable to impregnate carbon fiber reinforced panels for structural applications.

The histogram in Figure II.45 summarizes the results obtained on the activity of the two catalysts in the resin as a function of the treatment temperature.

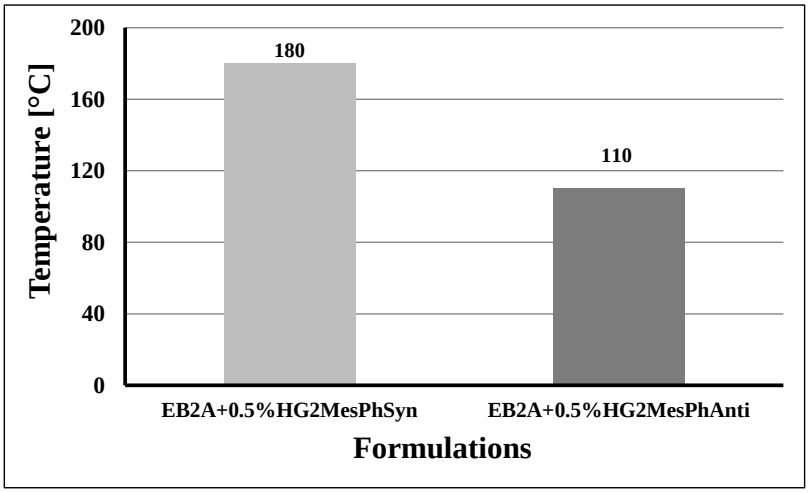

Figure II.45 *Histogram related to the activity of the catalysts as a function of the treatment temperature*

The catalyst with *syn* spatial orientation of the phenyl groups, $HG2_{MesPhSyn}$ catalyst, due to the very promising results, has been chosen between the two analyzed catalysts to formulate self-healing epoxy samples solidified using higher temperature for the curing cycle, as discussed in the previous section *II.3.5.2 Chemical stability of the initiator in self-healing epoxy mixture*.

II.4 Conclusion

The industrial need for "cost cutting" makes self-healing resins, based on commercial ruthenium initiators, untempting products. A reduction of material costs and the possibility to apply the ROMP initiators in epoxy resins aimed at manufacturing load-bearing structures is a relevant step to fulfill current industrial requirements.

During this research activity the synthesis of the initiator $HG2_{MesPhSyn}$ was performed. It is characterized by high thermal stability and tolerance towards the epoxy groups and the aromatic primary amines. The $HG2_{MesPhSyn}$ initiator has proven to be active in the synthesis in situ of polymers (PN/NB) inside thermosetting resins characterized by improved mechanical performance.

Furthermore, in the field of design of catalytic systems for self-healing structural materials, another very relevant result has been found: a slight difference in the molecular stereochemistry plays a key role in the development of self-healing materials for aeronautical and aerospace applications. The different spatial orientation plays a relevant influence on the activity of the catalyst within the epoxy resins and therefore the stereochemistry has to be taken in high consideration before to formulate structural self-healing resins. In fact, as here described and discussed, $HG2_{MesPhSyn}$ complex, which has a *syn* orientation of the phenyl groups, has proven to be very effective in the activation of ROMP reactions, being able to preserve its catalytic activity within aeronautical epoxy mixtures, also after curing cycles up to 180°C, which are typical of aeronautical industries.

Figure II.46 shows the design of the self-healing material. The autorepair mechanism is based on ROMP reaction of healing agent (DCPD/ENB) activated by the $HG2_{MesPhSyn}$ initiator solubilized in the form of molecular complex in the epoxy matrix.

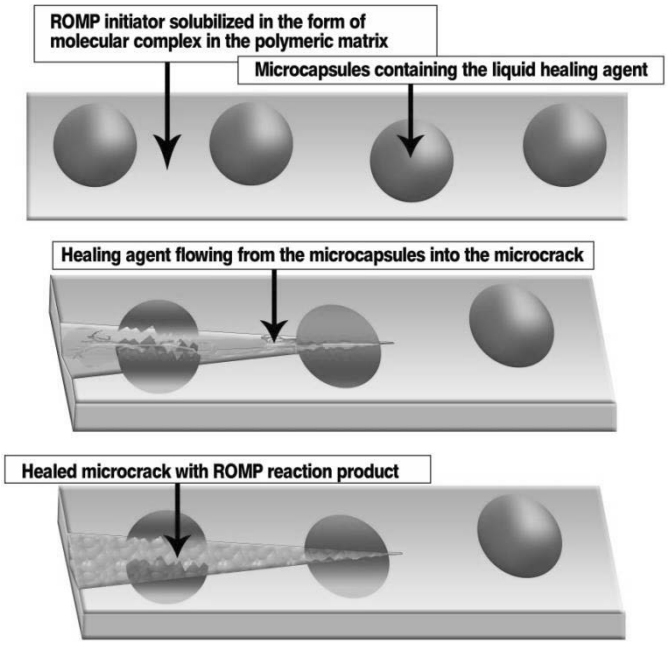

Figure II.46 *Design of the self-healing material*

The $HG2_{MesPhSyn}$ initiator, solubilized in the form of molecular complex, has proven to be active in structural resins hardened with aromatic primary amines (es. DDS) after curing cycles up to 180°C as those planned for high structural materials (aeronautical, naval or infrastructural etc.). One of the most relevant results concerning the use of $HG2_{MesPhSyn}$ is the possibility to reduce its percentage from 5% wt/wt to 0.5% wt/wt in self-healing resins. The stability at high temperatures in presence of aromatic primary amines allows to use $HG2_{MesPhSyn}$ in epoxy resins aimed at building load-bearing structures with the relevant advantage to reduce its percentage of 90% and hence the cost related to the self-healing materials of about 79% (compared to the material containing 5% wt/wt of HG1). The possibility to use the initiator solubilized in the form of molecular complex inside epoxy mixtures also allows high performance in the self-healing function (the ROMP reaction is activated whenever the healing agent contacts the matrix where the damaged capsule is embedded and not only when the healing agent contacts the initiator particles). It is worth noting that, in the field of structural composites, solutions able to overcome shortcomings related to the microencapsulated systems will also allow to fulfil other requirements of structural materials without additional costs. For instance, the inclusion of microcapsules in CFRCs (self-healing aeronautic laminates) aimed at imparting self-healing ability, is of relevant benefit also for the very appreciable damping performance of these kind of self-healing composites

compared to standard CFRC composites (Viscardi *et al.* 2016). This peculiar property of the microencapsulated systems further allows reducing the cost related to the noise/vibration control of aircraft structures. The synthetized initiator can pave the way towards the rational design of practically relevant applications in the field of self-healing multifunctional structural materials.

Chapter III
Supramolecular self-healing system based on functionalized MWCNTs

III.1 Introduction

The purpose of this chapter is to explore an alternative strategy for the integration of auto-repair mechanisms within structural composites, allowing the simultaneous transfer of other fundamental functionalities for the application of such materials.

Recently, new results have been achieved through different approaches falling within the domain of the supramolecular chemistry (Cheng *et al.* 2015). Selected supramolecular polymers, based on fourfold hydrogen bonding units, show self-healing capability as an intermediate layer in between plies of fiber reinforced composites (Sordo and Michaud 2016) In thermoplastic materials, functionalization of both matrix and fibers with this reversible binding unit enables the interfaces to re-bond spontaneously or at moderate temperature after damage (Amamoto *et al.* 2012; Herbst *et al.* 2013; Deng *et al.* 2015; Campanella *et al.* 2018). Polymer networks based on reversible covalent bonds manifest the benefits to be self-healed, remolded, and recycled through reshuffling and rearrangement of cross-linkages (Tian *et al.* 2009; Montarnal *et al.* 2011; Deng *et al.* 2012; Lu and Guan 2012; Michal *et al.* 2013; Yu *et al*. 2013; Brutman *et al.* 2014; Rekondo *et al*. 2014; Roy *et al.* 2014; Yuan *et al.* 2014; Cromwell *et al.* 2015; Denissen *et al.* 2015; Fortman *et al.* 2015; Imato *et al.* 2015; Ji *et al.* 2015; Obadia *et al.* 2015; Lai *et al.* 2016; Liu *et al.* 2017; Xu *et al*. 2016; ; Zhang Y. *et al.* 2016; Zhang Z. P. *et al.* 2016, 2018). These systems are usually characterized by repeatable and autonomous self-healing capability, which are interesting features for real applications.

In the perspective to find effective technical solutions, it is also important to consider recent developments in the field of nanotechnologies, where new

possibilities to simultaneously increase thermal and electrical conductivity, flame resistance, and durability in a single multifunctional polymer are foreseen (Guadagno et al. 2015a, 2015b, 2015d, 2015e, 2017a; Naddeo *et al.* 2017; Raimondo *et al.* 2018). In addition, the combination of self-healing functions with damage diagnosing based on piezoresistivity of carbon-based nanocomposites, can achieve timely healing autonomously, and it is expected to improve the reliability of materials (Pu *et al.* 2018). A variety of nanometric fillers has been dispersed in a wide spectrum of material to improve barrier properties, conductivity, and processability of thermoplastic and thermosetting polymers (De Santis and Pantani 2015; Sordo et Michaud 2016; Guadagno *et al.* 2018). The small size of the fillers leads to a dramatic increase of the interfacial area, which determines a significant volume fraction of interfacial polymer with properties different from the bulk polymer even at very low loadings (Guadagno *et al.* 2015f). Hybrid materials based on carbon nanostructured forms have been prepared to introduce self-healing mechanisms or impart other different functionalities (Shaygannia *et al.* 2015; Liu et al. 2018; Vertuccio *et al.* 2018; Guadagno *et al.* 2017d; Noack *et al*. 2017).

The research activity presented and discussed in this chapter is aimed to integrate self-healing ability, combined with other functionalities, in a single load-bearing material. Moieties able to act as hydrogen bond donors and acceptors at the same have been covalently bonded to MWCNT walls (see Fig. III.1).

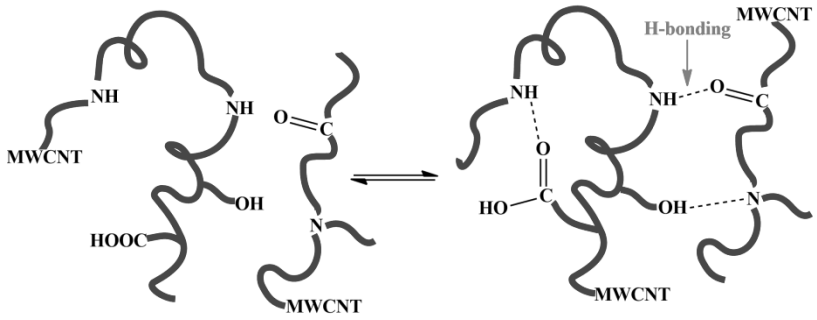

Figure III.1 *Moieties able to act as hydrogen bond donors and acceptors covalently bonded to MWCNT walls*

The reversibility of the opening and closing of hydrogen bonds enables a dynamic repetition of the repair events even at the same area, which is a well-known phenomenon in materials (Campanella *et al.* 2018; Herbst *et al.* 2013).

MWCNTs were functionalized with thymine (MWCNT-t) and barbituric (MWCNT-b) acid-based ligands via copper(I)-catalyzed alkyne/azide cycloaddition (CuAAC) “click” reaction. The functionalized carbon

nanotubes (MWCNT-t and MWCNT-b) have been embedded through sonication in an aeronautical epoxy formulation toughened *via* reaction between epoxy groups of tetraglycidyl methylene dianiline (TGMDA) and COOH groups of a liquid rubber carboxyl-terminated butadiene acrylonitrile (CTNB).

The performed functionalization is responsible for MWCNTs-bridges through the epoxy matrix due to strong attractive interactions between the rubber phase and MWCNT walls. For both functional groups, barbiturate and thymine-based moieties, self-healing efficiencies higher than 50% have been found. Hardener and components employed to design the here described self-healing nanocomposites are typical of load-bearing structures and therefore, suitable to formulate self-healing materials preserving the characteristics of mechanical properties of highly performant structures.

Furthermore, covalently functionalized MWCNTs can improve the nanofiller dispersion, as already found in literature for carbon nanotubes (Guadagno *et al.* 2011a; Ma *et al.* 2007, 2010; Lavorgna *et al*. 2013).

III.2 Experimental section

III.2.1 Materials

III.2.1.1 Preparation of epoxy matrices

III.2.1.1.1 Preparation of epoxy matrix TCTBD

The epoxy mixture was obtained by mixing the epoxy precursor tetraglycidyl methylene dianiline (TGMDA-acronym T) with 12.5 phr of carboxyl-terminated butadiene acrylonitrile (CTNB-acronym CT) and 10 phr of the catalyst triphenylphosphine (PPh_3). The chemical formulas of the liquid rubber CTNB and of the catalyst PPh_3 are shown in Figure III.2, while that of TGMDA has already been shown in figure II.4.

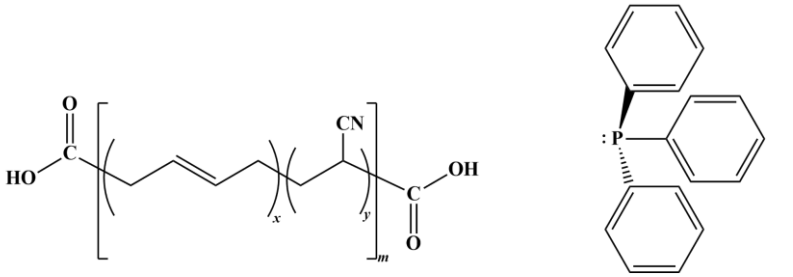

Carboxyl-terminated butadiene acrylonitrile (CTNB) **Triphenylphosphine (PPh_3)**

Figure III.2 *Chemical formulas of CTNB and PPh_3*

This mixture was heated at 170°C, using an oil bath and mechanical agitation promoted by an electric stirrer, for 24 h. The reaction related to the formation of the TGMDA-CTNB pre-polymer is shown in Figure III.3. The triphenylphosphine is used as a pre-reaction catalyst to promote the reaction between the epoxy groups and the carboxylic acid groups of the CTNB copolymer. In the first step, the nucleophilic attack by triphenylphosphine on the carbon of the oxirane ring causes its opening, producing then a phosphonium salt. The carboxylic anion reacts with the electrophilic carbon attached to the positive phosphorus, regenerating the catalyst PPh_3 and producing the TCT modified precursor, as shown in the second step of Figure III.3.

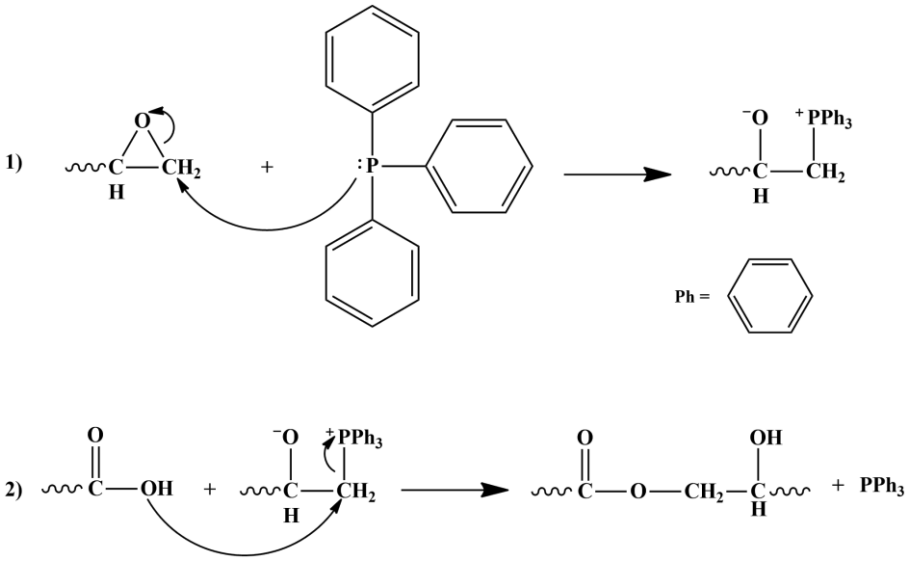

Figure III.3 *Reaction scheme showing the reaction between epoxy group of TGMDA and COOH group of CTNB*

The obtained TCT was cooled at 120°C and the reactive epoxy diluent 1,4-butanedioldiglycidylether (BDE-acronym B, for the chemical formula see Fig.II.4) was added at a concentration TGMDA/BDE of 80%:20% by wt, obtaining the mixture TCTB. An amount of curing agent 4,4′-diaminodiphenyl sulfone (DDS-acronym D, for the chemical formula see Fig.II.4) of 55 phr with respect to precursor TGMDA was added to the mixture TCTB to activate the curing reactions, obtaining the epoxy mixture TCTBD. The epoxy TCTBD was mixed at 120°C for 1 h and was degassed afterwards in vacuum at 100 °C for 1 h. The mixture was cured by a two-stage curing cycles: a first isothermal stage at the lower temperature of 125°C for 1 h followed by a second isothermal stage at the higher temperatures of 200°C for 3 h.

III.2.1.1.2 Preparation of epoxy matrix TCTBD charged with functionalized and unfunctionalized MWCNTs

Functionalized and unfunctionalized MWCNTs were added and incorporated in the matrix TCTBD by using an ultrasonication for 20 min (Hielscher model UP200S-24 kHz high power ultrasonic probe) in order to obtain a homogeneous dispersion. All the mixtures were cured by a two-stage curing cycles: a first isothermal stage at the lower temperature of 125°C for 1 h followed by a second isothermal stage at the higher temperatures of 200°C for 3 h (as already done for the unfilled formulation).

III.2.1.2 Synthesis of functionalized MWCNTs

III.2.1.2.1 Preparation of ethyl-2-(1-pentyn-5-yl) barbituric acid (1)

All synthetic steps were carried out under dry and inert conditions using common Schlenk techniques unless noted. In the first step ethyl-2- (1-pentyn-5-yl)malonate was prepared by adding a sodium hydride dispersion in mineral oil (60.00 mmol; 2.40 g) to dry DMF (25 mL), followed by the dropwise addition of diethyl ethyl-malonate (50.00 mmol; 9.4 mL) over a period of 30 min. The mixture was stirred for 1 h till the evolution of hydrogen had ceased. To the resulting oil solution 5-chloro-1-pentyne (50 mmol; 5.30 mL) was added and the mixture was stirred for 20 h at 65°C. Distilled water (75 mL) was added and the solution was extracted three times with diethyl ether (3x 100 mL). The combined ether portions were washed with distilled water (300 mL), dried over Na_2SO_4, filtered and the solvent was removed at a rotary evaporator. The crude product was purified by distillation (74–76°C; 2 mbar) to yield 8.01 g (31.49 mmol; 63.0%) of 2-ethyl-2-(1-pentyn-5-yl) malonate as a clear, colorless oil. In a second step urea (1260 mmol; 75.68 g) was dissolved in dry DMSO (250 mL) and potassium tert-butoxide (64.00 mmol; 7.2 g) was added, followed by the addition of 2-ethyl-2-(1-pentyn-5-yl)malonate (31.50 mmol; 8.01 g) as a solution in dry DMSO (10 mL). The resulting mixture was stirred at room temperature for 24 h. Distilled water (1000 mL) was added and the pH was adjusted to 10 by means of a 1M NaOH solution. The aqueous layer was extracted two times with diethyl ether (2x 500 mL). The diethyl ether portions were discarded. The pH of the aqueous layer was adjusted to 2 by means of a 1M HCl solution and extracted two times with diethyl ether (2x 500 mL). The diethyl ether fractions were combined, washed with distilled water (500 mL), dried over Na_2SO_4 and filtered. The solvent was removed by means of a rotary evaporator. Finally, the crude product was purified by crystallization from boiling benzene to yield 2-ethyl-2-(1-pentyn-5-yl)barbituric acid (1) (see Fig. III.9 in the section *III.3.1 Functionalization of MWCNTs*) of a white powder (74.6%).

H-NMR characterization: ^{1}H NMR (400 MHz, DMSO-d_6, at 27 °C, δ): 11.52 (s, 2H, H_a), 2.76 (t, 1H, H_b, $^{4}J_{H,H}$=2.62 Hz), 2.12 (dt, 2H, H_c, $^{4}J_{H,H}$=2.63 Hz), 1.89–1.80 (m, 4H, $H_{d,e}$), 1.26 (m, 2H, H_f), 0.74 (t, 3H, H_g, $^{3}J_{H,H}$=7.42 Hz) (see Fig. III.4).

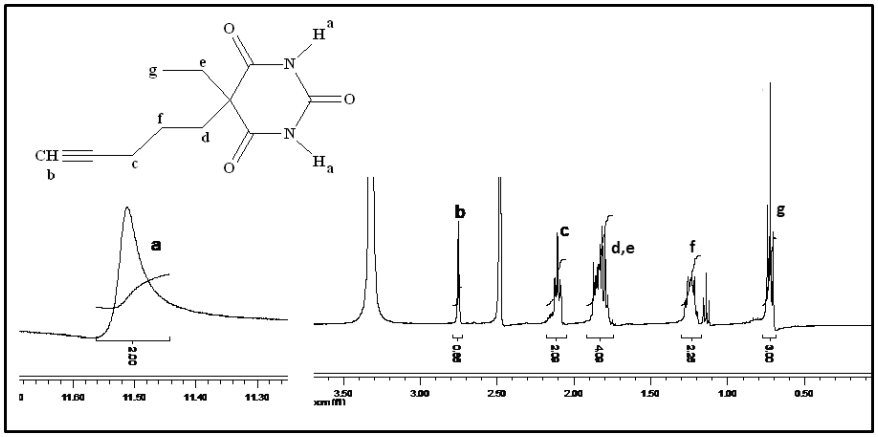

Figure III.4 *^{1}H-NMR spectrum of the ethyl-2-(1-pentyn-5-yl)barbituric acid*

III.2.1.2.2 Preparation of 1-(6-azidohexyl) thymine (2)

1-(6-bromohexyl) thymine (665 mg, 2.5 mmol) and sodium azide (195 mg, 3.0 mmol) were refluxed in acetonitrile for 18 h. The obtained solid was separated by filtration and the solution was concentrated to a gum, which slowly crystallized. The material was recrystallized from water and afforded 1-(6-azidohexyl) thymine (2) (see Fig. III.9 in the section *III.3.1 Functionalization of MWCNTs*) (76%).
H-NMR characterization: ^{1}H NMR (400 MHz, DMSO-d_6, J (Hz), at 27 °C, δ): 11,1 (s, 1H, H_a); 7,5 (s, 1H, H_b); 3,6 (t, 2H, ^{3}J (H,H)=7,47, H_c); 2,7 (t, 2H, ^{3}J (H,H)= 7,89; H_d); 1,7 (s, 3H, H_e); 1,5 (m, 4H, H_{f-g});1,3 (m, 4H, H_{h-i}). (see Fig. III.5).

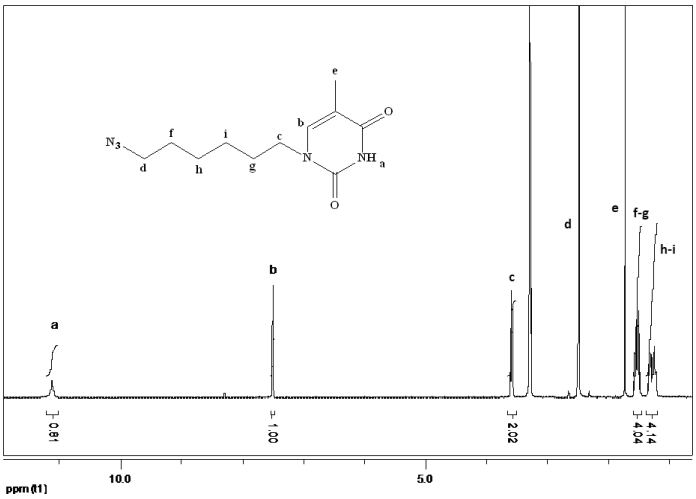

Figure III.5 *^{1}H- NMR spectrum of the 1-(6-azidohexy) thymine*

III.2.1.2.3 Preparation of alkyne modified MWCNTs (5)

Pristine MWCNTs (Nanocyl™ CN3101; 1 g) (3) were dispersed by ultrasonication in an aqueous HNO_3 solution (60 wt%, 40.0 mL) and stirred subsequently for 2 h under reflux. The suspension was afterwards filtered through a poly (tetrafluoroethylene) (PTFE) membrane and washed with distilled water until the pH of the filtrate was 7. The treated MWCNTs were dried under vacuum for 24 h at 40°C, yielding the carboxyl-functionalized MWCNTs (4) (0.95 g). In a second step, carboxyl-functionalized MWCNTs (4) (0.10 g) was suspended in $SOCl_2$ (10 mL) and stirred at 65°C for 24 h. After the excess $SOCl_2$ was removed under reduced pressure, the flask was cooled in an ice bath and a mixture of propargyl alcohol (1 mL, 16.9 mmol), $CHCl_3$ (2 mL), and anhydrous triethylamine (1 mL, 7.17 mmol) was added dropwise into the flask over a period of 0.5 h under magnetic stirring. The mixture was stirred for 1 h at 0°C and then for 24 h at room temperature. The

product was filtered through a PTFE membrane under vacuum, and the filter cake was washed with THF and distilled water for several times. The obtained alkyne modified MWCNTs (5) (see Fig. III.10 in the section *III.3.1 Functionalization of MWCNTs*)) were dried under vacuum at 25°C for 48 h.

The loading of the alkyne onto surface of MWCNTs was determined *via* TGA to 1.3×10^{-2} $mmol_{alkyne}/mg_{sample}$ (not shown here).

III.2.1.2.4 Preparation of thymine functionalized MWCNTs (6)

In a typical experiment, alkyne modified MWCNT (5) (50.0 mg) was dispersed in DMF/THF mixture using water bath sonicator. The sonication process has been chosen because it has proven to be a very effective method to obtain an optimal dispersion (Guadagno *et al.* 2010b; Martone *et al.*

2012). Afterwards the mixture was bubbled with nitrogen for 10 min, and 1-(6-azidohexyl) thymine (2) (500 mg), CuBr (120 mg, 0.8 mmol) as well as PMDETA (16 µL, 0.8 mmol) were added and stirred at 70°C for 24 h. The mixture was diluted with DMF (100 mL), sonicated for 5 min, and filtered through a PTFE membrane. After washing with THF, the obtained thymine functionalized MWCNTs (6) (see Fig. III.9 in the section *III.3.1 Functionalization of MWCNTs*) were dried under vacuum at 25°C for 48 h. The loading of the thymine onto the surface of MWCNTs was determined *via* TGA to 7.4×10^{-4} $mmol_{thymine}/mg_{sample}$ (see Fig. III.16 section III.3.2.2.3 Evaluation of the amount of functional groups bonded to MWCNT *via* of TGA analysis). The thymine functionalized MWCNTs are named with the acronym MWCNT-t.

III.2.1.2.5 Preparation of azide functionalized MWCNTs (8)

MWCNTs (Nanocyl™ CN3101; 50 mg) (3) were dispersed in DMF (5 mL) by sonication. 2-Chloroethyl isocyanate (0.85 g, 2 mmol) was added to the homogeneous suspension and the mixture was stirred at room temperature for 24 h. Afterwards the slurry reaction mixture was poured into methylene chloride (50 mL) to coagulate the product. The obtained MWCNT-Cl (7) was filtered, washed with methylene chloride (50 mL), and dried under vacuum. In a second step, the azide group was introduced via nucleophile substitution reaction of alkyl halide. MWCNT-Cl (7) (50 mg) was dispersed in DMSO (10 mL) by ultrasonication. Sodium azide (0.39 g, 6 mmol) was added and the mixture was stirred for 48 h at 50°C. After extraction with ethyl acetate, the azide functionalized MWCNTs (8) (see Fig. III.9 in the section *III.3.1 Functionalization of MWCNTs*) was filtered and dried under vacuum. The loading of azide groups onto the MWCNTs surface was estimated *via* TGA to 7.4×10^{-3} $mmol_{azide}/mg_{sample}$ (not shown here).

III.2.1.2.6 Preparation of barbiturate modified MWCNTs (9)

Azide functionalized MWCNTs (8) (50.0 mg) was dispersed in DMF via ultrasonication. Afterwards the mixture was purged with nitrogen for 10 min and an excess of ethyl-2-(1-pentyn-5-yl) barbituric acid (1) (500 mg), CuBr (120 mg, 0.8 mmol) and PMDETA (16 µL, 0.8 mmol) were added, followed by stirring under nitrogen at 70°C for 24 h. The mixture was diluted with DMF (100 mL), sonicated for 5 min, and filtered through a PTFE membrane and washed with excess of THF to obtain the barbiturate functionalized MWCNTs (9) (see Fig. III.10 in the section *III.3.1 Functionalization of MWCNTs*) named with the acronym MWCNT-b.

The loading of the barbiturate on the MWCNTs was determined via TGA

to 7.0×10^{-4} $mmol_{barbiturate}/mg_{sample}$ (see Fig. III.16 section III.3.2.2.3 Evaluation of the amount of functional groups bonded to MWCNT *via* TGA analysis).

III.2.2 Methods

III.2.2.1 Nuclear magnetic resonance spectroscopy (NMR)

NMR-spectra were recorded at 27 °C on Varian Gemini 400 spectrometer in $CDCl_3$ (Chemotrade, 99.8 atom%D) or DMSO-d_6 (Chemotrade, 99.8 atom%D). Chemical shifts (δ) are reported in parts per million (ppm) and referred to the residual signal of the deuterated solvent.

III.2.2.2 Morphological analysis

III.2.2.2.1 High-Resolution Transmission electron microscopy (HRTEM)

High-Resolution Transmission Electron Microscopy (HRTEM) characterization was performed on a Jeol 2010 LaBa6 microscope operating at 200 kV. MWCNTs were dispersed (in ethanol) by ultrasonic waves for 30 min. The obtained suspension was dropped on a copper grid (holey carbon).

III.2.2.2.2 Field Emission Scanning Electron Microscopy (FESEM)

Micrographs of the epoxy nanocomposites, based on functionalized MWCNTs, were obtained using FESEM (mod. LEO 1525, Carl Zeiss SMT AG, Oberkochen, Germany). All samples were placed on a carbon tab previously stuck to an aluminium stub and were covered with a 250 Å- thick gold film using a sputter coater (Agar mod. 108 A – Agar Scientific, Stansted, UK). Nanofilled sample sections were cut from solid samples by a sledge microtome. These slices were etched before the observation by FESEM. The etching reagent was prepared by stirring 1.0 g potassium permanganate in a solution mixture of 95 mL sulphuric acid (95–97%) and 48 mL orthophosphoric acid (85%). The filled resins were immersed into the fresh etching reagent at room temperature and held under agitation for 36 h. Subsequent washings were done using a cold mixture of two parts by volume of concentrated sulfuric acid and seven parts of water. Afterwards the samples were washed again with 30% aqueous hydrogen peroxide to remove any manganese dioxide. The samples were finally washed with distilled water and kept under vacuum for 5 days before being subjected to morphological analysis.

III.2.2.3 Differential Scanning Calorimetry (DSC) analysis

In this work, DSC curves have been obtained using a thermal analyser Mettler DSC 822/400 (Mettler-Toledo Columbus, OH, USA) equipped with DSC cell purged with nitrogen and chilled with liquid nitrogen for sub-ambient measurements. DSC has been used for the estimation of the curing degree (DC) of the samples under the assumption that the exothermic heat evolved during cure is proportional to the extent of reaction. The DC can be determined from the total heat of reaction (ΔH_T) of the curing reaction and the residual heat of reaction (ΔH_{Res}) of the partially cured epoxy resin according to Equation (III.1). To obtain fraction reacted at various temperatures, a series of isothermal experiments were performed. To secure accurate total ΔH_T values from isothermal studies, dynamic runs were made after the isothermal curing cycle to obtain the residual heat of reaction. The total heat of reaction was considered according to Equation (III.2), where ΔH_{iso} and ΔH_{Res} are the areas under the isothermal and dynamic thermograms, respectively.

$$DC = \frac{\Delta H_T - \Delta H_{Res}}{\Delta H_T} \times 100 \qquad \text{(III.1)}$$

$$\Delta H_T = \Delta H_{iso} + \Delta H_{Res} \qquad \text{(III.2)}$$

III.2.2.4 Thermogravimetric analysis (TGA)

TGA was carried out in air using a Mettler TGA/SDTA 851 thermal analyzer. The temperature range was 25–1000°C at heating rate of 10°C min^{-1}. The weight loss was recorded as a function of the temperature.

III.2.2.5 Dynamic mechanical analysis (DMA)

Dynamic mechanical characterization has been carried out on a DMA 2980 (TA instrument). Solid samples with dimensions 3×4×35mm^3 have been tested by applying a variable flexural deformation in three points bending geometry. The displacement amplitude was set to 0.1% and the frequency to 1 Hz. These conditions have been chosen to characterize the linear viscoelastic response of the materials and reduce the noise to signal ratio. The range of temperature analyzed was from −50°C to 300°C at the constant scanning rate of 3°C min^{-1}. Before tests, calibration of clamp compliance, force and furnace temperature has been carried out. The glass transition temperatures reported are obtained from the maxima in the loss tangent spectrum (tan δ versus temperature) by taking the derivative of tan δ with respect to temperature.

III.2.2.6 Evaluation of Self-healing efficiency

The healing efficiency η of the analyzed samples has been evaluated by fracture tests, as already described in section *II.2.2.3 Healing activity and self-healing efficiency evaluation*. The specimens (see in Fig.III.6 the photo of two formulated samples) were prepared in the metallic mould, shown in Figure III.7 from which they were extracted after the curing cycle and subsequently tested.

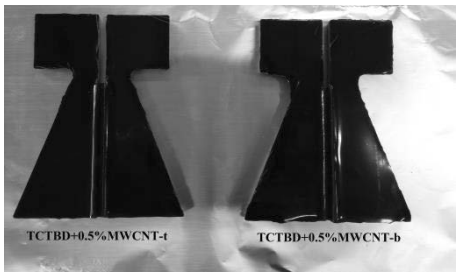

Figure III.6 *Photo of the samples TCTBD+0.5%MWCNT-t and TCTBD+0.5%MWCNT-b, after the extraction from the metallic mould*

Figure III.7 *Metallic mould for sample preparation*

III.2.2.7 Electrical properties

The measurements of the dc volume conductivity were performed by using disk-shaped specimens of about 2 mm thickness and 50 mm diameter; the measurement electrode is circular with a diameter of about 22 mm. The measurement system, remotely controlled by the software LABVIEW®, is composed of a suitable shielded cell with temperature control, of multimeter Keithley 6517A with function of voltage generator (max. _1000 V) and voltmeter (max. _200 V) and the ammeter HP34401A (min. current 0.1 mA) for samples above the percolation threshold. For ones below the percolation

threshold the system is composed only of multimeter Keithley 6517A with function of voltage generator (max. _1000 V) and pico-ammeter (min. current 0.1 fA).

III.3 Results and discussion

III.3.1 Functionalization of MWCNTs

The aim of the developed systems is to enable multiple autonomous self-healing at room temperature to fulfill the industrial requirements of high-performance structural materials. Hydrogen bonding approaches are known to be ideal solutions as the reversibility of the opening and closing of hydrogen bonds facilitate a dynamic repetition of the repair events even in the same area (Campanella *et al*. 2018, Herbst *et al.* 2012, 2013; Chen *et al.* 2015a, 2015b). Appearing stress will rupture the hydrogen bonds, which are able to restore the original donor/acceptor interaction without an additional intervention – fully autonomously. The combination of this approach with the advantages of nanofiller modified epoxy resins would allow to manufacture self-healing nanocomposites *via* reversible crosslinking (see Fig. III.8), which would ideally fulfill almost all above-mentioned requirements for structural material in aerospace applications.

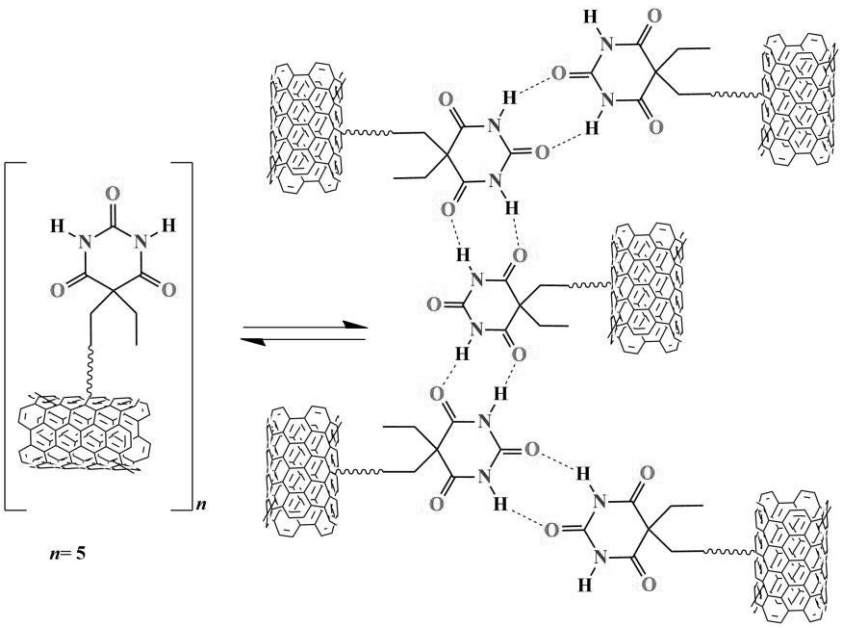

Figure III.8 *Example of barbiturate modified MWCNTs for reversible opening and closing of hydrogen bonds during damage and healing event*

Thymine and barbituric acid-based moieties have been selected as they are known to undergo hydrogen bonding leading to reversible crosslinking and are well suitable for self-healing applications (Herbst *et al.* 2012; Döhler *et al.* 2015). These moieties are able to establish hydrogen bonds via *NH*-donation and *CO*-acceptance either with another thymine or barbiturate, as shown in Figure III.9 for the barbiturate modified MWCNTs, or with the rubber modified and amino hardened epoxy matrix itself.

The modification of the MWCNTs with hydrogen bonding moieties has been performed via a CuAAC "click" reaction, as this kind of reaction is well known for its high efficiency and large tolerance against other functional groups (Döhler *et al.* 2017; Binder and Sachsenhofer 2007, 2008). For that purpose, the pristine MWCNTs (3) were modified in a first step either with alkyne (5) or azide groups (8), which were subsequently transformed via the CuAAC "click" reaction with the corresponding barbituric acid alkyne (1) or thymine azide (2) to generate the desired hydrogen bonding modified MWCNTs 6 and 9 (see Figure III.9).

All synthesis procedures for preparing functionalized MWCNTs are described in the section *III.2.1.2 Synthesis of functionalized MWCNTs*.

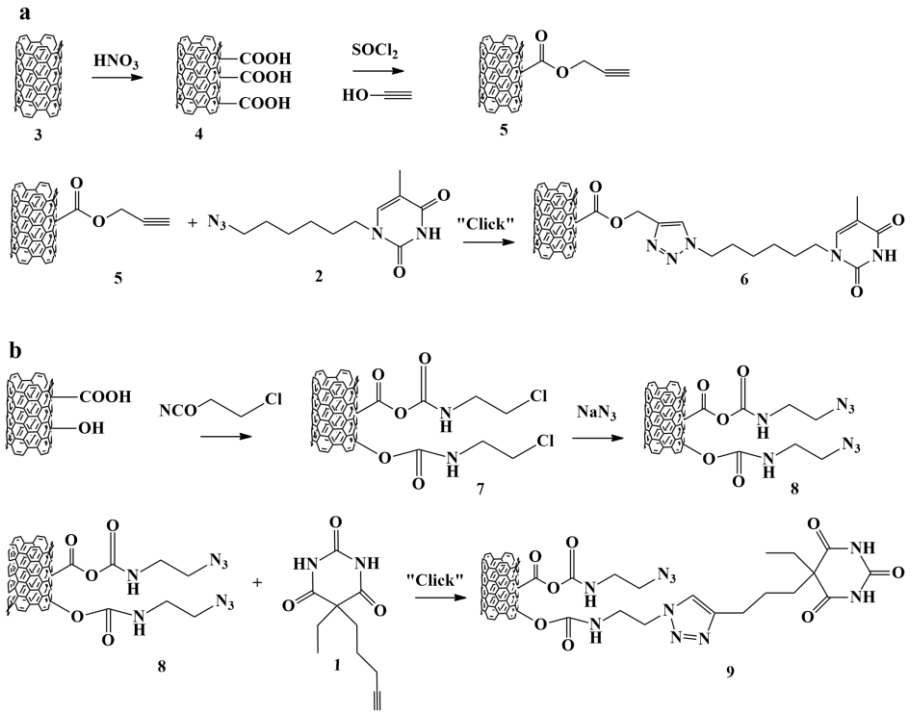

Figure III.9 *a) Preparation of thymine-acid-functionalized MWCNTs (6); b) Preparation of barbituric acid-functionalized MWCNTs (9)*

III.3.2 Epoxy matrix filled with unfunctionalized and functionalized MWCNTs

III.3.2.1 Morphological analysis

III.3.2.1.1 Transmission electron microscopy (TEM)

TEM analysis has been used to better investigate the effect of covalent functionalization on MWCNTs. Figure III.10 shows the comparison between the TEM image of the pristine MWCNTs (see image on the left) and the TEM image of the functionalized MWCNT-b (see image on the right). The comparition highlights that the functionalization procedure strongly affects the aspect ratio of the carbon nanofillers, attacking mainly the areas of defects and reducing the length of the MWCNTs. This effect could be responsible for the strong decrease in the electrical conductivity of the self-healing nanocomposites containing embedded functionalized MWCNTs (see section *III.3.2.5 Electrical properties*).

.

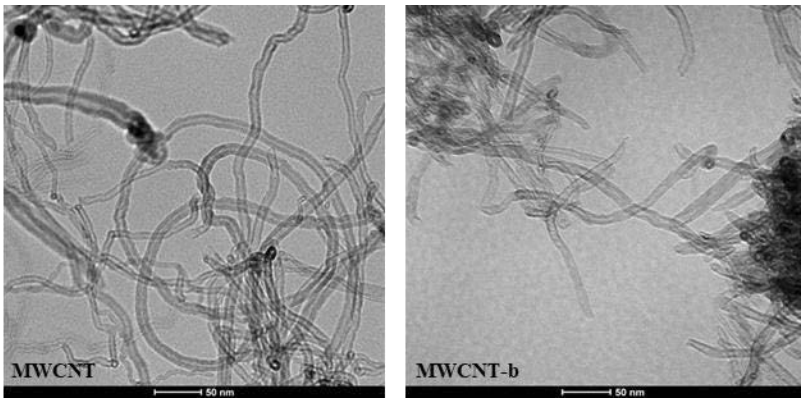

Figure III.10 *TEM images of the unfunctionalized MWCNTs (on the left) and of the functionalized MWCNT-b (on the right)*

III.3.2.1.2 Field Emission Scanning Electron Microscopy (FESEM) of Self-Healing Nanocomposites

Initially, morphological analysis has been carried out on the TCTBD+0.5%MWCNT-b (9) and TCTBD+0.5%MWCNT-t (6) samples without etching procedure (see Fig. III.11). In both samples, it was possible to glimpse spherical domains corresponding to the rubber phase. However, no clear information was obtained on the dispersion of MWCNTs in the

epoxy matrix, the arrangement of the rubber domains and the morphological feature of the inter-phase regions.

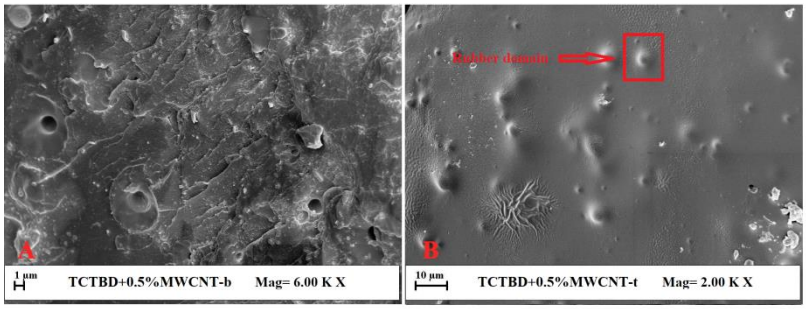

Figure III.11 *SEM images of the non-etched fracture surface of the samples. A)TCTBD+0.5% MWCNT-b (with MWCNTs functionalized with barbiturate-based ligand; B) TCTBD+0.5% MWCNT-t (with MWCNTs functionalized with thymine-based ligand)*

Therefore, to better study these morphological aspects, a strong etching procedure has been performed on the samples, as described in the section III.2.2.2.1 Field Emission Scanning Electron Microscopy (FESEM).

Figure III.12 shows SEM images of the etched fracture surface of the samples TCTBD (without MWCNTs) (Fig. III.12 A-B), TCTBD+0.5% MWCNT (with unfunctionalized MWCNTs) (Fig. III.12 C-D), TCTBD +0.5%MWCNT-b (Fig. III.12 E-F) and TCTBD+0.5% MWCNT-t (Fig. III.12 G-H) with MWCNTs functionalized with barbiturate (9) and thymine-based ligands (6), respectively. The comparison between unfilled and filled epoxy samples highlights that the ultrasonication procedure performed for dispersing MWCNTs in the fluid epoxy mixture (before the curing process) determines a strong reduction of the dimensions related to the rubber domains. The fracture surface of the sample filled with MWCNTs shows a three-phase morphology with a scattered rubber phase, characterized by approximately spherical domains with dimension ranging from hundreds of nanometers to few micrometers, a rigid continuous phase (epoxy matrix) and MWCNTs. It is worth noting that the etching procedure also consumes part of resin at the interface between the matrix and the rubber phase making clearly visible not only MWCNTs, but also the distribution of the rubber domains.

In the unfilled sample (Fig. III.12 A-B), and the samples containing unfunctionalized MWCNTs (Fig. III.12 C-D), the strong etching procedure determines more easily detachment regions between rubber domains and epoxy matrix (see inter-phase region in Fig. III.12 B), and the empty spherical region left by the rubber phase due to the agitation in the etching solution in Fig. III.12D).

SEM images in Fig. III.12 E and in Fig. III.12 H clearly evidence the effect of MWCNTs functionalization on the morphological features related to the inter-phase regions.

A very peculiar and interesting feature observed in the samples containing embedded functionalized MWCNTs is related to the distribution of MWCNTs. They have a particular affinity to the rubber phase as detectable by a higher concentration around the spherical domains (Fig. III.12 E-F and Fig. III.12 G-H).

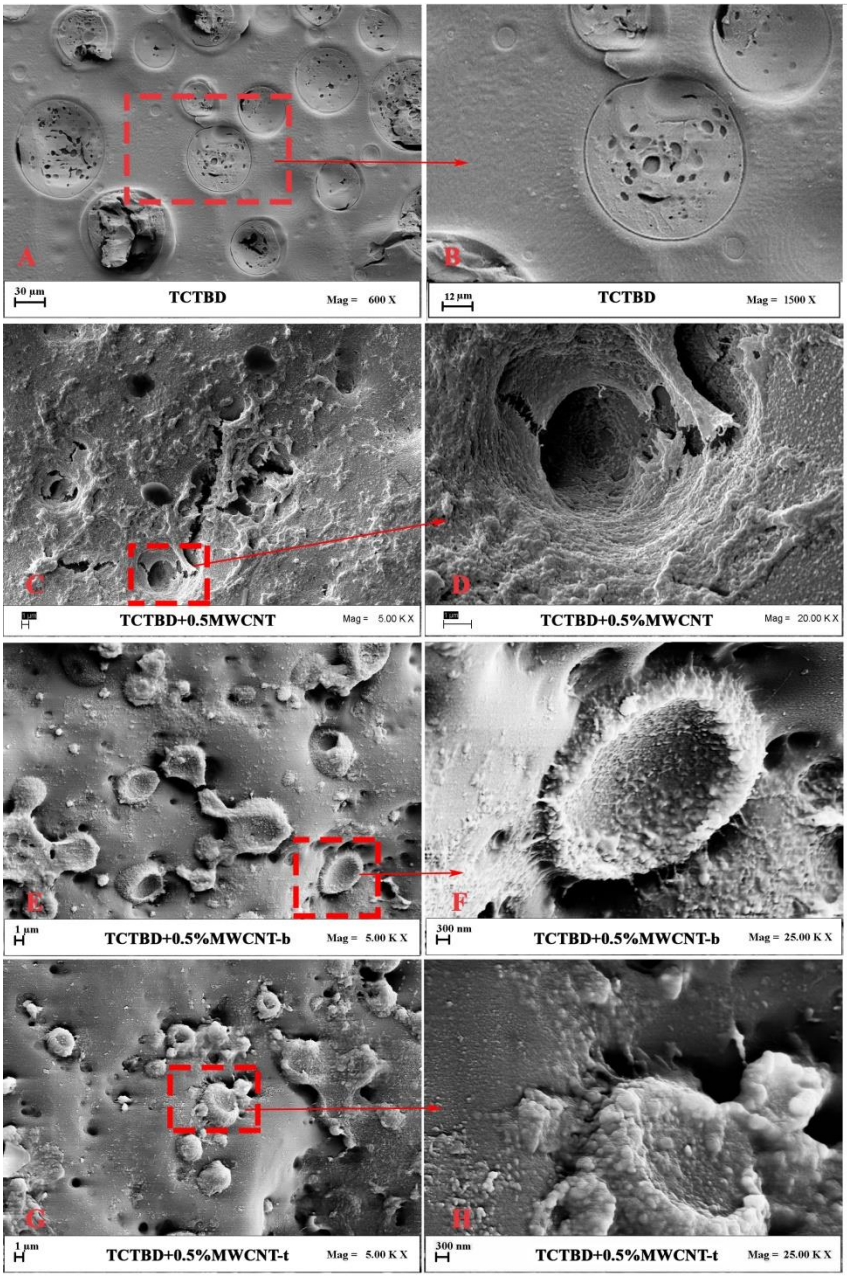

Figure III.12 *SEM images of the etched fracture surface of the samples. A-B) TCTBD (without MWCNTs); C-D) TCTBD+0.5% MWCNT (with unfunctionalized MWCNTs); E-F) TCTBD+0.5% MWCNT-b (with MWCNTs functionalized with barbiturate-based ligand; G-H) TCTBD+0.5% MWCNT-t (with MWCNTs functionalized with thymine-based ligand)*

Figure III.13 shows the SEM images at larger magnification of the interfacial zones between the rubber phase domains and the epoxy matrix in the sample TCTBD+0.5%MWCNT-b (Fig. III.13 A-C) and the sample TCTBD+0.5%MWCNT-t (Fig. III.13 B-D). The last images clearly show the influence of the functional groups attached to the wall of MWCNTs on their morphological arrangement in the matrix. Several nanotubes connect different rubber domains passing through the epoxy matrix (Fig. III.13 B); some of them have been highlighted with red arrows in Fig. III.13, where the nanotubes acting as bridges between different rubber domains are named MWCNTs-bridges. Furthermore, some MWCNTs seem to be strongly anchored with other MWCNTs dispersed in the epoxy matrix, acting as bridge between rubber domains and the epoxy matrix. It is worth noting that an epoxy matrix with high curing degree (see the next section III.3.2.2.1 Differential Scanning Calorimetry (DSC)) is characterized by a strong presence of OH groups (due to the conversion of epoxy groups into the corresponding cross-linked network) which can form hydrogen-bonding bridges with functional groups on the wall of MWCNTs. On the other hand, the strong affinity between functionalized MWCNTs and rubber domains is also responsible for MWCNTs-bridges between different rubber domains.

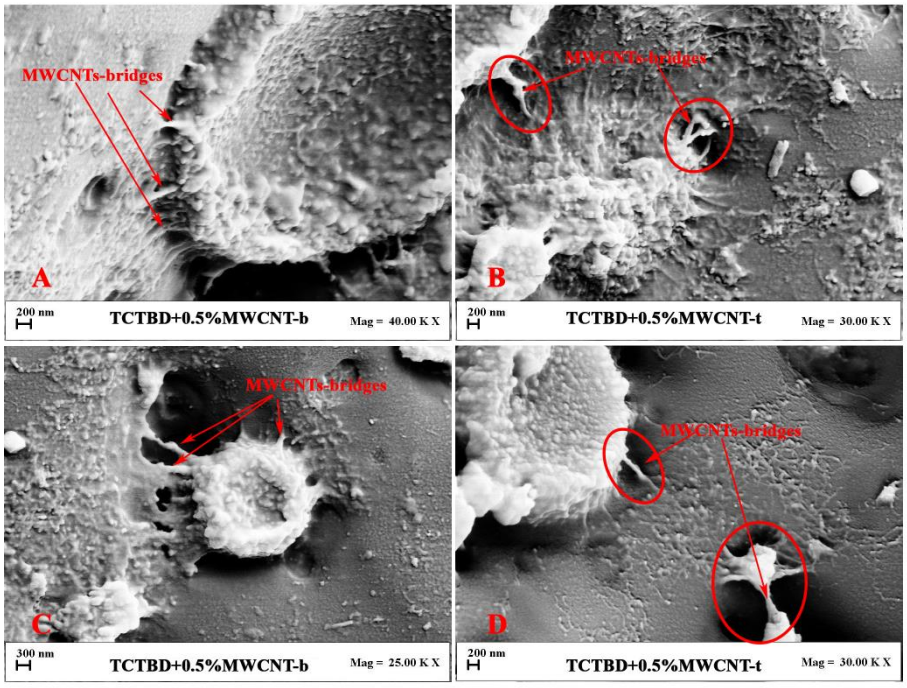

Figure III.13 *SEM images of the interfacial zones between the rubber phase domains and the epoxy matrix. A-C) TCTBD+0.5% MWCNT-b; B-D) TCTBD+0.5% MWCNT-t*

III.3.2.2 Thermal analysis

III.3.2.2.1 Differential Scanning Calorimetry (DSC)

DSC analysis has been performed to evaluate the curing degree (DC) of the samples. DC has been defined in the experimental section *III.2.2.3 Differential Scanning Calorimetry (DSC) analysis*, after a curing cycle composed of two steps: a first step of 125°C for 1 h followed by a second step at the higher temperature of 200°C for 3 h, where both steps have been carried out in isothermal condition in oven. Figure III.14b shows DSC curves of the cured toughened epoxy mixture TCTBD and of the same epoxy mixture filled with unfunctionalized and functionalized MWCNTs. All samples show a small fraction of uncured resin, which continues to cure in different temperature ranges. In particular, the unfilled resin and the resin filled with unfunctionalized MWCNTs complete their curing process between 175°C and 275°C; whereas for the resins filled with functionalized MWCNTs, MWCNT-b (9) and MWCNT-t (6), a further small exothermic peak, centered at about 280°C, is observed. It is very likely that these exothermic peaks are due to a beginning of decompositions of the organic substituents on MWCNTs, such as triazole rings or remaining azides in the temperature range higher than 270°C and before the degradation process of the epoxy matrix around 360 °C (see TGA curves in Fig. III.15a).

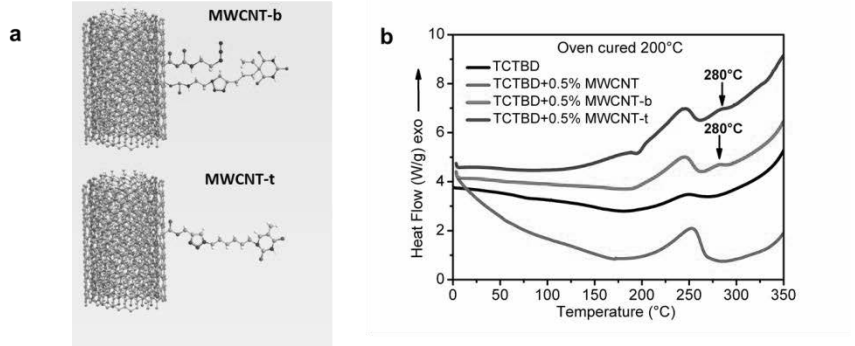

Figure III.14 *a) Functional groups, barbiturate and thymine-based ligands on MWCNTs; b) DSC curves of the cured epoxy mixture TCTBD and the nanocomposites TCTBD+0.5%MWCNT, TCTBD+0.5%MWCNT-b, TCTBD+0.5%MWCNT-t*

The initial decomposition reactions can cause free radicals responsible for a little additional curing of the resin. It is worth noting that the analyzed samples and the healing efficiency have been evaluated after a curing cycle up to 200°C; hence a temperature able to preserve the thermal stability of the functional groups. The degree of curing for the sample TCTBD was found to be 97%, calculated according to equation (III.1), as described in the

experimental section *III.2.2.3 Differential Scanning Calorimetry (DSC) analysis.* The inclusion of unfunctionalized MWCNTs in the epoxy formulation determines a non-trivial decrease in the DC value (DC=89); whereas for functionalized MWCNTs, only a slight decrease in DC values was found with respect to the unfilled formulation. It has already been observed that the inclusion of MWCNTs at low concentration (0.32%wt) in epoxy formulations leads to a decrease in the DC value due to a lower crosslinking density; therefore, in order to reach the same curing degree of the unfilled formulation, a curing cycle at higher temperature is required (Guadagno *et al.* 2018). On the other hand, higher curing degrees of up to 100% can usually be found only for structural resins filled with carbon nanoparticles solidified in dynamic regimes (Raimondo *et al*. 2018). For epoxy nanocomposites solidified through isothermal steps (able to simulate a real industrial processing condition), values higher than 91–92% make the resin suitable to meet industrial requirements. For the samples TCTBD+0.5%MWCNT-b and TCTBD+0.5% MWCNT-t, using the same curing cycle, the presence of the functional groups allows to reach a higher curing degree compared to the formulation containing unfunctionalized nanotubes, providing in this way also an effective strategy for energy-saving.

Table III.1 shows ΔH_T, ΔH_{Res} and DC values of the analyzed samples calculated as described in the experimental section *III.2.2.3 Differential Scanning Calorimetry (DSC) analysis.* For the samples TCTBD+0.5% MWCNT-b and TCTBD+0.5%MWCNT-t the ΔH_{Res} and ΔH_T calculation has been performed excluding the exothermic peak at 280°C, which is absent in the reference samples TCTBD and TCTBD+0.5%MWCNT. This experimental procedure prevents the overestimation of the curing degree for the samples with functionalized nanotubes.

Table III.1 *Calorimetric results of the analyzed samples*

Sample	Cure Degree DC [%]	ΔH_{Res} [Jg^{-1}]	ΔH_T [Jg^{-1}]
TCTBD	97	8.16	283.42
TCTBD+0.5%MWCNT	89	48.48	429.32
TCTBD+0.5%MWCNT-b	93	25.21	365.56
TCTBD+0.5%MWCNT-t	93	30.63	415.64

III.3.2.2.2 Thermogravimetric analyses (TGA)

Figure III.15 shows the TGA curves of the cured toughened epoxy mixture TCTBD and of the same epoxy mixture filled with unfunctionalized MWCNT and functionalized MWCNT-b (9) and MWCNT-t (6), in air and nitrogen flow. The beginning of thermal degradation process, defined as 5% mass loss temperature, is around 360°C for all analysed samples, both in air

and nitrogen atmosphere. The sample TCTBD+0.5% MWCNT-b, in air, seems to lose a small percentage of its weight in the temperature range higher than 270°C and before the main first step of the degradation process. This seems to be in agreement with the hypothesis of decomposition of the functional group mentioned before. In any case, TGA curve profiles highlight two distinct and well-separated turns. Both in nitrogen and air, the first step falls in the temperature range between 360°C and 450°C, evidencing that there is no appreciable influence of MWCNTs and functional groups on the first step of the degradation process.

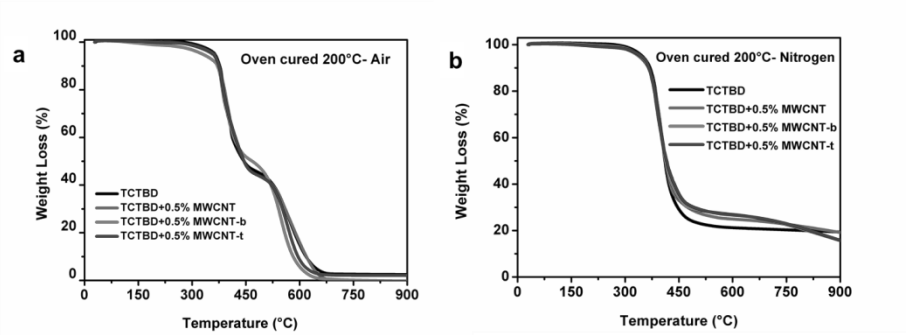

Figure III.15 *a) TGA curves of the cured toughened epoxy mixture TCTBD and of the same epoxy mixture filled with unfunctionalized and functionalized MWCNTs in airflow; b) TGA curves of the cured toughened epoxy mixture TCTBD and of the same epoxy mixture filled with unfunctionalized and functionalized MWCNTs in nitrogen flow*

A very interesting behaviour is observable in the mass loss after the first step of thermal decomposition in both air and nitrogen atmosphere. In fact, in air, the samples seem to be more stable than in nitrogen; the mass loss is 47–55% in air and 63–75% in nitrogen. This behaviour was already observed for epoxy formulation and it is due to the oxidation reactions take place primarily in the gas-phase by the flaming burning of the nanocomposites (Kashiwagi 2007). Thus, oxygen hardly reaches the thermally degrading sample surface beneath the evolved gaseous products. The results of thermo gravimetric tests performed in air for thermoset resins would apply to smouldering combustion instead of flaming combustion. Hence, it is important to analyse the TGA profiles of thermosetting nanocomposites also in inert atmosphere. In nitrogen atmosphere, a stabilizing effect of MWCNTs is observed in the second step of the degradation process in the temperature range between 450°C and 700°C. Concerning the influence of the functional groups attached to the MWCNTs, the curves are almost superimposable with the curve of the sample containing unfunctionalized MWCNTs. TGA analysis of uncured epoxy

formulation evidences the same steps and the same temperature ranges for the degradation processes.

All the collected results highlight that no degradation processes occur during the curing process; hence, the formulated nanocomposites are stable up to 350–360°C.

III.3.2.2.3 Evaluation of the amount of functional groups bonded to MWCNT *via* TGA analysis

The values of healing efficiency, shown and discussed in section *III.3.2.4 Evaluation of self-healing efficiency*, result from functional groups covalently attached to MWCNTs which are embedded in the epoxy formulation in a low percentage. In fact, the value of 0.5 wt%, also includes the weight percentage of MWCNTs, therefore the concentration of functional groups in the epoxy resins is even lower. This concentration has been determined by TGA analysis.

From the TGA curves, shown in Figure III.19, it can be observed the initial degradation temperature (T_d, evaluated after a weight loss of 5%) for the unfunctionalized MWCNT (T_d= 560°C) and for functionalized MWCNT (T_d= 310°C). The weight loss by weight of 24.6%, for both the functionalized MWCNT, corresponds to the degradation of the functional groups, thymine and barbituric acid-based ligands.

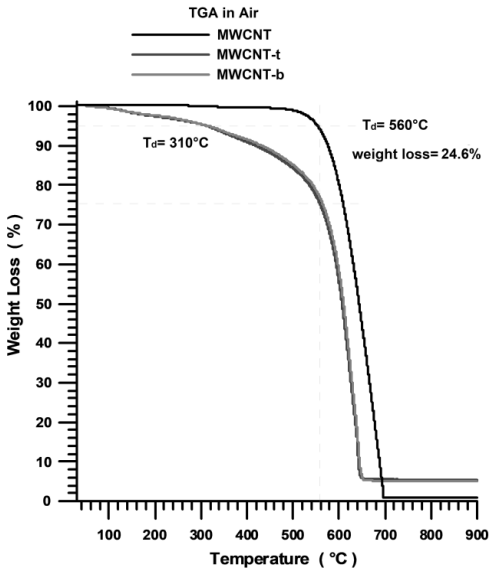

Figure III.16 *TGA curves of the unfunctionalized MWCNT (black curve), functionalized MWCNT-t (blue curve) and functionalized MWCNT-b (red curve) in airflow*

Therefore, considering the 0.5% by weight of functionalized nanofillers, the amount of pristine functional groups covalently bonded to MWCNT, corresponds to 0.12% by weight with respect to the epoxy matrix TCTBD, while the percentage of MWCNT is equal to 0.38% by weight.

III.3.2.3 Mechanical properties: dynamic mechanical analysis (DMA)

In order to fully understand the influence of the functional groups on the mechanical properties of the toughened epoxy matrix, loaded with functionalized and unfunctionalized MWCNTs, DMA analyses were performed. In particular, in this research work, DMA is mainly used to investigate the influence of filler content on the relaxation phenomena of the unfilled and filled modified epoxies TCTBD. DMA also provides supporting evidence of filler dispersion in a polymeric matrix and represents an important reference for thermal stability of nanocomposites.

Figure III.17b shows the plots of the storage modulus (E') as a function of temperature for all analysed nanocomposites. The storage modulus decreases with increasing temperature (see Fig. III.17c). In the range of temperatures between –50°C and 120°C, the addition of functionalized and unfunctionalized nanofiller leads to increased storage moduli. In particular, the functionalized MWCNTs show a smaller improvement compared to unfunctionalized MWCNTs. The lowest values observed for functionalized nanotubes are most likely due to a reduction of the stiffness and strength of functionalized nanotubes and a different MWCNT distribution due to a particular affinity of the functionalized MWCNTs with the rubber phase, as highlighted by SEM investigation.

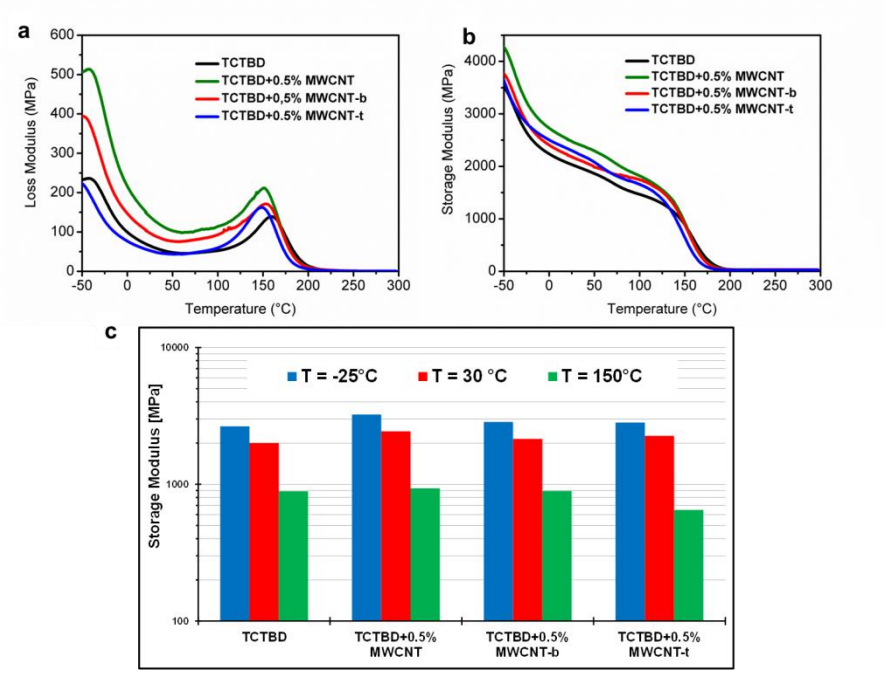

Figure III.17 *a) Evolution of the storage modulus as a function of the temperature; b) evolution of the loss modulus as a function of the temperature; c) storage modulus of composites at three different temperatures*

In any case, the differences between the individual nanocomposites are relatively small, if compared with the absolute values of the modulus. This is a clear indication of the good dispersion obtained. In fact, the linear deformation applied in this work assures the existence of a continuous morphology in all cases here exanimated.

For all analyzed nanocomposites the loss modulus (E″, Fig. III.17a) firstly decreases and then increases with increasing the temperatures up to a peak maximum at about 150°C. In addition, here, the similarity between the curves of the composite based on the unfilled MWCNT and the others demonstrates a good interaction between the filler particles and the epoxy matrix. The combined use of microscopic observations and DMA can help us to further identify the microstructure formations in epoxy composites.

The loss tangent (tan δ, Fig. III.18a) of the composites shows two distinct peaks that are indicative of two different temperature relaxation phenomena. The high temperature relaxation, located in the region between 170 and 200°C, corresponds to the glass transition region of the epoxy matrix. The lower temperature relaxation, located in the region between −30 and −50°C, is associated with both the glass transition region of the rubber and in minor

extend to the secondary relaxation of the epoxy resin. The position and shape of the two peaks in tan δ are affected by the nature of the composites. The glass transition temperature (which is determined here from the peak of loss tangent *versus* temperature curve) shows not trivial changes with the filler addition. With MWCNTs addition, the main relaxation increases in intensity while the peak broadens on the lower temperature side, indicating the appearance of new, faster relaxation modes. The main relaxation peak shifts to lower temperatures (see Fig. III.18b) for the filled formulations. This decrease is probably due to the enhancement in epoxy chain movements produced by the functional groups on MWCNTs.

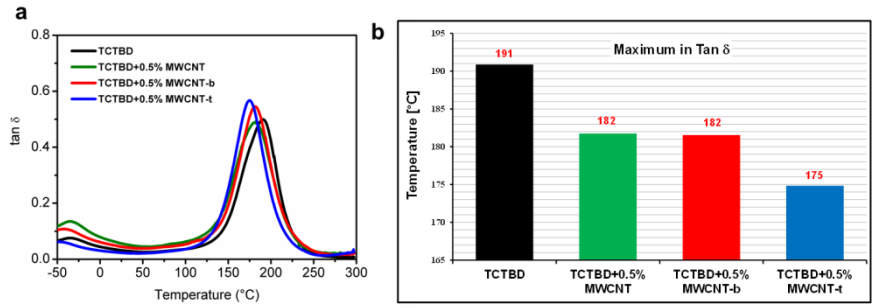

Figure III.18 *a) evolution of the loss factor (tan δ) as a function of the temperature; b) temperature of the maximum in loss factor for the composites*

III.3.2.4 Evaluation of Self-healing efficiency

Values of healing efficiency (η) have been calculated using equation (II.2), as described in the experimental section *II.2.2.3 Healing activity and self-healing efficiency evaluation*. Figure III.19 shows the load-displacement curves for TCTBD+0.5%MWCNT-b (see Fig. III.19a) and TCTBD+0.5% MWCNT-t (see Fig. III.19b), respectively. Healing efficiencies have been found to 52% and 55%. The samples filled with MWCNTs functionalized with thymine-based ligand (6) tend to manifest values in the healing efficiency slightly higher than the sample filled with MWCNTs functionalized with the barbituratebased ligand (9).

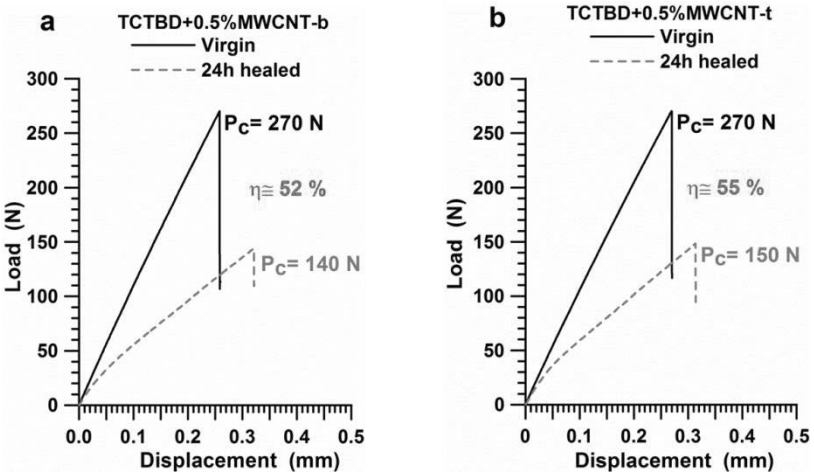

Figure III.19 *a) Load-Displacement curves for the TCTBD+0.5%MWCNT-b sample (black curve for the virgin sample, grey curve for the healed sample after the first cycle); b) Load-Displacement curves for the TCTBD+0.5% MWCNT-t sample (black curve for the virgin sample, grey curve for the healed sample after the first cycle)*

The healing efficiencies calculated for the sample TCTBD+0.5% MWCNT-b (on five virgin samples) have been found to be 51%, 52%, 52% and 53% and 54% respectively (average value-52.4%). Similarly, for TCTBD+0.5% MWCNT-t samples values in the healing efficiency of 54%, 53%, 55% 55% and 57% have been found (average value - 54.8%).

As already mentioned in section II.3.5.2.2 Self-healing efficiency assessed by metathesis test for TBD formulation, TDCB fracture test couldn't be performed on formulation based on the TGMDA epoxy precursor, due to the high rigidity of the matrix, that did not allow the control of fracture propagation along the centerline of the sample. The toughening of the matrix, obtained through the addition of the liquid rubber, has made possible to overcome this problem, reducing the fragility of the matrix and allowing a correct execution of the test.

III.3.2.5 Electrical properties

In order to evaluate the electrical behaviour of nano-charged materials, electrical conductivity measurements a have been performed, on disk-shaped specimens shown in Figure III.20. The obtained values of electrical conductivity are shown in Table III.2.

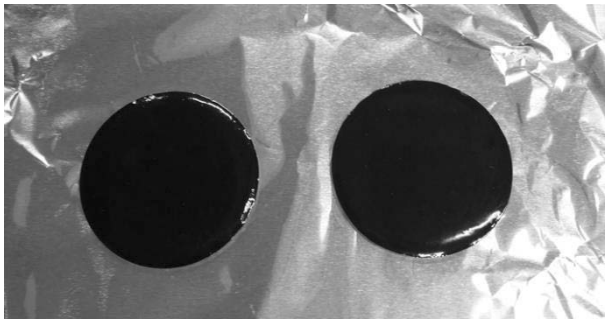

Figure III.20 *Disk-shaped specimens*

Table III.2 *Values of electrical conductivity for the analyzed samples*

Sample	Electrical Conductivity [S/m]
TCTBD	1.16×10^{-14}
TCTBD+0.5%MWCNT	2.56×10^{-2}
TCTBD+0.5%MWCNT-b (0.38% of MWCNT)	6.28×10^{-12}
TCTBD+0.5%MWCNT-t (0.38% of MWCNT)	6.47×10^{-12}
TCTBD+2.0%MWCNT-b (1.50% of MWCNT)	6.76×10^{-3}
TCTBD+2.0%MWCNT-t (1.50% of MWCNT)	3.77×10^{-2}

These results highlight that the addition of pristine MWCNT within the epoxy matrix TCTBD converts its electrical behaviour from an insulator to a conductor, thanks to the formation of conductive paths in the nano-composite. In fact, the sample TCTBD+0.5%MWCNT is characterized by a value in the electrical conductivity of 2.56×10^{-2} S/m, which is several orders of magnitude higher than the very low electrical conductivity of the unfilled sample TCTBD (1.16×10^{-14} S/m). Figure III.21 shows that for a concentration of MWCNTs corresponding to 0.5% by wt, the sample is beyond the Electrical Percolation Threshold (EPT).

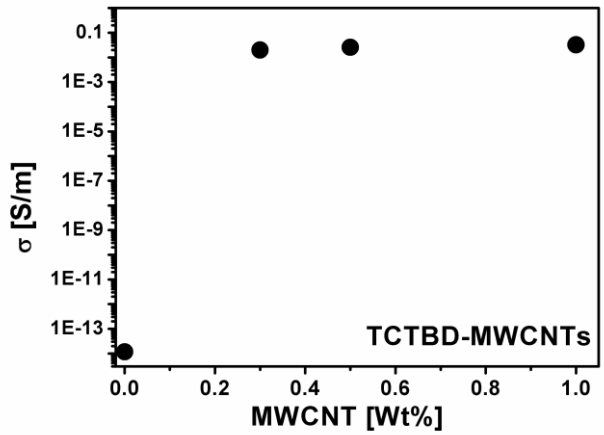

Figure III.21 *Electrical conductivity of TCTBD sample versus MWCNT weight percentage*

The values of electrical conductivity shown in Table III.2 evidence that the functionalization of MWCNTs strongly affects the electrical behaviour of the nanocomposites, reducing their electrical conductivity to values of pS/m. This result is most likely due to the changes in the aspect ratio of the nanofiller determined by the functionalization procedure as evidenced by Transmission electron microscopy (TEM) investigation. The functionalization partially compromises the sp^2 hybridization of carbon atoms and the π-electron delocalization typical of polynuclear aromatic rings, as it happens with other type of covalent functionalizations. In order to achieve values in the electrical conductivity of the self-healing nanocomposites comparable to those obtained with unfunctionalized MWCNTs, nanofiller loadings up to 2.0 by wt% (see Table III.2) are needed. This work is still in progress; in the future work, the EPT of the self-healing nanocomposites and the healing efficiency of samples loaded with 2% by weight of functionalized MWCNTs will be evaluated.

III.4 Conclusion

Multi-wall carbon nanotubes have been functionalized with barbituric acid and thymine-based moieties. These functional groups have been chosen for their potential to act as donor and acceptor of hydrogen bonds causing a reversible and repeatable opening and closing of the resultant hydrogen bonds. Functionalized MWCNTs have been embedded in a rubber-

toughened epoxy formulation to transfer auto-repair function based on attractive reversible hydrogen bonding interactions to thermosetting resins. The performed experiments highlight the possibility to adopt this self-healing strategy to the resins, mainly due to the preservation of the ability of the functional groups for hydrogen bonding interactions even after the curing cycle. The proposed design of nanofilled self-healing polymers based on hydrogen bonds combines highly dynamic properties, like a reversible, "sticker-like" bond opening and closing behaviour to enable a de-and subsequent reconnection, and thus supramolecular network formation with the possibility to restore the sensing functionality based on electrical properties. However, one of biggest challenge to apply this approach for epoxy resins is the limited dynamic properties of thermosetting matrix segments. In this work, the rigidity of the matrix has been reduced implementing a rubber material to modify the phase composition. Moreover, the reversibility of hydrogen bonds can be enhanced by a fine interpenetration of small rubber domains in the matrix. It was demonstrated that the higher mobility of this rubber phase finely distributed in the composite, is most likely responsible for favouring the arrangement of hydrogen bonding interactions to activate self-healing mechanisms.

It is worth noting that, despite the low concentration of functional groups (0.12% by wt), the values in the healing efficiency have been found higher than 50% for both the analysed samples. This is a very relevant result in light of the detected mechanical performance. In fact, the self-healing capability has been conferred to an epoxy formulation composed of thermosetting resins characterized by high values in the storage modulus (between 2000 and 3000 MPa up to 100°C) and in the main glass transition temperature (between 175°C and 191°C). The healing efficiency of the formulated nanocomposites can be due to the strong attractive interactions between the rubber phase, which is responsible for nano/micro domains at higher chain mobility, as highlighted by DMA results, and the functional groups attached on the walls of MWCNTs. This hypothesis is also supported by the presence of MWCNTs-bridge between rubber domains observed by SEM analysis. Furthermore, thermal investigations highlight important results from an industrial point of view: the formulations are thermally stable after the curing cycle and hence, the functional barbiturate and thymine-based groups on MWCNT walls are available to act as donors and acceptors of hydrogen bonds even after the "curing cycles" usually employed in industrial manufacturing processes. The functionalization of MWCNTs also affect the curing degree (DC) which is an important parameter for fulfilling industrial requirements. In fact, while the presence of unfunctionalized MWCNT substantially decreases the DC (from 97 to 89%) of the formulated epoxy material, the presence of functionalized MWCNTs causes only a slight decrease of about 4% in the same material. Furthermore, with the covalent functionalization of MWCNTs the composites show an insulating behaviour

and most likely this effect is a consequence of the change of the aspect ratio of carbon nanofillers, as highlighted by TEM analysis. By adding a higher concentration of functionalized MWCNTs, the formulations show tipical electrical conductivity values of samples above the percolation electrical threshold.

In conclusion, results from this study had led to the design of new materials for safe and cost-efficient self-healing composites in many sectors of loadbearing materials, as well depicted, in a futuristic way, in the Figure III.22.

Further developments can be done in the direction of tuning the concentration of functional groups on MWCNTs to further improve self-healing efficiency and restoration of functional properties or self- responsive functions.

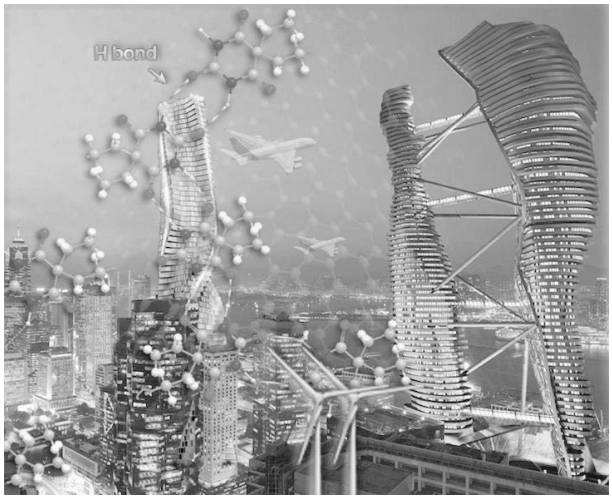

Figure III.22 *Graphical representation of possible application of self-healing composites in some sectors of loadbearing materials*

Chapter IV
Supramolecular self-healing system based on unfunctionalized MWCNTs

IV.1 Introduction

As already mentioned, self-healing supremolecular systems are based on non-covalent, transient bonds to generate networks able to heal the damaged site (Herbst *et al*. 2013). The possibility to repeatedly activate healing events even after that multiple damages have occurred (multiple self-healing cycles) is a central advantage of supramolecular self-healing materials, thus putting them on the frontline of industrial applications.

In this chapter, the attention is always focused on the development of multifunctional self-healing supramolecular systems, but the strategic approach is different from that discussed in the previous chapter. In fact, in order to integrate auto-repair mechanisms in structural materials, able to contrast the insulating property of epoxy resins, new nanocomposites have been developed, based on molecules acting as self-healing filles and unfunctionalized MWCNTs, which determine low values in EPT and allow to avoid the functionalization steps of MWCNTs (with relevant advantages for possible industrialization processes).

The first step of this research work has been the identification of molecules having the intrinsic potential to easily create cumulative effects of the reversible interactions based on hydrogen bonding in the epoxide networks. The biggest challenge is to generate autorepair networks in the epoxy matrix without decreasing mechanical performance of the self-healing structural material. After an intense bibliographic research study, some molecules, containing characteristic functional groups, able to establish reversible non-covalent bonds among themselves and with the matrix have been identified. The structure of the molecules has been chosen considering their peculiar property to activate interactions with the epoxy matrix through

the formation of reversible hydrogen bonds, generating a supramolecular network with the intrinsic property to repair themselves after damages.

In order to evaluate the solubility or the dispersion of self-healing fillers in the epoxy matrix, different tests have been performed. The solubility and the dispersion are very important conditions for simplifying the processing steps.

The epoxy matrix, in which the fillers and the MWCNTs have been added, is the toughened epoxy resin TCTBD, already used for the systems loaded with functionalized MWCNTs (see Chapter III).

In order to evaluate the properties of the formulated nanocomposites, such as its healing efficiency and processability, morphological analysis, mechanical tests, rheological and FT-IR investigation have been carried out.

IV.2 Experimental section

IV.2.1 Materials

The epoxy matrix is composed of: a) the terafunctional epoxy precursor tetraglycidylmethylenedianiline (TGMDA); b) the epoxy reactive diluent 1,4 butanedioldiglycidyl ether (BDE); c) the curing agent 4,4- diaminodiphenyl sulfone (DDS).They were purchased from Sigma-Aldrich Company.

This matrix has been toughened using a rubber phase, carboxyl-terminated butadiene acrylonitrile copolymer (CTBN), which was purchased from Hycar-Reactive Liquid Polymers. It is characterized by a Mn = 3600 containing terminal carboxy groups (COOH content of 0.67×10^{-3} equiv/g of CTBAC and 18 w/w% of CN).

Multi Wall Carbon Nanotubes (MWCNTs) (3100 Grade) were purchased from Nanocyl S.A.

The compounds were purchased from Sigma-Aldrich Company and were reagent of grade quality.

These products have been used without any further purification.

IV.2.1.1 Preparation of epoxy matrices

IV.2.1.1.1 Epoxy matrix TBD

The epoxy mixture was obtained by mixing the epoxy precursor TGMDA (acronym T) with the reactive monomer BDE (acronym B) at a concentration TGMDA/BDE of 80%:20% by wt. An amount of curing agent DDS (acronym D) of 44.4 phr with respect to precursor (TGMDA) was added to activate the curing reactions. The hardener agent was employed in a non-stoichiometric ratio amine/epoxy. Epoxy blend TBD was mixed at 120°C for 1 h and, after this time, the blend was degassed in vacuum at 100°C for 1 h. The mixture was cured by a two-stage curing cycles: a first isothermal stage at the lower temperature of 125°C for 1 h followed by a

second isothermal stage at the higher temperatures of 200°C for 3 h. The chemical formulas of TGMDA, BDE and DDS have already been shown in Figure II.4.

IV.2.1.1.2 Epoxy matrix TCTBD

The epoxy mixture TCTBD was obtained as described in section III.2.1.1.1 Preparation of epoxy matrix TCTBD. The chemical formulas of the components have been already shown in Figures II.4 and III.3.

IV.2.1.1.3 Epoxy matrix TCTBD+0.5%MWCNT

The epoxy mixture TCTBD+0.5%MWCNT was obtained as described in section III.2.1.1.2 Preparation of epoxy matrix TCTBD charged with functionalized and unfunctionalized MWCNTs. The chemical formulas of the MWCNTs have been already shown in Figure III.2.

IV.2.1.1.4 Epoxy matrix TCTBD+0.5%MWCNT+1% self-healing filler

The epoxy mixture was obtained by mixing the epoxy precursor TGMDA with 12.5 phr of CTNB and 10 phr of the catalyst triphenylphophine. This mixture was heated at 170°C, using an oil bath and mechanical agitation promoted by an electric stirrer, for 24 h. The TCT blend was cooled at 120°C and the reactive epoxy diluent was added at a concentration TGMDA/BDE of 80%:20% by wt. Then the compound was added at a concentration of 1% by weight with respect to the mixture TCTBD and the epoxy blend was mixed at 120°C for 30 min. An amount of curing agent DDS of 44.4 phr with respect to precursor (TGMDA) was added to activate the curing reactions. The Epoxy blend TCTBD+1% self-healing filler was mixed at 120°C for 1 h and, after this time, the blend was degassed in vacuum at 100°C for 1 h. The mixture was cured by a two-stage curing cycles: a first isothermal stage at the lower temperature of 125°C for 1 h followed by a second isothermal stage at the higher temperatures of 200°C for 3 h.

IV.2.1.2 Self-healing fillers

The molecules selected and added into the epoxy matrix, with the aim to activate self-healing mechanism, are defined “self-healing fillers” and are commercially available.

In a preliminary screening, nine compounds have been identified. They have been chosen for their structural characteristics, and therefore for their ability to establish hydrogen bonds thanks to the presence of characteristic

functional groups. Based on their nature, these functional groups can act as H-bonding acceptors or donors.
Among these nine compounds, three have been selected and chosen as self-healing fillers. They are shown in Figure IV.1.

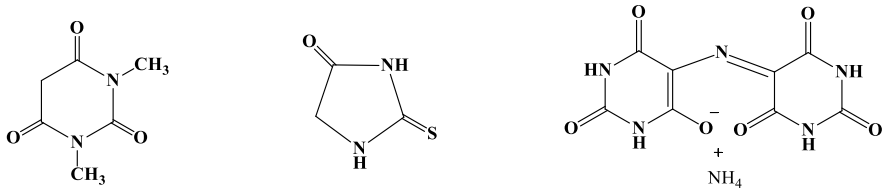

Figure IV.I *Molecular formulas of self-healing fillers*

The attention has been focused on these three molecules also because they are available at a lower cost with respect to other analyzed solutions.

IV.2.2 Methods

IV.2.2.1 Solubility tests

IV.2.2.1.1 Solubility tests in BDE diluent

The first solubility tests were performed in order to evaluate the solubility of the molecules in the reactive diluent BDE (employed for the epoxy formulations). These tests were carried out with reference to the indications of FUI XII (*Farmacopea ufficiale italiana*- Italian pharmaceutical code), which allow to evaluate the the approximate solubility, expressed as the parts of solvent (BDE) necessary to dissolve a part of solute (self-healing filler). The approximate solubility of the fillers has been attributed according to the indications reported in the Table IV.1

Table IV.1 *FUI XII indications to evaluate the solubility*

Solubility	Parts of solvent necessary to dissolve a part of solute	Range of solubility (mg/ml)
Highly soluble	<1	≥1000
Very soluble	1-10	100-1000
Soluble	10-30	33-100
Mildly soluble	30-100	100-33
Slightly soluble	100-1000	1-10
Very slightly soluble	1000-10000	0.1-1
Insoluble	>10000	≤0.1

The tests have been performed by starting from a fixed ratio filler/BDE and by diluting the heterogenous solution in case of insolubility, or by increasing the ratio (through the addition of another amount of filler), in case of solubility of the solute.

If the fillers were not soluble at room temperature, the solutions were heated up to 120°C using an oil bath and mechanical agitation promoted by a magnetic stirrer, until 1h.

IV.2.2.1.1 Evaluation of fillers' dispersion in the mixtures TB and TCTB

The tests were carried out by adding the fillers in the TB blend and in the TCTB blend and by heating the mixtures at 120°C, using an oil bath and mechanical agitation promoted by a magnetic stirrer, for 1 h.

Based on the solubility tests in BDE, the concentration chosen to evaluate the dispersion in the two blends has been 1% by weight respect to TCTBD matrix.

IV.2.2.2 Mechanical properties

IV.2.2.2.1 Dynamic mechanical analysis (DMA)

Dynamic mechanical analysis of the samples were performed with a dynamic mechanical thermo analyzer (Tritec 2000 DMA-Triton Technology). Solid samples with dimensions 2×10×35 mm^3 were tested by applying a variable flexural deformation in three points bending mode. The displacement amplitude was set to 0.03 mm, whereas the measurements were performed at the frequency of 1 Hz. The range of temperature was from -90°C to 315°C at the scanning rate of 3°C min^{-1}.

IV.2.2.2.2 Self-healing efficiency evaluation

The healing efficiency η of the samples was evaluated by fracture tests, which utilize a TDCB geometry as already described in section II.2.2.3 *Healing activity and self-healing efficiency evaluation*

IV.2.2.3 Scanning Electron Microscope (SEM)

SEM investigation has been performed as described in section III.2.2.2.1 Field Emission Scanning Electron Microscopy (FESEM). The samples have been subjected to the etching procedure before the observation.

IV.2.2.4 Rheological investigation

The rheological measuremets in the liquid state, before curing, were carried out using a Physica MCR 301 (Anton Paar) rotational rheometer equipped with a parallel plate geometry (50 mm diameter, 1mm gap) on the

following samples: the TCTBD mixture; the TCTBD+1%barbiturate mixtures; the TCTBD+0.5%MWCNT mixture; the TCTBD+1%1.3 DBA mixture at different concentrations of MWCNTs. Strain sweep tests, at the frequency of 1 rad/s, were previously performed to determine the linear viscoelastic region. Frequency sweep tests were carried out to acquire the mechanical spectra of the samples, by varying the frequency. Dynamic rheological measurements allow to observe the trend of the elastic modulus (G '), of the viscous one (G") and of the complex viscosity (η*) with the variation of the frequency (ω), once the amplitude of the deformation (γ) is fixed. The tests are carried out in nitrogen flow at temperatures of 25, 50, 75 and 90°C.

IV.2.2.5 Fourier Transform Infrared (FTIR) Spectroscopy

The procedure of FT-IR analysis is described in section II.2.2.2 Fourier Transform Infrared (FTIR) Spectroscopy.

IV.2.2.6 Thermal analysis

IV.2.2.6.1 Thermogravimetric analysis (TGA)

For the procedure, see section III.2.2.4 Thermogravimetric analysis (TGA).

IV.2.2.6.2 Differential Scanning Calorimetry

For the procedure see section III.2.2.3 Differential Scanning Calorimetry (DSC) analysis.

IV.2.2.7 Electrical properties

For the procedure, see section *III.2.2.7 Electrical properties*.

IV.3 Results and discussion

IV.3.1 Solubility and dispersion tests

The solubility tests were performed in order to evaluate the solubility of the selected molecules in the epoxy blend and such a way to identify the molecules to be used as agents activating auto-repair reversible interactions. The solubility is an important aspect for the processability of the composite materials because it can strongly affect its rheological properties. The solubility tests were carried out in the diluent BDE, as described in the experimental section, in the mixture TB, to evaluate the compatibility of the molecules with the epoxy precursor, and then in the mixture TCTB, to verify

if the presence of the liquid rubber affects the dispersion of the molecules in the finished formulation.

IV.3.1.1 Solubility tests in BDE diluent

The results of the tests for the fillers 1.3 DBA, 2T and M, in the BDE diluent, are summarized, respectively, in the Tables IV.2, IV.3 and IV.4.

Table IV.2 *Results of solubility tests for 1.3 DBA filler*

Ratio 1.3 DBA/BDE	Amount of 1.3 DBA with respect to TCTBD epoxy matrix (%)	Solubility
1:50	0.25	soluble
1:20	0.62	soluble
1:5	2.50	soluble*

* Solubility has been performed heating the solution up to 80°C for few minutes.

Table IV.3 *Results of solubility tests for 2T filler*

Ratio 2T/BDE	Amount of 2T with respect to TCTBD epoxy matrix (%)	Solubility
1:50	0.25	Soluble
1:20	0.62	Unsolube*

* Solubility test has been performed also heating the solution up to 120°C, under magnetic stirring.

Table IV.4 *Results of solubility tests for M filler*

Ratio M/BDE	Amount of M with respect to TCTBD epoxy matrix (%)	Solubility
1:50	0.25	Unsoluble*
1:500	0.025	Unsolube*
1:5000	0.0025	Unsolube*
1:10000	0.0012	Unsolube*

*Solubility tests have been performed also heating the solution up to 120°C, under magnetic stirring.

These data highlight that only the filler 1,3-Dimethylbarbituric acid (1.3 DBA) can be classified as “very soluble”, because it is soluble for all the analyzed filler/epoxy-mixture percentages. This is a very promising result

for the use of this molecule as healing agent in epoxy nano-filled formulations.

When the filler is very soluble in the diluent, no solid particles dispersed in the mixture are observed, as it is clearly visible for the solutions 1.3 DBA/BDE, shown in Figure IV.2.

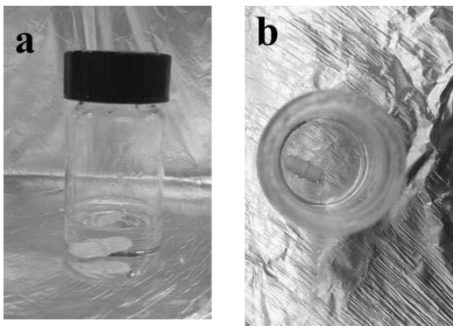

Figure IV.2 *Optical images of the vials containing the solution of the filler 1.3 DBA in the diluent BDE in different ratios: a) 1.3 DBA/BDE ratio of 1:20; b) 1.3 DBA/BDE ratio of 1:5, after heating*

The filler 2-Thiohydantoin (2T) also has shown a good solubility and it can be classified as “soluble”. It is totally soluble in the BDE until the ratio filler/diluent 1:50 (see Fig. IV.3a), while, increasing this ratio, a sedimentation of the filler particles on the bottom of the becker is observed as shown in Figure IV.3b.

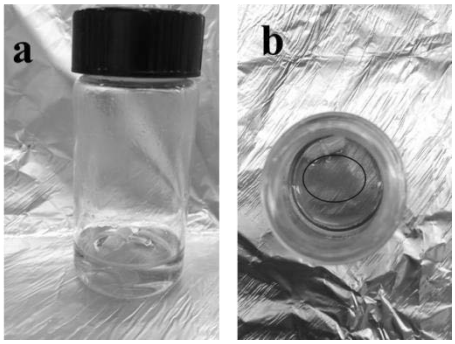

Figure IV.3 *Photos of the vials containing the solution of the filler 2T in the diluent BDE in different ratios: a) 2T/BDE ratio of 1:50; b) 2T/BDE ratio of 1:20, after heating. The black ellipse highlights the precipitate*

The filler Murexide (M), differently to previous molecules, has been classified as “insoluble”. In fact, as shown in Figure IV.4, even when the minimum filler/diluent ratio is reached, the solid particles continue to

sediment on the bottom of the becker, and the supernatant (BDE) remains totally transparent, because no particles of M are molecularly dissolved in it.

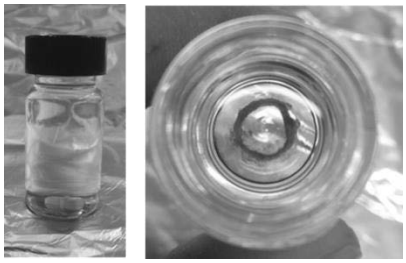

Figure IV.4 *Optical images of the vials containing the solution of the filler M in the diluent BDE in the ratio M/BDE of 1:10000*

IV.3.1.2 Evaluation of the fillers' dispersion in TB and TCTB mixtures

The dispersion of the filler in the matrix is an important aspect for the processability of the composite material and can strongly affect its rheological properties.

The tests were carried out in the mixture TB to evaluate the compatibility of the fillers with the epoxy precursor, and then they were carried out in the mixture TCTB, to verify if the presence of the liquid rubber affects the dispersion.

Based on solubility test in BDE diluent, the amount of filler used for the investigation was 1% by weight with respect to the epoxy mixture TCTBD. This concentration has been chosen to achieve the right balance between the self-healing required effect and the processability of the material.

The results of the tests are summarized in the Table IV.5.

Table IV.5 *Results of the evaluation of fillers' dispersion*

1% Self-healing filler	TB blend	TCTB blend
1,3-Dimethylbarbituric acid (1.3 DBA)	soluble	soluble
2-Thiohydantoin (2T)	partially soluble	partially soluble, good dispersion
Murexide (M)	unsoluble,	Unsolube, good dispersion

The filler 1.3 DBA solubilizes at molecular level in both the epoxy blends, while the other two fillers manifest a different behaviour. They give sedimentation in TB mixture, while in TCTBD mixture; they remain in suspension in the blend, showing a good dispersion. These results highlight a particular affinity between the fillers and the toughened matrix, in particular

with the rubber phase. This aspect has been investigated by means of FT-IR analysis.

Furthermore, the performed SEM investigation confirms the effective solubility or sospension of the fillers (*IV.3.2 Scanning Electron Microscope (SEM)*).

IV.3.2 Dynamic mechanical analysis (DMA)

In order to fully understand the influence of the self-healing fillers (1.3 DBA, 2T and M) on the mechanical properties of the toughened epoxy matrix unfilled and filled with MWCNTs, DMA analysis was performed.

The storage modulus, E' (MPa), and the loss factor, tanδ, of the analysed formulations are shown in Figures IV.5-IV.10, where in particular, tanδ, expressed as the ratio of loss modulus to storage modulus, is a measure of the energy lost, expressed in terms of the recoverable energy.

IV.3.2.1 TBD-TCTBD epoxy mixtures

Before evaluating the influence of self-healing compounds on the unfilled and filled epoxy mixture, a comparison between the unfilled epoxy resin hardened in non-stoichiometric condition (TBD) and the unfilled toughened epoxy matrix hardened in non-stoichiometric condition (TCTBD) has been performed (see Fig. IV.5a and IV.5b), with the aim to fully understand the the influence of the rubber phase on the formulated systems.

This comparison, in terms of storage modulus (see Fig. IV.5a), evidences that both samples show high values of the storage modulus, higher than 2000 MPa up to 100°C, highlighting that the TCTBD epoxy formulation can be advantageously applied in the range of service temperature of structural materials (i.e. aeronautical, shipbuilding industries, wind turbine blades, as electronic device, etc.).

The curve related to tanδ of the sample TBD (black curve) exhibits two distinct peaks centred at about 200°C and 265°C respectively (see Fig. IV.5b). The presence of two peaks in the dynamic-mechanical spectra of unfilled epoxy resins was already found in literature (Guadagno *et al*. 2017d). It was correlated to fractions with different crosslinking density characterized by two different values of Tg. The amount of these different phases, related to the intensity of the peaks in the tanδ curves, depends on the curing degree and on the stoichiometric ratio of oxirane rings/hardener.

The introduction of the liquid rubber CTBN in the epoxy matrix determines significant changes in the profile of the tanδ curve. In particular, the glass transition temperature appears as a single phase shifted at lower temperature with respect to both the Tg values of 200°C and 265°C. Furthermore, the highest peak, which is centered at about 190°C and associated with the sample glass transition, is widened and more intense than

each peak observable for the sample TBD. This is a clear indication that the two phases with different crosslinking density converge in a single phase, which presents relaxation mechanisms in a wider range of temperature. The same trend is observed for the other two weak transitions, the β transition (between -100°C and 30°C), due to crankshaft rotations of the glycidyl crosslinking segments (Huang and Kinloch 1992; Saadati *et al*. 2005), and the γ transition (between 30°C and 120°C), due to unreacted molecular segments and/or material inhomogeneities from region of different crosslink density (see the inset in Fig. IV.5b). The peaks associated with these weak transitions are more pronounced for the TBD blend, and converge in a single wider peak for the TCTBD mixture, that presents relaxation mechanisms in a range of low temperatures (-100°C and 60°C). The lower intensity of γ transition may be due to a reduction of the material inhomogeneity, hence of the regions with different crosslink density, related to the presence of the liquid rubber.

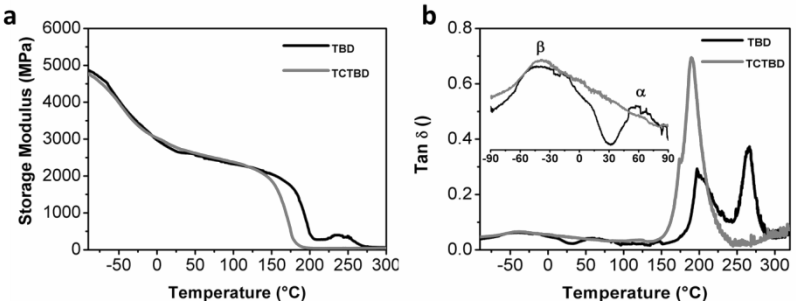

Figure IV.5 *DMA curves of the cured formulations TBD and TCTBD : a) storage modulus as a function of temperature; b) loss factor (Tanδ) as a function of temperature*

It can be hypothesized that the use of epoxy matrix toughened with the liquid rubber CNTB enhances the activation of supramolecular self-healing mechanisms (without altering the mechanical properties of the materials) for two different reasons:

1) the reduced crosslink density increases the chain flexibility and mobility, hence enhancing the ability of the composite to activate auto-repair mechanisms;
2) the modified epoxy matrix can better interact with self-healing fillers generating a dense supramolecular network;

IV.3.2.2 TCTBD-TCTBD+1%self-healing filler epoxy mixtures

In this section, the influence of the filler's addition in the TCTBD matrix has been investigated.

The samples loaded with 1% of fillers 1.3 DBA and 2T show high values in the storage modulus in the usual operational temperature range of structural materials. The profile of the curves in Figure IV.6 shows that E' is higher than 2000 MPa in a very wide temperature range of -100 ÷ 100°C. It is observed a slow and progressive decrease of E' up to 50°C, followed by an almost constant value in the range between 50 ÷ 150°C before the principal drop, due to the glass transition temperature Tg, which is evident between 150 ÷ 200°C.

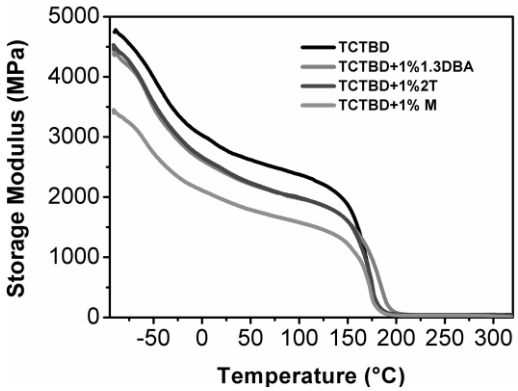

Figure IV.6 *Storage modulus of the cured unfilled epoxy formulations TCTBD and of the cured epoxy formulation TCTBD loaded with 1% of self-healing filler 1.3 DBA, 2T and M*

The presence of the Tg in this range is also confirmed by the mechanical spectra of the samples shown in Figures IV.7a and IV.7b.

The sample loaded with 1% of filler M shows a lower value of storage modulus, which is anyway higher than 2000 MPa up to about 30°C. Also for this filler, E' shows a progressive decrease up to 50°C, followed by an almost constant value in the range between 50 ÷ 150°C before the principal drop, due to the glass transition temperature Tg which is evident between 150 ÷ 200 °C. The presence of the Tg in this range is also confirmed by the mechanical spectra of the sample shown in Figure IV.7c.

It can be observed that, while the presence of the fillers 1.3 DBA and 2T slightly affects the storage modulus of the epoxy matrix, the filler M determines a decrease in the value of the strorage modulus of about 1000 - 500 MPa (depending on the temperature range). Despite this, the values of Tg observed in the mechanical spectra of all samples are not affected by the filler presence (see Fig. IV.7). The significant decrease observed in the storage modulus for M filler is most likely due to the presence of M crystals, which interrupt the crosslinking in many regions of the matrix, as also confirmed by SEM investigation.

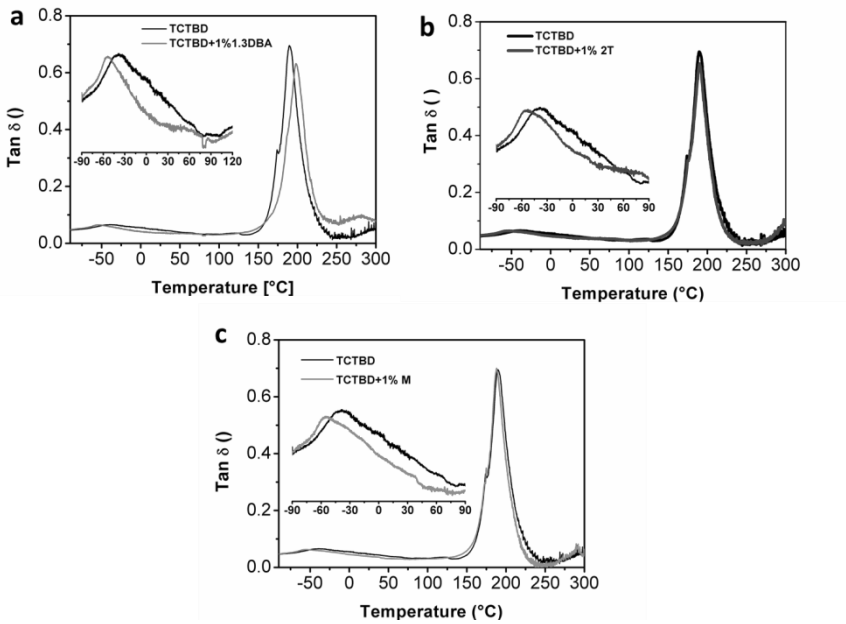

Figure IV.7 *Loss factor (tanδ) of the unfilled epoxy formulations TCTBD and the epoxy formulation loaded with 1% of self-healing fillers: a) 1.3 DBA; b) 2T; c) M*

The insets in Figure IV.7, related to the loss factor, highlight that the presence of the self-healing fillers inside the epoxy matrix causes a shift of the β transition to lower temperatures (from -40 to -60 °C).

IV.3.2.3 TCTBD-TCTBD+0.5%MWCNT

Before evaluating the influence of self-healing fillers on the epoxy mixture loaded with MWCNTs, a comparison between the toughened epoxy matrix not loaded with the MWCNT (TCTBD) and the toughened epoxy matrix loaded with MWCNT (TCTBD+0.5%MWCNT) was performed (see Fig. IV.8a and IV.8b). MWCNTs, embedded in the matrix, cause an increase of the storage modulus in the temperature range from -90°C to 0°C (see Fig. IV.8a) and a shift of the glass transition temperature to the higher value of 210°C. Furthermore, the inclusion of MWCNTs affects the intensity of the transition observed in the lower temperature range, from -45°C to about -60°C (see inset in Fig. IV.8b).

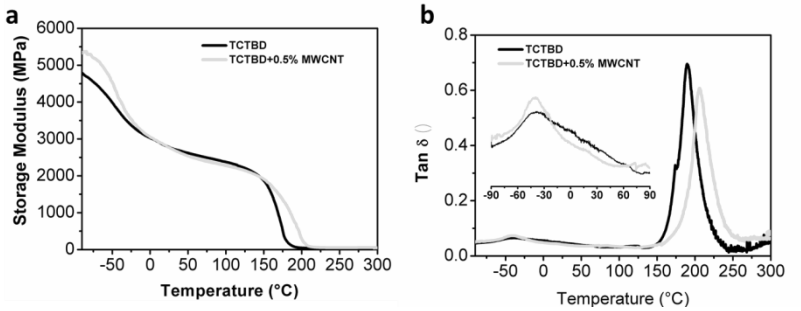

Figure IV.8 *DMA curves of TCTBD and TCTBD+0.5%MWCNT: a) storage modulus; b) loss factor (Tanδ)*

IV.3.2 4 TCTBD+0.5%MWCNT - TCTBD+0.5%MWCNT+1%self-healing filler

The presence of self-healing fillers in the epoxy matrix loaded with carbon nanotubes determines a decrease in the storage modulus, as shown in Figure IV.9. Contrarily to what is observed in absence of MWCNT, the filler M does not cause large differences in the storage modulus with respect to the fillers 13 DBA and 2T. The curve related to the sample containing the filler 2T is superimposed to the curve of the formulation loaded with the filler M. The lowest values in the storage modulus are observed for the filler 13 DBA, which also causes a decrease in the glass transition temperature, as shown in Figure IV.10a.

Figures IV.10b and IV.10c, show that, in presence of the fillers 2T and M, the glass transition temperatures values are higher than 200°C, but the associated peaks are characterized by a lower intensity. Furthermore, another small peak at lower temperature appears in both samples. This peak is centred at about 190°C for TCTBD+0.5%MWCNT+1%2T sample and at about 200°C for TCTBD+0.5%MWCNT+1%M sample. The presence of the double peak observed for the fillers 2T and M is most likely due to a slight disomogeneity in the crossilinking density enhanced by the interaction with CNT walls.

Furthermore, also for these samples, the transition observed in the lower temperature range is shifted at higher values of temperatures; respect to those observed for the samples loaded only with the self-healing fillers (see inset in Fig. IV.10).

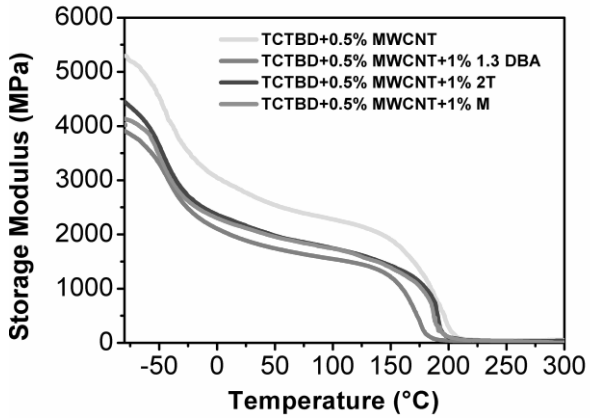

Figure IV.9 *Storage modulus of the epoxy formulations TCTBD loaded with 0.5% of MWCNT and with 1% of self-healing fillers 1.3 DBA, 2T and M*

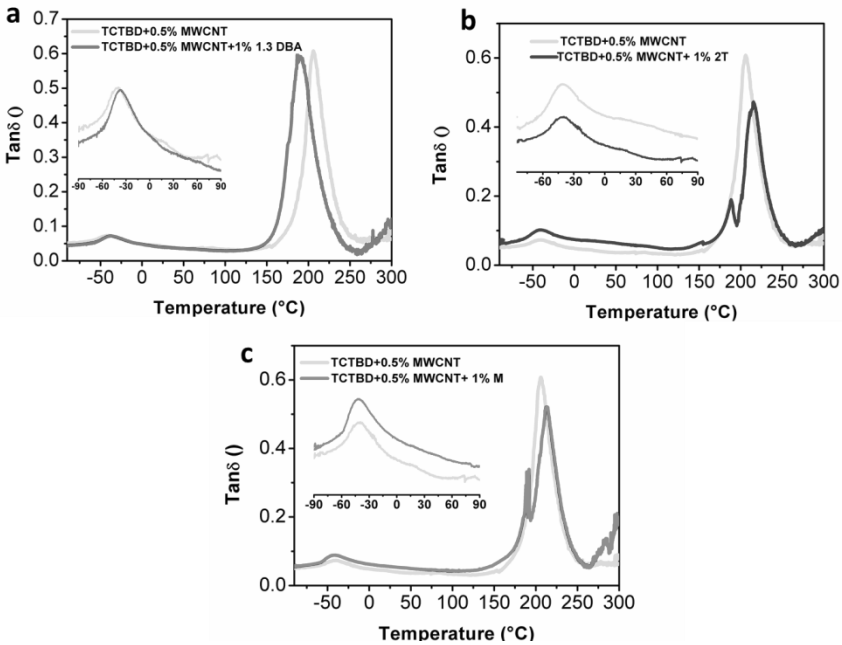

Figure IV.10 *Loss factor (tanδ) of the epoxy formulations TCTBD loaded with 0.5% MWCNT and with 1% of self-healing fillers: a) 1.3 DBA; b) 2T; c) M*

Dynamic mechanical results have shown that the simultaneous presence of MWCNT and the self-healing fillers 2T and M in the toughened epoxy matrix, tends to create a phase with increased mobility of the chains, as

evident from the appearance in the spectrum of tanδ of the peak at lower temperature with respect to the peak corresponding to the main transition. The barbituric filler 1.3 DBA shows a different beahavior, but also in this case, it is possible to observe an increase in the chain mobility as evident from the translation of the main peak, in the spectrum of tanδ, at lower temperature. This phase characterized by higher mobility could be responsible for a better promotion of auto-repair mechanisms, as highlighted by the results of self-healing efficiency evaluation (see section *IV.3.7 Self-healing efficiency evaluation*).

IV.3.3 Scanning Electron Microscope (SEM) investigation

The self-healing filler dispersion in the toughened epoxy matrix, both in presence and absence of MWCNT, was analysed by SEM investigation on etched samples. The etching procedure consumes part of the surface layers of the epoxy matrix making possible a clearer observation of the dispersion state of the fillers. Furthermore, the surface of the observed samples has been obtained by means of breaking in liquid nitrogen, to block all the movements of the rubbery phase chains.

Figure IV.11 shows SEM image of the toughened epoxy matrix without MWCNT and self-healing filler. The etching procedure has allowed observing the globular domains of the rubbery phase within the sample, highlighting their uniform sizes and homogeneous distribution in the rigid continuous phase. The observation of rubbery domains has been possible since the etching process corroded more the interface zone between the rubbery phase and the matrix, where the crosslink density is lower.

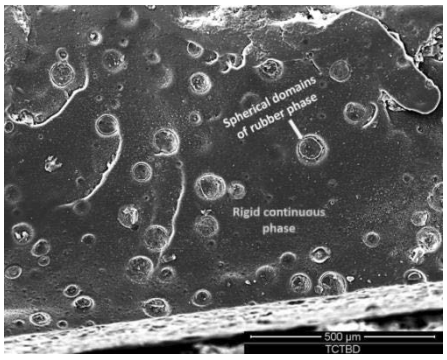

Figure IV.11 *SEM image of the fracture surface of the unfilled epoxy composite TCTBD*

Figure IV.12 shows SEM images of the toughened epoxy matrix TCTBD loaded with carbon nanotubes at different magnifications. In these images, it

is possible to discriminate between rubbery phase, rigid continuous phase, and MWCNTs which form percolated paths (for this sample it was found a conducibility value of 2.5×10^{-2} S/m). It can be also observed that the nanotubes are mainly incorporated in the resin, with poor affinity with the rubbery phase. In the dark zone of the last image (Fig. IV. 12d), the etching procedure has better highlighted the presence of nanotubes that form a continuous network in the matrix.

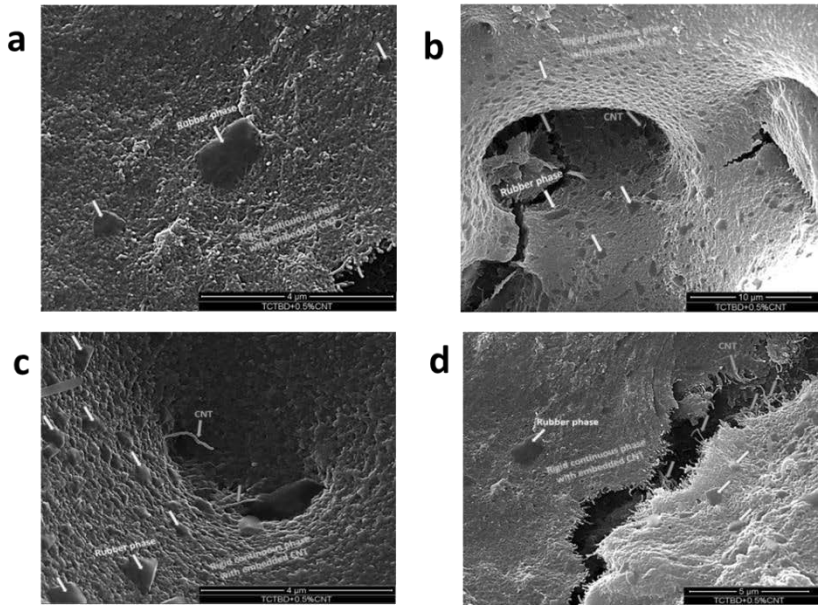

Figure IV.12 *SEM image at different magnifications of the fracture surface of the epoxy composite TCTBD loaded with 0.5% of MWCNT*

Figure IV.13 shows SEM images of the epoxy formulation TCTBD loaded with 1% of barbituric compound 1.3 DBA. The complete solubilization of the filler determines the absence of crystalline particles and promotes a more effective and homogeneous distribution of rubbery domains.

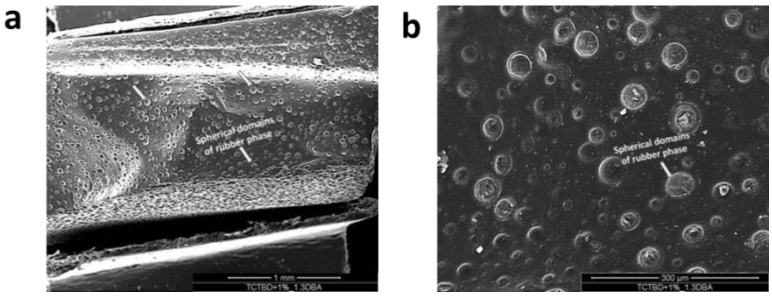

Figure IV.13 *SEM images at different magnifications of the fracture surface of the epoxy composite TCTBD loaded with 1% of barbituric compound 1.3 DBA*

Figure IV.14a shows the SEM images of the epoxy formulation TCTBD loaded with 1% of the compound 2T. It can be observed the presence of 2T filler crystals, not completely solubilized in the epoxy matrix. These crystals are characterized by a well-defined geometry, which can be distinguished from the globular shape of the rubbery phase.

Figure IV.14b shows the SEM image of the epoxy formulation TCTBD loaded with 1% of the compound 2T and 0.5% by weight of MWCNT. In this selected image, it can be observed an area where the rigid continuous phase of the resin has been well corroded by etching, highlighting the conductive network of nanotubes strongly anchored to the matrix.

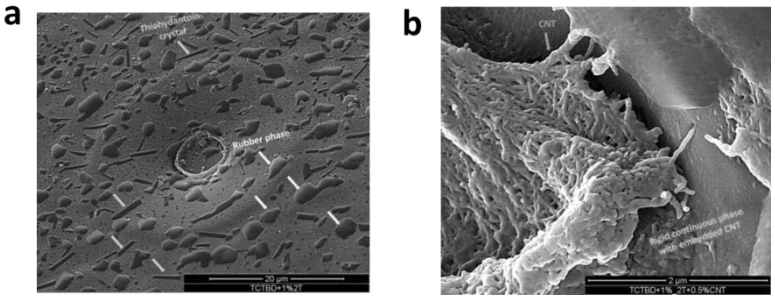

Figure IV.14 *SEM images of the fracture surface of the epoxy composite TCTBD loaded with: a) 1% of the filler 2T; b) 1% of the filler 2T and 0.5% by weight of MWCNT*

Figure IV.15a shows the SEM image of the epoxy formulation TCTBD loaded with 1% of the compound M. The globular rubbery domains are clearly distinguisble in the epoxy matrix. Furthermore, the dark area in Figure IV.15a corresponds to the matrix corroded by the etching procedure.

Figure IV.15b, corresponding to the epoxy formulation TCTBD loaded with 1% of the compound M and with 0.5% of MWCNT, shows the

presence of not solubilized murexide crystals, characterized by a well-defined geometry, and the nanotube networks strongly bounded to the epoxy matrix.

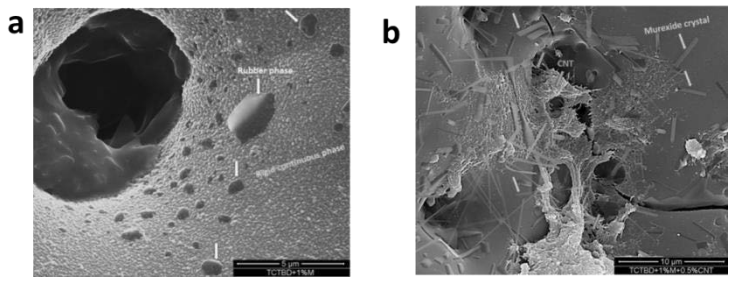

Figure IV.15 *SEM image of the fracture surface of the epoxy composite TCTBD loaded with: a) 1% of the filler M; b) 1% of the filler M and 0.5% MWCNT*

For a better evaluation of the morphology of the materials, SEM investigations on the powder of the self-healing fillers, have been performed and are shown in the following figures.

Figure IV.16 shows the SEM images of the filler's powder 1.3 DBA at two different magnification. This compound has a scaled morphology, without a well-defined geometric shape. These flakes are not observed in the final composite, as expected considering the solubility tests.

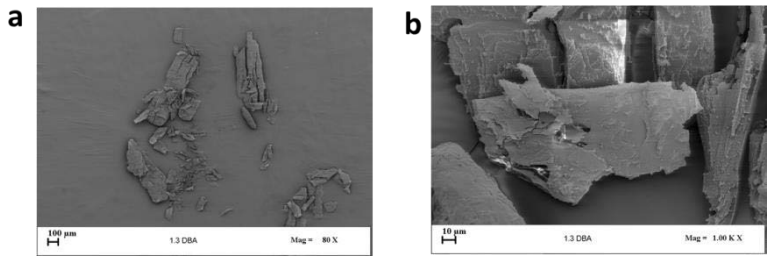

Figure IV.16 *SEM image of the powder of the barbituric filler 1.3 DBA, at two different magnifications*

Figure IV.17 shows the SEM images of the filler 2T at two different magnifications. This filler has a morphology characterized by crystals with a well-defined geometry, which can be observed also in the final composite (see Fig. IV.14a) because of the filler's insolubility.

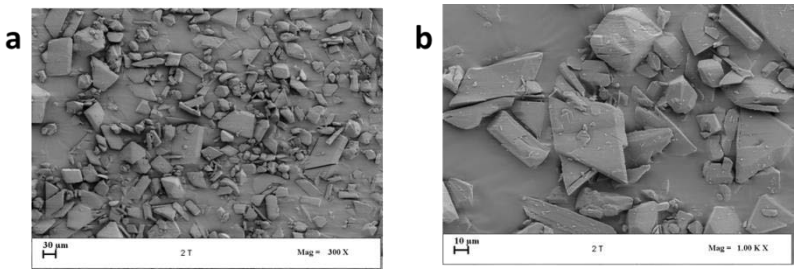

Figure IV.17 *SEM image of the powder of the filler 2T, at two different magnifications*

Figure IV.18 shows the SEM images of the filler M at three different magnifications. Also for this filler, crystals characterized by a well-defined morphology are observable. However, the morphological feature of these crystals in the finished nanocomposites is very different from the initial morphology. In particular, in the nanocomposites, as a consequence of the preparation procedure, the murexide phase appears in the form of needle-like crystals (see Fig. IV.15b).

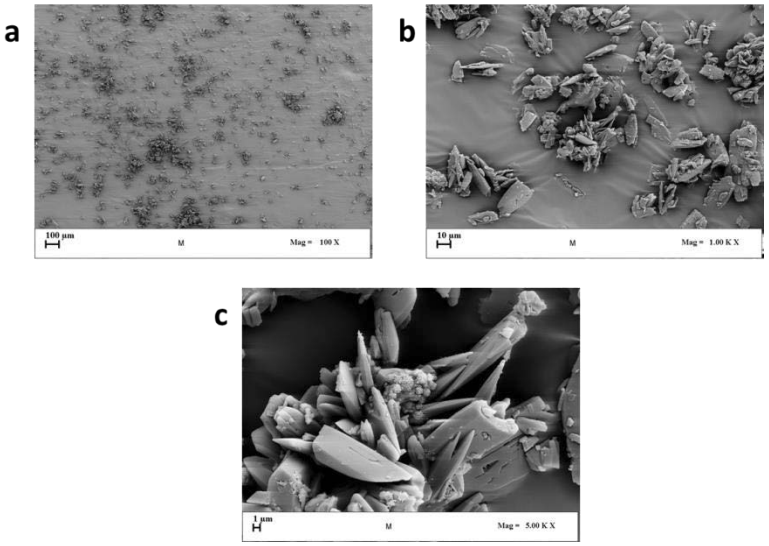

Figure IV.18 *SEM image of the powder of the filler M, at three different magnifications*

Summarizing, SEM analysis has allowed to better understand many aspects of the material morphology:

- a homogeneous distribution of the rubbery phase with dimensionally uniform globular domains;
- the confirmation of total solubility of barbiturate filler 1.3 DBA, an important aspect for the processability of the material;

- the presence of a dense conductive network of nanotubes well distributed and strongly anchored to the epoxy matrix, but not dispersed in the rubber phase
- a homogeneous dispersion of compound crystals 2T and M, which, although not solubilized, are well distributed in the material.

IV.3.4 Rheological investigation

One of the engineering aspects associated with the use of self-healing multifunctional formulations, loaded with carbon nanotubes (MWCNTs), is the optimization of processing steps for their production. In this concern, the study and the control of the rheological properties of the epoxy mixtures are of fundamental importance. The choice of the manufacturing processes and the optimization of the various processing parameters strongly depend on the rheological behaviour of the samples.

In order to study the viscoelastic properties of self-repairing epoxy formulations loaded with multi-walled carbon nanotubes and with self-healing fillers, rheological analysis on the samples in the liquid state, before curing, has been performed. Rheological measurements of the functional uncured formulations were carried out on a Physica-MCR301 (Anton-Paar) rotational rheometer. Small amplitude oscillatory shear measurements were performed at different temperatures.

IV.3.4.1 TCTBD epoxy mixture

At first, the rheological behavior of the toughened epoxy matrix TCTBD was evaluated. Figure IV.19 shows the trend of the complex viscosity (η^*) as a function of the frequency (ω) for the TCTBD blend, obtained through a frequency sweep test in strain-controlled mode performed at temperatures of 25, 50, 75 and 90°C.

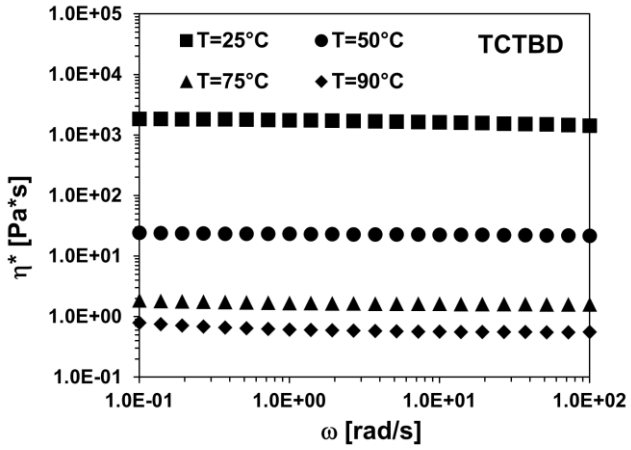

Figure IV.19 *Complex viscosity (η*) vs frequency (ω) for the TCTBD blend, at different temperatures*

In the considered range of frequency and at each tested temperature, the TCTBD mixture is characterized by a Newtonian behavior with constant values of the complex viscosity, which decreases by about four orders of magnitude, as the temperature increases (see Table IV.6).

Table IV.6 *Values of complex viscosity (η*) at different temperatures (T) for TCTBD blend*

T [°C]	η* [Pa*s]
25	1726,552
50	22,89545
75	1,668182
90	0,610136

IV.3.4.2 TCTBD+1%self-healing filler epoxy mixture

The trends of the complex viscosity as a function of the frequency, for the TCTBD+1%self-healing filler blends, were obtained through frequency sweep tests in strain controlled mode performed at temperatures of 25, 50, 75 and 90°C. Figures IV.20a and IV.20b show, respectively, the tests performed at 50 and 90°C and highlight that the inclusion of self-healing agents does not influence the Newtonian behavior of the matrix TCTBD. Furthermore, the toughened epoxy matrix TCTBD with the addition of the self-healing agents 1.3 DBA, M and 2T, is characterized by an increase in viscosity compared to the TCTBD blend.

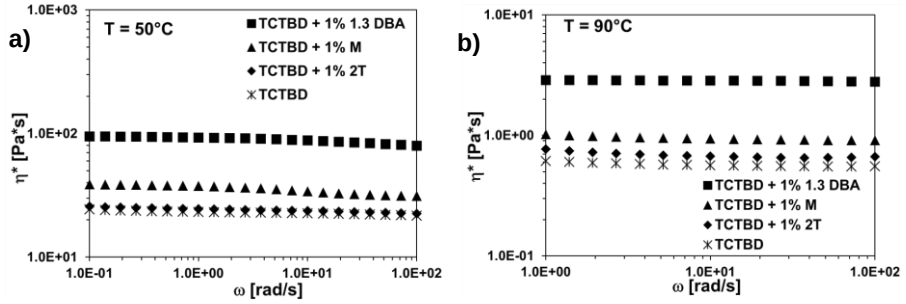

Figure IV.20 *Complex viscosity (η*) vs frequency (ω) for TCTBD, TCTBD+1% 1.3 DBA, TCTBD+1% M and TCTBD+1% 2T epoxy mixtures, at: a) T= 50°C; b) T= 90°C*

Table IV.7 shows the values related to the decrease of the complex viscosity as a function of temperature. It can be observed that the viscosity decreases as the temperature increases of about 4 orders of magnitude for TCTBD+1% 1.3 DBA blend (at 90°C), of about 5 orders of magnitude for TCTBD+1% 2T blend (at 90°C) and of about three orders of magnitude for TCTBD+1% M blend (at 90°C).

Table IV.7 *Values of complex viscosity (η*) at different temperatures (T) for TCTBD+1% self-healing filler blend*

T [°C]	η* TCTBD+1% 1.3 DBA [Pa*s]	η* TCTBD+1% 2T [Pa*s]	η* TCTBD+1% M [Pa*s]
25	11100	-	2550
50	92,8	24,5	37,6
75	6,43	2,04	2,63
90	2,87	0,77	1,02

IV.3.4.3 TCTBD+0.5% MWCNT epoxy mixture

The inclusion of 0.5wt% MWCNTs in the toughened epoxy matrix TCTBD, determines a change in the viscosity trend, which begins to show a shear-thinning behavior already at T= 25°C and this trend is more evident at higher temperatures (see Figure IV.21a). Therefore, the addition of the nanotubes involves the transformation from a Newtonian behavior to a non-Newtonian behavior. Moreover, the inclusion of the 0.5wt% MWCNTs, in the TCTBD epoxy matrix, produces a plateau in the storage modulus (G') at low frequencies, indicative of a clear solid-like behaviour (see Figure IV.21b) and highlighting that the TCTBD+0.5% MWCNT liquid dispersion

is above the rheological percolation threshold, as also confirmed by the electrical results.

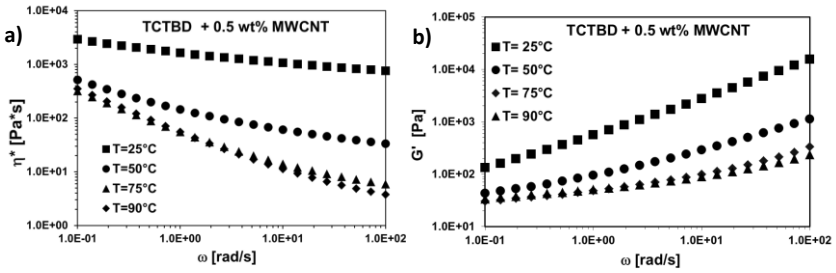

Figure IV.21 *a) Complex viscosity (η*) vs frequency (ω) for TCTBD+0.5% MWCNT, at different temperatures; b) Storage modulus (G') vs frequency (ω) for TCTBD+0.5% MWCNT, at different temperatures*

IV.3.4.4 TCTBD+1%self-healing filler+0.5% MWCNT epoxy mixture

The inclusion of self-healing agents in the mixture TCTBD+0.5% MWCNT does not significantly alter the rheological behavior, in terms of viscosity and storage modulus trends (see Figures IV.21 and IV.22). In particular, at the temperature of 25°C and in all the analysed range of frequencies, the complex viscosity shows a shear thinning behaviour and it is characterized by higher values than those corresponding to the nano-composite containing only the 0.5% by weight of MWCNTs (see Figure IV.21a). At the temperature of 50°C, the complex viscosity shows a shear-thinning trend much more marked than that occuring at 25°C (see Figure IV.21b). Furthermore, in the range of high frequencies, the mixture containing the barbituric filler 1.3 DBA, shows the highest viscosity. At the temperatures of 75°C and 90°C, in the range of high frequencies, this difference in the viscosity values between the various analysed systems tends to decrease (see Figures IV.22c and IV.22d).

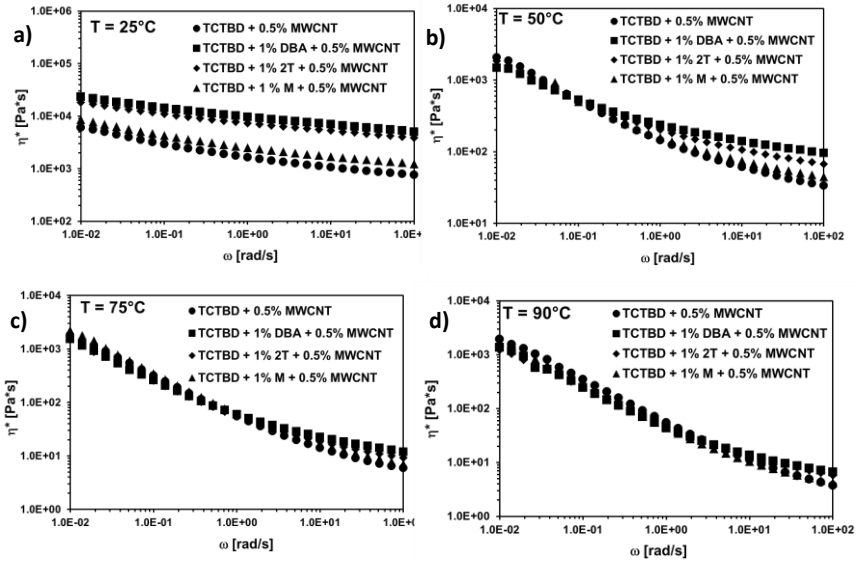

Figure IV.22 *Complex viscosity (η*) vs frequency (ω) for TCTBD+0.5% MWCNT, TCTBD+1% 1.3 DBA+0.5% MWCNT, TCTBD+1% 2T+0.5% MWCNT and TCTBD+1% M+0.5% MWCNT at a) T= 25°C; b) T= 50°C; c) T= 75°C; d) T= 90°C*

The analysis of the storage modulus as a function of the oscillation frequency highlights that, when the temperature increases, a plateau in the area of the low oscillation frequencies is observed for all the nanocomposite systems. In particular, at the temperature of 50, 75 and 90°C, the materials are above the rheological percolation threshold (see Figure IV.23).

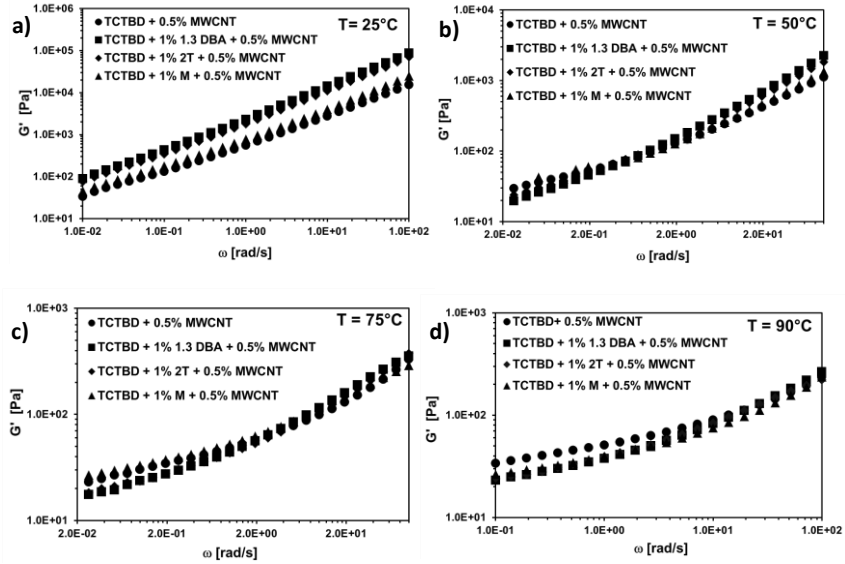

Figure IV.23 *Storage modulus (G') vs frequency (ω) for TCTBD+0.5% MWCNT, TCTBD+1% 1.3 DBA+0.5% MWCNT, TCTBD+1% 2T+0.5% MWCNT and TCTBD+1% M+0.5% MWCNT at a) T= 25°C; b) T= 50°C; c) T= 75°C; d) T= 90°C*

IV.3.4.5 TCTBD+1% 1.3 DBA+ 0.1-1% MWCNT epoxy mixture

In order to evaluate the rheological percolation threshold, rheological tests at different temperatures have been performed on the mixture TCTBD containing the barbituric filler 1.3 DBA with different concentration by weight of MWCNTs. This acid-based barbituric filler was chosen because the performed solubility tests (*IV.3.1 Solubility and dispersion tests) have* established that this molecule is completely soluble at 1% by weight within the TCTBD epoxy matrix. Increasing the concentration of MWCNTs from 0.1 to 1 wt% within the TCTBD+1% 1.3 DBA matrix, the complex viscosity, in the low frequencies area, gradually increases, highlighting a shear thinning behaviour. The complex viscosity trend modifies from a Newtonian to a shear-thinning behavior when the MWCNT's content is about 0.3 wt% (see Figure IV.24).

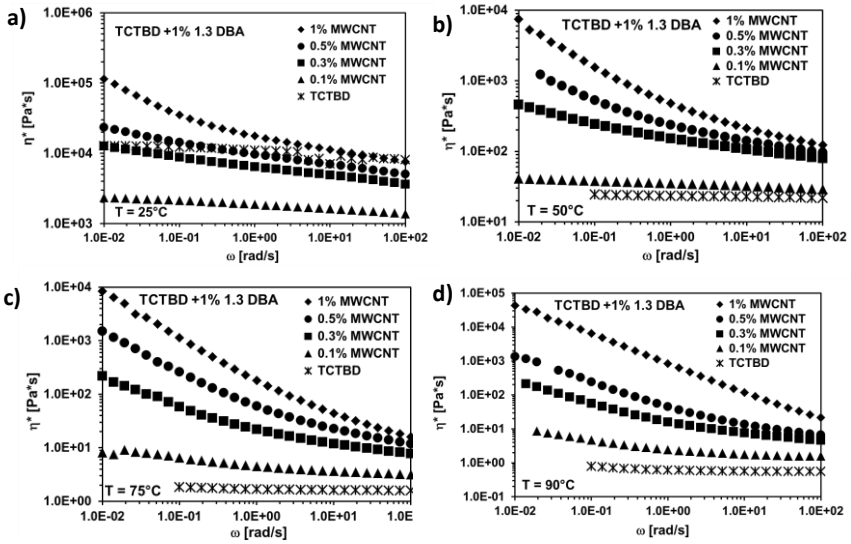

Figure IV.24 *Complex viscosity (η*) vs frequency (ω) for TCTBD+1% 1.3 DBA with different concentration of MWCNTs at: a) T= 25°C; b) T= 50°C; c) T= 75°C; d) T= 90°C*

Analogously, the analysis of storage modulus shows that the inclusion of the nanofiller gradually modifies the terminal liquid-like behaviour of the pure matrix. In particular, at a temperature of 25°C, the system shows a plateau for the storage modulus, in the area of the low oscillation frequencies, when the concentration of carbon nanotubes is 1% by weight (see Figure IV.25a). At a temperature of 50°C, in the area of the low oscillation frequencies, it is possible to observe, already for the nanocomposite containing 0.5% by weight of carbon nanotubes, a plateau value for the elastic modulus (see Figure IV.25b). Considering the higher temperatures of 75 and 90°C, the presence of a plateau for G 'is observed already for the percentage of 0.3% by weight of carbon nanotubes (see Figures IV.25c and IV.25d), indicating, for this value, the rheological percolation threshold. Therefore, the transition from liquid-like to solid-like behaviour, due to the formation of an interconnected network in the nanocomposite, occurs between 0.1 and 0.3 wt % MWCNT.

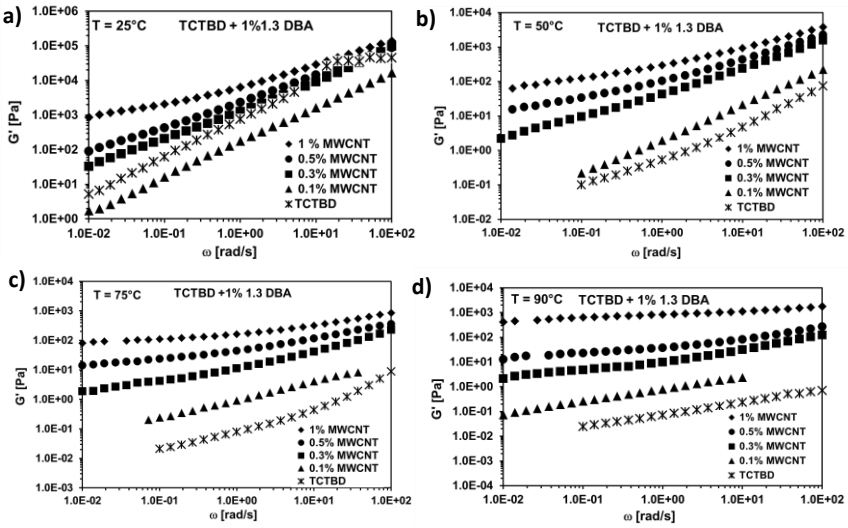

Figure IV.25 *Storage modulus (G') vs frequency (ω) for TCTBD+1% 1.3 DBA with different concentration of MWCNTs at: a) T= 25°C; b) T= 50°C; c) T= 75°C; d) T= 90°C*

In conclusion, the rheological measurements, carried out on the epoxy TCTBD system, have shown that the presence of the fillers at 1wt% does not alter the Newtonian behavior of the epoxy matrix. The addition of carbon nanotubes, in the epoxy formulations containing the healing agents, shows that the complex viscosity and the storage modulus are mainly dominated by the presence of the nanofillers. The addition of different amounts of MWCNTs to the TCTBD+1% 1.3 DBA mixture has highlighted that the rheological percolation threshold is between 0.1 and 0.3% by weight of MWCNT, similarly to what has been previously observed for the nanocomposite without acid-based barbituric filler.

IV.3.5 FT-IR investigation

In order to evaluate the interactions that the barbiturate acid derivatives can establish with the components of the toughened epoxy blend, FT-IR analysis has been performed.

FT-IR spectroscopy is a useful technique for the recognition of functional groups in molecules.

Different factors can determine a variation in the absorption frequency of a functional group with respect to its theoretical value, one of this is the molecular association. Within a sample, the molecular segments, bringing functional groups, can establish bonds between them or with other components, and in particular they can form intermolecular and intra-molecular hydrogen bonding. The hydrogen bonding is formed in any

system containing a proton *donor* group X-H (carboxyls, hydroxyls, amines, amides) and an *acceptor* group Y (oxygen, nitrogen, halogens).

The hydrogen bonding modifies the force constant of both groups, therefore the vibration frequencies of both stretching and bending are altered; more precisely, a general shift of frequencies is observed towards lower values, which leads to more intense and enlarged bands.

The analyzed molecules can establish hydrogen bonding interactions with the matrix because they have these donor and acceptor sites, just like the same matrix (carboxylic and hydroxyl groups). With the aim to confirm these interactions, FT-IR spectra have been carried out on the solid samples cured up to 200°C.

In a first qualitative evaluation, the spectra of the samples oven cured and those of the uncured formulations, containing the self-healing fillers, have been compared, in order to understand if the signals of the characteristic fuctional groups of these molecules have been shifted to different values of frequency, because of H-bonding interactions.

IV.3.5.1 FT-IR investigation for the system with 1.3 DBA filler

The comparison between the spectra of the oven cured epoxy formulations, shown in Figure IV.26, highlights that only the samples containing the molecule 1.3 DBA have a characteristic peak around 1680 cm^{-1} (see the inset in Fig. IV.26). This signal is located in the range of frequency of carbonyl group, and it may be due to the imide carbonyl C=O stretching band of the barbiturate acid derivative 1.3 DBA. In fact, in the spectrum of the single filler (see Fig. IV.27), two peaks can be observed in this region and they belong to the carbonyl groups C=O. There are two different peaks for the same functional group because the chemical surrounding environments is different: it can be distinguished an imide C_1=O stretching group about at 1700 cm^{-1} and an imide C_2=O stretching group about at 1660 cm^{-1}. The characteristic value of C=O stretching bond for cyclic imides with six carbon atoms is around 1710-1700 cm^{-1}, but the presence of two nitrogen atoms bonded to C_2=O group causes the shift of the signal to lower frequencies for inductive effects.

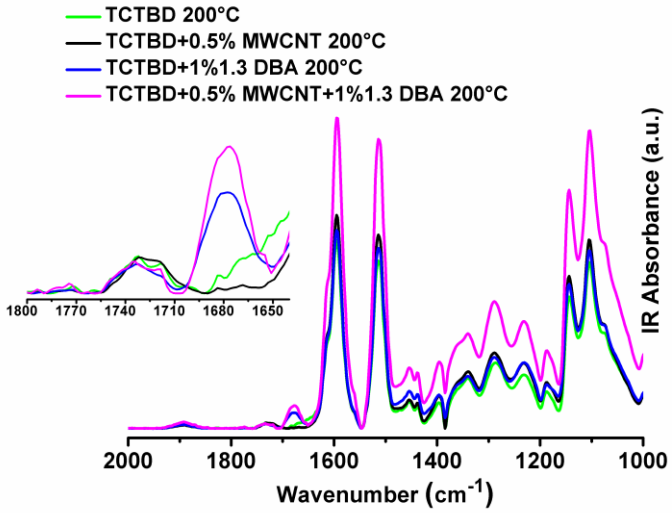

Figure IV.26 *FT-IR spectra of the cured formulations: TCTBD (green curve), TCTBD+0.5%MWCNT (black curve), TCTBD+1%1.3DBA (blue curve) and TCTBD+0.5%MWCNT+1%1.3 DBA (violet curve)*

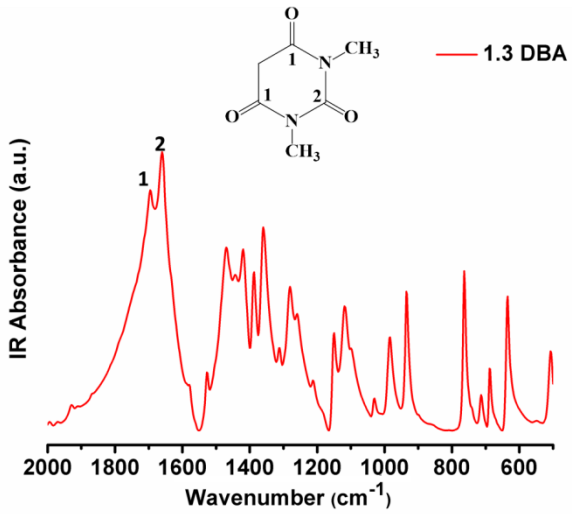

Figure IV.27 *FT-IR spectrum of the barbituric filler 1.3 DBA*

These two signals, belonging to two different carbonyl groups, converge into one peak when the filler is added in the toughened epoxy formulation.

In particular, Figure IV.28a highlights that, when the filler is added to the TB mixture, the two peaks are still separated, instead, they converge into a broadened peak when the filler is added to the toughened epoxy matrix TCTB: the peak at about 1700 cm^{-1} shifts at a lower value of frequency, forming a single wider signal with the other signal (red and green curves).

This broadening effect of the signal is even more pronounced in the cured epoxy formulation loaded with 1% by weight of 1.3 DBA filler (see Fig. IV.28b).

In light of the above, it can be hypothesized that this behavior is a clear evidence that C=O functional groups of 1.3 DBA filler are involved in hydrogen bonding interactions (as acceptors) with the O-H groups (formed during the toughening reaction, see Fig. III.4) of the TCTB mixture and of the cured mixtures. It is worth noting that during the curing process of the resin, the number of OH group increase, enhancing the H-bonding interactions and causing an increased broadening of the signal at around 1680 cm^{-1}.

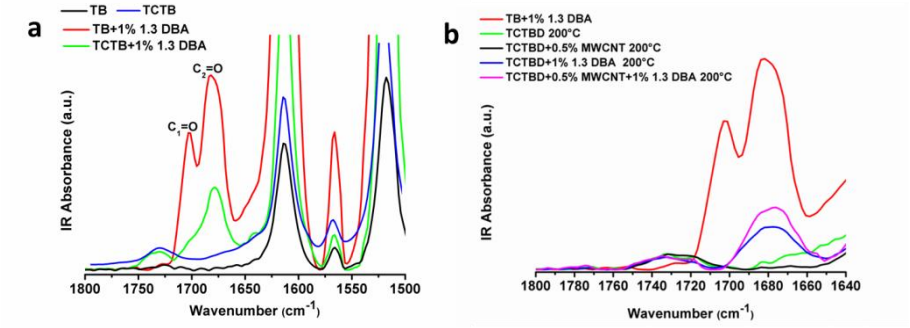

Figure IV.28 *a) FT-IR spectra of the uncured liquid formulations, TB (black curve), TCTB (blue curve), TB+1% 1.3 DBA (red curve) and TCTB+1%1.3 DBA (green curve); b)FT-IR spectra of the cured formulations, TCTBD (green curve), TCTBD+0.5%MWCNT (black curve), TCTBD+1%1.3DBA (blue curve) and TCTBD+0.5%MWCNT+1%1.3 DBA (violet curve)and of the liquid uncured mixture TB+1%1.3 DBA (red curve)*

IV.3.5.2 FT-IR investigation for the system with 2T filler

A similar trend is also observed in the samples with the barbiturate acid derivative 2T. The spectra shown in Figure IV.29 (see inset Fig. IV.29), highlight that, in the range of frequencies between 1750 and 1640 cm^{-1}, an intense signal (1707 cm^{-1}) is present only in the samples containing the molecule 2T (blue and violet curves). Considering the FT-IR spectrum of the single filler 2T (see Fig. IV.30), and focusing the attention in that same region, there is a similar peak, at about 1730 cm^{-1}, which can be associated with the C=O stretching band of the carbonyl functional group of 2T molecule: the molecule 2T could be considered as a cyclic amide with 5 atoms (a γ-lactam), for this class of compounds the C=O FT-IR signal is around 1750-1700 cm^{-1}.

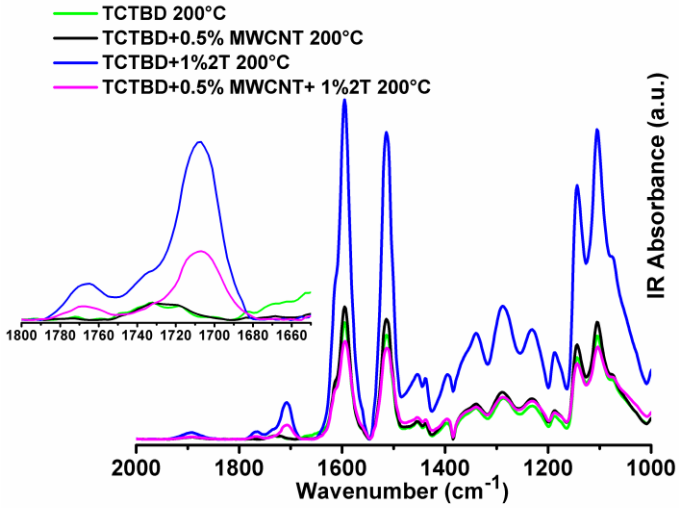

Figure IV.29 *FT-IR spectra of the cured formulations: TCTBD (green curve), TCTBD+0.5%MWCNT (black curve), TCTBD+1%2T (blue curve) and TCTBD+0.5%MWCNT+1%2T (violet curve)*

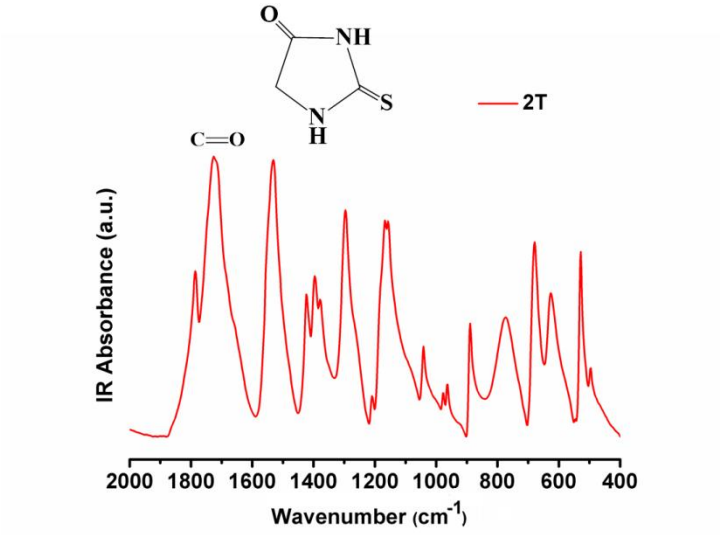

Figure IV.30 *FT-IR spectrum of the filler 2T*

This amide carbonyl signal broadens and is shifted to lower values of frequency when the filler is added in the toughened epoxy formulation.

In particular, Figure IV.31a highlights that the signal starts to change when the filler is added to the toughened epoxy matrix TCTB (green curve).

It is worth noting that the ester carbonyl group in the mixture TCTB (Vertuccio *et al.* 2017) (see blue curve in Fig. 31a) has a value of frequency very similar to that of the amide C=O of the filler 2T (see red curve in Fig. 31a), so these two signals overlap in the spectrum of TCTB+1%2T (see green curve in Fig. 31a).

The comparison shown in Figure IV.31b, clearly highlights the shift of amide C=O from 1731 to 1707 cm^{-1} in the cured epoxy formulation loaded with 1% by weight of 2T filler.

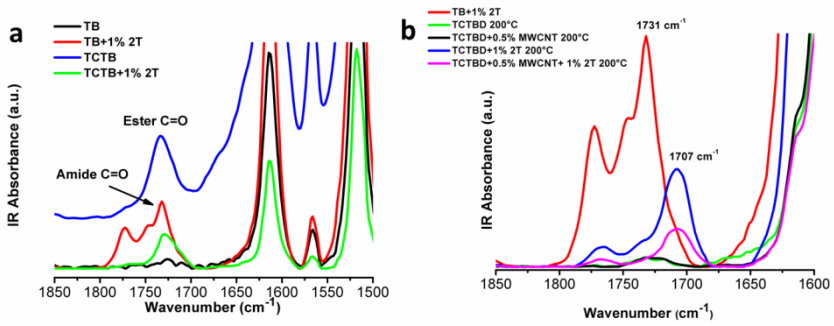

Figure IV.31 *a) FT-IR spectra of the uncured liquid formulations, TB (black curve), TCTB (blue curve), TB+1% 2T (red curve) and TCTB+1%2T (green curve); b)FT-IR spectra of the cured formulations, TCTBD (green curve), TCTBD+0.5%MWCNT (black curve), TCTBD+1%2T (blue curve) and TCTBD+0.5%MWCNT+1%2T (violet curve)and of the liquid uncured mixture TB+1%2T (red curve)*

Also, in this system it can be supposed that C=O functional group of 2T filler is involved in hydrogen bonding interactions (as acceptor) with the OH groups of the TCTB mixture and of the cured mixtures.

IV.3.5.3 FT-IR investigation for the system with M filler

In the spectrum of Murexide, no the same trend is observed. Most likely, the possible presence of any signals' shift is not visible due to total insolubility of the molecule. In fact, as shown in Figure IV.32, the characteristic absorbance bands of different carbonyl groups present in the spectrum of molecule M in the range of frequencies between 1800-1600 cm^{-1} (see Fig. IV. 32a), are not observable in the spectra of the liquid mixture loaded with the filler (see Fig. IV. 32b).

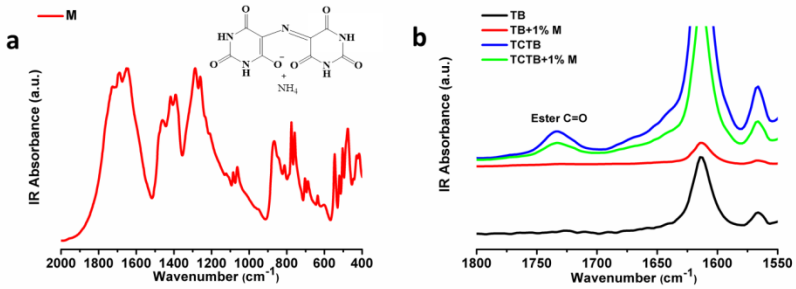

Figure IV.32 *a)FT-IR spectrum of the filler M; b) FT-IR spectra of the uncured liquid formulations, TB (black curve), TCTB (blue curve), TB+1% M (red curve) and TCTB+1%M (green curve)*

However, it is evident an intensification of the absorption band at about 1730 cm^{-1} (see Fig. IV.33, spectra violet and blue), belonging to the ester functional groups of the toughened epoxy formulation, as above mentioned.

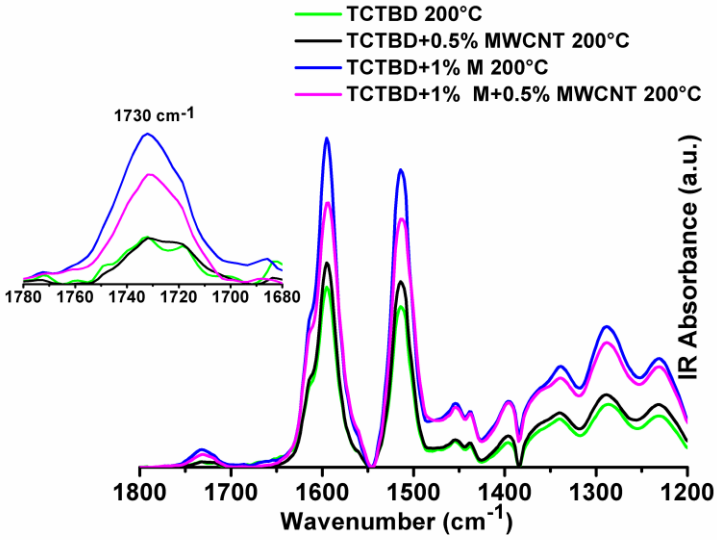

Figure IV.33 *FT-IR spectra of the cured formulations: TCTBD (green curve), TCTBD+0.5%MWCNT (black curve), TCTBD+1%M (blue curve) and TCTBD+0.5%MWCNT+1%M (violet curve)*

This effect is not observed in the other two analysed systems (see Figs. IV.26 and IV.29). In particular, for the system with the 1.3 DBA filler (see inset of Fig. IV.26) it is clearly observable that all the spectra show the signal at 1730 cm^{-1} with about the same intensity for all the samples (for the system containing the filler 2T, the absence of the intensification effect is less detectable due to overlap of the signals).

In order to support this qualitative assessment, in Fig. IV.34 an histogram with the values of the ratio *R*, between the intensity of the peak at 1730 cm^{-1} and the intensity of a reference peak at 1513 cm^{-1} (associated with the phenyl group, assumed chemically unmodified during the reaction) (Vertuccio *et. al* 2017), is shown for the samples containing the molecules 1.3 DBA and M, and for the samples without these two acid barbiturate derivatives. While for almost all the samples, the values of *R* are comparable, for the formulations containing the Murexide these values highly increase.

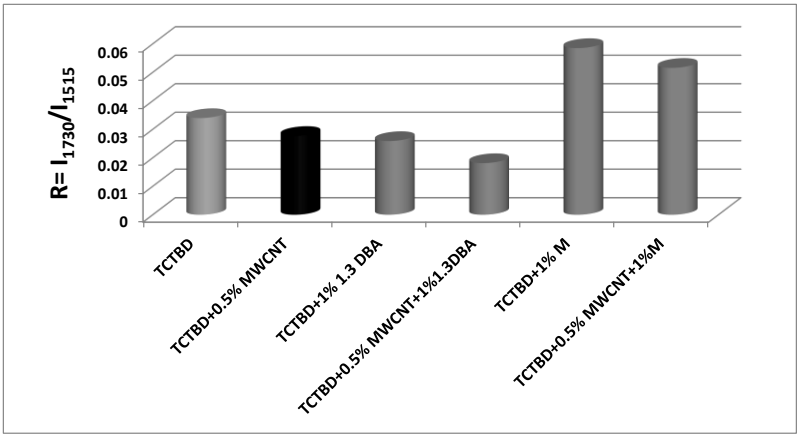

Figure IV.34 *Comparison of the R values for different formulations*

It could be hypothesize a role of Murexide as catalyst in the reaction between the rubber phase CTNB and the epoxy precursor TGMDA, just like PPh_3 (see Fig. III.4), according to the reaction scheme proposed in Figure IV.35. The nucleophilic attack by the oxygen atom of Murexide's enolate anion opens the epoxy ring, producing an intermediate containing a vinyl ether functional group. The carboxylic anion of the elastomer CTNB reacts with the electrophilic carbon of the intermediate, regenerating the catalyst and producing an ester functional group.

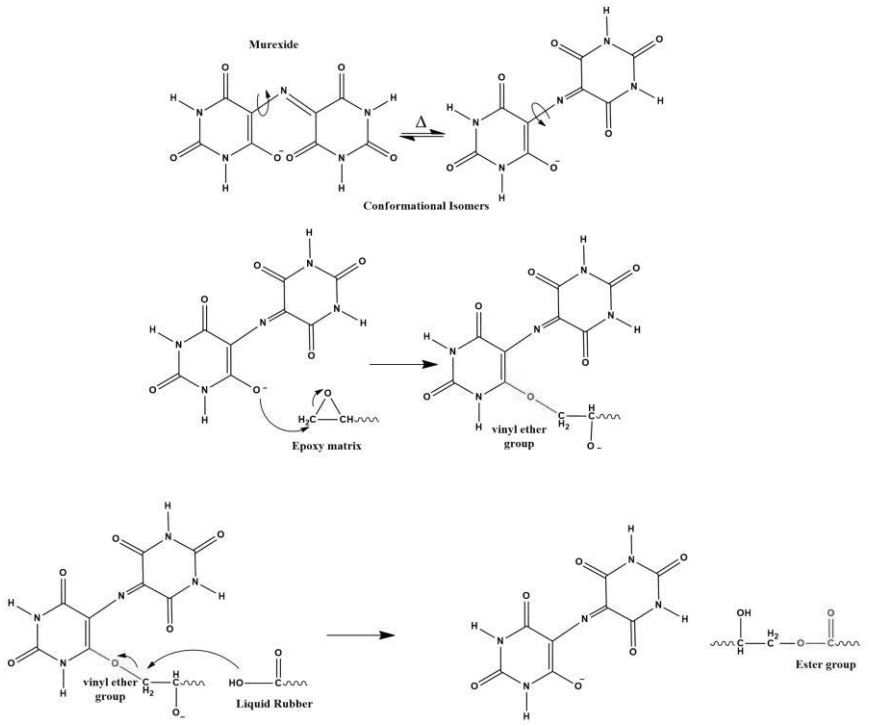

Figure IV.35 *Supposed reaction mechanism catalysed by Murexide*

Also, if the oxygen atom of the enolate anion seems to be sterically hindered, the high temperatures, reached during the curing process, could promote the rotation of the molecule around the C-N single bond, making the nucleophilic attack of the oxygen atom to the oxirane ring possible.

This hypothesis could also allow to explain the lowering of the storage modulus observed in the DMA analysis for the cured sample TCTBD+1%M (see section IV.3.2 Mechanical properties), caused by a greater toughening of the matrix.

However, further investigations on this supposed mechanism are planned.

IV.3.5.4 Further FT-IR investigation on the analysed systems

In order to better highlight the formation of H-bonding interactions between the self-healing fillers and the epoxy matrix, further evaluations by means of FT-IR analysis have been performed on the cured samples. In particular, for the systems loaded with both components, self-healing fillers and MWCNTs, a detailed investigation on the OH groups' absorbance bands has been carried out.

Infrared spectroscopy can be used to observe the O-H stretching band in the region between 3200 and 3650 cm^{-1}. This vibration is sensitive to hydrogen bonding. Generally, sharp bands related to this vibration are never observed in the FT/IR spectra of epoxy resins because they are related to free hydroxyl groups, which can be observed in the vapor phase, in very dilute solution of non-polar solvents or for hindered OH groups. In these last cases, the additional formation of intermolecular hydrogen bonding appears as additional bands at lower frequencies between 3550 and 3200 cm^{-1}. In the solid state, the O-H stretching signal of an epoxy resin appears as a broad band because of the intermolecular hydrogen bonding formed during the curing cycle. However, the profile of the band in the region of the hydroxyl groups and the presence of more or less accentuated shoulders and/or additional peaks can provide information about the nature of hydrogen bonding interactions (Guadagno *et al.* 2017b).

In order to better analyse the profile of OH stretching band, a deconvolution has been performed on the signal in the range of frequencies between 3600-3100 cm^{-1}. The used peak function has been a mixed Gauss–Lorentz line shape; this is calculated, by a non-linear curve fitting of data, the height, the full width al half height (FWHH) and the position of the individual components. This valuation method has also been applied in literature (Vertuccio *et al*. 2017). The result of this procedure has led to the identification of two peaks (see red curves in Fig.IV.36) for each O-H stretching band (see black curve, real peak, in Fig. IV.36): one peak at higher values of frequencies, that is associated to the free hydroxyl groups, and an another peak, shifted to lower values of frequencies, that is associated to O-H groups involved in H-bonding interaction as donors. The ratio R, between the area of the O-H H-bonded signal ($A_{OH\text{-}bond}$) and the area of the free O-H signal ($A_{OH\text{-}free}$), has allowed to make a quantitative evaluation of the H-bonding interactions formed in the composites: a greater value of this ratio, indicates that a greater number of OH groups is involved in hydrogen bond interactions with self-healing fillers.

Figure IV.36 shows the results of the deconvolutions, while Figure IV.37 shows the values of the ratio $R= A_{OH\text{-}bond}/A_{OH\text{-}free}$ for the different formulations. The data highlight that the presence of the self-healing fillers increases the amount of H-bonding interactions, in particular in the composite loaded with the 1% by weight of the filler M, favouring the formation of a supramolecular network, which promotes the activation of self-healing mechanisms (*IV.3.7 Self-healing efficiency evaluation*).

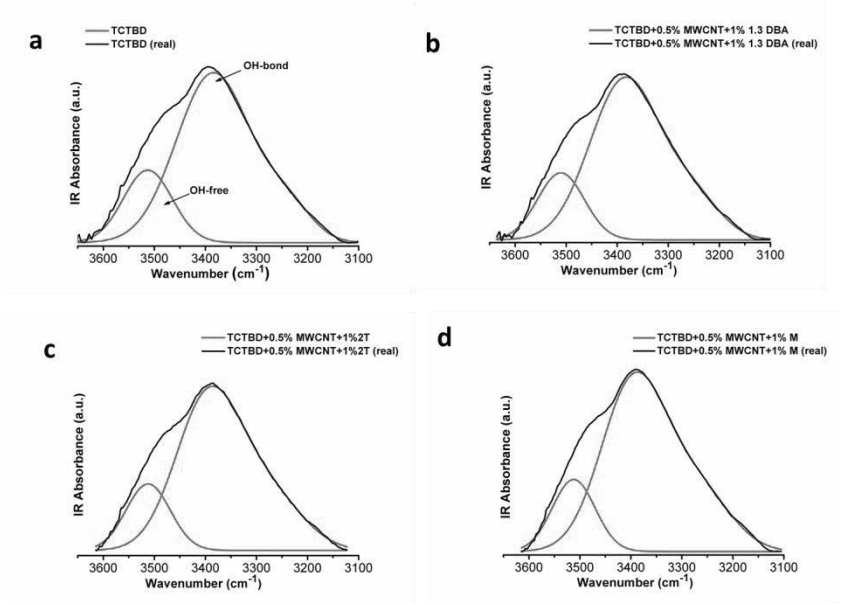

Figure IV.36 *Deconvolution performed on the O-H absorbance band of the FT-IR spectra of the samples: a) TCTBD; b) TCTBD+0.5% MWCNT+1%1.3 DBA; c) TCTBD+0.5%MWCNT+1%2T; d) TCTBD+0.5%MWCNT+1%M*

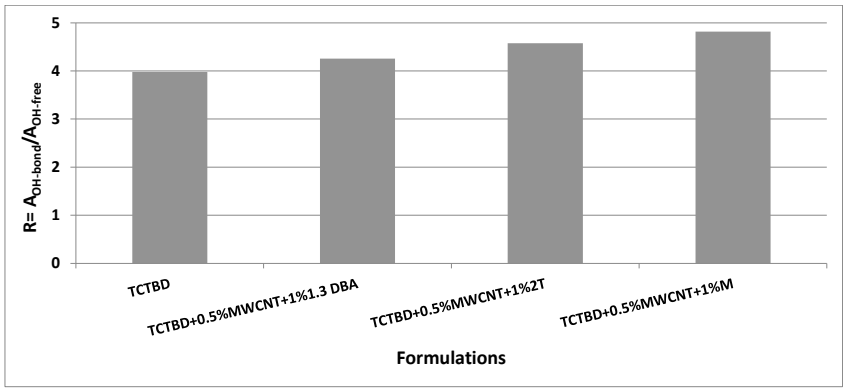

Figure IV.37 *Values of the ratio $R= A_{OH\text{-}bond}/A_{OH\text{-}free}$ for the different formulations*

IV.3.6 Thermal analysis

IV.3.6.1 Differential Scanning Calorimetry

DSC analysis has been performed for the estimation of the curing degree (DC), defined in the experimental section *III.2.2.3 Differential Scanning Calorimetry (DSC) analysis*, after a curing cycle composed of two steps: a first step of 125°C for 1 h followed by a second step at the higher temperature of 200°C for 3 h, where both steps have been carried out in isothermal condition in oven. Figure IV.38 shows DSC curves of the cured toughened epoxy mixture TCTBD and of the same epoxy mixture filled with MWCNTs and with both, MWCNTs and self-healing fillers. Almost all samples show a small fraction of uncured resin, which continues to cure in the range of temperature between 175°C and 275°C, except for resin filled with the compound M, which seems to show a further small exothermic peak, centered at about 280°C, just like it has been observed for the resins filled with functionalized MWCNT-b and MWCNT-t (see section III.3.2.2.1 Differential Scanning Calorimetry (DSC)).

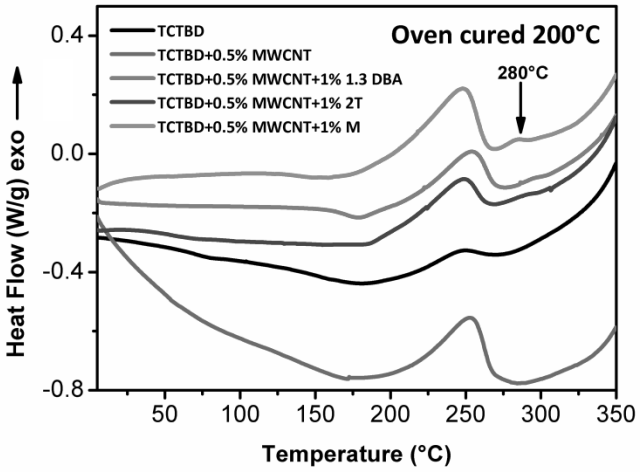

Figure IV.38 *DSC curves of the cured epoxy mixtures: TCTBD, TCTBD+0.5%MWCNT, TCTBD+0.5%MWCNT+1%1.3 DBA, TCTBD+0.5%MWCNT+1%2T and TCTBD+0.5%MWCNT+1%M*

It is very likely that these exothermic peaks are due to a beginning of decomposition of the organic molecule Murexide (M), in the temperature range higher than 270°C and before the degradation process of the epoxy matrix, around 360°C (see TGA curves in Fig. IV.40). This initial decomposition reactions can cause free radicals responsible for a little additional curing of the resin. It is worth noting that the analysed samples

and the healing efficiency have been evaluated after a curing cycle up to 200°C; hence a temperature able to preserve the thermal stability of the functional groups. The degree of curing for the sample TCTBD was found to be 97%, calculated according to equation (III.1), as described in the experimental section *III.2.2.3 Differential Scanning Calorimetry (DSC) analysis.* The inclusion of MWCNTs in the epoxy formulation determines a non-trivial decrease in the DC value (DC=89, due to a lower crosslinking density); whereas for the resin loaded with both, MWCNTs and the barbiturate fillers 1.3 DBA and 2T, only a slight decrease in DC values was found with respect to the unfilled formulation (see Table IV.4). Instead, for the epoxy nanocomposite filled with the filler M, a further decrease in the DC value, with respect to the unfilled formulation, has been found (DC=86).

It is likely that this decrease is due to a competition between two reactions of nucleophilic attack on the oxirane ring of the epoxy precursor: the neceophilic attack of the amine group (-NH_2) of the hardener DDS and the nucleophilic attack of the negative charged oxygen atom (O^-) of the Murexide (see reaction scheme in Fig. IV.39). This possible competition can hinder the curing process of the material, decreasing the cure degree of the final composite.

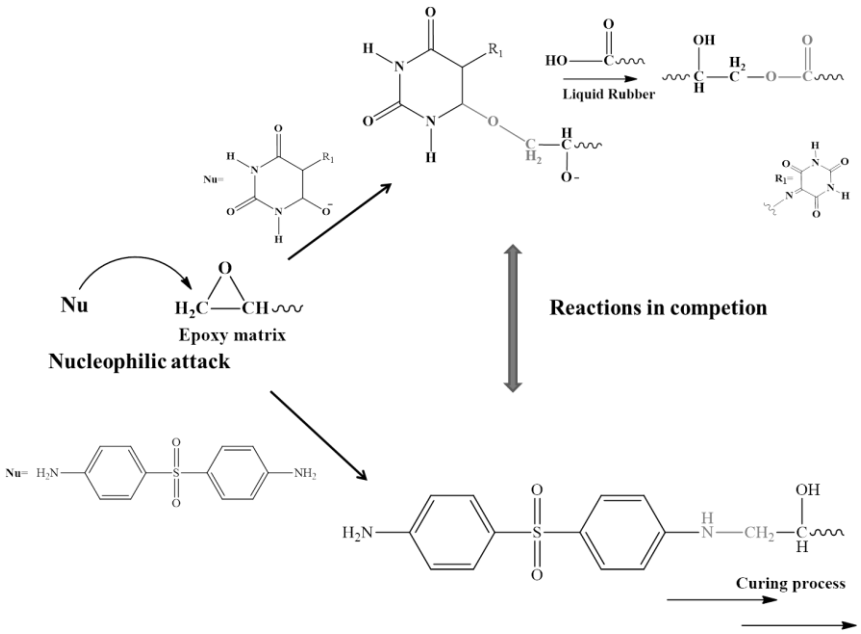

Figure IV.39 *Reaction scheme of the two possible nucleophilic attacks on the oxirane ring of the epoxy precursor*

For the samples loaded with the self-healing fillers 1.3 DBA and 2T, using the same curing cycle, the presence of these molecules allows to reach a higher curing degree compared to the formulation containing only

MWCNTs, making in this way the resin suitable to meet industrial requirements.

Table IV.8 shows ΔH_T, ΔH_{Res} and DC values of the analysed samples calculated as described in the experimental section *III.2.2.3 Differential Scanning Calorimetry (DSC) analysis.* For the sample TCTBD+0.5% MWCNT+1%M the ΔH_{Res} and ΔH_T calculation has been performed excluding the exothermic peak at 280°C, which is absent in the reference samples TCTBD and TCTBD+0.5%MWCNT. This experimental procedure prevents the overestimation of the curing degree for the samples with functionalized nanotubes.

Table IV.8 *Calorimetric results of the analysed samples*

Sample	Cure Degree DC [%]	ΔH_{Res} [Jg^{-1}]	ΔH_T [Jg^{-1}]
TCTBD	97	8.16	283.42
TCTBD+0.5%MWCNT	89	48.48	429.32
TCTBD+0.5%MWCNT+1%1.3 DBA	92	30.10	354.80
TCTBD+0.5%MWCNT+1%2T	92	27.22	348.32
TCTBD+0.5%MWCNT+1%M	86	54.27	392.17

IV.3.6.2 Thermogravimetric analysis (TGA)

Figure IV.40 shows TGA curves of the cured toughened epoxy mixture TCTBD and of the same epoxy mixture filled with MWCNTs and with both, MWCNTs and self-healing fillers, in air and nitrogen flow. The beginning of thermal degradation process, defined as 5% mass loss temperature, is around 360°C for all analysed samples, both in air and nitrogen atmosphere.

The samples TCTBD+0.5%MWCNT+1%2T and TCTBD+0.5%MWCNT+1%M, in air seem to lose a small percentage of their weight in the temperature range higher than 250°C and before the main first step of the degradation process. This seems to be in agreement with the hypothesis of decomposition of the self-healing filler, mentioned before. In any case, TGA curve profiles highlight two distinct and well-separated turns. Both in nitrogen and air, the first step falls in the temperature range between 360°C and 450°C, evidencing that there is no appreciable influence of MWCNTs and of self-healing fillers on the first step of the degradation process.

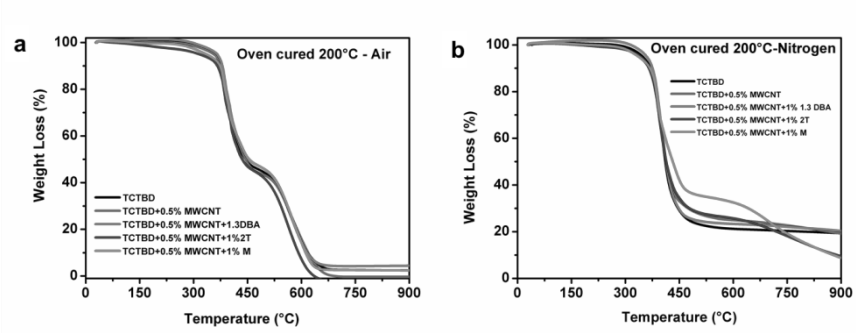

Figure IV.40 *TGA curves of the cured toughened epoxy mixtures TCTBD, TCTBD+0.5%MWCNT, TCTBD+0.5%MWCNT+1%1.3DBA, TCTBD+0.5%MWCNT+1%2T and TCTBD+0.5%MWCNT+1%M in a) air flow; b) nitrogen flow*

As already seen for systems loaded with functionalized MWCNTs, in air the samples seem to be more stable than in nitrogen; the mass loss is 52–57% in air and 69–76% in nitrogen, except for the system containing the Murexide, for which the mass loss is about 60% in nitrogen flow.

In nitrogen atmosphere, a stabilizing effect of MWCNTs is observed in the second step of the degradation process in the temperature range between 450°C and 750°C. Concerning the influence of the self-healing fillers, while the 1.3 DBA compound tends to minimally decrease this effect, the filler M highly increases it. The curve of the sample TCTBD+0.5%MWCNT+1%2T is superimposable to that of the sample loaded only with MWCNTs.

TGA analysis of uncured epoxy evidences the same steps and the same temperature ranges for the degradation processes.

All the collected results highlight that no degradation processes occur during the curing process; hence, the formulated nanocomposites are stable up to 350–360°C.

IV.3.7 Self-healing efficiency evaluation

Values of healing efficiency (η) have been calculated (according to Eq. (II.2) shown in section *II.2.2.3 Healing activity and self-healing efficiency evaluation*) for the formulations containing both, the MWCNTs and the self-healing fillers. For all samples, only one cycle has been carried out: after the closure of the crack, the sample has been kept for 24 h and a first cycle has been performed after the healing of the sample.

Figure IV.41 shows the load-displacement curves for the epoxy matrix loading the MWCNTs and the fillers 1.3 DBA (see Fig. IV.41a), 2T (see Fig. IV.41b) and M (see Fig. IV.41c).

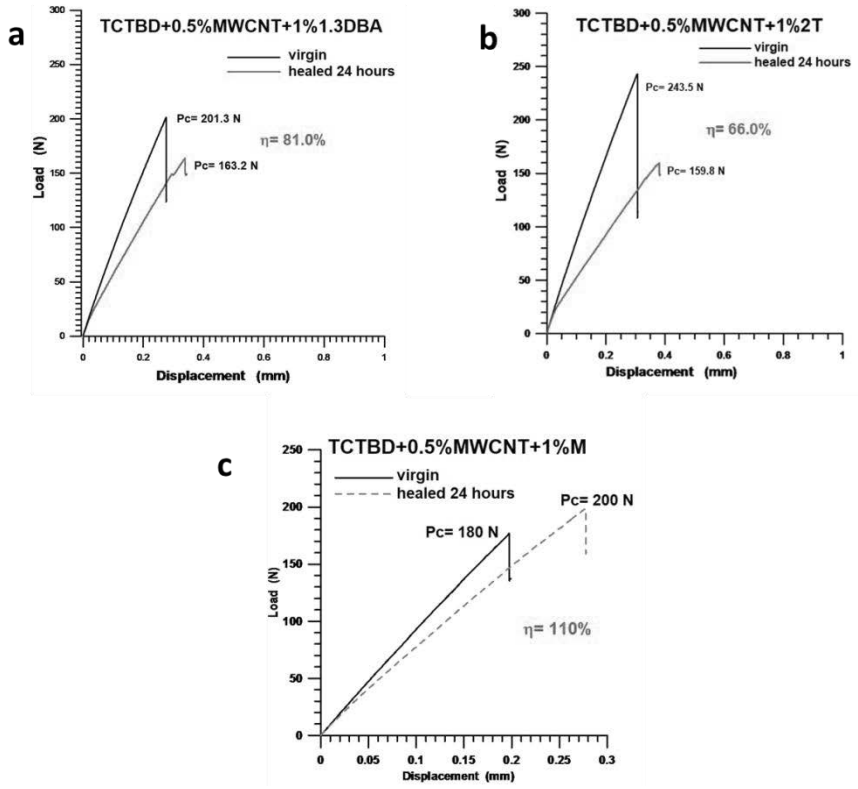

Figure IV.41 *Load-Displacement curves for the TCTBD+0.5%MWCNT samples embedded with filler: a) 1.3 DBA; b) 2T; c) M*

Good values of self-healing efficiencies have been obtained, in particular for the system containing the filler Murexide (M).

In order to confirm the supposed synergistic effect between the different components of the samples, in the activation of self-healing mechanisms, a complete set of TDCB fracture tests has been performed. The results of these tests are shown in Figure IV.42 and are summarized in the Table IV.9.

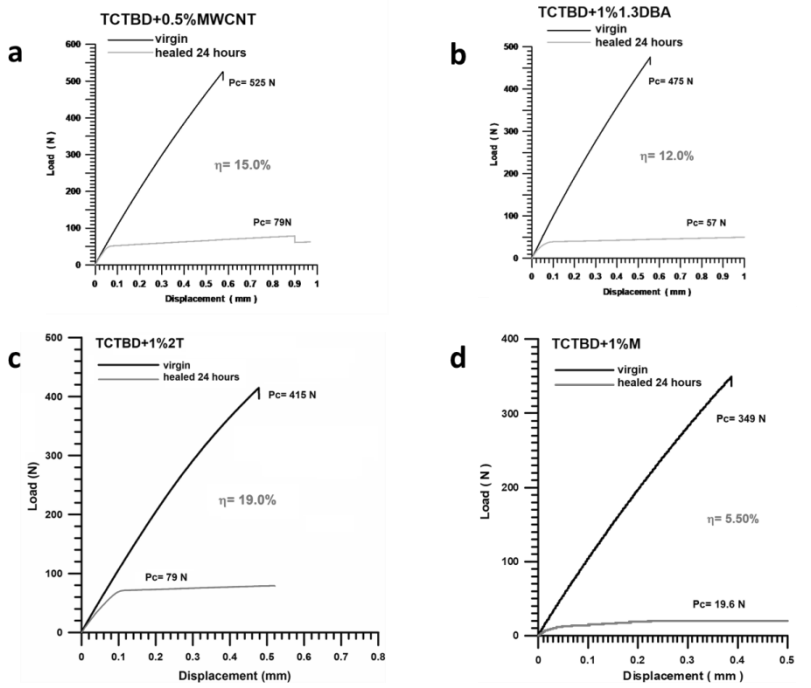

Figure IV.42 *Load-Displacement curves for the samples: a) TCTBD+0.5%MWCNT; b) TCTBD+1%1.3DBA; c) TCTBD+1%2T; d) TCTBD+1%M*

Table IV.9 *Healing efficiency values after the first healing cycle*

Sample	Healing efficiency (η)
TCTBD+0.5%MWCNT	15.0
TCTBD+1%1.3DBA	12.0
TCTBD+1%2T	19.0
TCTBD+1%M	5.50

The samples loaded only with MWCNTs or with the self-healing filler, show low values of healing efficiency with respect to the formulations containing both the components. These data highlight that there is a synergistic action between the various components of the mixture, which interacting each other could generate a supramolecular network able to activate self-healing mechanisms. As shown by dynamic mechanical results, the samples containing MWCNT and self-healing fillers tend to create a phase with increased mobility of the chains. This particular phase arrangement is most likely responsible for better promoting reversible hydrogen bonds determined by interaction between epoxy resin and self-

healing fillers. The presence of a more mobile phase in the formulation seems to enhance the self-healing efficiency of the composite material.

Moreover, the high efficiency value obtained for the sample TCTBD+0.5%MWCNT+1%M could be due to the chemical nature of the molecule, which is characterized by a bigger number of hydrogen bonding donor and acceptor sites, than the other two compounds (see Fig. IV.43), and, in addition, it presents sites that can establish ionic interactions.

Figure IV.43 shows the analyzed molecules, highlighting the sites that can establish non-covalent interactions with the matrix, in particular with the carbonyl and hydroxyl groups of the toughened epoxy matrix (see Fig. III.4 in the section III.2.1.1.1 Preparation of epoxy matrix TCTBD).

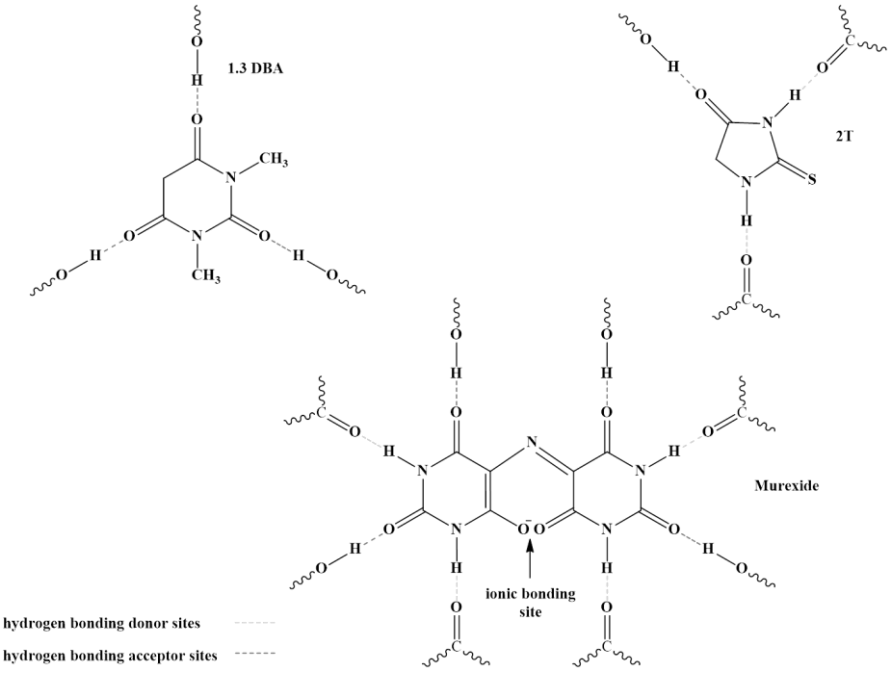

Figure IV.43 *Hydrogen bonding donor and acceptor sites in the analysed self-healing fillers*

IV.2.2.7 Electrical properties

In order to evaluate the electrical behaviour of nano-charged materials, electrical conductivity measurements have been performed. The obtained values of electrical conductivity are shown in Table IV.10.

Table IV.10 *Values of electrical conductivity for the analyzed samples*

Sample	Electrical Conductivity [S/m]
TCTBD	$1.16x10^{-14}$
TCTBD+0.5%MWCNT	$2.56\ x10^{-2}$
TCTBD+0.5%MWCNT+1%1.3DBA	$1.15\ x10^{-2}$
TCTBD+0.5%MWCNT+1%2T	$2.27\ x10^{-4}$
TCTBD+0.5%MWCNT+1%M	$1.29\ x10^{-2}$

These results have highlighted that the presence of the self-healing fillers in the nanofilled epoxy matrix does not decrease its electrical conductivity. The conductive paths in the nano-composite are not affected by the addition of self-healing fillers and the good values of electrical conductivity, together with the promising results of self-healing efficiency tests, confirm the success of this strategic approach aimed to propose a multifunctional load-bearing material with auto-repair ability.

In future, measurements aimed to determine the Electrical Percolation Threshold (EPT) for this formulation are planned.

IV.4 Conclusion

During this last part of research work, performed in the third year of PhD activity, very promising results have been achieved.

Molecules containing specific functional groups (self-healing fillers) have been selected and added to a nano-charged toughened epoxy matrix with the aim to integrate self-healing mechanism in structural materials: polymeric composites with auto-repair ability and good electrical conductivity have been formulated.

Concerning the mechanical properties of the formulated materials, all the systems are characterized by high values in the storage modulus (between 2000 and 3000 MPa up to 100°C) and in the main glass transition temperature (between 170°C and 200°C). Furthermore, very good values of self-healing efficiency have been obtained.

A very detailed FT-IR analysis has highlighted the formation of H-bonding interaction between the self-healing fillers and the components of the epoxy mixture.

Solubility tests and SEM analysis have evidenced a good dispersion of the compounds in the epoxy mixture.

Furthermore, thermal investigations highlight important results from an industrial point of view: the formulations are thermally stable after the curing cycle and hence, the self-healing fillers are available to act as donors and acceptors of hydrogen bonds even after the “curing cycles” usually employed in industrial manufacturing processes.

Chapter V
Conclusions and future work

V.1 Results of this PhD thesis

A multifunctional material "heals" only if it restores also other functionalities. The healing agent/healing resin must be able to activate self-healing mechanisms together with the simultaneous restoration of electrical conductivity. The self-healing resin must contain electrically conductive nanoparticles in a concentration able to restore the "electrical conductivity" function.

In this context, during this PhD research activity, two main strategies have been proposed, a first one based on the development of microencapsulated self-healing system and a second one based on the activation of self-healing mechanism through hydrogen bonding interaction of conductive healing agent/healing components.

Both strategic approaches have led to very successful and promising results for the structural applications of the composites, but still a lot can be done, in particular in the field of supramolecular self-healing systems.

A supramolecular self-healing system is based on the possibility to control the number and mobility of hydrogen bonding moieties (covalently or non-covalent attached to specific nanofillers) to activate auto-reapeair mechanisms integrated in multifunctional materials. The design of nanofilled self-healing polymers based on hydrogen bonding combines highly dynamic properties, such as bonds showing a reversible "sticker-like" behavior enabling connection and reconnection, and thus supramolecular network formation with the possibility to restore the sensing functionality based on electrical properties. The real challenge to face in apply this approach is the limited dynamic properties of thermosetting matrix segments. The idea, to overcome this difficulty, has been to reduce the rigidity of the matrix acting on the phase composition of the resin. Therefore, to enhance the effect of hydrogen bonding forces, small domains of polymeric matrix at lower mobility, finely interpenetrated in the resin, have been considered. The higher mobility of the resin finely distributed in the composite has favored

the arrangement of hydrogen bonding interactions to activate self-healing mechanisms.

Therefore, the relevant results of this PhD thesis, obtained for the two different analysed systems, are listed below:

Microencapsulated systems

- A stable initiator for ROMP reactions, suitably designed to be embedded in structural resins, has been synthetized. It is named with the acronym $HG2_{MesPhSyn}$.
- It rapidly polymerizes cyclic olefins in reactive environments.
- The thermal stability and chemical inertness towards oxirane rings allow its employment in the form of molecular complex in epoxy precursors thus reducing the amount of initiator in structural self-healing materials of 90% wt/wt, simultaneously preserving the catalytic activity at high temperatures (180–200°C) also in presence of the aromatic primary amine (DDS).
- NMR and FTIR spectroscopy highlighted a relevant initiator stability able to activate self-healing mechanisms in aeronautical resins and to fulfill industrial requirements.
- Self-healing efficiency has been found to be 103%.
- The $HG2_{MesPhSyn}$ complex, with the *syn* orientation of the phenyl groups, is able to activate metathesis reactions within the highly reactive environment of the epoxy thermosetting resins, cured up to 180°C, while the other stereoisomer, with the anti-orientation of the phenyl groups, does not preserve itscatalytic activity in these conditions.
- The comparison between the self-healing functionality of two catalytic systems has been performed, using metathesis tests and FTIR spectroscopy. In the field of the design of catalytic systems for self-healing structural materials, a very relevant result has been found: a slight difference in the molecular stereochemistry plays a key role in the development of self-healing materials for aeronautical and aerospace applications.

Self-healing systems based on hydrogen bondings

- Hydrogen bonding moieties, able to act as reversible healing-elements, have been covalently linked to MWCNTs to generate self-healing nanocomposites.
- Functionalized MWCNTs, embedded in a rubber-toughened epoxy formulation, lead to reversible MWCNTs-bridges through the matrix.

- Multifunctional self-healing systems characterized by an electrical conductivity beyond the EPT have been formulated.
- Healing efficiencies have been assessed for nanocharged epoxy formulations loaded with 0.5% wt/wt of MWCNTs decorated with barbituric acid and thymine groups.
- Molecules containing specific functional groups have been selected and added to a nano-charged toughened epoxy matrix with the aim to integrate self-healing mechanism in structural materials: polymeric composites with auto-repair ability and good electrical conductivity have been formulated.
- Very good values of self-healing efficiency have been obtained.
- The detailed FT-IR analysis has highlighted the formation of H-bonding interaction between the self-healing fillers and the components of the epoxy mixture.
- Thermal and mechanical investigations have highlighted that the formulated composites are able to meet industrial requirments.
- Results from this study allow new design concepts of self-healing structures, opening new horizons in aeronautical, automotive, civil engineering and wind power industries.

V.2 Future work

In order to reach the above-mentioned goal, other different strategies can be planned:

- chemical modification of self-healing materials;
- chemical modification of nitrogen bases;
- mixing strategy

These strategies have been discussed in the following sections and represent the starting point for a future research activity.

V.2.1 Chemical modification of self-healing materials

New materials for self-healing mechanisms have been already commercially developed by Suprapolix. The current limits of these existing materials (if not modified) are the absence of mechanical performance suitable for structural materials (planned for primary structures and then for epoxy resins). These drawbacks can be overcome through a very innovative functionalization able to simultaneosly impart (to the self-healing material) “electrical conductivity” and “compatibility” with the epoxy matrix. The possibility to add self-healing mechanisms based on π-π stacking interactions (controlling the viscosity of the formulation) can be explored.

In order to realize this innovative functionalization, the polymer Ureidopyrimidone (UPy), provided by Suprapolix and shown in Figure V.1, can be covalently functionalized with a pyrene tail and with epoxy groups.

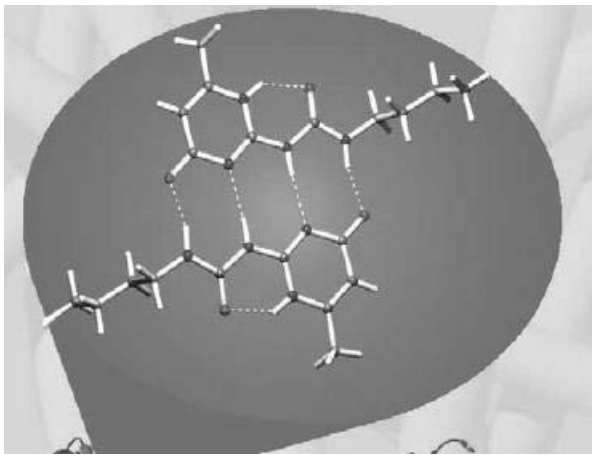

Figure V.1 ***Polymer*** *Ureidopyrimidone (UPy)*

The design of the self-healing material, as theoretical planned, is shown in Figure V.2

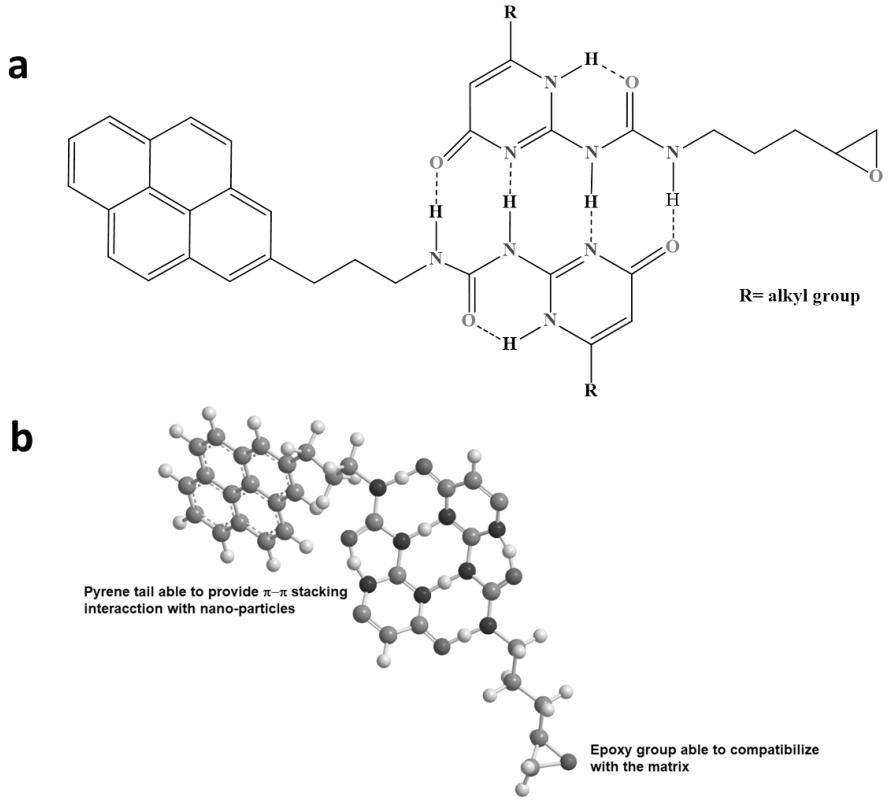

Figure V.2 *a) Theoretical design of self-healing material; b) theoretical design of self-healing material in 3D configuration*

Pyrene group is able to activate π-π stacking interactions with MWCNTs or graphene nanoparticles (embedded in the self-healing material to impart "sensing" function), as shown in Figure V.3.

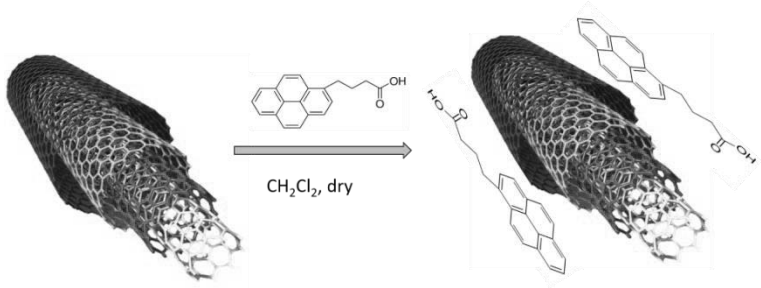

Figure V.3 *Rapresentation of π-π stacking interactions*

Non-covalent functionalization of MWCNTs and graphene-based nanoparticles with pyrene derivatives are able to preserve the structure of the nanofiller simultaneously promoting high degree of dispersion due to π-stacking interaction between nanofiller and pyrene (covalently attached to the self-healing material). This type of chemical functionalization of particles not only prevents the agglomeration during the filler dispersion within the viscous resin, but is also able to decrease the viscosity of the nanofilled formulation, thus optimizing the manufacturing process and the electrical properties of the resulting materials.

The functionalization of UPy with epoxy groups is aimed to better compatibilize the self-healing materials with the epoxy hosting matrix.

The eventual obtained material could be dispersed together with carbon nanoparticle (MWCNTs, in the range of nanofiller concentration able to maximize the "electrical conductivity") in the epoxy resin, which should be tested to prepare carbon fiber reinforced composites at lab scale.

The simultaneous use of the functionalized UPy (or other molecules) and carbon nanofiller can assure the "sensing function" in addition to the self-repair.

The new functionalized material, the epoxy dispersion and the CFRP can be characterized with the following techniques:

- Spectroscopic Investigation, to verify the effectiveness of the functionalization.
- Rheological measurements, to determine the process parameters.
- TDCB fracture test for self-healing efficiency evaluation.
- AFM-TUNA, to analyze the restoration of the conductive network at nanoscale level (domains).

V.2.2 Chemical modification of nitrogen bases

As an alternative to the use of functionalized UPy, nitrogen bases can be used to obtain similar interactions (see Fig. V.4).

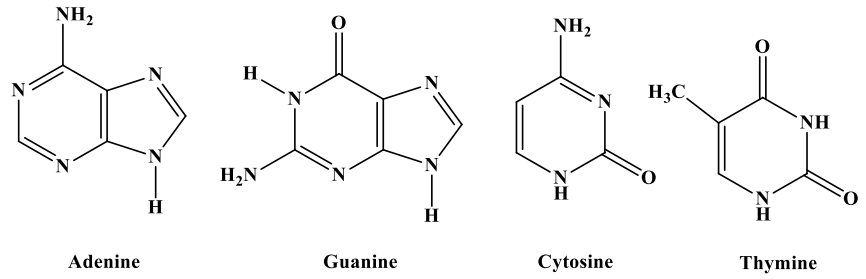

Figure V.4 *Chemical formulas of nitrogen bases*

In particular, among the nitrogenous bases, Guanine should be the most suitable, due to a bigger amount of H-bonding donor and acceptor sites. Furthermore, Guanine is commercially available at low costs.

The idea is that to use "Click-chemistry" to covalently functionalize the Guanine with a Pyrene-tail, for the aims above discussed. (see Fig. V.5).

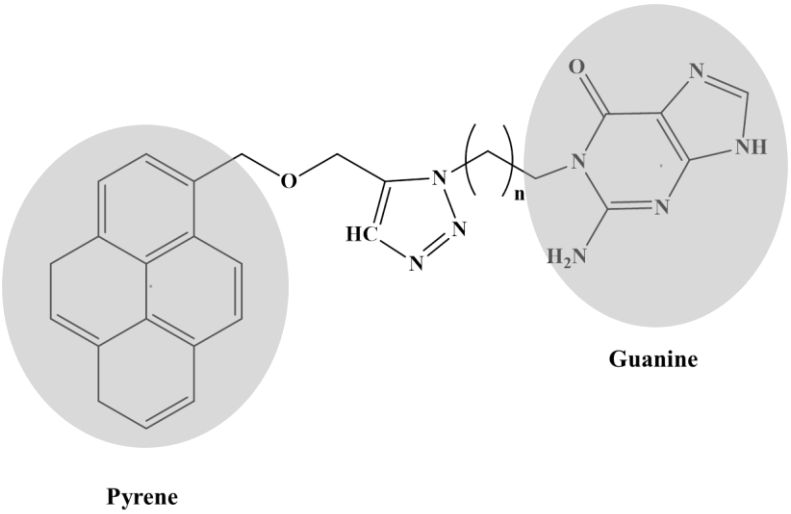

Figure V.5 *Guanine-Pyrene modified*

V.2.3 Mixing strategy

The mixing strategy is based on the possibility to include in the epoxy resin components able to create cumulative hydrogen bondings with the self-healing polymer of Suprapolix or with the functionalized nitrogen bases. This strategy has been (in part) already verified with components able to give high self-healing efficiency for a nanofilled formulation (see section *IV.3.7 Self-healing efficiency evaluation*).

Components able to create cumulative hydrogen bonding with the self-healing polymer of Suprapolix should be selected and characterized from different points of view:

- healing efficiency in the nanofilled epoxy resin;
- viscosity;
- solubility;
- mechanical performance.

The more promising components should be mixed with UPy self-healing materials, and healing efficiency in the nanofilled epoxy resin should be evaluated.

The most promising blend should be loaded with MWCNTs (in the range of nanofiller concentration able to maximize the “sensing function”) and used in CFRPs.

References

Amamoto, Y., Otsuka, H., Takahara, A. and Matyjaszewski, K. (2012). Self - healing of covalently cross - linked polymers by reshuffling thiuram disulfide moieties in air under visible light. Adv Mater, **24**, 3975‑3980.

Amendola, E., Dello Iacono, S., Pastore, A., Curcio, M., Giordano, M. and Iadonisi, A. (2015) Epoxy Thermosets with Self-Healing Ability. J. Mater. Sci. Chem. Eng., **3**, 162-167.

Annable, T., Buscall, R. and Ettelaie, R. (1996). Network formation and its consequences for the physical behaviour of associating polymers in solution. *Colloids Surf A*, **112**, 97-116.

Bazan, G. C., Schrock, R. R., Cho, H. N. and Gibson, V. C. (1991) Polymerization of Functionalized Norbornenes Employing Mo(CH-*t*-Bu)(NAr)(0-*t*-Bu)$_2$ as the Initiator. *Macromolecules*, 24, 4495-4502.

Beck, J. B. and Rowan, S. J. (2003). Multistimuli, Multiresponsive Metallo-Supramolecular Polymers. *J Am Chem Soc*, **125**, 13922-13923.

Binder, W. H. (2013) Self-healing polymers. From principles to applications. *Wiley-VCH, Verlag GmbH & Co. KGaA*, Weinheim, Germany, pp. 440.

Binder, W. H. and Sachsenhofer, R. (2007). 'Click' chemistry in polymer and materials science. *Macromol Rapid Commun*, **28**, 15‑54.

Binder, W. H. and Sachsenhofer, R. (2008). 'Click' chemistry in polymer and material science: an update. *Macromol Rapid Commun*, **29**, 952-981.

Brown, E.N., White, S.R. and Sottos, N.R. (2004). Microcapsule induced toughening in a self-healing polymer composite. *J. Mater. Sci.*, **39**, 1703-1710.

Brown, E.N., White, S.R. and Sottos, N.R. (2005a). Retardation and repair of fatigue cracks in a microcapsule toughened epoxy composite - Part I: Manual infiltration. *Compos. Sci. Technol*, **65**, 2466-2473.

Brown, E. N., White, S.R. and Sottos, N.R. (2005b). Retardation and repair of fatigue cracks in a microcapsule toughened epoxy composite - Part II: In situ self-healing. *Compos. Sci. Technol*, **65**, 2474-2480.

References

Brown, E. N., Kessler, M. R., Sottos, N. R. and White, S. R. (2003) *In situ* poly(urea-formaldehyde) microencapsulation of dicyclopentadiene. *J. Microencapsul*., **20**, 719-730.

Brown, E. N., Sottos, N. R. and White, S. R. (2002) Fracture testing of a self-healing polymer composite. *Exp. Mech.*, **42**, 372-379.

Brutman, J. P., Delgado, P. A. and Hillmyer, M. A. (2014). Polylactide vitrimers. ACS Macro Lett, **3**, 607–610.

Buchmeiser, M. R. (2000). Homogeneous Metathesis Polymerization by Well-Defined Group VI and Group VIII Transition-Metal Alkylidenes: Fundamentals and Applications in the Preparation of Advanced Materials. *Chem. Rev*, **100**, 1565-1604.

Busseron, E., Ruff, Y., Moulin, E. and Giuseppone, N. (2013). Supramolecular self-assemblies as functional nanomaterials. *Nanoscale*, **5**, 7098-7140.

Calabrese, E., Longo, P., Naddeo, C., Mariconda, A., Vertuccio, L., Raimondo, M. and Guadagno, L. (2019). Design of Self-Healing Catalysts for Aircraft Application, *Int. J. Struct. Integr.*, **9**, 732-736.

Campanella, A., Döhler, D. and Binder, W. H. (2018). Self-healing in supramolecular polymers. *Macromol. Rapid Commun.*, **39**, 1700739.

Chen, S., Mahmood, N., Beiner, M. and Binder, W. H. (2015a) Self-Healing Materials from V- and H-Shaped Supramolecular Architectures. *Angew. Chemie Int. Ed.*, **54**, 10188-10192.

Chen, S., Mahmood, N., Beiner, M. and Binder, W. H. (2015b) Self-Healing Materials from V- and H-Shaped Supramolecular Architectures. *Angew. Chemie Int. Ed.*, **127**, 10326–10330.

Cheng, C. C., Chang, F. C., Chen, J. K., Wang, T. Y. and Lee, D. J. (2015). High-efficiency self-healing materials based on supramolecular polymer networks. *RSC Adv.*, **5**, 101148–54.

Cho, S. H, White, S.R. and Braun, P. V., (2009). Self-Healing Polymer Coatings. *Adv. Mater*., **21**, 645-649.

Chowdhury, R. A., Hosur, M.V., Nuruddin, Md., Tcherbi-Narteh, A., Kumar, A., Boddu, V. and Jeelani, S. (2015) Self-healing epoxy composites: preparation, characterization and healing performance. *J Mater Res Technol*, **4**, 33-43.

Chung, K., Lee, S., Park, M., Yoo, P. and Hong, Y. (2015). Preparation and characterization of microcapsule-containing self-healing asphalt. *J. Ind. Eng. Chem*., **29**, 330-337.

Chung, C. K. and. Grubbs, R. H. (2008). Olefin Metathesis Catalyst: Stabilization Effect of Backbone Substitutions of N-Heterocyclic Carbene. *Org. Lett.*, **10**, 2693-2696.

Cordier, P., Tournilhac, F., Soulie-Ziakovic, C. and Leibler, L. (2008). Self-healing and thermoreversible rubber from supramolecular assembly. *Nature*, **451**, 977-980.

Costabile, C. and Cavallo, L. (2004) Origin of Enantioselectivity in the Asymmetric Ru-Catalyzed Metathesis of Olefins. *J. Am. Chem. Soc.*, **126**, 9592–9600.

Cromwell, O. R., Chung. J. and Guan, Z. (2015). Malleable and self-healing covalent polymer networks through tunable dynamic boronic ester bonds. *J Am Chem Soc*, **137**, 6492–6495.

Denissen, W., Rivero, G., Nicolaÿ, R., Leibler, L., Winne, J. M. and Du Prez, F. E. (2015). Vinylogous urethane vitrimers. *Adv Funct Mater*, **25**, 2451–2457.

Deng, W., You, Y. and Zhang, A. (2015). Supramolecular network-based self-healing polymer materials. *Recent advances in smart self-healing polymers and composites*. Elsevier p. 181–210.

Deng, G., Li, F., Yu, H., Liu, F., Liu, C., Sun, W., et al. (2012). Dynamic hydrogels with an environmental adaptive self-healing ability and dual responsive sol–gel transitions. *ACS Macro Lett*, **1**, 275–279.

De Santis, F. and Pantani, R. (2015). Melt compounding of poly (Lactic Acid) and talc: assessment of material behavior during processing and resulting crystallization. *J Polym Res*, **22**, 242.

Deshmukh, P. H. and Blechert, S. (2007). Alkene metathesis: the search for better catalysts. *Dalton Trans*., **24**, 2479-2491.

Döhler, D., Peterlik, H. and Binder, W. H. (2015) A dual crosslinked self-healing system: supramolecular and covalent network formation of four-arm star polymers. *Polymer*, **69**, 264-273.

Döhler, D., Michael, P. and Binder, W. H. (2017). CuAAC-based click chemistry in self-healing polymers. *Accounts Chem Res*, **50**, 2610–2620.

Dry, C. (2007) Multiple function, self-repairing composites with special adhesives. *International Patent* WO/2007/005657.

D'Urso, L., Acocella, M. R., Guerra, G., Iozzino, V., De Santis, F. and Pantani, R. (2018). PLA melt stabilization by high-surface-area graphite and carbon black. *Polymers*, **10**, 139.

Eigler, S., Grimm, S., Hof, F. and Hirsch, A. (2013). Graphene oxide: a stable carbon framework for functionalization. *J Mater Chem A*, **1**,11559-11562.

Eigler, S. and Hirsch, A., (2014). Chemistry with Graphene and Graphene Oxide—Challenges for Synthetic Chemists. *Angew Chem Int Ed Engl*, **53**, 7720-7738.

Eisenberg, A., Hird, B. and Moore, R. B. (1990). A new multiplet-cluster model for the morphology of random ionomers. *Macromolecules*, **23**, 4098-4107.

Everitt, D.T., Luterbacher, R., Coope, T.S., Trask, R.S., Wass, D.F. and Bond, I.P. (2015). Optimisation of epoxy blends for use in extrinsic self-healing fibre-reinforced composites. *Polymer*, **69**, 283-292.

Faghihnejad, A., Feldman, K. E., Yu, J., Tirrell, M. V., Israelachvili, J. N., Hawker, C. J., Kramer, E. J. and Zeng, H. (2014). Adhesion and Surface

Interactions of a Self-Healing Polymer with Multiple Hydrogen-Bonding Groups. *Adv Funct Mater*, **24**, 2322-2333.

Fortman, D. J., Brutman, J. P., Cramer, C. J., Hillmyer, M. A. and Dichtel, W. R. (2015). Mechanically activated, catalyst-free polyhydroxyurethane vitrimers. *J Am Chem Soc*, **137**, 14019–14022.

Frenzel, U. and Nuyken, O. (2002) Ruthenium-based metathesis initiators: Development and use in ring-opening metathesis polymerization. *Polym. Sci. Part*, 40, 2895-2916.

Garber, S. B., Kingsbury, J. S., Gray, B. L. and. Hoveyda, A.H (2000). Efficient and Recyclable Monomeric and Dendritic Ru-Based Metathesis Catalysts. *J. Am. Chem. Soc.*, **122**, 8168-8179.

Georgakilas, V., Otyepka, M., Bourlinos, A. B., Chandra, V., Kim, N., Kemp, K.C., Hobza, P., Zboril, R. and Kim, K. S. (2012). Functionalization of Graphene: Covalent and Non-Covalent Approaches, Derivatives and Applications. *Chem Rev*, **112**, 6156-6214.

Gessler, S., Randl, S. and Blechert, S. (2000). Synthesis and metathesis reactions of a phosphine-free dihydroimidazole carbene ruthenium complex. *Tetrahedron Lett.*, **41**, 9973-9976.

González-Rodríguez, D. and Schenning, A. P. H. J. (2011). Hydrogen-bonded Supramolecular π-Functional Materials. *Chem. Mater*., **23**, 310-325.

Grisi, F., Mariconda, A., Costabile, C., Bertolasi, V. and Longo, P. (2009) Influence of *syn* and *anti* Configurations of NHC Backbone on Ru-Catalyzed Olefin Metathesis. *Organometallics*, **28**, 4988–4995.

Grubbs, R. H. and Khosravi, E. (1999). Ring-Opening Metathesis Polymerization (ROMP) and Related Processes. *Mater. Sci. Technol.*, **20**, 65.

Gu, X., Qi, W., Xu, X., Sun, Z., Zhang, L., Liu, W., Pan, X. and Su, D. (2014). Covalently functionalized carbon nanotube supported Pd nanoparticles for catalytic reduction of 4-nitrophenol. Nanoscale, **6**, 6609-6616.

Guadagno, L., Longo, P., Raimondo, M., Naddeo, C., Mariconda, A., Vittoria, V., Iannuzzo, G. and Russo, S. (2011a) Use of Hoveyda–Grubbs' second-generation catalyst in self-healing epoxy mixtures. *Composites Part B*, **42**, 296-301.

Guadagno, L., Raimondo, M., Naddeo, C., Longo, P., Mariconda, A. and Binder, W. H. (2014a) Healing efficiency and dynamic mechanical properties of self-healing epoxy systems. *Smart Mater Struct*, **23**, 045001 (11 pp).

Guadagno, L., Raimondo, M., Vittoria, V., Vertuccio, L., Naddeo, C., Lamberti, P., et al. (2015a). Epoxy resin with low humidity content Aermacchi SpA, EP2873682A1.

Guadagno, L., Raimondo, M., Longo, P., Bonnaud, L., Murariu, O., Dubois, P., et al. (2015b). Multifunctional epoxy resin with enhanced flame resistance EP2883896A1, Leonardo SpA,

Guadagno, L., Longo, P., Mariconda, A., Calabrese, E., Raimondo, M., Naddeo C., Vertuccio, L., Russo, S. and Iannuzzo, (2017a). G. Grubbs-hoveyda type catalyst for metathesis reactions in highly reactive environments. European Patent EP 3 141 303 A1, 2017-03-15, Leonardo S.p.A 00195 Roma / IT

Guadagno, L., Naddeo, C., Raimondo, M., Barra, G., Vertuccio, L., Sorrentino, A., Binder, W. H. and Kadlec, M. (2017b) Development of self-healing multifunctional materials. *Composites Part B,* **128**, 30-38

Guadagno, L., Longo, P., Raimondo, M., Naddeo, C., Mariconda, A., Sorrentino, A., Vittoria, V., Iannuzzo, G. and Russo, S. (2010a). Cure behavior and mechanical properties of structural self-healing epoxy resins**.** *J. Polym. Sci. Part B: Polym. Phys*., **48**, 2413-2423.

Guadagno, L., Raimondo, M., Naddeo, C., Longo, P. and Mariconda, A. (2014b). Self-healing materials for structural applications. *Polym. Eng. Sci*., **54**, 777-784.

Guadagno, L., Raimondo, M., Vietri, U., Naddeo, C., Stojanovic, A., Sorrentino, A. and Binder, W. H. (2016a) Evaluation of the Mechanical Properties of Microcapsule-Based Self-Healing Composites. *Int. J. Aerosp. Eng.*, Article ID 7817962 (10 pp).

Guadagno., L., Raimondo, M., Naddeo, C. and Longo, P., (2013a) Application of self-healing materials in aerospace Engineering. In: Wolfgang H. Binder (editor) Self-Healing Polymers: From Principles to Applications. *Wiley-VCH Verlag*, chapter 17, pp. 401-412.

Guadagno, L. and Raimondo, M., (2012). Use of FTIR Analysis to Control the Self-Healing Functionality of Epoxy Resins. In: Prof. Theophanides Theophile (Ed.), Infrared Spectroscopy - Materials Science, Engineering and Technology, *InTech, Rijeka - Croatia*, chapter 14, pp. 285-300.

Guadagno, L., Mariconda, A., Agovino, A., Raimondo, M. and Longo, P., (2017c). Protection of graphene supported ROMP catalyst through polymeric globular shell in self-healing materials. *Composites Part,* **116**, 352-360.

Guadagno, L., Raimondo, M., Vertuccio, L., Mauro, M., Guerra, G., Lafdi, K., De Vivo, B., Lamberti, P., Spinelli, G. and Tucci, V. (2015c). Optimization of graphene-based materials outperforming host epoxy matrices. *RSC Advances*, **5**, 36969-36978.

Guadagno, L., Vertuccio, L., Naddeo, C., Calabrese, E., Barra, G., Raimondo, M., Sorrentino, A., Binder, W. H., Michael, P. and Rana, S. (2019). Self-healing epoxy nanocomposites via reversible hydrogen bonding. *Composites Part B*, **157**, 1-13.

Guadagno, L. and Raimondo, M. (2013b) Process for preparing self-healing composite materials of high efficiency for structural applications. *US Patent*, US8481615.

Guadagno, L., Raimondo, M., Vittoria, V., Vertuccio, L., Naddeo, C., Russo, S., De Vivo, B., Lamberti, P., Spinelli, G. and Tucci, V. (2014c). Development of epoxy mixtures for application in aeronautics and aerospace**.** *RSC Adv.*, **4**, 1547415488.

Guadagno, L., Vietri, U., Raimondo, M., Vertuccio, L., Barra, G., De Vivo, B., Lamberti, P., Spinelli, G., Tucci, V., De Nicola, F., Volponi, R. and Russo S. (2015d). Correlation between electrical conductivity and manufacturing processes of nanofilled carbon fiber reinforced composites. *RSC Adv.*, **80**, 7-14.

Guadagno, L., Raimondo, M., Vietri, U., Vertuccio, L., Barra, G., De Vivo, B., et al. (2015e). Effective formulation and processing of nanofilled carbon fiber reinforced composites. *RSC Adv*, **5**, 6033‑6042.

Guadagno, L., Raimondo, M., Vertuccio, L., Naddeo, C., Barra, G., Longo, P., Lamberti, P., Spinelli, G. and Rossella, M. R.. (2018). Morphological, rheological and electrical properties of composites filled with carbon nanotubes functionalized with 1-pyrenebutyric acid. *Compos B Eng*, **147**, 12‑21.

Guadagno, L., Sarno, M., Vietri, U., Raimondo, M., Cirillo, C. and Ciambelli, P. (2015f). Graphenebased structural adhesive to enhance adhesion performance. *RSC Adv*, **5**, 27874‑27886.

Guadagno, L., Naddeo, C., Raimondo, M., Barra, G., Vertuccio, L., Russo, S., et al. (2017d). Influence of carbon nanoparticles/epoxy matrix interaction on mechanical, electrical and transport properties of structural advanced materials. *Nanotechnology*, **28**, 094001.

Guadagno, L., De Vivo, B., Di Bartolomeo, A., Lamberti, P., Sorrentino, A., Tucci, V., et al. (2011b). Effect of functionalization on the thermo-mechanical and electrical behavior of multi-wall carbon nanotube/epoxy composites. *Carbon* 2011b, **49**, 1919‑1930.

Guadagno, L., Naddeo, C., Vittoria, V., Sorrentino, A., Vertuccio, L., Raimondo, M., et al. (2010b). Cure behavior and physical properties of epoxy resin-filled with multiwalled carbon nanotubes. *J Nanosci Nanotechnol*, **10**, 2686‑2693.

Halake, K. and Lee, J. (2017) *J. Ind. Eng. Chem*. doi:http://dx.doi.org/10.1016/j. jiec.2017.04.018 (in press), Corrected Proof, Available online 15 April 2017.

Herbst, F., Döhler, D., Michael, P. and Binder, W. H. (2013) Self-Healing Polymers via Supramolecular Forces. *Macromol. Rapid Commun.*, **34**, 203–220.

Herbst, F., Seiffert, S. and Binder, W. H. (2012) Dynamic supramolecular poly(isobutylene)s for self-healing materials. *Polym. Chem.*, **3**, 3084-3092.

Hia, I. L., Vahedi, V. and Pasbakhsh, P. (2016) Self-Healing Polymer Composites: Prospects, Challenges, and Applications. *Polymer Reviews*, **56**, 225–261.

Hong, S. H., Wenzel, A. G., Salguero, T. T., Day, M. W. and. Grubbs, R. H. (2007). Decomposition of Ruthenium Olefin Metathesis Catalysts. *J. Am. Chem. Soc.*, **129**, 7961-7968.

Huang, J., Stevens, E. D., Nolan, S. P. and Petersen, J. L. (1999) Olefin Metathesis-Active Ruthenium Complexes Bearing a Nucleophilic Carbene Ligand. *J. Am. Chem. Soc.*, **121**, 2674-2678.

Huang, Y. and Kinloch, A. (1992). The toughness of epoxy polymers containing microvoids. *Polymer*, **33**, 1330-1332.

Imato, K., Takahara, A. and Otsuka, H. (2015). Self-healing of a cross-linked polymer with dynamic covalent linkages at mild temperature and evaluation at macroscopic and molecular levels. *Macromolecules*, **48**, 5632‑5639.

Ivin, J. K. and Mol, J. C. (1997) Olefin Metathesis and Metathesis Polymerization. Academic Press, San Diego (CA).

Jazzar, R. F. R., Macgregor, A. S., Mahon, M. F., Richards, S. P. and Whittlesey, M. K. (2002). C−C and C−H Bond Activation Reactions in N-Heterocyclic Carbene Complexes of Ruthenium. *J. Am. Chem. Soc*., **124**, 4944-4945.

Ji S, Cao W, Yu Y, Xu H. Visible - light - induced self - healing diselenide - containing polyurethane elastomer. Adv Mater 2015;27(47):7740‑5.

Jin, H., Hart, K. R., Coppola, A. M., Gergely, R. C., Moore, J. S., Sottos, N. R. and White, S. R. (2013) Self-Healing Epoxies and Their Composites. In: WH Binder (editor), Self-Healing Polymers. From Principles to Applications, *Wiley-VCH Verlag GmbH & Co. KGaA*, Weinheim, Germany, chapter 15, pp. 361-380.

Jones, A. S., Rule, J. D., Moore, J. S., White, S. R. and Sottos, N. R. (2006) Catalyst Morphology and Dissolution Kinetics of Self-Healing Polymers. *Chem. Mater.*, **18**, 1312-1317.

Jones, A. S., Rule, J. D., Moore, J. S., Sottos, N. R. and White, S. R. (2007). Life extension of self-healing polymers with rapidly growing fatigue cracks. *Journal of the Royal Society Interface*, **4**, 395-403.

Kadlec, M., Nováková, L., Mlch, I. and Guadagno, L. (2016). Fatigue delamination of a carbon fabric/epoxy laminate with carbon nanotubes. *Composites Science and Technology*, **131**, 32-39.

Kanaoka, S. and Grubbs, R. H. (1995) Synthesis of Block Copolymers of Silicon-Containing Norbornene Derivatives via Living Ring-Opening Metathesis Polymerization Catalyzed by a Ruthenium Carbene Complex. *Macromolecules,* **28**, 4707-4713.

Kashiwagi, T. (2007). Progress in flammability studies of nanocomposites with new types of nanoparticles. *Flame retardant polymer nanocomposites*, **10**, 285‑324.

Keitz, B. K. and Grubbs, R. H. (2010). Ruthenium Olefin Metathesis Catalysts Bearing Carbohydrate-Based N-Heterocyclic Carbenes. *Organometallics*, **29**, 403-408.

Kessler, M. R., Sottos, N. R. and White, S. R. (2003) Self-healing structural composite materials. *Compos. Part A: Appl. Sci. Manuf*, 34, 743-753.

Kessler, M. R. and White, S.R. (2001). Self-activated healing of delamination damage in woven composites. *Composites Part A*: Applied Science and Manufacturing, 32, 683-699.

Lai, J. C., Mei, J. F., Jia, X. Y., Li, C. H., You, X. Z. and Bao, Z. (2016). A stiff and healable polymer based on dynamic - covalent boroxine bonds. *Adv Mater*, **28**, 8277‑8282.

Lavorgna, M., Romeo, V., Martone, A., Zarrelli, M., Giordano, M., Buonocore, G., et al. (2013). Silanization and silica enrichment of multiwalled carbon nanotubes: synergistic effects on the thermal-mechanical properties of epoxy nanocomposites. *Eur Polym J*, **49**, 428‑438.

Liu, W., Liu, Y. and Wang, R. (2011). MD Simulation of Single-wall Carbon Nanotubes Employed as Container in Self-healing Materials. *Polym. Polym. Compos*., **19**, 333-338.

Liu, W. X., Zhang, C., Zhang, H., Zhao, N., Yu, Z. X. and Xu, J. (2017). Oxime-based and catalyst-free dynamic covalent polyurethanes. *J Am Chem Soc*, **139**, 8678–8684.

Liu, X., Su, G., Guo, Q., Lu, C., Zhou, T., Zhou, C., et al. (2018). Hierarchically structured self-healing sensors with tunable positive/negative piezoresistivity. *Adv Funct Mater*, 1706658.

Longo, P., Mariconda, A., Calabrese, E., Raimondo, M., Naddeo, C., Vertuccio, L., Russo, S., Iannuzzo, G., and Guadagno, L., (2017a) Development of a new stable ruthenium initiator suitably designed for self-repairing applications in high reactive environments. *Int. J. Struct. Integr.*, **54**, 234-251.

Lu, Y. X. and Guan, Z. (2012). Olefin metathesis for effective polymer healing via dynamic exchange of strong carbon–carbon double bonds. *J Am Chem Soc*, **134**, 14226–14231.

Ma P. C., Kim, J. K. and Tang, B. Z. (2007). Effects of silane functionalization on the properties of carbon nanotube/epoxy nanocomposites. Compos Sci Technol, **67**, 2965–2972.

Ma, P. C., Siddiqui, N. A., Marom, G., Kim and J. K. (2010). Dispersion and functionalization of carbon nanotubes for polymer-based nanocomposites: a review. *Compos Appl Sci Manuf*, **41**, 345–367.

Mariconda, A., Longo, P., Agovino, A., Guadagno, L., Sorrentino, A. and Raimondo, M., (2015). Synthesis of ruthenium catalysts functionalized graphene oxide for self-healing applications. *Polymer*, **69**, 330-342.

Martone, A., Formicola, C., Piscitelli, F., Lavorgna, M., Zarrelli, M., Antonucci, V., et al. (2012). Thermo-mechanical characterization of epoxy nanocomposites with different carbon nanotube distributions obtained by solvent aided and direct mixing. *Express Polym Lett*, **6**, 520–531.

Michal, B. T., Jaye, C. A., Spencer, E. J. and Rowan S. J. (2013). Inherently photohealable and thermal shape-memory polydisulfide networks. *ACS Macro Lett.*, **2**, 694–699.

Montarnal, D., Capelot, M., Tournilhac, F. and Leibler, L. (2011). Silica-like malleable materials from permanent organic networks. *Science*, **334**, 965–968.

Motuku, M., Vaidya, U. K. and Janowski, G. M. (1999) Parametric studies on self-repairing approaches for resin infused composites subjected to low velocity impact. *Smart Mater. Struct.*, **8**, 623-638.

Naddeo, C., Vertuccio, L., Barra, G. and Guadagno, L. (2017). Nano-charged polypropylene application: realistic perspectives for enhancing durability. *Materials*, **10**, 943.

Nia, A. S., Rana, S., Döhler, D., Osim, W. and Binder, W. H., (2015). Nanocomposites via a direct graphene-promoted "click"-reaction. *Polymer*, **79**, 21-28.

Nguyen, S. T., Johnson, L. K. and Grubbs, R. H. (1992) Ring-opening metathesis polymerization (ROMP) of norbornene by a Group VIII carbene complex in protic media. *J. Am. Chem. Soc.*, **114**, 3974-3975.

Nguyen, S. T. and Grubbs, R. H. (1993) Syntheses and activities of new single-component, ruthenium-based olefin metathesis catalysts. *J. Am. Chem. Soc.*, **115**, 9858-9859.

Noack, M., Merindol, R., Zhu, B., Benitez, A., Hackelbusch, S., Beckert, F., et al. (2017). Light - fueled, spatiotemporal modulation of mechanical properties and rapid self-healing of graphene - doped supramolecular elastomers. *Adv Funct Mater*, **27**, 1700767.

Nobile, M. R., Raimondo, M., Lafdi, K., Fierro, A., Rosolia, S. and Guadagno, L. (2015). Relationships between nanofiller morphology and viscoelastic properties in CNF/epoxy resins. *Polym. Compos.*, **36**, 1152-1160.

Novak, B. M., Risse, W. and Grubbs, R. H. (1992) The development of well-defined catalysts for ring-opening olefin metathesis polymerizations (ROMP). *Adv. Polym. Sci.*, **102**, 47-72.

Obadia, M. M., Mudraboyina, B. P., Serghei, A., Montarnal, D. and Drockenmuller, E. (2015). Reprocessing and recycling of highly cross-linked ion-conducting networks through transalkylation exchanges of C-N bonds. *J Am Chem Soc*, **137**, 6078‑6083.

Osim, W., Stojanovic, A., Akbarzadeh, J., Peterlik, H. and Binder, W. H. (2013). Surface modification of MoS2 nanoparticles with ionic liquid-ligands: towards highly dispersed nanoparticles. *Chem Commun*, **49**, 9311-9313

Perfetto, A., Costabile, C., Longo, P., Bertolasi, V. and Grisi, F. (2013) Probing the Relevance of NHC Ligand Conformations in the Ru-Catalysed Ring-Closing Metathesis Reaction. *Chem. Eur. J.*, **19**, 10492 – 10496.

Perfetto, A., Costabile, C., Longo, P. and Grisi, F. (2014) Ruthenium Olefin Metathesis Catalysts with Frozen NHC Ligand Conformations. *Organometallics*, **33**, 2747−2759.

Pu, W., Fu, D., Wang, Z., Gan, X., Lu, X., Yang, L., et al. (2018). Realizing crack diagnosing and selfhealing by electricity with a dynamic crosslinked flexible polyurethane composite. *Advanced Science*, **5**, 1800101.

Raimondo, M. and Guadagno, L. (2013). Healing efficiency of epoxy-based materials for structural applications. *Polym. Compos.*, **34**, 1525-1532.

Raimondo, M., Longo, P., Mariconda, A. and Guadagno, L. (2015) Healing agent for the activation of self-healing function at low temperature. *Adv. Compos. Mater*, **24**, 519-529.

Raimondo, M., De Nicola, F., Volponi, R. Binder, W., Michael, P., Russo, S. and Guadagno, L. (2016) Self-repairing CFRPs targeted towards structural aerospace applications. *Int. J. Struct. Integr.*, **7**, 656-670.

Raimondo, M. and Guadagno, L., (2012). Healing efficiency of epoxy-based materials for structural application. AIP Conference Proceedings, **1459**, 223-225.

Raimondo, M., Guadagno, L., Vertuccio, L., Naddeo, C., Barra, G., Spinelli, G., et al. (2018). Electrical conductivity of carbon nanofiber reinforced resins: potentiality of Tunneling Atomic Force Microscopy (TUNA) technique. *Compos B Eng*, **143**, 148‑160.

Rekondo, A., Martin, R., de Luzuriaga, A. R., Cabañero, G., Grande, H. J. and Odriozola, I. (2014). Catalyst-free room-temperature self-healing elastomers based on aromatic disulphide metathesis. *Materials Horizons*, **1**, 237‑240.

Roy, N., Buhler, E. and Lehn, J. M. (2014). Double dynamic self - healing polymers: supramolecular and covalent dynamic polymers based on the bis - iminocarbohydrazide motif. *Polym Int*, **63**, 1400-1405.

Rule, J. D., Brown, E. N., Sottos, N. R., White S. R. and Moore, J. S. (2005a) Wax-Protected Catalyst Microspheres for Efficient Self-Healing Materials. *Adv. Mater*, **17**, 205-208.

Rule, J.D., Sottos, N.R., White, S.R. and Moore, J.S. (2005b). The Chemistry of Self-Healing Polymers. *Education in Chemistry*, **42**, 130-132.

Saadati, P., Baharvand, H., Rahimi, A. and Morshedian, J. (2005). Effect of modified liquid rubber on increasing toughness of epoxy resin. *Iran Polym.*, **14**, 637–646.

Sahoo, N.G., Rana, S., Cho, J.W., Li, L. and Chan, S. H. (2010). Polymer nanocomposites based on functionalized carbon nanotubes. *Prog Polym Sci*, **35**, 837-867.

Samojłowicz, C., Bieniek, M. and Grela, K. (2009). Ruthenium-Based Olefin Metathesis Catalysts Bearing *N*-Heterocyclic Carbene Ligands. *Chem. Rev.*, **109**, 3708-3742.

Sarkar, S., Moser, M. L., Tian, X., Zhang, X., Al-Hadeethi, Y. F. and Haddon, R. C., (2014). Metals on Graphene and Carbon Nanotube Surfaces: From Mobile Atoms to Atomtronics to Bulk Metals to Clusters and Catalysts. *Chem Mater*, **26**, 184-195.

Savoie, T., Stenne, B. and Collins, S. K. (2009). Improved Chiral Olefin Metathesis Catalysts: Increasing the Thermal and Solution Stability via Modification of a C1-Symmetrical N-Heterocyclic Carbene Ligand. *Adv. Synth. Catal*., **351**, 1826-1832.

Scheuermann, G. M., Rumi, L., Steurer, P., Bannwarth, W. and Mülhaupt, R. (2009). Palladium Nanoparticles on Graphite Oxide and Its Functionalized Graphene Derivatives as Highly Active Catalysts for the Suzuki−Miyaura Coupling Reaction. *J Am Chem Soc*, **131**, 8262-8270.

Scholl, M., Ding, S., Lee, C. W. and Grubbs, R. H. (1999). Synthesis and Activity of a New Generation of Ruthenium-Based Olefin Metathesis Catalysts Coordinated with 1,3-Dimesityl-4,5-dihydroimidazol-2-ylidene Ligands. *Org. Lett.*, **1**, 953-956.

Schrock, R. R. (1990) Living Ring-Opening Metathesis Polymerization Catalyzed by Well-Characterized Transition-Metal Alkylidene Complexes. *Acc. Chem. Res.*, 23, 158-165.

Schrodi, Y. and Pederson, R. L. (2007). *Aldrichim. Acta*, **40**, 45-52

Schwab, P., Grubbs R. H. and Ziller, J.W. (1996) Synthesis and Applications of $RuCl_2(=CHR')(PR_3)_2$: The Influence of the Alkylidene Moiety on Metathesis Activity. *J. Am. Chem. Soc.*, **118**, 100-110.

Shaygannia, A., Rana, S., Döhler, D., Jirsa, F., Meister, A., L. Guadagno, et al., (2015) Carbon-Supported Copper Nanomaterials: Recyclable Catalysts for Huisgen [3+2] Cycloaddition Reactions. *Chem Eur J*, **21**, 10763‑10770.

Sijbesma, R. P., Beijer, F. H., Brunsveld, L., Folmer, B. J., Hirschberg, J. H., Lange, R. F., Lowe, J. K. and Meijer, E. W. (1997). Reversible polymers formed from self-complementary monomers using quadruple hydrogen bonding. *Science*, **278**, 1601-1604.

Sivakova, S., Bohnsack, D. A., Mackaym M. E., Suwanmala, P. and Rowan, S. J. (2005). Utilization of a Combination of Weak Hydrogen-Bonding

Interactions and Phase Segregation to Yield Highly Thermosensitive Supramolecular Polymers. *J Am Chem Soc*, **127**, 18202-18211.

Sordo, F. and Michaud, V. (2016). Processing and damage recovery of intrinsic self-healing glass fiber reinforced composites. Smart Mater Struct., **25**, 084012 (9pp).

Stupp, S. I. and Palmer, L. C. (2014). Supramolecular Chemistry and Self-Assembly in Organic Materials Design. *Chem. Mater.*, **26,** 518.

Tam, K. C., Jenkins, R. D., Winnik, M. A. and Bassett, D. R. (1998). A Structural Model of Hydrophobically Modified Urethane−Ethoxylate (HEUR) Associative Polymers in Shear Flows. *Macromolecules*, **31**, 4149-4159.

Tian, Q., Yuan, Y. C., Rong, M. Z. and Zhang, M. Q. (2009). A thermally remendable epoxy resin. *J Mater Chem*, **19**, 1289‑1296.

Tiede, S., Berger, A., Schlesiger, D., Rost, D., Luhl, A. and Blechert, S. (2010a). Hochaktive chirale Ruthenium-Metathesekatalysatoren durch Monosubstitution im N-heterocyclischen Carben. *Angew. Chem.* **122** 4064-4067.

Tiede, S., Berger, A., Schlesiger, A., Rost, D., Luhl, A. and Blechert, S. (2010b). Highly Active Chiral Ruthenium-Based Metathesis Catalysts through a Monosubstitution in the N-Heterocyclic Carbene. *Angew. Chem. Int. Ed*., **49**, 3972-3975.

Toohey, K. S., Sottos, N. R., Lewis, J. A., Moore, J. S. and White, S. R. (2007) Self-healing materials with microvascular networks. *Nature Mater.*, 6, 581-585.

Toohey, K. S., Sottos, N.R. and White, S. R (2009a). Characterization of Microvascular-Based Self-Healing Coatings. *Exp. Mech.*, **49**, 707-717.

Toohey, K.S., Hansen, C.J., Lewis, J.A., White, S.R. and Sottos, N. R. (2009b). Delivery of Two-Part Self-Healing Chemistry via Microvascular Networks. *Adv. Funct. Mater.*, **19**, 1399-1405.

Van der Zwaag, S. (2007). In: Sybrand van der Zwaag (editor), Self Healing materials: an alternative approach to 20 centuries of materials science, *Springer Series in Materials, Springer*, *Dordrecht*, The Netherlands, **100**, 1-18.

Vertuccio, L., Guadagno, L., Spinelli, G., Russo, S. and Iannuzzo, G. (2017). Effect of carbon nanotube and functionalized liquid rubber on mechanical and electrical properties of epoxy adhesives for aircraft structures. *Composites Part B*, **129**, 1-10.

Vertuccio, L., Guadagno, L., Spinelli, G., Lamberti, P., Zarrelli, M., Russo, S., et al. (2018). Smart coatings of epoxy based CNTs designed to meet practical expectations in aeronautics. *Compos B Eng*, **147**, 42‑46.

Vieille-Petit, L., Luan, X., Gatti, M., Blumentritt, S., Linden, A., Clavier, H., Nolan, S. P. and Dorta, R. (2009). Improving Grubbs' II type ruthenium catalysts by appropriately modifying the N-heterocyclic carbene ligand. *Chem. Commun.*, **0**, 3783-3785.

Vieille-Petit, L., Clavier, H., Linden, A., Blumentritt, S., Nolan, S. P. and Dorta, R. (2010). Ruthenium Olefin Metathesis Catalysts with N-Heterocyclic Carbene Ligands Bearing *N*-Naphthyl Side Chains. *Organometallics*, **29**, 775-788.

Viscardi, M., Arena, M., Barra, G. and Guadagno, L. (2017). Smart carbon-epoxy laminate with high dissipation properties for vibro-acoustic optimization in the turboprop aircraft. *Int. J. Mech.*, **11**, 51-57.

Viscardi, M., Arena, M. Barra, G. and Guadagno, L. (2016). Structural performance analysis of smart carbon fiber samples supported by experimental investigation. Int. J. Mech. 10, 376-382.

Vougioukalakis, G. C. and Grubbs, R. H. (2010). Ruthenium-Based Heterocyclic Carbene-Coordinated Olefin Metathesis Catalysts. *Chem. Rev.*, **110**, 1746-1787.

Weng, W., Beck, J. B., Jamieson, A. M. and Rowan, S. J. (2006). Understanding the Mechanism of Gelation and Stimuli-Responsive Nature of a Class of Metallo-Supramolecular Gels. *J Am Chem Soc*, **128**, 11663-11672.

Weck, M., Schwab, P. and Grubbs, R. H. (1996) Synthesis of ABA Triblock Copolymers of Norbornenes and 7-Oxanorbornenes via Living Ring-Opening Metathesis Polymerization Using Well-Defined, Bimetallic Ruthenium Catalysts. *Macromolecules*, **29**, 1789-1793.

Weskamp, T., Schattenmann, W. C., Spiegler, M. and Herrman, W. A. (1998a) Eine neue Generation von Rutheniumkatalysatoren für die Olefinmetathese. Angew. Chem., 110, 2631-2633.

Weskamp, T., Schattenmann, W. C., Spiegler, M. and Herrman, W. A. (1998b) A Novel Class of Ruthenium Catalysts for Olefin Metathesis. Angew. Chem., 37, 2490-2493.

Weskamp, T., Kohl, F. J., Hieringer, W., Gleich, D. and Herrman, W. A. (1999a) Hochaktive Rutheniumkatalysatoren für die Olefinmetathese: die Synergie N-heterocyclischer Carbene und koordinativ labiler Liganden Angew. Chem., 111, 2573-2576.

Weskamp, T., Kohl, F. J., Hieringer, W., Gleich, D. and Herrman, W. A. (1999b) Highly Active Ruthenium Catalysts for Olefin Metathesis: The Synergy of N-Heterocyclic Carbenes and Coordinatively Labile Ligands. Angew. Chem., 38, 2416-2419.

White, S. R., Sottos, N. R., Geubelle, P. H., Moore, J. S., Kessler, M. R., Sriram, S. R., Brown, E. N. and Viswanathan, S. (2001) Autonomic healing of polymer composites. *Nature*, **409**, 794-797.

Wilson, G. O., Moore, J. S., White, S. R., Sottos, N. R. and Andersson, H. M. (2008a). Autonomic healing of epoxy vinyl esters via ring opening metathesis polymerization. *Adv. Funct. Mater*,**18**, 44-52.

Wilson, G. O., Caruso, M. M., Reimer, N. T., White, S. R., Sottos, N. R. and Moore, J. S. (2008b). Evaluation of Ruthenium Catalysts for Ring-

Opening Metathesis Polymerization-Based Self-Healing Applications. *Chem Mater*, **20**, 3288-3297 (Supporting Information).

Wool, R. P. and O'Conner, K.M. (1981). A theory crack healing in polymers. *J. Appl. Phys*., **52**, 5953.

Wu, D. Y., Meure, S. and Solomon, D. (2008) Self-healing polymeric materials: A review of recent developments. *Prog Polym Sci*, **33**, 479-522.

Yang, S., Bachman, R. E., Feng, X. and Müllen, K. (2013). Use of Organic Precursors and Graphenes in the Controlled Synthesis of Carbon-Containing Nanomaterials for Energy Storage and Conversion. *Acc Chem Res*, **46**, 116-128.

Yu, S., Zhang, R., Wu, Q., Chen, T. and Sun, P. (2013). Bio - Inspired high - performance and recyclable cross - linked polymers. *Adv Mater* **25**, 4912‐4917.

Yuan, Y. C., Yin, T., Rong, M. Z. and Zhang, M. Q. (2008a) Self healing in polymers and polymer composites. Concepts, realization and outlook: A review. *EXPRESS Polymer Letters,* **2**, 238–250.

Yuan, C. E., Rong, M. Z. and Zhang, M. Q. (2014). Self-healing polyurethane elastomer with thermally reversible alkoxyamines as crosslinkages. *Polymer*, **55**, 1782-1791.

Xu, W. M., Rong, M. Z. and Zhang, M. Q. (2016). Sunlight driven self-healing, reshaping and recycling of a robust, transparent and yellowing-resistant. *J. Mater. Chem*., **4**, 10683‐10690.

Zhang, M. Q. and Rong, M. Z. (2011) Self-healing Polymers and Polymer Composites, *John Wiley & Sons*, Inc., Hoboken.

Zhang, Z. P, Lu, Y., Rong, M. Z. and Zhang, M. Q. (2016). A thermally remendable and reprocessable crosslinked methyl methacrylate polymer based on oxygen insensitive dynamic reversible C‐ON bonds. *RSC Adv* , **6**, 6350‐6357.

Zhang, Z. P., Rong, M. Z. and Zhang M. Q. (2018). Mechanically robust, self - healable, and highly, stretchable "living" crosslinked polyurethane based on a reversible C-C bond. *Adv Funct Mater*, **28**, 1705060.

Zhang, Y., Ying, H., Hart, K. R., Wu, Y., Hsu, A. J., Coppola, A.M., et al. (2016). Malleable and recyclable poly (urea - urethane) thermosets bearing hindered urea bonds. *Adv Mater*, **28**, 7646‐7651.

Zwaag, S. van der (2007) Self Healing Materials: An Alternative Approach to 20 Centuries of Materials Science, ed. van der Zwaag, Sybrand, Springer, Dordrecht, The Netherlands, **100**, Springer Series in Materials Science.